

Myosin 5c is a class V myosin that functions in secretory granule trafficking

Damon Todd Jacobs

A dissertation submitted to the faculty of the University of North Carolina at Chapel Hill
in partial fulfillment of the requirements for the degree of Doctor of Philosophy in the
School of Medicine (Department of Cell and Molecular Physiology)

Chapel Hill
2008

Approved by:

Carol A. Otey, Ph.D.

Richard E. Cheney, Ph.D.

C. William Davis, Ph.D.

Ann Erickson, Ph.D.

James M. Anderson, MD, Ph.D.

Abstract:

DAMON JACOBS: Myosin Vc is Class V Myosin that Functions in Secretory Granule Trafficking

(Under the direction of Richard E. Cheney, Ph.D.)

Myosin motor proteins are a super family of mechanoenzymes that carry out diverse functions in plants and animals. Class V myosins power the movement of membranous organelles along tracks composed of actin filaments. Myosin Vc (Myo5c) is the third and final member of the myosin V family to be discovered. The mRNA distribution of Myo5c indicated that it is preferentially expressed in epithelial cells and glandular tissues. Initial studies in HeLa cells indicated that Myo5c was associated with an endocytic recycling compartment. Kinetic studies showed that Myo5c is a non-processive vertebrate class V myosin. These studies revealed that, unlike Myo5a and Myo5b, Myo5c is a low duty ratio motor and the rate limiting step of the ATPase cycle is in a prehydrolysis state. More recently, we began to explore the functions of Myo5c in exocrine secretion. Tissue surveys and immunoblots of rat tissues showed that Myo5c is expressed most abundantly in acinar cells and localizes to the apical domain. Our studies utilized exocrine-derived MCF-7 cells to reveal the first endogenous localization of Myo5c in human cells. Myo5c clearly labeled distinct membrane compartments consisting of puncta and long, slender tubules. Our generation of a full-length, GFP-tagged Myo5c expression construct showed that in living cells Myo5c-associated puncta and tubules exhibit differing localization, dynamics, and dependence upon the cytoskeleton. Our key results in MCF-7 cells demonstrated that Myo5c is tightly

associated with secretory granules and that expression of a dominant-negative Myo5c tail disrupts the distribution of secretory granules. Furthermore, in acinar cells of the lacrimal gland, Myo5c tail partially inhibited carbachol stimulated secretion. Together these results strongly indicate that Myo5c is a unique vertebrate class V myosin with important functions in exocrine secretion.

Dedication

This work documents a great personal achievement and is dedicated to my American Indian ancestors who did not have opportunities or were denied opportunities for education. This dissertation is also dedicated to our daughter, Sophia Zavarine Jumping Eagle Jacobs, who was born in our home in Chapel Hill, North Carolina.

“Sophia, may all your dreams come true”

Acknowledgements:

First and foremost, I wish to acknowledge my graduate advisor, Dr. Richard E Cheney, whose guidance and mentorship through my graduate studies was invaluable. I wish to thank Dr. Cheney for demanding a rigorous approach toward scientific investigation and his commitment toward education. I appreciate the many great discussions over good coffee, covering topics such as cell biology, wildland firefighting, and the natural world.

I wish to acknowledge my family, particularly Mom, Carmen Marie Jacobs, for understanding and support during my graduate studies.

I wish to thank the Thompson family in Fort Hall, Idaho for their lifelong friendship and support during all endeavors of my life, you guys are the best!

I wish to acknowledge Dr. Debra Kendall for a note on the back page of a Bluebook test booklet that sparked my initial interest in pursuing graduate studies. I also wish to thank Dr. Shere Byrd, for guidance while attending Fort Lewis College and for providing my first opportunity to perform biological research.

I wish to thank Dr. Sharon Milgram and Jan McCormick of the Cell and Molecular Physiology department at the University of North Carolina-Chapel Hill.

Most of all, I wish to acknowledge and thank Diane Marie Gercke, for her unwavering support and commitment to our family. Diane, my partner in life, has been a great source of inspiration and motivation, and has provided invaluable perspective, patience, and understanding during my graduate studies.

Preface:

This dissertation is the culmination of several years of intense study focused on unconventional myosins. My attention was directed primarily toward investigating the fundamental physiology and cell biology of myosin Vc (Myo5c). The first paper reporting the sequence and discovery of this molecular motor had just been published (Rodriguez and Cheney, 2002) when I began working on this project. Although Myo5a had been the subject of intensive research, almost nothing was known concerning the function(s) of Myo5c. This study of Myo5c allowed me to explore the mechanisms of actin-based membrane transport in vertebrate cells and tissues. In addition to Myo5c, I also performed studies with myosin X (Myo10) that revealed a novel form of motility within filopodia. A brief summary of my accomplishments are listed below:

1. As a first step toward determining the function(s) of Myo5c and identifying the organelle(s) that it is associated with, I began a systematic analysis of Myo5c localization in rat tissues. This led to the discovery of the striking localization at the apical domain of acinar cells in exocrine glands such as the lacrimal gland. These results were presented at a Gordon Research Conference (Salivary Glands and Exocrine Secretion) where I won a student poster award for this work. This presentation of my results also led to a collaboration with the Hamm-Alvarez lab

at the University of Southern California to investigate the role of Myo5c in lacrimal gland acinar cells.

2. In the introduction (Chapter 1) I provide a detailed background on class V myosins and the functions they perform in organelle trafficking. This chapter was commissioned by Nature Reviews Molecular Cell Biology and will serve as the basis of a review article title “Class V Myosins: Motors for organelle transport”. It is currently undergoing revision by Dr. Richard Cheney.
3. Chapter 2 is a data chapter that contains the manuscript, Marchelletta et al., 2008, “The Class V Myosin Motor, Myosin 5c, Localizes to Mature Secretory Vesicles and Facilitates Exocytosis in Lacrimal Acini.” This manuscript was published in the American Journal of Physiology-Cell Physiology. This collaboration with the Hamm-Alvarez lab at USC is a study on the role of Myo5c in secretion from isolated rabbit lacrimal glands. I am second author on this publication and my contributions to this study included the initial localization of Myo5c in a lacrimal gland and showing the presence of all three class V myosins (Myo5a, Myo5b, and Myo5c) by immunoblot. In addition, I generated a green fluorescent protein (GFP) tagged, full-length human Myo5c cDNA, and provided other constructs and Myo5c-specific antibodies, all of which made this study possible. I also contributed to the intellectual conception of the study, provided drafts of a portion of the introduction, results, and discussion, and provided comments on several draft manuscripts.

4. In chapter three, I present a manuscript of my core work on the localization, dynamics, and functions of Myo5c. This manuscript is titled “Myosin Vc is a class V myosin that functions in secretory granule trafficking”, and is currently in revision at *Molecular Biology of the Cell*. This study utilized an exocrine-derived cell line (MCF-7) that expresses an abundance of Myo5c protein, which allowed the first immunolocalization of Myo5c in a cell line. Furthermore, in this study a clonal line that stably expresses Myo5c at near physiological levels was generated and utilized in numerous experiments. Although the MCF-7 cells do not exhibit classic epithelial polarity, they provided a model system in which to obtain high-resolution, time-lapse images of secretory granule trafficking using TIRF microscopy. I am the first author on this manuscript and I am deeply involved in the intellectual conception of the study. I also designed and carried out all experiments, and I wrote the initial draft of the manuscript. Drs. Julie Donaldson and Roberto Weigert, at the NIH, are collaborators on this manuscript. This collaboration originally focused on the endocytic recycling of MHC class I molecules in HeLa cells, however, when many endocytic recycling assays did not consistently support a role for Myo5c in recycling, the focus shifted to the localization and dynamics of Myo5c on secretory granules in MCF-7 cells.

5. The concluding chapter (Chapter 4) will discuss results from previous chapters and present original ideas on the functions of Myo5c in secretory granule

trafficking. Potential regulatory mechanisms of class V myosins associating with cargo will also be discussed.

6. Appendix Chapter 1 is a manuscript published in the Journal of Biological Chemistry (Takagi et al., 2008) that determined the kinetic parameters of human Myo5c. This paper is important because it demonstrated that, in contrast to Myo5a and Myo5b, Myo5c is a non-processive vertebrate class V myosin. My primary contribution to this study consisted of generating a GFP-tagged Myo5c-HMM construct that made this study possible.
7. Appendix Chapter 2 is a manuscript on the discovery of a novel form of motility in filopodia. This manuscript represents the first direct visualization of the dynamics of single molecules of Myosin 10 in living cells. We also provide evidence that Myo5a can also undergo similar movements at the single molecule level. My contributions to this study included setting up the TIRF imaging system that made these studies possible and acquiring the first data revealing this novel form of motility.

Additionally, during my graduate studies I was actively involved with minority issues and recruitment activities sponsored by the Graduate School. These activities included serving as the president of the First Nations Graduate Circle student organization, organizing American Indian recruitment events and American Indian research conferences at UNC-CH, serving on the Provost's Committee on Native American Issues

(PCNAI) at UNC-CH, serving on the search committee for the inaugural director of the American Indian Center at UNC-CH, and serving on the American Indian Center Advisory Committee. These activities allowed me to take advantage of valuable professional development opportunities offered at the University of North Carolina-Chapel Hill.

Table of Contents

CHAPTER 1: INTRODUCTION.....	1
CLASS V MYOSINS: MOTORS FOR ORGANELLE TRANSPORT	1
Abstract.....	3
Introduction.....	4
Structure of class V myosins.....	5
Functions of class V myosins	8
Biophysical and biochemical properties of class V myosins.....	22
Regulatory mechanisms of class V myosins.....	24
Conclusions.....	40
References.....	42
CHAPTER 2: THE CLASS V MYOSIN MOTOR, MYOSIN 5C, LOCALIZES TO MATURE SECRETORY VESICLES, AND FACILITATES EXOCYTOSIS IN LACRIMAL ACINI.....	53
Abstract.....	55
Introduction.....	56
Materials and Methods.....	60
Results.....	70
Discussion.....	108
Text Footnotes	115
Acknowledgements.....	116
References.....	117

CHAPTER 3: MYOSIN VC IS A CLASS V MYOSIN THAT FUNCTIONS IN SECRETORY GRANULE TRAFFICKING.....	122
Abstract.....	124
Introduction.....	125
Materials and Methods.....	129
Results.....	137
Discussion.....	181
Acknowledgements.....	190
Supplemental Methods.....	197
References.....	198
CHAPTER 4: CONCLUSIONS AND FUTURE DIRECTIONS	206
Class V myosins are actin-based molecular motors that transport organelles.....	207
How is organelle specificity achieved?.....	207
Myo5c is a class V myosin for exocrine secretion	211
Myo5c, non-processivity, and exocrine secretion.....	219
References.....	231
APPENDICES	237
APPENDIX 1: MYOSIN VC IS A LOW DUTY RATIO, NON-PROCESSIONAL MOLECULAR MOTOR	238
Abstract.....	240
Introduction.....	242
Materials and Methods.....	246
Results.....	251
Discussion.....	282

Acknowledgments.....	290
References.....	291
APPENDIX 2: SINGLE MOLECULE IMAGING OF MYOSIN-X REVEALS A NOVEL FORM OF MOTILITY IN FILOPODIA.....	298
Abstract.....	300
Introduction.....	301
Materials and Methods.....	304
Results.....	307
Discussion.....	329
Acknowledgements.....	331
References.....	336

List of Tables

Table 1-1: Class V myosins associate with several organelles.....	11
Table 2-1. Bulk Protein release in LGAC transduced with GFP or GFP-Myo5c-tail.	89
Table A1-1: Kinetic parameters of the MVc-S1 ATPase cycle with corresponding values for myosins Va, Vb and Drosophila myosin V.....	256

List of Figures

Figure 1-1: Structure of the vertebrate class V myosins.....	6
Figure 1-2: Current models of class V myosin organelle transport functions.....	9
Figure 1-3: Crystal structure of the Myo2p globular tail.....	26
Figure 1-4: Diagram of docking complexes for different organelles.....	30
Figure 1-5: Rab proteins label distinct organelles.....	32
Figure 1-6: General mechanisms of regulation of Class V myosins.....	38
Figure 2-1. Localization of endogenous Myo5c and actin filaments in LG and LGAC.....	71
Figure 2-2: Myo5c and Rab3D co-localized in LGAC.....	74
Figure 2-3: GFP-Myo5c-tail associates with mature SVs.....	79
Figure 2-4: Expression of GFP-Myo5c-tail suppresses CCh-stimulated syncollin-GFP release in LGAC.....	82
Figure 2-5: Expression of GFP-Myo5c-tail suppresses CCh-stimulated SC release in LGAC.....	86
Figure 2-6: Electron Microscopy micrographs of Myo5c and GFP-Myo5c-tail enriched around mSV in resting and CCh-stimulated LGAC.....	90
Figure 2-7: GFP-Myo5c-full is localized to mSVs.....	94
Figure 2-8: GFP-Myo5c-full and GFP-Myo5c-tail both localize to pIgAR/SC enriched mSVs beneath the APM.....	96
Figure 2-9: GFP-Myo5c-tail-enriched mSVs exhibit reduced diameter and infrequent association with actin-coated structures relative to GFP-Myo5c-full-enriched mSVs in stimulated LGAC.....	100
Figure 2-10. GFP-Myo5c-tail-enriched mSVs exhibit reduced diameter in the presence and absence of CCh, and reduced association with actin-coated structures in CCh-stimulated LGAC.....	104
Supplemental Figure 2-1: Myo5c and endogenous Rab3D are co-localized on mSVs in LGAC.....	106

Figure 3-1. Endogenous Myo5c localizes to small puncta and slender tubules.	138
Figure 3-2. Dynamics of GFP-Myo5c associated puncta and tubules.....	143
Movie 3-1: Timelapse movie illustrating the dynamics of Myo5c puncta.....	145
Movie 3-2: Timelapse movie demonstrating that Myo5c associated tubules move rapidly and microtubule-dependently whereas Myo5c puncta move slowly and microtubule-independently.....	147
Figure 3-3. The localization of Myo5c is distinct from that of Myo5a and Myo5b.....	150
Movie 3-3: The localization and dynamics of Myo5c are distinct from those of Myo5b.	152
Figure 3-4. Distribution of Myo5c relative to selected membrane compartments.	155
Figure 3-5. Myo5c localizes on secretory granules.	158
Movie 3-4: mCherry-Myo5c localizes on chromogranin A-GFP labeled secretory granules.	160
Movie 3-5: mCherry-Myo5b does not localize on chromogranin A-GFP labeled secretory granules.....	163
Movie 3-6: Myo5c associated secretory granules can be triggered to undergo secretion.....	168
Figure 3-6: Myo5c labeled secretory granules can be triggered to undergo secretion.....	172
Movie 3-7: Myo5c remains associated with secretory granule membranes following exocytosis.....	174
Movie 3-8: Myo5c labeled secretory granules are not perturbed by exogenous markers of secretory granules.....	176
Figure 3-7. Dominant negative Myo5c disrupts the distribution of secretory granules.....	179
Figure 3-8: Summary Diagram: Myo5c is associated with dynamic tubules and regulated secretory granules.....	183
Supplemental Figure 1. Myo5c is expressed in exocrine secretory tissues.....	191

Supplemental Figure 2: Class V myosin constructs used to investigate the cellular functions of Myo5c.....	193
Supplemental Figure 3: Dominant-negative Myo5c specifically associates with secretory granules and disrupts their distribution in MCF-7 cells.....	195
Movie 4-1: Myo5c localizes to vacuole-like structures in a temporally-regulated manner.....	227
Figure 4-1: Myo5c is enriched in regions of protrusive activity in MCF-7 cells.....	229
Figure A1-1: SDS polyacrylamide electrophoretogram of MVc-S1.....	252
Figure A1-2: Steady-state actin-activated ATPase activity of MVc-S1.....	254
Figure A1-3: Interaction of MVc-S1 with actin in the absence of nucleotide and in the presence of ADP.....	259
Figure A1-4: Interaction of ATP with acto-MVc-S1.....	262
Figure A1-5: MANT-ADP release from acto-MVc-S1.....	265
Figure A1-6: Acto-MVc-S1 ADP affinity.....	267
Figure A1-7: Transient kinetics of ATP hydrolysis by MVc-S1 monitored by quenched-flow.....	270
Figure A1-8: Pi release from MVc-S1 and acto-MVc-S1 monitored by MDCC-PBP fluorescence.....	273
Figure A1-9: in vitro actin gliding assay of eGFP-MVc-HMM.....	276
Figure A1-10: Dependence of steady-state parameters (ATPase activity, duty ratio) of MVc-S1 on (A) actin and (B) background ADP concentration.....	280
Figure A1- 11: Phylogenetic analysis of various myosin Vs from different organisms.....	287
Movie A2-1. TIRF microscopy of single GFP molecules adsorbed on a coverslip.....	308
Movie A2-2. TIRF microscopy of GFP-Myo10 in HeLa cell filopodia.....	310
Movie A2-3. TIRF microscopy reveals fast forward movements of faint particles of GFP-Myo10 in a filopodium.....	312

Figure A2-1. TIRF microscopy reveals fast forward movements of faint particles of GFP-Myo10 in living cells.....	314
Figure A2-2. Faint particles of GFP-Myo10 exhibit characteristics of single molecules.....	318
Figure A2-3. Fast forward movements require the Myo10 motor domain.....	321
Figure A2-4. Fast forward movements are inhibited by latrunculin B.....	325
Figure A2-5. Faint particles of GFP-Myo5a can also move forward and rearward in living cells.....	327
Figure A2-S1. Dynamics of GFP-Myo10 in living HeLa cells imaged with TIRF.....	332
Figure A2-S2. Tip localization of different Myo10 constructs and TIRF imaging of a forced dimer and a motor domain point mutant.	334

List of Abbreviations

Ad- adenovirus

APM- apical plasma membrane

ATP- Adenosine Triphosphate

BSA- bovine serum albumin

Ca⁺⁺ - calcium

CgA- Chromogranin A

DIC- differential interference contrast

DNA- deoxyribonucleic acid

DN- dominant negative

EM- electron microscopy

ER- endoplasmic reticulum

F-actin- Filamentous actin

GFP- green fluorescent protein

HA- hemagglutinin epitope

Kd- Kilodalton

LG-lacrimal gland

LGAC- lacrimal gland acinar cells

MANT-ATP- 2'-(or-3')-O-(N-methylanthraniloyl) adenosine 5'-triphosphate, trisodium salt;

MANT-ADP- 2'-(or-3')-O-(N-methylanthraniloyl)adenosine 5'-diphosphate, disodium salt;

MOPS, N-morpholino-propanesulfonic acid

mRNA- messenger RNA

mSV- mature secretory vesicle

nm - nanometer

NPY- neuropeptide -Y

pIgAR- polymeric immunoglobulin A receptor

SC- secretory component

SEM- standard error of the mean

sIgA- secretory immunoglobulin A

TIRF- total internal reflection fluorescence

μm - micrometer

μM - micromolar

CHAPTER 1: INTRODUCTION

CLASS V MYOSINS: MOTORS FOR ORGANELLE TRANSPORT

Class V myosins: Motors for organelle transport

Damon T Jacobs and Richard E Cheney

University of North Carolina-Chapel Hill,
Cell and Molecular Physiology department
5314 Medical Biomolecular Research Building
Chapel Hill, NC 27599-7545

Corresponding author:

Richard E Cheney, Professor of Cell and Molecular Physiology
cheneyr@med.unc.edu
919-966-0331

Abstract

Myosins are actin-based molecular motors that are responsible for carrying out a variety of biological processes such as muscle contraction, mRNA transport, and cell signaling. Class V myosins are an evolutionarily conserved class of myosin with key functions in organelle transport. This family of motor proteins is essential for normal physiology, and mutations to class V myosins can cause lethal diseases. Studies of class V myosins have led to important insights on membrane trafficking, molecular motor function, and the determinants of organelle/cargo specificity.

Introduction

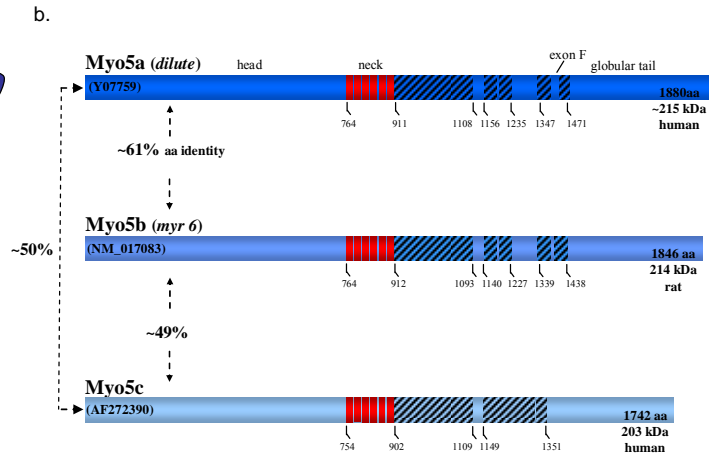
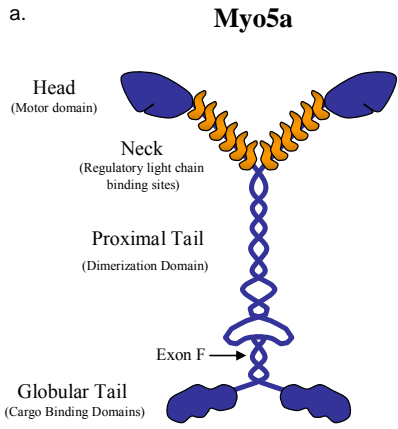
Class V myosins are among the most ancient and broadly distributed class of myosin (Berg *et al.*, 2001; Odronitz and Kollmar, 2007). Class V myosins are also leading candidates to carry out actin-based organelle transport (Berg *et al.*, 2001). In the budding yeast, *Saccharomyces cerevisiae*, there are two class V myosins (Myo2p and Myo4p) that function in polarized secretion, organelle inheritance, and mRNA transport (Valiathan and Weisman, 2008). In mammals, the three class V myosins, myosin Va (Myo5a), myosin Vb (Myo5b), and myosin Vc (Myo5c), appear to be differentially expressed in a tissue specific manner (Rodriguez and Cheney, 2002). In humans, defects in class V myosins can cause serious diseases such as Griscelli Syndrome Type I (Pastural *et al.*, 1997) and microvillar inclusion disease (Muller *et al.*, 2008). These disorders are a direct result of trafficking defects of class V myosin-associated organelles. Studies in isolated melanocytes (pigment producing cells) showed that Myo5a stably associates with melanosomes (pigment granules) by forming a tripartite protein docking complex on the surface of the organelle (Wu *et al.*, 2002b). These studies also revealed that melanosomes undergo long-range, microtubule-based transport from the cell center and are retained in the actin-rich cell periphery by Myo5a, leading to a dual-filament transport model for organelle transport (Wu *et al.*, 1998). Since the discoveries of the association of Myo2p with secretory vesicles in yeast (Johnston *et al.*, 1991) and Myo5a with melanosomes in vertebrates (Provance *et al.*, 1996), the number of organelles associated with class V myosins has increased substantially. This list now includes neuronal secretory vesicles (Prekeris and Terrian, 1997; Bridgman, 1999), endoplasmic reticulum (Takagishi *et al.*, 1996; Estrada *et al.*, 2003), and several plasma membrane

receptors (Roland *et al.*, 2007), among others. Recent structural studies have afforded much progress in determining the basis for cargo selection and regulation of motor activity (Liu *et al.*, 2006; Pashkova *et al.*, 2006). Here we will review recent progress and key ideas on the roles of class V myosins in membrane trafficking and will emphasize recent research in budding yeast and mammals.

Structure of class V myosins

Vertebrate class V myosins are motor proteins composed of two identical heavy chains with six light chains per heavy chain (Espreafico *et al.*, 1992) (Figure 1-1). At the N-terminus of each heavy chain there is a highly conserved myosin motor domain, which is then followed by a region that contains six tandem repeats of a light chain binding motif, and finally a tail domain at the C-terminus that can be divided into a proximal tail and a distal globular tail. The head or motor domain hydrolyzes ATP and binds to F-actin during the catalytic cycle to produce force (Cheney *et al.*, 1993). The neck or light chain binding domain consists of six tandem repeats of a conserved consensus sequence (IQxxxRGxxxR), termed “IQ motif” that binds to calmodulin or calmodulin-like light chains with high affinity (Cheney and Mooseker, 1992). This region of the molecule also serves as a rigid lever arm that is important for force transduction and step size (Sakamoto *et al.*, 2003). The proximal tail is predicted to consist largely of coiled-coil and mediates dimerization of the myosin V heavy chains (Cheney *et al.*, 1993). The globular tail of class V myosins is required for cargo attachment and interacts with a docking complex on the surface of the organelle (Wu *et al.*, 2002b; Ishikawa *et al.*, 2003). This globular tail region can be further divided into two separate subdomains that

Figure 1-1: Structure of the vertebrate class V myosins. a. The predicted structure of Myo5a consists of a conserved head domain, a neck domain containing six IQ motifs (light chain binding motifs), followed by a region of predicted coiled coil and a globular tail. Each molecule consists of two identical heavy chains and six accessory light chains/heavy chain. **b.** Domain alignment of mouse Myo5a, rat Myo5b, and human Myo5c shows that vertebrate class V myosins are highly homologous and amino acid sequence alignment (not shown) predicts ~ 50% overall identity between family members. Class V myosin domains are conserved within the family and the structures are predicted to be highly homologous. (Figure adapted from Cheney and Rodriguez, 2002).



are important for providing cargo specificity (Pashkova *et al.*, 2005) (discussed below). The general model of vertebrate class V myosin function consists of a two-headed motor transporting an organelle in a hand-over-hand fashion along an actin filament (Liu *et al.*, 2006).

Functions of class V myosins

Class V myosins are broadly expressed and have important functions in vertebrates. Messenger RNA expression data indicates that, although most tissues express all three class V myosins, one family member appears to predominate over the others (Rodriguez and Cheney, 2002). Yeast have been utilized extensively as a model system where much of our knowledge of class V myosins has been demonstrated. Functional studies in both yeast and mammals show that class V myosins perform transport and tethering tasks and that many functions are conserved across species. (Figure 1-2) These studies show that each class V myosin appears to associate with a specific set of organelles in a cell type specific manner (See table 1). The two class V myosins in budding yeast perform such tasks as transporting membranous organelles and mRNAs along actin cables (Estrada *et al.*, 2003). Since most studies in yeast have focused on the budding yeast, we will limit our discussion to Myo2p and Myo4p.

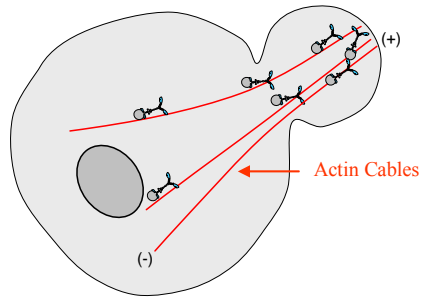
Yeast

Myo2p transports secretory vesicles in yeast.

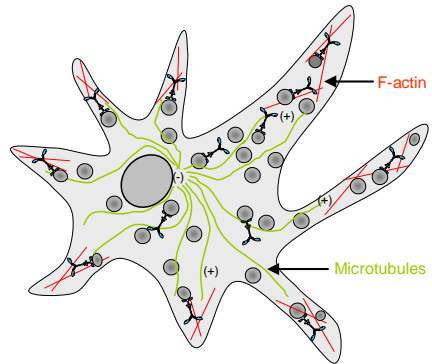
Myo2p was the first class V myosin to be discovered and was initially shown to transport secretory vesicles to sites of active cell growth, such as the tip of a growing bud (Johnston *et al.*, 1991; Govindan *et al.*, 1995). (Figure 1-2a) Mutants of Myo2p exhibit an accumulation of secretory vesicles within the mother cell during bud formation,

Figure 1-2: Current models of class V myosin organelle transport functions. **a.** In yeast class V myosins transport secretory vesicles and organelles along actin cables into the bud tip during cell division. **b.** Myo5a functions to tether or transport melanosomes in the actin-rich dendritic extensions of melanocytes. **c.** Myo5a is implicated in the recruitment and anchoring of smooth endoplasmic reticulum in dendritic spines of Purkinje neurons in mice. **d.** In neuroendocrine cells, Myo5a maintains a normal distribution of dense-core secretory granules.

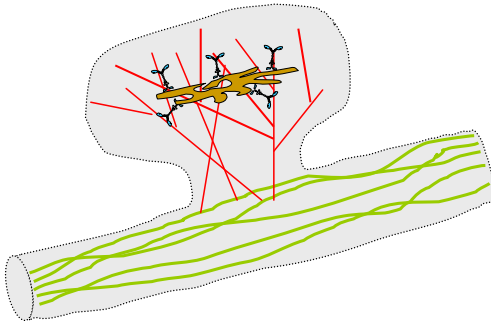
a. Transport of secretory vesicles and cellular organelles in yeast



b. Transport/tethering of melanosomes



c. Anchoring of calcium stores/SER in dendritic spines



d. Distributing secretory granules in neuroendocrine cells

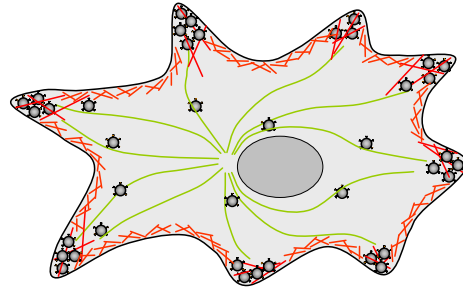


Table 1-1: Class V myosins associate with several organelles

	<u>Cell type</u>	<u>organelle/cargo</u>	<u>Reference</u>
• Myo2p	<i>S. cerevisiae</i>	secretory vesicle	(Johnston <i>et al.</i> , 1991)
		vacuole	(Hill <i>et al.</i> , 1996)
		Late golgi	(Rossanese <i>et al.</i> , 2001)
		Peroxisome	(Fagarasanu <i>et al.</i> , 2006)
		Mitochondrion	(Itoh <i>et al.</i> , 2002)
• Myo4p	<i>S. cerevisiae</i>	mRNA	(Takizawa <i>et al.</i> , 1997)
		endoplasmic reticulum	(Estrada <i>et al.</i> , 2003)
• Myo5a 1997)	Melanocyte	melanosome	(Provance <i>et al.</i> , 1996; Wu <i>et al.</i> ,
	Purkinje neuron	ER-like structure	(Takagishi <i>et al.</i> , 1996)
	WIF-B	?	(Lionne <i>et al.</i> , 2001)
	Macrophage	phagosome	(Al-Haddad <i>et al.</i> , 2001)
	Chromaffin	secretory vesicle	(Rose <i>et al.</i> , 2002)
	PC-12	secretory granules	(Rudolf <i>et al.</i> , 2003)
	Spermatid (acroplaxome)	?	(Kierszenbaum <i>et al.</i> , 2003)
	Photoreceptor synapse	?	(Libby <i>et al.</i> , 2004)
	Min-6 (Beta)	secretory granule	(Varadi <i>et al.</i> , 2005)
	Several endocrine tissues	?	(Espindola <i>et al.</i> , 2008)
• Myo5b	HeLa	TfnR, Rab11a	(Lapierre <i>et al.</i> , 2001)
	MDCK II	pIgAR, Rab11a	(Lapierre <i>et al.</i> , 2001)
	PC-12	M4 muscarinic receptor	(Volpicelli <i>et al.</i> , 2002)
	MDCK	Resp. Sync. virus	(Brock <i>et al.</i> , 2003)
	HEK 293/leukocytes	CXCR2	(Fan <i>et al.</i> , 2004)
	WIF-B9	ABC Transporters	(Wakabayashi <i>et al.</i> , 2005)
	Hippocampal neurons	GluR1 AMPA receptor	(Lise <i>et al.</i> , 2006)
	Airway epithelial	CFTR	(Swiatecka-Urban <i>et al.</i> , 2007)
	Collecting duct-Principal	AQP2	(Nedvetsky <i>et al.</i> , 2007)
	HeLa	MHC I, Rab8a	(Roland <i>et al.</i> , 2007)
	HeLa	Rab10	(Roland <i>et al.</i> , 2008)
• Myo5c	HeLa	TfnR, Rab8a	Rodriguez and Cheney, 2002
	Pancreas	zymogen granule	Chen <i>et al.</i> , 2006
	Lacrimal acinar cell	Secretory granule	Marchelletta <i>et al.</i> , 2008

indicating Myo2p transports and targets secretory vesicles (Johnston *et al.*, 1991).

Myo2p mutants also display synthetic lethality with mutant genes required for actin cable formation (*TPM1*) and a Rab8 homolog protein important for secretory vesicle fusion (*SEC4*) (Liu and Bretscher, 1992; Govindan *et al.*, 1995). Much evidence shows that Myo2p is a molecular motor that functions to transport vesicles along actin cables to sites of polarized secretion (Karpova *et al.*, 2000).

Myo2p transports several additional organelles

In addition to secretory vesicle transport, Myo2p is also required for proper transport/localization of several other cellular organelles, including vacuoles, peroxisomes, late golgi, and mitochondria (Hill *et al.*, 1996; Catlett and Weisman, 1998; Hoepfner *et al.*, 2001; Rossanese *et al.*, 2001; Itoh *et al.*, 2002; Boldogh *et al.*, 2004; Fagarasanu *et al.*, 2006; Altmann *et al.*, 2008; Valiathan and Weisman, 2008). Several of these associations appear to be cell cycle dependent and indicate distinct functions in organelle partitioning and inheritance. It is clear that Myo2p interacts with several different organelles and thus mediates several different trafficking functions. As will be discussed below, specific docking complexes have been identified that mediate the attachment of Myo2p to the various organelles.

In addition to organelle trafficking functions, Myo2p also functions to orient the mitotic spindle and to position the spindle pole body by guiding Bim1p/Kar9p-labeled microtubule plus ends along actin cables into the daughter bud tip (Yin *et al.*, 2000; Gundersen and Bretscher, 2003; Hwang *et al.*, 2003). Additionally, an exciting recent study also implicates Myo2p in P-body disassembly and suggests that Myo2p plays a role in regulating translation of mRNA (Chang *et al.*, 2008). P-bodies are cytoplasmic foci

that contain enzymes important for mRNA turnover and act to inhibit translational machinery by sequestering mRNA for eventual degradation. cRNA hybridization to yeast microarray assays suggest that Myo2p-associated P-bodies contain as many as 2300 mRNA. This study suggests that Myo2p associates with many different mRNAs and is the first report of an association of Myo2p with mRNA turnover.

Myo4p in mRNA and ER transport

Myo4p, the other class V myosin in *S. cerevisiae* (Haarer *et al.*, 1994), along with a complex of She proteins, is required to transport a specific set of 24 mRNAs (Gonsalvez *et al.*, 2005). This set includes Ash1, which is important in regulating mating-type switching in the daughter cell (Takizawa *et al.*, 1997). In addition to mRNA transport, Myo4p has also functions during inheritance of cortical endoplasmic reticulum (ER) (Estrada *et al.*, 2003). These observations indicate that Myo4p functions to transport mRNA's and cortical ER tubules along actin cables from the mother cell to the bud tip.

Vertebrates

Myo5a and melanosome transport

The role of Myo5a in melanosome transport is one of the best characterized functions of a vertebrate class V myosin. Melanocytes synthesize and package melanin (pigment) into membranous organelles (melanosomes) and distribute them to surrounding hair follicle cells and keratinocytes. In humans, mutations to Myo5a cause Griscelli Syndrome Type I (Pastural *et al.*, 1997), which is characterized by partial albinism and neurological disorders that include hypotonia, delayed motor development, and mental

retardation. A similar phenotype is observed in *dilute-lethal* mice (Myo5a^{-/-}) which also display pigmentation defects and a neurological disorder. Studies in wild-type melanocytes demonstrate that Myo5a localizes on melanosomes that are distributed throughout the cell and are especially enriched in dendritic extensions (Provance *et al.*, 1996; Wu *et al.*, 1997). (Figure 1-2b) In wild-type melanocytes, melanosomes move from the cell center to the periphery via microtubules and microtubule motors. However, in *dilute-lethal* melanocytes, melanosomes accumulate in the cell center (Provance *et al.*, 1996). These results argue strongly that Myo5a functions to terminate microtubule-based transport and tether the melanosome in the cell cortex (Provance *et al.*, 1996; Wu *et al.*, 1998). Several observations support the hypothesis that Myo5a is required for melanosome transport in melanocytes, including, 1) Myo5a is present on melanosomes (Wu *et al.*, 1997), 2) wild-type melanophores treated with F-actin destabilizers exhibit a similar melanosome distribution as *dilute-lethal* melanocytes (Rogers and Gelfand, 1998), 3) overexpression of dominant-negative Myo5a tail mimics the *dilute-lethal* phenotype in wild-type cells (Wu *et al.*, 1998), and 4) in *dilute-lethal* melanocytes, overexpression of the wild-type Myo5a protein rescues the defect in melanosome distribution (da Silva Bizario *et al.*, 2002). In the melanocyte model system, it is clear that Myo5a is required for maintaining melanosomes in the cell periphery. Whether Myo5a also plays a direct role in transferring the organelles from melanocytes to surrounding keratinocytes is not clear.

Myo5a and trafficking in dendritic spines

Myo5a is expressed most abundantly in brain and neuronal tissues, and *dilute-lethal* mice and *dilute-opisthotonis* rats, which also have mutated Myo5a, suffer from a

serious neurological disorder that is lethal within three weeks of birth (Dekker-Ohno *et al.*, 1996; Takagishi *et al.*, 1996). Although no gross abnormalities in overall brain morphology were detected, mutant animals exhibit severe seizures and ataxia. Subsequent ultrastructural studies of dendritic spines of Purkinje neurons in the cerebellum revealed the absence of smooth endoplasmic reticulum (SER), which serves as a calcium storage organelle and labels with inositol triphosphate receptors (IP3R). These observations suggest that Myo5a functions to transport/tether SER into the actin-rich dendritic spines (Dekker-Ohno *et al.*, 1996; Takagishi *et al.*, 1996). (Figure 2c) Although immunogold labeling of Purkinje neurons in *dilute-lethal* mice revealed that dendritic spines contained a normal contingent of several protein components essential for synaptic function (Petralia *et al.*, 2001), the Myo5a mutant mice suffered from a loss of long term depression (LTD) (Miyata *et al.*, 2000). These results indicate that loss of Myo5a function inhibits LTD through an inability to transport or tether SER in dendritic spines of Purkinje neurons.

In the dendrites of rat hippocampal neurons, Myo5a appears to associate with organelles containing GluR1 AMPA receptors (Correia *et al.*, 2008). Using a dominant negative approach or RNA interference against Myo5a inhibited GluR1 AMPA receptor trafficking from dendritic shafts into the spine. This transport defect altered activity-induced synaptic potentiation. These results indicate that Myo5a is responsible for short-range transport of organelles containing receptors important for long term potentiation (LTP), thus Myo5a appears to be involved with the regulation of learning and memory.

Myo5a and neuroendocrine secretion

Myo5a is expressed in neuroendocrine cells and exhibits a striking localization on secretory granules (Rose *et al.*, 2002; Varadi *et al.*, 2005; Desnos *et al.*, 2007b). Several

studies in neuroendocrine cells have demonstrated that filamentous actin is required for efficient exocytosis (Neco *et al.*, 2003; Giner *et al.*, 2005) and that an actin-based molecular motor likely mediates transport of secretory organelles (Neco *et al.*, 2002; Rose *et al.*, 2002). Several methods demonstrated that Myo5a facilitates a more direct role in secretory granule dynamics in the cell periphery. Both RNA interference against Myo5a and over expression of a dominant negative Myo5a tail alter the distribution of secretory granules and decrease a secretory response in neuroendocrine cells (Rudolf *et al.*, 2003; Varadi *et al.*, 2005; Desnos *et al.*, 2007b), thus supporting a direct association with secretory granules. Although the precise mechanistic role of Myo5a in neuroendocrine secretion is still not clear, Desnos *et al.* (Desnos *et al.*, 2007b) demonstrate that knock down of Myo5a in chromaffin cells appears to decrease the dwell time of individual granules near the plasma membrane, which then decreases the likelihood of granules becoming docked prior to secretion. These results support the hypothesis that Myo5a tethers secretory granules in the actin-rich cell cortex and may also facilitate short range movements toward sites of secretion (Wu *et al.*, 1998; Desnos *et al.*, 2007b). (Figure 2d)

Espindola *et al.* (Espindola *et al.*, 2008) have recently surveyed several neuroendocrine tissues from rat and determined that Myo5a is expressed in the pineal gland (pinealocytes), pituitary gland (parenchymal cells), thyroid/parathyroid glands (parafollicular and principal cells), pancreas (almost exclusively endocrine islet cells), adrenal gland (chromaffin cells), testis (spermatogonia), and ovary (follicular and granulosa cells). These studies indicate a clear association of Myo5a with endocrine cells and suggest that Myo5a is important in endocrine physiology. Although endocrine

defects have not been detected in *dilute-lethal* mice thus far, this may be due to their brief lifetimes. For additional information on Myo5a and neuroendocrine secretion, two recent reviews are available (Eichler *et al.*, 2006; Desnos *et al.*, 2007a).

Myo5b and plasma membrane receptor recycling

Myo5b was originally cloned from rat (Zhao *et al.*, 1996), and is about ~60% identical to Myo5a and ~49% identical to Myo5c by amino acid sequence (Rodriguez and Cheney, 2002). Myo5b has a broad tissue distribution, with the highest levels detected in brain, kidney, liver, and lung (Zhao *et al.*, 1996). Several studies in cultured cells that utilized a dominant negative approach (GFP-Myo5b tail) have indicated that Myo5b associates with endocytic cargoes that undergo recycling to the plasma membrane (Lapierre *et al.*, 2001; Brock *et al.*, 2003; Nedvetsky *et al.*, 2007; Swiatecka-Urban *et al.*, 2007). Consistent with this, Myo5b interacts with Rab11a, which is an important component of the recycling endosome (Casanova *et al.*, 1999; Lapierre *et al.*, 2001). These studies led to the hypothesis that Myo5b is involved in the outbound trafficking of cell surface receptors from an internal recycling compartment back to the plasma membrane. Overexpression of the Myo5b tail appears to induce a collapse of an endocytic perinuclear recycling compartment and also inhibit an exocytic arm of a plasma membrane recycling pathway. In HeLa cells, a non-polarized cell type, Myo5b tail inhibited the recycling of internalized transferrin and transferrin receptor out of the perinuclear compartment back to the plasma membrane (Lapierre *et al.*, 2001). Using this approach, Myo5b appears to be important in the trafficking of several plasma membrane receptors including the M4 muscarinic receptor in PC12 cells (Volpicelli *et al.*, 2002) and the CXCR2 chemokine receptor (Fan *et al.*, 2004) in leukocytes. In HeLa

cells, it was recently reported that Myo5b can associate with Rab8a, suggesting that Myo5b functions in an additional trafficking pathway that is distinct from the rab11a recycling pathway (Roland *et al.*, 2007). Yeast two-hybrid screening and Fluorescence Resonance Energy Transfer (FRET), Goldenring and colleagues showed that Myo5b tail can directly interact with wild-type and GTP-bound, (but not GDP-bound), Rab8a (Roland *et al.*, 2007). In these cells, endogenous Rab8a labels long, membranous tubules and full-length Myo5b (GFP-Myr6) colocalizes at distinct points along the length. Furthermore, in pulse labeling assays, puncta of Myo5b tail were also shown to accumulate MHCI molecules. Interestingly, MHCI molecules were also shown to associate with long, membranous tubules during recycling assays in HeLa cells (Weigert *et al.*, 2004). These results suggest that Myo5b can form a direct association with Rab8a and/or Rab11a-associated organelles and also demonstrates that Myo5b can interact with at least two distinct compartments in a single cell type.

In polarized epithelial cells, Myo5b appears to specifically associate with cargoes destined for the apical plasma membrane (Lapierre *et al.*, 2001). In fully polarized MDCK cell monolayers, expressed polymeric IgA receptor (pIgAR) was found to localize to Myo5b tail puncta and Rab11a in a subapical recycling endosome. Interestingly, transferrin receptor was excluded from this compartment. The pIgARs was inhibited from being expressed at the apical membrane by the dominant negative Myo5b tail, indicating that Myo5b regulates apically directed transcytotic trafficking in MDCK cells (Lapierre *et al.*, 2001). In addition to a role in inhibiting transcytosis, the Myo5b tail also inhibits the polarized distribution of several transmembrane proteins, including the Na/H⁺ exchanger in gastric parietal cells (Hales *et al.*, 2001), the GluR1 glutamate

receptor in dendritic spines of hippocampal neurons (Lise *et al.*, 2006), the aquaporin-2 channel in rat kidney (Nedvetsky *et al.*, 2007), the respiratory syncytial virus (Brock *et al.*, 2003), and the cystic fibrosis transmembrane conductance regulator (CFTR) in human airway epithelial cells (Swiatecka-Urban *et al.*, 2007). Importantly, all of these cargoes appear to undergo regulated insertion into the apical plasma membrane.

In these studies, the *internalization* of receptors from the plasma membrane did not appear to be affected by the dominant negative Myo5b tail, which strongly suggests that Myo5b performs an exocytic trafficking function in these cells. However, an alternative hypothesis suggests that Myo5b functions primarily during the endocytic phase of plasma membrane receptor recycling (Provance *et al.*, 2004; Provance *et al.*, 2008). Mercer and colleagues utilize a full-length Myo5b that has been genetically engineered to bind an oversized ADP analog with specificity, which locks the motor domain into a tight actin-binding state. By locking Myo5b onto actin, uptake of fluorescent transferrin into a perinuclear recycling compartment was inhibited (Provance *et al.*, 2004). In these studies full length GFP-Myo5b localized to enlarged peripheral puncta and correlated with an apparent increase of transferrin labeling on the plasma membrane. This work suggests that overexpression of full-length Myo5b inhibits inward transport of endocytosed transferrin, and shunts it toward a “fast recycling” pathway, thus explaining the increase in transferrin on the plasma membrane (Provance *et al.*, 2008). This hypothesis also suggests that the inability of the Myo5b tail to bind actin causes the peripheral endocytic compartment to collapse into the cell center. In support of an endocytic function, Yan *et al.* (Yan *et al.*, 2005) report that Myo5b associates with the CART complex of proteins, which includes the early endosomal associated proteins, Hrs,

actinin-4, and BERP. Provance et al., (Provance *et al.*, 2008) suggest that Myo5b tethers an endosomal compartment in the cortical actin and functions to oppose inward transport of endocytic cargoes mediated by microtubules to the perinuclear recycling compartment. Although this is an intriguing hypothesis, further data are required to definitively show whether Myo5b functions to oppose retrograde endocytic transport or support anterograde exocytic transport, or both.

Myo5b and epithelial polarity

The establishment of cell polarity is vital for epithelial cell function. Polarity establishment requires a segregation of membrane proteins and a complex membrane trafficking system to maintain the polarized distribution of newly synthesized and recycled membrane proteins. Myo5b has been hypothesized to mediate polarity establishment in several systems. In the hepatocyte-derived WIF-B9 cells, Myo5b and rab11a localized near the centrosome and at the canilicular membrane, indicating Myo5b is associated with apically targeted cargoes (Wakabayashi *et al.*, 2005). Knockdown of Rab11a or expression of dominant-negative forms of Rab11a (S25N) or Myo5b (tail domain) inhibited canilicular formation significantly in these cells. These observations indicate that Myo5b is required for the establishment of polarity and canilicular formation. Importantly, a genetic screen in humans identified Myo5b as a gene responsible for microvillus inclusion disease (Muller *et al.*, 2008). Mutations in the motor domain or a C-terminal truncation appears to cause a loss of microvilli structure on the luminal surface of mature enterocytes and causes the appearance of villin-labeled, microvilli-like structures within internal inclusions. These cells also exhibited a defect in the localization of basolateral markers into a subapical distribution, indicating the polarity

of the enterocyte was compromised. These studies indicate that Myo5b functions to transport organelles that contain cargoes that require a polarized distribution, however more studies are required to determine whether this effect is direct or indirect.

Myo5c: a motor for exocrine secretion?

Myo5c is the third and final member of the class V myosin family to be identified in vertebrates (Berg *et al.*, 2001; Rodriguez and Cheney, 2002). Myo5c was originally cloned from a pancreas cDNA library and the initial characterization of human Myo5c showed that it is expressed most abundantly in exocrine tissues and epithelial cells (Rodriguez and Cheney, 2002). This study also showed that in cultured HeLa cells, expression of a dominant negative, GFP-tagged Myo5c tail construct induced the formation of large, peripheral punctate structures that accumulated Myo5c tail, exogenous transferrin, and the transferrin receptor. Intriguingly, these puncta also stained positive with antibodies to Rab8, but not rab11a, which suggests that Myo5c associates with one or more organelles that are distinct from the Myo5b-labeled recycling endosome (Rodriguez and Cheney, 2002). Although HeLa cells are a well characterized model for membrane transport, unfortunately the levels of endogenous Myo5c are low, thus making studies in these cells difficult. Future studies are thus required to determine the exact function of Myo5c in recycling of endocytic membranes.

The distribution of Myo5c mRNA in exocrine glands (Rodriguez and Cheney, 2002) and the localization of Myo5c protein in mouse and rat tissues suggested that it is most abundantly expressed in the acinar cells (Rodriguez and Cheney, 2002; Chen *et al.*, 2006; Marchelletta *et al.*, 2008). Consistent with this, Myo5c was identified in a proteomics study as a component on isolated zymogen granule membranes from rat

exocrine pancreas (Chen *et al.*, 2006). This approach also identified Rab3D, Rab27b, Rab11a, and Rab8a on the surface of zymogen granules. It is tempting to speculate whether Myo5c may associate with one or more of these Rab proteins to mediate an association with the granule membrane. Consistently, rab8a was shown to function in secretory granule biogenesis in a rat pancreatic acinar cell line (Faust *et al.*, 2008). Using yeast two-hybrid screening, a direct interaction between Myo5c tail and Rab8a was shown using wild-type and GTP-bound Rab8a, but not GDP-bound Rab8a (Roland *et al.*, 2007). Tissue expression and localization data suggests that Myo5c may have a secretory function, and more recent studies have shown that a dominant negative Myo5c tail can partially inhibit stimulated secretion from isolated rabbit lacrimal gland acinar cells (Marchelletta *et al.*, 2008). Although the precise role in acinar cells is not clear, Myo5c likely functions at the late stages of regulated secretion, which may be to transport secretory granules through the F-actin barrier, facilitate fusion of secretory granules with the plasma membrane or with each other, provide force to extrude contents, or provide a cytoskeletal link to membranes targeted for recycling following exocytosis.

Biophysical and biochemical properties of class V myosins

Myo5a has been studied intensively and has biochemical properties that make it ideal for single molecule studies (Trybus, 2008). The first experiments using purified, chick brain myosin V showed that it has ATPase activity, does not form filaments, and was regulated by calcium (Cheney *et al.*, 1993). A distinct characteristic of Myo5a is the 36 nm step size (Mehta *et al.*, 1999; Rief *et al.*, 2000; Sakamoto *et al.*, 2000). Since the step size is dictated by lever arm length (Sakamoto *et al.*, 2005), all class V myosins are

predicted to have a 36 nm step size. Thirty-six nanometers closely matches the pseudo-helical repeat of F-actin, which allows a class V myosin to walk along an actin filament without following the spiral of the helix (Trybus, 2008). The 36 nm step size may be an advantage for a motor protein that functions to transport large organelles along actin filaments. The average velocity reported for vertebrate Myo5a is ~300 nm/s (Cheney *et al.*, 1993; Watanabe *et al.*, 2007). Similarly, the velocity for Myo5b was reported to be ~220 nm/s (Watanabe *et al.*, 2006) and the reported velocities for Myo5c are 24 nm/s (Takagi *et al.*, 2008) and 160 nm/s (Watanabe *et al.*, 2007).

These studies also revealed that Myo5a is a processive motor, meaning it can undergo multiple rounds of ATP hydrolysis (ie. multiple steps) before dissociating from an actin filament (Mehta *et al.*, 1999; Trybus, 2008). A defining determinant of processivity for single myosin molecules is the duty ratio, which is defined as the fraction of the ATPase cycle spent in a tight actin-bound state. Myosin Va has a high duty ratio of ~ 0.7, therefore each motor domain spends 70% of its ATPase cycle tightly bound to actin (Watanabe *et al.*, 2006). Similar kinetic studies of human Myo5b showed that it is also a processive motor with a duty ratio of ~0.8 (80%) (Watanabe *et al.*, 2006). Interestingly, two independent groups showed that human Myo5c does not exhibit processivity (Watanabe *et al.*, 2007; Takagi *et al.*, 2008). The calculated duty ratios for Myo5c are ~10% (Takagi *et al.*, 2008) and ~30% (Watanabe *et al.*, 2007), which are low values, similar to skeletal muscle myosin II (Takagi *et al.*, 2008). This result is intriguing because it highlights that not all vertebrate class V myosins are processive. Thus, Myo5c exhibits characteristics similar to Myo2p and Myo4p in yeast (Reck-Peterson *et al.*, 2001), and also myosin V in *Drosophila melanogaster* (Toth *et al.*, 2005), which do not

exhibit processivity. It is interesting to speculate concerning the selective advantage of a non-processive or processive class V myosin. For more detailed information on the biophysics of class V myosins see Trybus (Trybus, 2008).

Regulatory mechanisms of class V myosins

In order for class V myosins to function as motors for organelle transport the motor domain must bind to actin and hydrolyze ATP in a cyclical manner, and the tail domain must provide a stable and specific attachment to the organelle. Hence, regulating motor activity and regulating the association with cargoes provide distinct points to modulate class V myosin function. Recent studies focused on the structure of class V myosins have led to insights on the mechanisms by which the motor activity can be regulated, as well as identifying subdomains important for organelle recognition. In addition, several protein complexes that facilitate the attachment of the motor to the organelle have been described.

How do class V myosins associate with organelles?

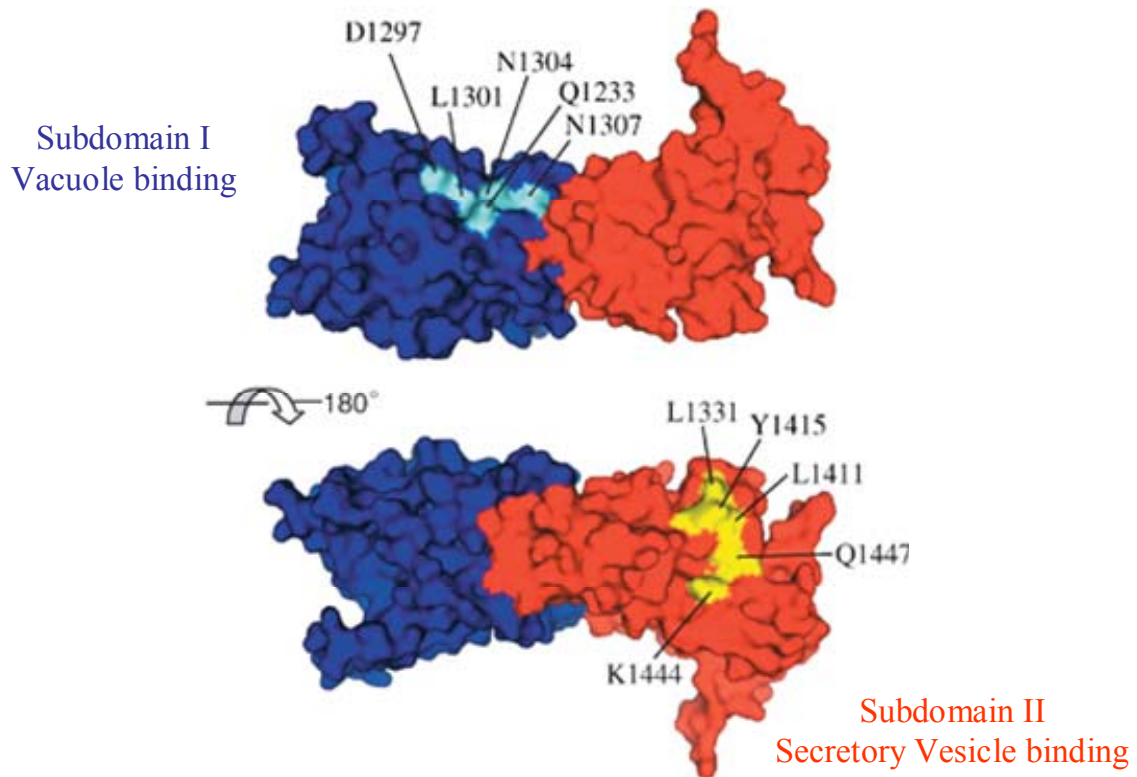
Since the globular tail domain of class V myosins has been shown to be important for cargo association (Wu *et al.*, 1998; Reck-Peterson *et al.*, 1999; Schott *et al.*, 1999), the tail domain may also provide binding specificity and form a stable attachment to the organelle. Recent biochemical and structural studies have revealed the presence of distinct domains important for binding specific cargoes. Here we discuss the solution of the crystal structure of the globular tail and the growing list of multi-protein organelle receptors that form specific docking complexes.

Crystal structure of the globular tail

Myo2p associates with several different organelles within the same cell (see Table 1). This observation implies that determinants of organelle specificity may be present in the Myo2p globular tail. To address this, an early mutagenesis screen identified two distinct clusters of residues essential for vacuole (aa 1297-1307) and secretory vesicle (aa 1439-1491) binding (Catlett *et al.*, 2000). The clusters are positioned ~132 amino acids apart, thus indicating that two distinct regions of the globular tail mediate vacuole and secretory vesicle binding (Catlett 2000). Subsequent studies showed that mild proteolysis of the Myo2p globular tail produced two intact globular tail fragments, termed subdomain I (aa 1131-1345) and subdomain II (aa 1346-1574) (Pashkova *et al.*, 2005). This study showed that residues essential for vacuole binding reside in subdomain I and many of the residues important for secretory vesicle binding are in subdomain II. Subdomain I was shown to associate with subdomain II with high affinity, and in living yeast cells, only simultaneous overexpression of both domains yielded a dominant negative phenotype (Pashkova *et al.*, 2005). Importantly, a high resolution crystal structure consisting of subdomain I and subdomain II of the Myo2p globular tail was obtained (Pashkova *et al.*, 2006). The tertiary structure confirmed the tight association of the subdomains and that the residues essential for vacuole binding and secretory vesicle binding appear to be simultaneously exposed ~180° from each other. (Figure 1-3)

Figure 1-3: Crystal structure of the Myo2p globular tail. The Myo2p crystal structure consists of two separate subdomains. Subdomain I (blue) has been shown to be important for vacuolar binding and subdomain II (red) is important for secretory vesicle binding. Clusters of residues in both subdomain I and subdomain II have been identified that mediate attachment to the yeast vacuole and secretory vesicles, respectively. Residues were identified through mutagenesis studies in *S.cerevisiae*. Each subdomain requires a tight association with the other to be functional. Figure reproduced from Pashkova et al. (2006), and with permission from the Nature Publishing Group.

Crystal structure of the Myo2p globular tail domain



Class V myosins bind organelles through protein complexes

What are the molecular components utilized by class V myosins to attach to an organelle and how is specificity ensured? The answers to these questions are being elucidated and we now are gaining an understanding of the molecular players that determine organelle attachment. The association of Myo5a with the melanosome provides a clear example of how a motor protein attaches to its cargo. It is well established that Myo5a is one member of a tripartite protein docking complex that includes Rab27a and melanophilin/Slac2-a (Wu *et al.*, 2002b; Wu *et al.*, 2006). (Figure 1-4a) Rab27a is a member of the Rab family of small Ras-related GTPases that function in organelle identity and vesicle trafficking (Zerial and McBride, 2001) (Figure 1-5). Melanophilin/Slac2-a is a melanocyte-specific member of the Slac2 family of proteins that appear to function as “adaptor” molecules for Rab27-based organelle transport (Izumi, 2007). The Myo5a motor protein has six exons (exon A-exon F) in the tail domain and three undergo alternative splicing (exons B, D, and F) in a cell type specific manner (Lambert *et al.*, 1998). The melanocyte-specific isoform of Myo5a expresses exon F, which is required for proper melanosome distribution (Wu *et al.*, 2002b). Biochemical studies of deletion mutants have shown that melanophilin acts as a “linker” protein by binding to Rab27a at its N-terminus and to exon F of Myo5a at the C-terminus (Au and Huang, 2002; Wu *et al.*, 2002b; Fukuda and Itoh, 2004). In humans, Griscelli Syndrome Type I, II, and III, and the equivalent genetic disorders in mice, (*Dilute*, *Ashen*, and *Leaden*) are the result of mutations to Myo5a, Rab27a, and melanophilin/Slac2-a, respectively (Mercer *et al.*, 1991; Wilson *et al.*, 2000; Matesic *et al.*, 2001). Each gene, when mutated, induces a virtually identical coat color phenotype as well as a perinuclear accumulation of melanosomes in isolated melanocytes (Wu *et al.*, 2006). Recently,

Hammer and colleagues have reconstituted *in vitro* motility using purified components, thus confirming that Myo5a, melanophilin, and Rab27a are essential to an actin-based transport complex (Wu *et al.*, 2006). These studies convincingly demonstrate that all three proteins are essential to maintaining proper organelle distribution in melanocytes.

Myo5b also associates with a tripartite protein complex that regulates attachment to the recycling endosome. (Figure 1-4b) The Myo5b-associated docking complex is composed of Rab11a and a member of the Rab11-family of interacting proteins (Rab11-FIP), Rab11-FIP2 (Hales *et al.*, 2002). The Rab11 family of Rab GTPases consists of Rab11a, Rab11b, and Rab25, and yeast two-hybrid screens showed the all four Rab11-FIPs are able to bind to each member of the Rab11 family (Hales *et al.*, 2001). However, Rab11-FIP2 bound to Rab11a, regardless of nucleotide state, and also showed a specific interaction with the tail domain of Myo5b. (Figure 1-4b) Of note, in a yeast two-hybrid screen, the Myo5b tail domain also demonstrated a direct interaction with Rab11a (Roland *et al.*, 2007). These results indicate that all three members of this docking complex interact with each other to form a specific and stable interaction with the organelle(s). Also, in *Drosophila melanogaster*, the single class V myosin (MyoV) expressed in this species forms a ternary complex with Rab11 and dRip11 (*D. melanogaster* Rab11-FIP) to facilitate the delivery of organelles important for rhabdomere biogenesis (Li *et al.*, 2007). Although yeast two hybrid demonstrated that MyoV and dRip11 can each bind Rab11 independently, all three proteins are required for normal organelle transport.

As discussed above, Myo2p functions to transport several different organelles and our knowledge of Myo2p-associated organelle receptors is growing rapidly. Myo2p

Figure 1-4: Diagram of docking complexes for different organelles. **a.** Myo5a associates with melanosomes through a tripartite protein docking complex that includes Rab27a and melanophilin. **b.** Myo5b attaches to endocytic organelles through a tripartite protein adaptor complex that consists of Rab11a and Rab11-FIP2. The Myo5b tail domain interacts directly with Rab11a and Rab11-FIP2 by yeast two-hybrid screen. **c.** Although a Myo5c-associated docking complex has not been identified, proteins have been identified on secretory granules. **d.** Myo2p interacts with secretory vesicles through Ypt31/32 (mammalian Rab11). The Myo2p interaction with secretory vesicles is mediated through the globular tail subdomain II. Sec4p, a rab protein, is known to be present and is required for secretory vesicle fusion in the bud tip. **e.** Myo2p attaches to the vacuole through a tripartite protein organelle receptor that includes Vac8p and Vac17p. Vac8p, which is not a rab protein, is linked to globular tail subdomain I by Vac17p. Of note, Vac17p undergoes regulated expression and degradation. **f.** Myo4p indirectly associates with mRNA through She3p and She2p, to form an mRNA transport complex. Myo2p and She3p can also associate with cortical ER and functions during inheritance.

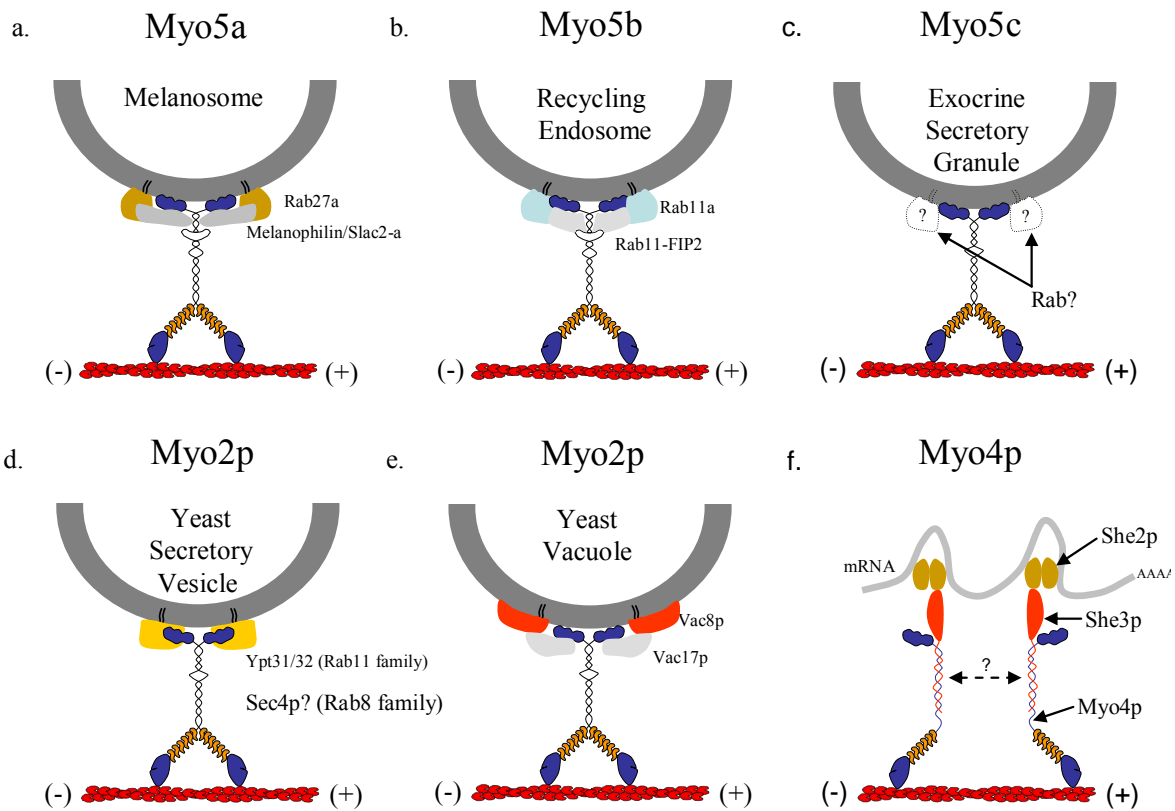
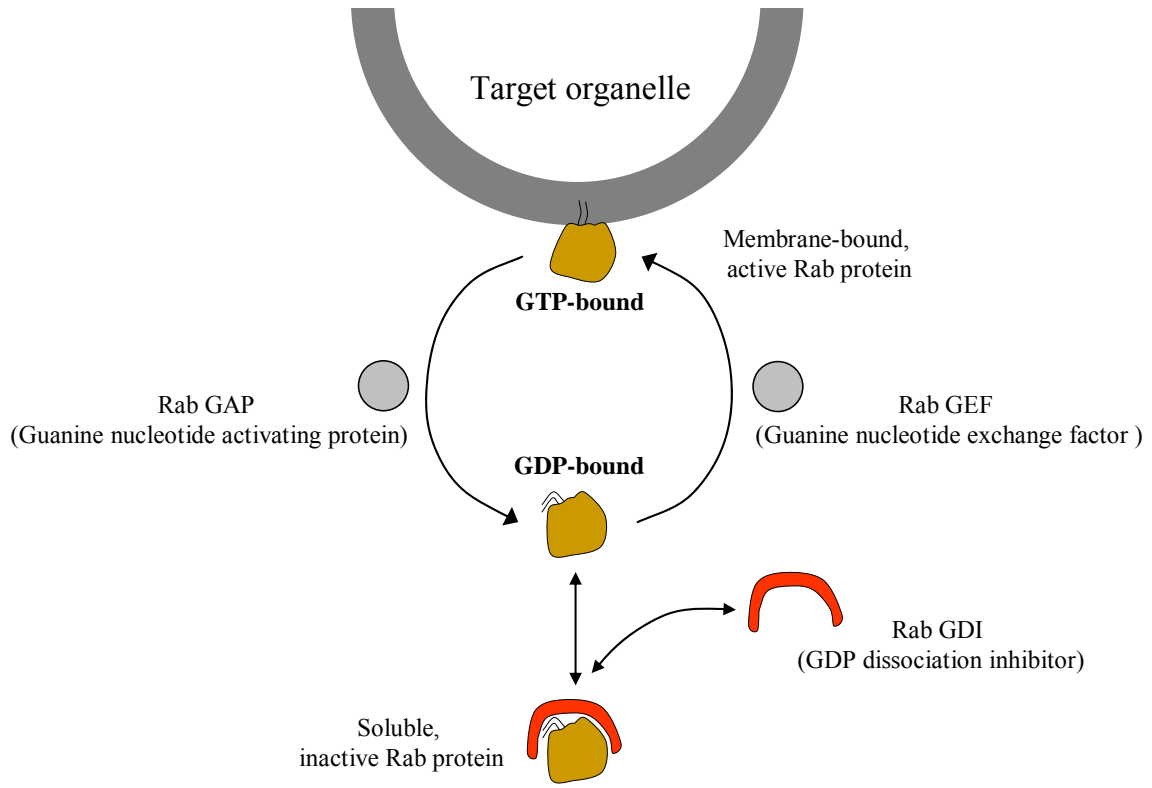


Figure 1-5: Rab proteins label distinct organelles. Rab proteins are required for distinct steps in membrane trafficking such as *budding* of vesicles from a donor compartment, *transporting* vesicles by associating with motor proteins, *tethering* of vesicles near acceptor membranes, and *fusion* of vesicles to acceptor membranes (Grosshans *et al.*, 2006). In yeast and vertebrates several rab proteins function in receptor complexes that link organelles to motor proteins (Hales *et al.*, 2002; Wu *et al.*, 2002b; Lipatova *et al.*, 2008). There are >60 rab proteins in humans and ~11 rab proteins in yeast, which make them the largest family of the Ras superfamily of small GTPases (Zerial and McBride, 2001). Individual rab proteins, when active, associate with specific organelles, which make them ideal docking complex components. Rab proteins function as molecular switches by cycling between a GTP-bound, “active” state and a GDP-bound, “inactive” state. The nucleotide state is controlled by rab effectors known as guanine nucleotide exchange factors (GEF’s) and guanine nucleotide activating proteins (GAP’s). Rab GDI proteins (Guanine Dissociation Inhibitor) stabilize inactive rab proteins in the cytoplasm by masking the prenylation groups and inhibiting GDP exchange. Rab proteins are prenylated and associate with membranes through geranylgeranyl groups on C-terminal cysteine residues (). Although it is unknown how a rab protein distinguishes a specific membrane, they are poised to function as a highly specific, initial recognition factor for an organelle receptor complex. (For more complete reviews see Grosshans *et al.*, 2006; Zerial *et al.*, 2002)



associates with secretory vesicles through a rab GTPase, Ypt31/32, which likely functions to recruit the motor to the organelle at the Golgi complex (Lipatova *et al.*, 2008). (Figure 1-4d) Although a linker protein has not been identified, Ypt31/32 (mammalian Rab11a homolog) interacts directly with subdomain II of the Myo2p globular tail (Casavola *et al.*, 2008). Although the function is unclear, the authors suggest that Sec2p, which is a GEF for Sec4p, also associates with this complex at an early transport time point (Lipatova *et al.*, 2008).

In addition to secretory vesicles Myo2p also associates with cellular organelles undergoing partitioning and inheritance. The interaction between Myo2p and the vacuole during vacuolar inheritance is mediated by a tripartite receptor complex that includes Myo2p, Vac17p, and Vac8p (Ishikawa *et al.*, 2003; Tang *et al.*, 2003), and serves to transport vacuole membranes to the bud tip. (Figure 1-4e) It appears that Vac8p is a peripheral membrane protein on the surface of the vacuole and that Vac17p provides a link between it and Myo2p to form a transport complex (Ishikawa *et al.*, 2003). As an important mechanism to terminate the Myo2p-mediated vacuole transport into the daughter bud, Vac17p undergoes regulated degradation (Tang *et al.*, 2003). Weisman and colleagues showed that Vac17p expression levels are regulated by a cell-cycle dependent mechanism and deletion analysis identified a PEST sequence required for Vac17p degradation. This is the first demonstration of a temporally-controlled, Myo2p-associated organelle receptor complex in yeast.

In the budding yeast, Myo2p also associates with late golgi elements (Rossanese *et al.*, 2001; Arai *et al.*, 2008) and mitochondria (Itoh *et al.*, 2002; Boldogh *et al.*, 2004; Altmann *et al.*, 2008) to transport or tether them into the daughter bud during cell

division. Myo2p appears to be recruited to these organelles by the rab protein, Ypt 11. The peroxisome also undergoes partitioning and inheritance during cell division and Myo2p carries out this transport process as well. Myo2p is linked to the peroxisome through the adaptor protein, Inp2p (Fagarasanu *et al.*, 2006). It was demonstrated through knockdown and overexpression studies that the level of peroxisomal inheritance directly correlated with the amount of Inp2p protein in the cell (Fagarasanu *et al.*, 2006).

Myo4p, which transports specific mRNAs from mother to daughter cell during cell division, also utilizes a tripartite protein complex to associate with the mRNA. She2p binds to specific mRNAs and She3p links that complex to Myo4p (Takizawa and Vale, 2000). (Figure 1-4f) She3p also provides a linkage between Myo4p and cortical ER membranes for transport during organelle inheritance (Estrada *et al.*, 2003). Myo4p is a monomer and does not self assemble *in vitro*, however it was suggested that Myo4p ensembles may form through She3p and/or She2p (Dunn *et al.*, 2007). Thus, She3p appears to be a multifunctional adaptor for Myo4p.

Additional mechanisms may regulate the attachment of a motor protein to an organelle that include phosphorylation of the motor protein (Rogers *et al.*, 1999; Karcher *et al.*, 2001; Legesse-Miller *et al.*, 2006), alternative splicing of the motor protein (Wu *et al.*, 2002a), and expression of different adaptor molecules such as members of the Slac2 family of adaptor proteins (Izumi, 2007). For instance, the expression of MyRip/Slac2-c in retinal pigment epithelial cells forms a transport complex with Rab27a and myosin VIIa, not Myo5a. Thus, MyRip/Slac2-c appears to be a specific Rab27a adaptor for Myosin VIIa in these cells. These studies highlight the progress being made in identifying organelle receptors and illustrate the complexities involved in docking

complex formation. The similarity in docking complex formation between class V myosins suggests that a general mechanism of attachment may exist.

Intramolecular regulation of motor activity

Regulation of class V myosin motor activity is vital to modulating the biological processes it carries out. The minimum requirements for myosin ATPase activity are Mg^{2+} -ATP (fuel) and F-actin (substrate). Novel regulatory mechanisms of Myo5a have been revealed through structural and biochemical studies using expressed and purified protein. Through image averaging of negatively stained electron micrographs of Myo5a it is predicted that the motor domains associate with the globular tail domains and form an intramolecular interaction *in vitro* (Liu *et al.*, 2006; Thirumurugan *et al.*, 2006).

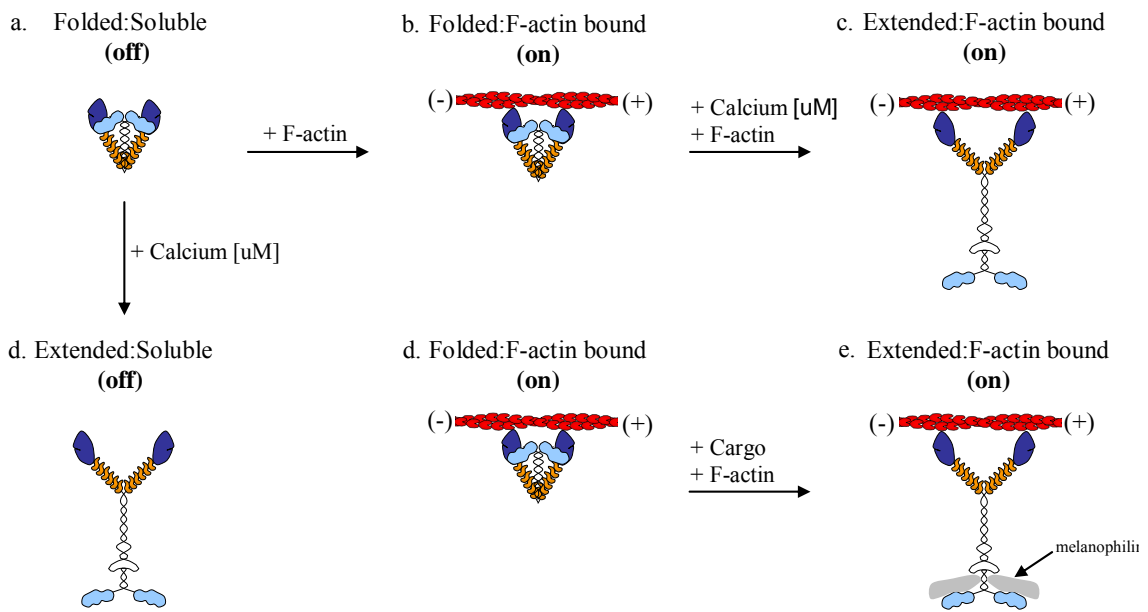
(Figure 1-6a) These observations were made in the absence of calcium and F-actin and, under these conditions, Myo5a does not exhibit ATPase activity. Although several groups have shown that Myo5a can fold back upon itself, there is disagreement about the precise details of this interaction (Li *et al.*, 2006; Liu *et al.*, 2006; Thirumurugan *et al.*, 2006). Calcium appears to be a key regulator of Myo5a conformation since a folded conformation occurs in the absence (or nM levels) of calcium, whereas at micromolar levels, Myo5a becomes extended (Krementsov *et al.*, 2004; Li *et al.*, 2004).

Ultracentrifugation studies of Myo5a in solution showed that the addition of calcium changed the rate of sedimentation from a 11s extended conformation to a 14s globular conformation (Krementsov *et al.*, 2004; Li *et al.*, 2004). (Figure 1-6d) The early observation that Myo5a ATPase activity was upregulated ~100-fold under micromolar levels of calcium (Cheney *et al.*, 1993) fits well with these recent observations and supports the hypothesis that *folded* Myo5a is “inactive” and *extended* Myo5a is “active”

(Liu *et al.*, 2006). (Figure 1-6c) These studies are complicated by the presence of up to twelve calmodulin light chains per dimer. Since the function of calmodulin on the neck of class V myosins is not entirely understood, the addition of calcium may mediate secondary effects on motor activity. Further, ATPase assays of full length Myo5a (containing exon F) showed that the addition of melanophilin increased ATPase activity four-fold in the absence of calcium (Li *et al.*, 2005). (Figure 1-6e) This result suggests that cargo binding to the tail domain of Myo5a can inhibit the intramolecular interaction and shift Myo5a into an “active” state. Current models suggest that the physical interaction of the globular tail with the motor domain can either, 1) inhibit nucleotide exchange (Liu *et al.*, 2006) or 2) physically block an ATPase induced conformational change of the lever arm (Li *et al.*, 2008), which renders the molecule inactive. The regulation of enzymatic activity through intramolecular interactions has precedence by signaling molecules (ie. src) and also an actin-based motor, non-muscle myosin II (Sellers and Knight, 2007).

Figure 1-6: General mechanisms of regulation of class V myosins. **a.** Myo5a, purified in solution and in the absence of calcium and F-actin, adopts a folded conformation and exhibits no ATPase activity. **b.** The addition of F-actin to soluble Myo5a, activates low ATPase activity. Myo5a remains in a folded conformation. **c.** Myo5a obtains an extended conformation following the addition of micromolar amounts of calcium. In the presence of F-actin, “active” Myo5a has high ATPase activity. The addition of cargo to the C-terminal globular tail domain is not predicted to affect ATPase activity. **d.** The addition of micromolar amounts of calcium to purified Myo5a in solution induces an extended conformation and ATPase activity remains undetected. **e.** The addition of melanophilin increases Myo5a ATPase activity in the absence of calcium. This result indicates cargo binding can activate motor activity.

No ATPase activity \longrightarrow Low ATPase activity \longrightarrow High ATPase activity



Conclusions

In this review we have highlighted the multitude of organelle trafficking and non-organelle trafficking functions that class V myosins carry out. It is clear that even within the class V myosin family, significant diversity of biophysical and cell biological function exists. Although many important questions have been answered, the future holds many challenges for researchers in the class V myosin field. Since more than one class V myosin can be expressed in a single cell type, and each one can potentially perform several functions, dissecting out the roles each are playing will be a major challenge. Recent observations have provided insights into mechanisms of organelle association and motor regulation. Although *in vitro* observations are extremely exciting it will be important to confirm these observations in a physiological setting. Despite the complexity, a general mechanism of docking complex formation is beginning to emerge.

It is clear that considerable data exists on the cell biological functions for Myo5a and Myo5b, however much less is known about Myo5c. The initial characterization of Myo5c indicated that it functions in trafficking of Rab8-positive endocytic organelles in a plasma membrane recycling pathway (). Although Myo5c is chiefly expressed in exocrine secretory cells, the precise identity of the Myo5c-associated organelles remains elusive. Future studies will be required to determine whether Myo5c also associates with an organelle docking complex and to learn the identity of those components. It will also be important to determine the kinetic parameters of the Myo5c motor and compare it to the kinetics of Myo5a and Myo5b. Furthermore, *in vivo* studies that examine the localization and intracellular dynamics of Myo5c are important to begin to understand

Myo5c's function(s). Most importantly, a critical first step to determining the function of Myo5c will be to identify the Myo5c-associated organelle(s).

References

- Al-Haddad, A., Shonn, M.A., Redlich, B., Blocker, A., Burkhardt, J.K., Yu, H., Hammer, J.A., 3rd, Weiss, D.G., Steffen, W., Griffiths, G., and Kuznetsov, S.A. (2001). Myosin Va bound to phagosomes binds to F-actin and delays microtubule-dependent motility. *Mol Biol Cell* *12*, 2742-2755.
- Altmann, K., Frank, M., Neumann, D., Jakobs, S., and Westermann, B. (2008). The class V myosin motor protein, Myo2, plays a major role in mitochondrial motility in *Saccharomyces cerevisiae*. *J Cell Biol* *181*, 119-130.
- Arai, S., Noda, Y., Kainuma, S., Wada, I., and Yoda, K. (2008). Ypt11 functions in bud-directed transport of the Golgi by linking Myo2 to the coatamer subunit Ret2. *Curr Biol* *18*, 987-991.
- Au, J.S., and Huang, J.D. (2002). A tissue-specific exon of myosin Va is responsible for selective cargo binding in melanocytes. *Cell Motil Cytoskeleton* *53*, 89-102.
- Berg, J.S., Powell, B.C., and Cheney, R.E. (2001). A millennial myosin census. *Mol Biol Cell* *12*, 780-794.
- Boldogh, I.R., Ramcharan, S.L., Yang, H.C., and Pon, L.A. (2004). A type V myosin (Myo2p) and a Rab-like G-protein (Ypt11p) are required for retention of newly inherited mitochondria in yeast cells during cell division. *Mol Biol Cell* *15*, 3994-4002.
- Bridgman, P.C. (1999). Myosin Va movements in normal and dilute-lethal axons provide support for a dual filament motor complex. *J Cell Biol* *146*, 1045-1060.
- Brock, S.C., Goldenring, J.R., and Crowe, J.E., Jr. (2003). Apical recycling systems regulate directional budding of respiratory syncytial virus from polarized epithelial cells. *Proc Natl Acad Sci U S A* *100*, 15143-15148.
- Casanova, J.E., Wang, X., Kumar, R., Bhartur, S.G., Navarre, J., Woodrum, J.E., Altschuler, Y., Ray, G.S., and Goldenring, J.R. (1999). Association of Rab25 and Rab11a with the apical recycling system of polarized Madin-Darby canine kidney cells. *Mol Biol Cell* *10*, 47-61.
- Casavola, E.C., Catucci, A., Bielli, P., Di Pentima, A., Porcu, G., Pennestri, M., Cicero, D.O., and Ragnini-Wilson, A. (2008). Ypt32p and Mlc1p bind within the vesicle binding region of the class V myosin Myo2p globular tail domain. *Mol Microbiol* *67*, 1051-1066.
- Catlett, N.L., Duex, J.E., Tang, F., and Weisman, L.S. (2000). Two distinct regions in a yeast myosin-V tail domain are required for the movement of different cargoes. *J Cell Biol* *150*, 513-526.

- Catlett, N.L., and Weisman, L.S. (1998). The terminal tail region of a yeast myosin-V mediates its attachment to vacuole membranes and sites of polarized growth. *Proc Natl Acad Sci U S A* 95, 14799-14804.
- Chang, W., Zaarour, R.F., Reck-Peterson, S., Rinn, J., Singer, R.H., Snyder, M., Novick, P., and Mooseker, M.S. (2008). Myo2p, a class V myosin in budding yeast, associates with a large ribonucleic acid-protein complex that contains mRNAs and subunits of the RNA-processing body. *Rna* 14, 491-502.
- Chen, X., Walker, A.K., Strahler, J.R., Simon, E.S., Tomanicek-Volk, S.L., Nelson, B.B., Hurley, M.C., Ernst, S.A., Williams, J.A., and Andrews, P.C. (2006). Organellar proteomics: analysis of pancreatic zymogen granule membranes. *Mol Cell Proteomics* 5, 306-312.
- Cheney, R.E., and Mooseker, M.S. (1992). Unconventional myosins. *Curr Opin Cell Biol* 4, 27-35.
- Cheney, R.E., O'Shea, M.K., Heuser, J.E., Coelho, M.V., Wolenski, J.S., Espreafico, E.M., Forscher, P., Larson, R.E., and Mooseker, M.S. (1993). Brain myosin-V is a two-headed unconventional myosin with motor activity. *Cell* 75, 13-23.
- Correia, S.S., Bassani, S., Brown, T.C., Lise, M.F., Backos, D.S., El-Husseini, A., Passafaro, M., and Esteban, J.A. (2008). Motor protein-dependent transport of AMPA receptors into spines during long-term potentiation. *Nat Neurosci* 11, 457-466.
- da Silva Bizario, J.C., da Cunha Nascimento, A.A., Casaletti, L., Patussi, E.V., Chociay, M.F., Larson, R.E., and Espreafico, E.M. (2002). Expression of constructs of the neuronal isoform of myosin-Va interferes with the distribution of melanosomes and other vesicles in melanoma cells. *Cell Motil Cytoskeleton* 51, 57-75.
- Dekker-Ohno, K., Hayasaka, S., Takagishi, Y., Oda, S., Wakasugi, N., Mikoshiba, K., Inouye, M., and Yamamura, H. (1996). Endoplasmic reticulum is missing in dendritic spines of Purkinje cells of the ataxic mutant rat. *Brain Res* 714, 226-230.
- Desnos, C., Huet, S., and Darchen, F. (2007a). 'Should I stay or should I go?' myosin V function in organelle trafficking. *Biol Cell* 99, 411-423.
- Desnos, C., Huet, S., Fanget, I., Chapuis, C., Bottiger, C., Racine, V., Sibarita, J.B., Henry, J.P., and Darchen, F. (2007b). Myosin va mediates docking of secretory granules at the plasma membrane. *J Neurosci* 27, 10636-10645.
- Dunn, B.D., Sakamoto, T., Hong, M.S., Sellers, J.R., and Takizawa, P.A. (2007). Myo4p is a monomeric myosin with motility uniquely adapted to transport mRNA. *J Cell Biol* 178, 1193-1206.

Eichler, T.W., Kogel, T., Bukoreshtliev, N.V., and Gerdes, H.H. (2006). The role of myosin Va in secretory granule trafficking and exocytosis. *Biochem Soc Trans* 34, 671-674.

Espindola, F.S., Banzi, S.R., Calabria, L.K., Custodio, R.J., Oliveira, R.A., Procopio, L.D., Lima, A.B., Cunha-Junior, J.P., Coelho, M.V., Guedes, I.M., Pellizzon, C.H., Larson, R.E., and Espreafico, E.M. (2008). Localization of myosin-Va in subpopulations of cells in rat endocrine organs. *Cell Tissue Res* 333, 263-279.

Espreafico, E.M., Cheney, R.E., Matteoli, M., Nascimento, A.A., De Camilli, P.V., Larson, R.E., and Mooseker, M.S. (1992). Primary structure and cellular localization of chicken brain myosin-V (p190), an unconventional myosin with calmodulin light chains. *J Cell Biol* 119, 1541-1557.

Estrada, P., Kim, J., Coleman, J., Walker, L., Dunn, B., Takizawa, P., Novick, P., and Ferro-Novick, S. (2003). Myo4p and She3p are required for cortical ER inheritance in *Saccharomyces cerevisiae*. *J Cell Biol* 163, 1255-1266.

Fagarasanu, A., Fagarasanu, M., Eitzen, G.A., Aitchison, J.D., and Rachubinski, R.A. (2006). The peroxisomal membrane protein Inp2p is the peroxisome-specific receptor for the myosin V motor Myo2p of *Saccharomyces cerevisiae*. *Dev Cell* 10, 587-600.

Fan, G.H., Lapierre, L.A., Goldenring, J.R., Sai, J., and Richmond, A. (2004). Rab11-family interacting protein 2 and myosin Vb are required for CXCR2 recycling and receptor-mediated chemotaxis. *Mol Biol Cell* 15, 2456-2469.

Faust, F., Gomez-Lazaro, M., Borta, H., Agricola, B., and Schrader, M. (2008). Rab8 is involved in zymogen granule formation in pancreatic acinar AR42J cells. *Traffic* 9, 964-979.

Fukuda, M., and Itoh, T. (2004). Slac2-a/melanophilin contains multiple PEST-like sequences that are highly sensitive to proteolysis. *J Biol Chem* 279, 22314-22321.

Giner, D., Neco, P., Frances Mdel, M., Lopez, I., Viniestra, S., and Gutierrez, L.M. (2005). Real-time dynamics of the F-actin cytoskeleton during secretion from chromaffin cells. *J Cell Sci* 118, 2871-2880.

Gonsalvez, G.B., Urbinati, C.R., and Long, R.M. (2005). RNA localization in yeast: moving towards a mechanism. *Biol Cell* 97, 75-86.

Govindan, B., Bowser, R., and Novick, P. (1995). The role of Myo2, a yeast class V myosin, in vesicular transport. *J Cell Biol* 128, 1055-1068.

Grosshans, B.L., Ortiz, D., and Novick, P. (2006). Rabs and their effectors: achieving specificity in membrane traffic. *Proc Natl Acad Sci U S A* 103, 11821-11827.

- Gundersen, G.G., and Bretscher, A. (2003). Cell biology. Microtubule asymmetry. *Science* 300, 2040-2041.
- Haarer, B.K., Petzold, A., Lillie, S.H., and Brown, S.S. (1994). Identification of MYO4, a second class V myosin gene in yeast. *J Cell Sci* 107 (Pt 4), 1055-1064.
- Hales, C.M., Griner, R., Hobdy-Henderson, K.C., Dorn, M.C., Hardy, D., Kumar, R., Navarre, J., Chan, E.K., Lapierre, L.A., and Goldenring, J.R. (2001). Identification and characterization of a family of Rab11-interacting proteins. *J Biol Chem* 276, 39067-39075.
- Hales, C.M., Vaerman, J.P., and Goldenring, J.R. (2002). Rab11 family interacting protein 2 associates with Myosin Vb and regulates plasma membrane recycling. *J Biol Chem* 277, 50415-50421.
- Hill, K.L., Catlett, N.L., and Weisman, L.S. (1996). Actin and myosin function in directed vacuole movement during cell division in *Saccharomyces cerevisiae*. *J Cell Biol* 135, 1535-1549.
- Hoepfner, D., van den Berg, M., Philippsen, P., Tabak, H.F., and Hettema, E.H. (2001). A role for Vps1p, actin, and the Myo2p motor in peroxisome abundance and inheritance in *Saccharomyces cerevisiae*. *J Cell Biol* 155, 979-990.
- Hwang, E., Kusch, J., Barral, Y., and Huffaker, T.C. (2003). Spindle orientation in *Saccharomyces cerevisiae* depends on the transport of microtubule ends along polarized actin cables. *J Cell Biol* 161, 483-488.
- Ishikawa, K., Catlett, N.L., Novak, J.L., Tang, F., Nau, J.J., and Weisman, L.S. (2003). Identification of an organelle-specific myosin V receptor. *J Cell Biol* 160, 887-897.
- Itoh, T., Watabe, A., Toh, E.A., and Matsui, Y. (2002). Complex formation with Ypt11p, a rab-type small GTPase, is essential to facilitate the function of Myo2p, a class V myosin, in mitochondrial distribution in *Saccharomyces cerevisiae*. *Mol Cell Biol* 22, 7744-7757.
- Izumi, T. (2007). Physiological roles of Rab27 effectors in regulated exocytosis. *Endocr J* 54, 649-657.
- Johnston, G.C., Prendergast, J.A., and Singer, R.A. (1991). The *Saccharomyces cerevisiae* MYO2 gene encodes an essential myosin for vectorial transport of vesicles. *J Cell Biol* 113, 539-551.
- Karcher, R.L., Roland, J.T., Zappacosta, F., Huddleston, M.J., Annan, R.S., Carr, S.A., and Gelfand, V.I. (2001). Cell cycle regulation of myosin-V by calcium/calmodulin-dependent protein kinase II. *Science* 293, 1317-1320.

- Karpova, T.S., Reck-Peterson, S.L., Elkind, N.B., Mooseker, M.S., Novick, P.J., and Cooper, J.A. (2000). Role of actin and Myo2p in polarized secretion and growth of *Saccharomyces cerevisiae*. *Mol Biol Cell* *11*, 1727-1737.
- Kierszenbaum, A.L., Rivkin, E., and Tres, L.L. (2003). The actin-based motor myosin Va is a component of the acroplaxome, an acrosome-nuclear envelope junctional plate, and of manchette-associated vesicles. *Cytogenet Genome Res* *103*, 337-344.
- Krementsov, D.N., Krementsova, E.B., and Trybus, K.M. (2004). Myosin V: regulation by calcium, calmodulin, and the tail domain. *J Cell Biol* *164*, 877-886.
- Lambert, J., Naeyaert, J.M., Callens, T., De Paepe, A., and Messiaen, L. (1998). Human myosin V gene produces different transcripts in a cell type-specific manner. *Biochem Biophys Res Commun* *252*, 329-333.
- Lapierre, L.A., Kumar, R., Hales, C.M., Navarre, J., Bhartur, S.G., Burnette, J.O., Provance, D.W., Jr., Mercer, J.A., Bahler, M., and Goldenring, J.R. (2001). Myosin vb is associated with plasma membrane recycling systems. *Mol Biol Cell* *12*, 1843-1857.
- Legesse-Miller, A., Zhang, S., Santiago-Tirado, F.H., Van Pelt, C.K., and Bretscher, A. (2006). Regulated phosphorylation of budding yeast's essential myosin V heavy chain, Myo2p. *Mol Biol Cell* *17*, 1812-1821.
- Li, B.X., Satoh, A.K., and Ready, D.F. (2007). Myosin V, Rab11, and dRip11 direct apical secretion and cellular morphogenesis in developing *Drosophila* photoreceptors. *J Cell Biol* *177*, 659-669.
- Li, X.D., Ikebe, R., and Ikebe, M. (2005). Activation of myosin Va function by melanophilin, a specific docking partner of myosin Va. *J Biol Chem* *280*, 17815-17822.
- Li, X.D., Jung, H.S., Mabuchi, K., Craig, R., and Ikebe, M. (2006). The globular tail domain of myosin Va functions as an inhibitor of the myosin Va motor. *J Biol Chem* *281*, 21789-21798.
- Li, X.D., Jung, H.S., Wang, Q., Ikebe, R., Craig, R., and Ikebe, M. (2008). The globular tail domain puts on the brake to stop the ATPase cycle of myosin Va. *Proc Natl Acad Sci U S A* *105*, 1140-1145.
- Li, X.D., Mabuchi, K., Ikebe, R., and Ikebe, M. (2004). Ca²⁺-induced activation of ATPase activity of myosin Va is accompanied with a large conformational change. *Biochem Biophys Res Commun* *315*, 538-545.
- Libby, R.T., Lillo, C., Kitamoto, J., Williams, D.S., and Steel, K.P. (2004). Myosin Va is required for normal photoreceptor synaptic activity. *J Cell Sci* *117*, 4509-4515.

Lionne, C., Buss, F., Hodge, T., Ihrke, G., and Kendrick-Jones, J. (2001). Localization of myosin Va is dependent on the cytoskeletal organization in the cell. *Biochem Cell Biol* 79, 93-106.

Lipatova, Z., Tokarev, A.A., Jin, Y., Mulholland, J., Weisman, L.S., and Segev, N. (2008). Direct interaction between a myosin V motor and the Rab GTPases Ypt31/32 is required for polarized secretion. *Mol Biol Cell* 19, 4177-4187.

Lise, M.F., Wong, T.P., Trinh, A., Hines, R.M., Liu, L., Kang, R., Hines, D.J., Lu, J., Goldenring, J.R., Wang, Y.T., and El-Husseini, A. (2006). Involvement of myosin Vb in glutamate receptor trafficking. *J Biol Chem* 281, 3669-3678.

Liu, H., and Bretscher, A. (1992). Characterization of TPM1 disrupted yeast cells indicates an involvement of tropomyosin in directed vesicular transport. *J Cell Biol* 118, 285-299.

Liu, J., Taylor, D.W., Kremntsova, E.B., Trybus, K.M., and Taylor, K.A. (2006). Three-dimensional structure of the myosin V inhibited state by cryoelectron tomography. *Nature* 442, 208-211.

Marchelletta, R.R., Jacobs, D.T., Schechter, J.E., Cheney, R.E., and Hamm-Alvarez, S.F. (2008). The Class V Myosin Motor, Myosin 5c, Localizes to Mature Secretory Vesicles and Facilitates Exocytosis in Lacrimal Acini. *Am J Physiol Cell Physiol*.

Matesic, L.E., Yip, R., Reuss, A.E., Swing, D.A., O'Sullivan, T.N., Fletcher, C.F., Copeland, N.G., and Jenkins, N.A. (2001). Mutations in *Mlph*, encoding a member of the Rab effector family, cause the melanosome transport defects observed in leaden mice. *Proc Natl Acad Sci U S A* 98, 10238-10243.

Mehta, A.D., Rock, R.S., Rief, M., Spudich, J.A., Mooseker, M.S., and Cheney, R.E. (1999). Myosin-V is a processive actin-based motor. *Nature* 400, 590-593.

Mercer, J.A., Seperack, P.K., Strobel, M.C., Copeland, N.G., and Jenkins, N.A. (1991). Novel myosin heavy chain encoded by murine dilute coat colour locus. *Nature* 349, 709-713.

Miyata, M., Finch, E.A., Khiroug, L., Hashimoto, K., Hayasaka, S., Oda, S.I., Inouye, M., Takagishi, Y., Augustine, G.J., and Kano, M. (2000). Local calcium release in dendritic spines required for long-term synaptic depression. *Neuron* 28, 233-244.

Muller, T., Hess, M.W., Schiefermeier, N., Pfaller, K., Ebner, H.L., Heinz-Erian, P., Ponstingl, H., Partsch, J., Rollinghoff, B., Kohler, H., Berger, T., Lenhartz, H., Schlenck, B., Houwen, R.J., Taylor, C.J., Zoller, H., Lechner, S., Goulet, O., Utermann, G., Ruemmele, F.M., Huber, L.A., and Janecke, A.R. (2008). MYO5B mutations cause microvillus inclusion disease and disrupt epithelial cell polarity. *Nat Genet* 40, 1163-1165.

- Neco, P., Gil, A., Del Mar Frances, M., Viniegra, S., and Gutierrez, L.M. (2002). The role of myosin in vesicle transport during bovine chromaffin cell secretion. *Biochem J* 368, 405-413.
- Neco, P., Giner, D., del Mar Frances, M., Viniegra, S., and Gutierrez, L.M. (2003). Differential participation of actin- and tubulin-based vesicle transport systems during secretion in bovine chromaffin cells. *Eur J Neurosci* 18, 733-742.
- Nedvetsky, P.I., Stefan, E., Frische, S., Santamaria, K., Wiesner, B., Valenti, G., Hammer, J.A., 3rd, Nielsen, S., Goldenring, J.R., Rosenthal, W., and Klusmann, E. (2007). A Role of myosin Vb and Rab11-FIP2 in the aquaporin-2 shuttle. *Traffic* 8, 110-123.
- Odrionitz, F., and Kollmar, M. (2007). Drawing the tree of eukaryotic life based on the analysis of 2,269 manually annotated myosins from 328 species. *Genome Biol* 8, R196.
- Pashkova, N., Catlett, N.L., Novak, J.L., Wu, G., Lu, R., Cohen, R.E., and Weisman, L.S. (2005). Myosin V attachment to cargo requires the tight association of two functional subdomains. *J Cell Biol* 168, 359-364.
- Pashkova, N., Jin, Y., Ramaswamy, S., and Weisman, L.S. (2006). Structural basis for myosin V discrimination between distinct cargoes. *Embo J* 25, 693-700.
- Pastural, E., Barrat, F.J., Dufourcq-Lagelouse, R., Certain, S., Sanal, O., Jabado, N., Seger, R., Griscelli, C., Fischer, A., and de Saint Basile, G. (1997). Griscelli disease maps to chromosome 15q21 and is associated with mutations in the myosin-Va gene. *Nat Genet* 16, 289-292.
- Petralia, R.S., Wang, Y.X., Sans, N., Worley, P.F., Hammer, J.A., 3rd, and Wenthold, R.J. (2001). Glutamate receptor targeting in the postsynaptic spine involves mechanisms that are independent of myosin Va. *Eur J Neurosci* 13, 1722-1732.
- Prekeris, R., and Terrian, D.M. (1997). Brain myosin V is a synaptic vesicle-associated motor protein: evidence for a Ca²⁺-dependent interaction with the synaptobrevin-synaptophysin complex. *J Cell Biol* 137, 1589-1601.
- Provance, D.W., Jr., Addison, E.J., Wood, P.R., Chen, D.Z., Silan, C.M., and Mercer, J.A. (2008). Myosin-Vb functions as a dynamic tether for peripheral endocytic compartments during transferrin trafficking. *BMC Cell Biol* 9, 44.
- Provance, D.W., Jr., Gourley, C.R., Silan, C.M., Cameron, L.C., Shokat, K.M., Goldenring, J.R., Shah, K., Gillespie, P.G., and Mercer, J.A. (2004). Chemical-genetic inhibition of a sensitized mutant myosin Vb demonstrates a role in peripheral-pericentriolar membrane traffic. *Proc Natl Acad Sci U S A* 101, 1868-1873.

- Provance, D.W., Jr., Wei, M., Ipe, V., and Mercer, J.A. (1996). Cultured melanocytes from dilute mutant mice exhibit dendritic morphology and altered melanosome distribution. *Proc Natl Acad Sci U S A* *93*, 14554-14558.
- Reck-Peterson, S.L., Novick, P.J., and Mooseker, M.S. (1999). The tail of a yeast class V myosin, myo2p, functions as a localization domain. *Mol Biol Cell* *10*, 1001-1017.
- Reck-Peterson, S.L., Tyska, M.J., Novick, P.J., and Mooseker, M.S. (2001). The yeast class V myosins, Myo2p and Myo4p, are nonprocessive actin-based motors. *J Cell Biol* *153*, 1121-1126.
- Rief, M., Rock, R.S., Mehta, A.D., Mooseker, M.S., Cheney, R.E., and Spudich, J.A. (2000). Myosin-V stepping kinetics: a molecular model for processivity. *Proc Natl Acad Sci U S A* *97*, 9482-9486.
- Rodriguez, O.C., and Cheney, R.E. (2002). Human myosin-Vc is a novel class V myosin expressed in epithelial cells. *J Cell Sci* *115*, 991-1004.
- Rogers, S.L., and Gelfand, V.I. (1998). Myosin cooperates with microtubule motors during organelle transport in melanophores. *Curr Biol* *8*, 161-164.
- Rogers, S.L., Karcher, R.L., Roland, J.T., Minin, A.A., Steffen, W., and Gelfand, V.I. (1999). Regulation of melanosome movement in the cell cycle by reversible association with myosin V. *J Cell Biol* *146*, 1265-1276.
- Roland, J.T., Kenworthy, A.K., Peranen, J., Caplan, S., and Goldenring, J.R. (2007). Myosin Vb interacts with Rab8a on a tubular network containing EHD1 and EHD3. *Mol Biol Cell* *18*, 2828-2837.
- Roland, J.T., Lapierre, L.A., and Goldenring, J.R. (2008). Alternative splicing in class V myosins determines association with RAB10. *J Biol Chem*.
- Rose, S.D., Lejen, T., Casaletti, L., Larson, R.E., Pene, T.D., and Trifaro, J.M. (2002). Molecular motors involved in chromaffin cell secretion. *Ann N Y Acad Sci* *971*, 222-231.
- Rossanese, O.W., Reinke, C.A., Bevis, B.J., Hammond, A.T., Sears, I.B., O'Connor, J., and Glick, B.S. (2001). A role for actin, Cdc1p, and Myo2p in the inheritance of late Golgi elements in *Saccharomyces cerevisiae*. *J Cell Biol* *153*, 47-62.
- Rudolf, R., Kogel, T., Kuznetsov, S.A., Salm, T., Schlicker, O., Hellwig, A., Hammer, J.A., 3rd, and Gerdes, H.H. (2003). Myosin Va facilitates the distribution of secretory granules in the F-actin rich cortex of PC12 cells. *J Cell Sci* *116*, 1339-1348.

- Sakamoto, T., Amitani, I., Yokota, E., and Ando, T. (2000). Direct observation of processive movement by individual myosin V molecules. *Biochem Biophys Res Commun* 272, 586-590.
- Sakamoto, T., Wang, F., Schmitz, S., Xu, Y., Xu, Q., Molloy, J.E., Veigel, C., and Sellers, J.R. (2003). Neck length and processivity of myosin V. *J Biol Chem* 278, 29201-29207.
- Sakamoto, T., Yildez, A., Selvin, P.R., and Sellers, J.R. (2005). Step-size is determined by neck length in myosin V. *Biochemistry* 44, 16203-16210.
- Schott, D., Ho, J., Pruyne, D., and Bretscher, A. (1999). The COOH-terminal domain of Myo2p, a yeast myosin V, has a direct role in secretory vesicle targeting. *J Cell Biol* 147, 791-808.
- Sellers, J.R., and Knight, P.J. (2007). Folding and regulation in myosins II and V. *J Muscle Res Cell Motil* 28, 363-370.
- Swiatecka-Urban, A., Talebian, L., Kanno, E., Moreau-Marquis, S., Coutermarsh, B., Hansen, K., Karlson, K.H., Barnaby, R., Cheney, R.E., Langford, G.M., Fukuda, M., and Stanton, B.A. (2007). Myosin Vb is required for trafficking of the cystic fibrosis transmembrane conductance regulator in Rab11a-specific apical recycling endosomes in polarized human airway epithelial cells. *J Biol Chem* 282, 23725-23736.
- Takagi, Y., Yang, Y., Fujiwara, I., Jacobs, D., Cheney, R.E., Sellers, J.R., and Kovacs, M. (2008). Human myosin Vc is a low duty ratio, non-processive molecular motor. *J Biol Chem*.
- Takagishi, Y., Oda, S., Hayasaka, S., Dekker-Ohno, K., Shikata, T., Inouye, M., and Yamamura, H. (1996). The dilute-lethal (dl) gene attacks a Ca²⁺ store in the dendritic spine of Purkinje cells in mice. *Neurosci Lett* 215, 169-172.
- Takizawa, P.A., Sil, A., Swedlow, J.R., Herskowitz, I., and Vale, R.D. (1997). Actin-dependent localization of an RNA encoding a cell-fate determinant in yeast. *Nature* 389, 90-93.
- Takizawa, P.A., and Vale, R.D. (2000). The myosin motor, Myo4p, binds Ash1 mRNA via the adapter protein, She3p. *Proc Natl Acad Sci U S A* 97, 5273-5278.
- Tang, F., Kauffman, E.J., Novak, J.L., Nau, J.J., Catlett, N.L., and Weisman, L.S. (2003). Regulated degradation of a class V myosin receptor directs movement of the yeast vacuole. *Nature* 422, 87-92.
- Thirumurugan, K., Sakamoto, T., Hammer, J.A., 3rd, Sellers, J.R., and Knight, P.J. (2006). The cargo-binding domain regulates structure and activity of myosin 5. *Nature* 442, 212-215.

Toth, J., Kovacs, M., Wang, F., Nyitray, L., and Sellers, J.R. (2005). Myosin V from *Drosophila* reveals diversity of motor mechanisms within the myosin V family. *J Biol Chem* *280*, 30594-30603.

Trybus, K.M. (2008). Myosin V from head to tail. *Cell Mol Life Sci*.

Valiathan, R.R., and Weisman, L.S. (2008). Pushing for answers: is myosin V directly involved in moving mitochondria? *J Cell Biol* *181*, 15-18.

Varadi, A., Tsuboi, T., and Rutter, G.A. (2005). Myosin Va transports dense core secretory vesicles in pancreatic MIN6 beta-cells. *Mol Biol Cell* *16*, 2670-2680.

Volpicelli, L.A., Lah, J.J., Fang, G., Goldenring, J.R., and Levey, A.I. (2002). Rab11a and myosin Vb regulate recycling of the M4 muscarinic acetylcholine receptor. *J Neurosci* *22*, 9776-9784.

Wakabayashi, Y., Dutt, P., Lippincott-Schwartz, J., and Arias, I.M. (2005). Rab11a and myosin Vb are required for bile canalicular formation in WIF-B9 cells. *Proc Natl Acad Sci U S A* *102*, 15087-15092.

Watanabe, S., Mabuchi, K., Ikebe, R., and Ikebe, M. (2006). Mechanoenzymatic characterization of human myosin Vb. *Biochemistry* *45*, 2729-2738.

Watanabe, S., Watanabe, T., Sato, O., Awata, J., Homma, K., Umeki, N., Higuchi, H., Ikebe, R., and Ikebe, M. (2007). Human myosin Vc is a low duty ratio non-processive motor. *J Biol Chem*.

Weigert, R., Yeung, A.C., Li, J., and Donaldson, J.G. (2004). Rab22a regulates the recycling of membrane proteins internalized independently of clathrin. *Mol Biol Cell* *15*, 3758-3770.

Wilson, S.M., Yip, R., Swing, D.A., O'Sullivan, T.N., Zhang, Y., Novak, E.K., Swank, R.T., Russell, L.B., Copeland, N.G., and Jenkins, N.A. (2000). A mutation in Rab27a causes the vesicle transport defects observed in ashen mice. *Proc Natl Acad Sci U S A* *97*, 7933-7938.

Wu, X., Bowers, B., Rao, K., Wei, Q., and Hammer, J.A., 3rd. (1998). Visualization of melanosome dynamics within wild-type and dilute melanocytes suggests a paradigm for myosin V function *In vivo*. *J Cell Biol* *143*, 1899-1918.

Wu, X., Bowers, B., Wei, Q., Kocher, B., and Hammer, J.A., 3rd. (1997). Myosin V associates with melanosomes in mouse melanocytes: evidence that myosin V is an organelle motor. *J Cell Sci* *110 (Pt 7)*, 847-859.

Wu, X., Sakamoto, T., Zhang, F., Sellers, J.R., and Hammer, J.A., 3rd. (2006). In vitro reconstitution of a transport complex containing Rab27a, melanophilin and myosin Va. *FEBS Lett* 580, 5863-5868.

Wu, X., Wang, F., Rao, K., Sellers, J.R., and Hammer, J.A., 3rd. (2002a). Rab27a is an essential component of melanosome receptor for myosin Va. *Mol Biol Cell* 13, 1735-1749.

Wu, X.S., Rao, K., Zhang, H., Wang, F., Sellers, J.R., Matesic, L.E., Copeland, N.G., Jenkins, N.A., and Hammer, J.A., 3rd. (2002b). Identification of an organelle receptor for myosin-Va. *Nat Cell Biol* 4, 271-278.

Yan, Q., Sun, W., Kujala, P., Lotfi, Y., Vida, T.A., and Bean, A.J. (2005). CART: an Hrs/actinin-4/BERP/myosin V protein complex required for efficient receptor recycling. *Mol Biol Cell* 16, 2470-2482.

Yin, H., Pruyne, D., Huffaker, T.C., and Bretscher, A. (2000). Myosin V orientates the mitotic spindle in yeast. *Nature* 406, 1013-1015.

Zerial, M., and McBride, H. (2001). Rab proteins as membrane organizers. *Nat Rev Mol Cell Biol* 2, 107-117.

Zhao, L.P., Koslovsky, J.S., Reinhard, J., Bahler, M., Witt, A.E., Provance, D.W., Jr., and Mercer, J.A. (1996). Cloning and characterization of myr 6, an unconventional myosin of the dilute/myosin-V family. *Proc Natl Acad Sci U S A* 93, 10826-10831.

**CHAPTER 2: THE CLASS V MYOSIN MOTOR, MYOSIN 5C, LOCALIZES TO
MATURE SECRETORY VESICLES, AND FACILITATES EXOCYTOSIS IN
LACRIMAL ACINI**

THE CLASS V MYOSIN MOTOR, MYOSIN 5C, LOCALIZES TO MATURE SECRETORY VESICLES AND FACILITATES EXOCYTOSIS IN LACRIMAL ACINI

Ronald R. Marchelletta¹, Damon T. Jacobs³, Joel E. Schechter², Richard E. Cheney³ and Sarah F. Hamm-Alvarez^{1*}

¹Department of Pharmacology and Pharmaceutical Sciences and the ²Department of Cell and Neurobiology, University of Southern California, Los Angeles; ³Department of Cell and Molecular Physiology, University of North Carolina, Chapel Hill, NC

*Address Correspondence to:
Sarah F. Hamm-Alvarez, Ph. D.
Department of Pharmacology and Pharmaceutical Sciences
USC School of Pharmacy
1985 Zonal Avenue
Los Angeles CA 90033
323-442-1445 O
323-442-1390 F

Running Head: Myosin 5c facilitates acinar exocytosis

Key Words: Actin, myosin, lacrimal gland, tear film

Abstract

We investigated the role of the actin-based myosin motor, Myosin 5c (Myo5c) in vesicle transport in exocrine secretion. Lacrimal gland acinar cells (LGAC) are the major source for the regulated secretion of proteins from the lacrimal gland into the tear film. Confocal fluorescence and immunogold electron microscopy revealed that Myo5c was associated with secretory vesicles in primary rabbit LGAC. Upon stimulation of secretion with the muscarinic agonist, carbachol, Myo5c was also detected in association with actin-coated fusion intermediates. Adenovirus-mediated expression of GFP fused to the tail domain of Myo5c (Ad-GFP-Myo5c-tail) showed that this protein was localized to secretory vesicles. Furthermore, its expression induced a significant ($p \leq 0.05$) decrease in carbachol-stimulated release of two secretory vesicle content markers, secretory component and syncollin-GFP. Adenovirus-mediated expression of GFP appended to the full length Myo5c (Ad-GFP-Myo5c-full) was used in parallel with adenovirus-mediated expression of GFP-Myo5c-tail in LGAC to compare various parameters of secretory vesicles labeled with either GFP-labeled protein in resting and stimulated LGAC. These studies revealed that the carbachol-stimulated increase in secretory vesicle diameter associated with compound fusion of secretory vesicles that was also exhibited by vesicles labeled with GFP-Myo5c-full was impaired in vesicles labeled with GFP-Myo5c-tail. A significant decrease in GFP labeling of actin-coated fusion intermediates was also seen in carbachol-stimulated LGAC transduced with GFP-Myo5c-tail relative to LGAC transduced with GFP-Myo5c-full. These results suggest that Myosin 5c participates in apical exocytosis of secretory vesicles.

Introduction

The lacrimal gland (LG)¹ is the principal source of proteins released into the tear film. These proteins play critical roles in protection of the ocular surface from pathogens, and also provide nutrients and growth factors essential for maintenance of the cornea (Chen *et al.*, 2006; Wu *et al.*, 2006). The lacrimal gland acinar cells (LGAC) constitute about 85% of the LG, and are largely responsible for this regulated secretion of tear proteins including secretory immunoglobulin A (sIgA), secretory component (SC), lysosomal hydrolases and growth factors among others (Wu *et al.*, 2006). The development of decreased LG output occurs in individuals with syndromes ranging in severity from mild dry eye to the autoimmune disorder, Sjögren's Syndrome (SjS) (Fox and Stern, 2002; Wu *et al.*, 2006). In the most severe case, SjS, initial changes in the LG are followed by lymphocytic infiltration of the gland, resulting in functional atrophy and some destruction of the tissue (Fox and Stern, 2002). However, LG biopsies have shown that the actual destruction of the tissue in patients with SjS is insufficient to account for the extreme decrease in LG output (Fox and Stern, 2002), raising the possibility that the functional atrophy of the LG may be reversed to provide some relief for affected patients. Such a strategy would depend upon a mechanistic understanding of the normal effectors that regulate secretion in the gland.

We and others have established that mature secretory vesicles (mSVs) sized ~0.5-1 μm are located beneath the actin-enriched apical plasma membrane (APM) domain of LGAC (Jerdeva *et al.*, 2005b). These SVs are enriched in the small GTPase, Rab3D (Wang *et al.*, 2003). Recent preliminary data in our laboratory and studies in acinar

¹ See text footnotes

epithelial cells from pancreas and parotid gland (Waselle *et al.*, 2003; Imai *et al.*, 2004) suggest that mSVs may also be enriched in Rab27a and/or Rab27b. Exposure of the LG to neurotransmitters released from innervating parasympathetic and sympathetic neurons triggers exocytosis of mSV at the APM, and can be mimicked in vitro by agents such as the muscarinic agonist, carbachol (CCh). Apical exocytosis is accompanied by significant actin filament remodeling including thinning of the apical actin layer (cortical actin/ terminal web) separating mSVs from the APM (Jerdeva *et al.*, 2005b). In parallel, assembly of an actin coat around the base of multiple fusing mSVs and contraction of this network occurs; we have proposed that this formation of an actin-coated fusion intermediate is important in facilitating compound fusion and extrusion of the contents of these vesicles (Jerdeva *et al.*, 2005b). Non-muscle myosin II has been implicated in contraction of the actin coat around fusing vesicles in LGAC, but inhibition of its activity only partially impairs CCh-stimulated exocytosis and actin remodeling, suggesting that additional actin-dependent motors may participate in these events.

Myosins are a superfamily of proteins that consist of a conserved N-terminal motor domain (head) that associates with actin filaments and can generate force, a neck region that binds light chains, and a class specific C-terminal tail (Provance and Mercer, 1999; Reck-Peterson *et al.*, 2000; Krendel and Mooseker, 2005; Abu-Hamdah *et al.*, 2006; O'Connell C *et al.*, 2007). One of the most ancient classes of myosins are the class V myosins (Richards and Cavalier-Smith, 2005; Foth *et al.*, 2006). Class V myosins are expressed in organisms as diverse as fungi, *Saccharomyces Cerevisiae*, *Drosophila Melanogaster*, and mammals and are leading candidates to function as motors for actin-based organelle transport (Richards and Cavalier-Smith, 2005; Foth *et al.*, 2006). In the

budding yeast, a class V myosin (Myo2p) and a rab protein (Sec4p) are required for targeted delivery of secretory vesicles from the mother to the daughter bud tip, thus facilitating polarized secretion (Pruyne *et al.*, 1998; Karpova *et al.*, 2000). The tail domain of Myo2p associates with secretory vesicles and acts as a dominant negative for polarized secretion, presumably by competing with endogenous Myo2p for its vesicle binding sites (Johnston *et al.*, 1991). Polarized secretion can also be blocked by treating wild-type yeast with latrunculin A; this and other evidence indicates that Myo2p binds to secretory vesicles and transports them along actin cables to sites of polarized secretion (Karpova *et al.*, 2000; Schott *et al.*, 2002).

Vertebrates express three class V myosins: Myosin 5a (Myo5a), Myosin 5b (Myo5b), and Myosin 5c (Myo5c) (Reck-Peterson *et al.*, 2000; Rodriguez and Cheney, 2002). Loss-of-function Myo5a leads to a defect in subcellular localization of melanosomes (pigment granules) (Wu *et al.*, 1997). Myo5b, the second of the class V myosins to be discovered in vertebrates, is associated with a plasma membrane recycling compartment in several cell types (Zhao *et al.*, 1996; Lapierre *et al.*, 2001; Fan *et al.*, 2004; Wakabayashi *et al.*, 2005; Lise *et al.*, 2006; Nedvetsky *et al.*, 2007; Swiatecka-Urban *et al.*, 2007).

Myo5c, the third member of the class V myosin family in vertebrates, is expressed most abundantly in exocrine secretory tissues. Myo5c localizes to the apical domain of epithelial cells and is hypothesized to function as a motor for actin-based organelle trafficking (Rodriguez and Cheney, 2002). In HeLa cells, the expression of a dominant negative Myo5c tail led to an accumulation of transferrin receptors in large cytoplasmic puncta and inhibited transferrin recycling (Rodriguez and Cheney, 2002).

Interestingly, Myo5c, as well as several Rab proteins, were identified in a proteomics study as components on secretory granules of pancreatic acinar cells (Chen, 2006). The distribution and abundance of Myo5c in exocrine tissues prompted us explore the function of this motor in secretory vesicle exocytosis in our LGAC model system.

Materials and Methods

Reagents: Carbachol (CCh) was purchased from Sigma Aldrich (St. Louis, Mo). Pepstatin A, Tosyl Phenylalanyl Chloromethyl Ketone, Leupeptin, Tosyl Lysyl Chloromethyl Ketone, Soybean Trypsin Inhibitor, and Phenylmethane Sulphonyl Fluoride were also purchased from Sigma Aldrich (St. Louis, MO) and used in the protease inhibitor cocktail for preparation of gland or cellular homogenate as described (Vilalta *et al.*, 1998). The antibodies to Myo5a, Myo5b and Myo5c used here have been characterized previously (Rodriguez and Cheney, 2002). Mouse monoclonal anti-hemagglutinin epitope (HA) antibody was purchased from Covance (Berkeley, CA). FITC-conjugated goat anti-rabbit secondary antibody, Alexa Fluor-680 conjugated donkey anti-sheep secondary antibody, Alexa Fluor-568 conjugated goat anti-mouse secondary antibody, Alexa Fluor-488 conjugated goat anti-rat secondary antibody, Alexa Fluor 647-phalloidin, Alexa Fluor-568 phalloidin, rhodamine phalloidin and Prolong anti-fade medium were purchased from Molecular Probes/Invitrogen (Carlsbad, CA). FITC-conjugated goat anti-rabbit secondary antibody was purchased from MP Biomedical (Solon, OH). Rabbit anti-green fluorescent protein (GFP) antibody was purchased from Santa Cruz Biotechnology (Santa Cruz, CA). Sheep polyclonal antisera to rabbit polymeric immunoglobulin A receptor (pIgAR) was prepared by Caprilogics (Hardwick, MA) using secretory component (SC) from rabbit gall bladder bile as antigen. Bovine serum albumin fraction (BSA) V was purchased from EMD chemicals (Gibbstown, NJ). Anti-rab3D polyclonal antibodies were generated in rabbits against recombinant (His)₆ epitope-tagged wild-type rab3D expressed in *E. coli* and purified by chromatography over protein A/G agarose (Antibodies Inc., Davis, CA) in accordance

with (9). IR800-conjugated and IR700-conjugated goat anti-rabbit and goat anti-mouse secondary antibodies were purchased from Rockland (Gilbertsville, PA) for use in Western blotting. Blocking buffer was purchased from Li-Cor Biosciences (Lincoln, Nebraska). Doxycycline was obtained from Clontech (Mountain View, CA).

Primary rabbit LGAC culture: Primary LGAC were isolated as described (Wang *et al.*, 2003; Jerdeva *et al.*, 2005a; Jerdeva *et al.*, 2005b) from New Zealand White Rabbits (1.8-2.2 kg) obtained from Irish Farms (Norco, CA) and sacrificed in accordance with all institutional IACUC guidelines. Isolated LGAC were cultured for 2-3 days in 100 mm round culture dishes at a density of 3.0×10^7 cells or on glass coverslips in 12-well dishes coated with Matrigel (Invitrogen, Carlsbad, CA) at a density of 2.0×10^7 cells. We have established that under these conditions the cultured cells re-establish distinct apical and basolateral domains, form mSVs and position these vesicles beneath lumina formed between adjacent APM of adjoining cells (Da Costa *et al.*, 2002; Wang *et al.*, 2003; Jerdeva *et al.*, 2005a; Jerdeva *et al.*, 2005b).

Confocal fluorescence microscopy: LGAC were cultured on Matrigel-coated coverslips for 2-3 days and then exposed without or with CCh (100 μ M, 5-15 min). Cells were fixed and permeabilized with ice-cold ethanol for 10 min in -20°C as previously described (Da Costa *et al.*, 2003). After fixation and permeabilization at RT, the cells were washed 3 times in PBS for 5 min at RT. The cells were then blocked with 1% BSA for 15 min at RT and processed for immunofluorescence detection for the proteins of interest (Rab3D, Myo5c, pIgAR, syncollin-GFP) with appropriate primary and

fluorophore-conjugated secondary antibody before fixation with Prolong anti-fade mounting medium as previously described (Da Costa *et al.*, 2003; Jerdeva *et al.*, 2005a; Jerdeva *et al.*, 2005b). Fixed samples were imaged using a Zeiss LSM 510 Meta NLO confocal imaging system equipped with software for quantitation of fluorescent pixel co-localization and for measurement of vesicle diameter. Use of the LSM co-localization tool with auto-threshold to assess pixel co-localization was done in accord with (Jerdeva *et al.*, 2005a). Images obtained were then compiled in Photoshop Version 8.0 (Mountain View, CA).

For dual labeling with rabbit polyclonal antibodies against Myo5c and Rab3D, shown as **Supplemental Figure 2-1**, cells were fixed and processed as described above up to the addition of the first primary antibody. Rabbit polyclonal antibody to Rab3D was incubated with the cells for 1 hr at 37°C, washed well in PBS, and then incubated with goat anti-rabbit secondary antibody conjugated to rhodamine for 1 hr at 37°C. Cells were then washed well with PBS and incubated overnight in 10% BSA containing 0.4 µg/µl of whole molecule goat anti-rabbit IgG (Sigma) at 4°C. Cells were then washed well with PBS and incubated with rabbit polyclonal antibody against Myo5c for 1 hr at 37°C. After washing well with PBS, cells were incubated with goat anti-rabbit secondary antibody conjugated to FITC for 1 hr at 37°C. Finally, cells were washed well in PBS and mounted as described above.

Preparation and analysis of LG tissue sections: Tissue sections were processed by surgically removing the LG from an anesthetized rat and immediately immersing into 2% paraformaldehyde in PBS for 4 hrs at 4°C. The excised rat LG was rinsed and washed

for 24 hrs in PBS through several changes. The rat LG was then infused with 15% sucrose over several days with 3 changes of the sucrose medium. The tissue was then immersed in OCT and flash frozen using dry ice and isopentane. Serial cryosections were cut at 10 μm each using a Bright/Hacker model 5030 cryostat (Huntington, England) and thaw-mounted onto warm slides, which were stored at 4°C until use.

Sections were encircled using a PAP pen, permeabilized using 0.5% Triton X-100 for 15 min at RT, washed 3x for 15 min each, then treated with 0.05% NaBH_3 for 15 min at RT. The sections were subsequently blocked with 5% heat-inactivated goat serum in PBS, incubated with rabbit anti-Myo5c antibody in 5% goat serum, rinsed three times in PBS, incubated with Alexa-488 goat anti-rabbit secondary antibody in 5% goat serum, and then rinsed three times again in PBS. During the second wash, Alexa-568 phalloidin was added to label F-actin and slides were mounted in Prolong anti-fade according to the manufacturer's instructions. Tissue sections were imaged with a 63X 1.4 NA lens on a Zeiss Axiovert 100-TV inverted microscope equipped with an Orca-II cooled CCD camera (Hamamatsu). Images were adjusted for optimal brightness and contrast by Metamorph Imaging software (Molecular Devices, Downingtown, PA).

Production and Purification of Recombinant Adenovirus (Ad): An Ad-GFP-Myo5c-tail construct was generated from the human GFP-Myo5c-tail construct in pEGFP-C2 (Clontech) described in (Rodriguez and Cheney, 2002). The pEGFP-C2 Myo5c-tail was digested with NheI and XbaI restriction enzymes at the 592bp (5' end) and the 3919bp (3' end) site of the pEGFP-C2 Myo5c-tail vector, respectively. A 3327 bp fragment digest encoding GFP-Myo5c-tail was subcloned into the pShuttle vector from

the Adeno X expression system kit 1 (Clontech, Mountain View, CA) and further subcloned into the Adeno X vector in accordance with the manufacturer's protocol. A GFP-tagged Myo5c full length construct was derived by ligating a PCR product containing the head, neck, and proximal tail into XhoI and SmaI sites of the pEGFP-Myo5c tail construct. Sequence analysis verified that full length construct in pEGFP-C2 was identical to the published sequence of human Myo5c (Accession number AF272390; aa 1-1742, nt 20-5245) except for a silent t>c change at nt 907. This construct was digested with nheI and Sall (at the 601bp (5' end) and the 6587bp (3' end) of the pEGFP-Myo5c full length vector) and the resulting fragment encoding GFP-Myo5c full length was subcloned into the pShuttle vector from the Adeno X Tet-on expression system kit 1 (Clontech, Mountain View, CA) and further subcloned into the Adeno X tet-on vector in accordance with the manufacturer's protocol.

Ad-Rab3D-HA was kindly provided by Dr. John Williams from the University of Michigan (Chen *et al.*, 2002). Ad-Syncollin-GFP was kindly provided by Dr. Christopher Rhodes, University of Chicago (Ma *et al.*, 2004). Ad-GFP was generated as described previously (Wang *et al.*, 2004).

All Ad vectors were amplified in the HEK293 derived helper cell line, QBI. Once QBI cells displayed evidence of a cytopathic effect of the transfected Ad, the virally-infected QBI cells were lysed with 3 cycles of freeze-thaw with liquid nitrogen. The supernatant was used to further infect more plated QBI cells. The process of infection and freeze/thaw was repeated until the appropriate viral titer was attained. Virus was then purified using CsCl₂ gradients according to established protocols (Wang *et al.*, 2003).

Viral Transduction: Transduction of LGAC was done in accordance with (Wang *et al.*, 2003) on day 2 of culture. Cells were rinsed with DPBS and aspirated and medium was then replaced with fresh culture media. The LGAC were exposed to replication-deficient Ad constructs (Ad-GFP, Ad-GFP-Myo5c-tail, Ad-GFP-Myo5c-full, Ad-Rab3D-HA, Ad-Syncollin-GFP) as described below, followed by aspiration of the medium, rinsing in PBS and addition of fresh culture medium. For Ad-GFP-Myo5c-full transduction which requires a helper virus, LGAC were incubated for 3 hrs at 37°C with Ad-GFP-Myo5c-full at an MOI of 5, rinsed once with PBS and incubated 3 hrs more with the tet-on Ad helper virus at an MOI of 5 in the presence of 1µg/ml doxycycline. After rinsing, doxycycline was maintained in the culture medium for the duration of the experiment. All Ad constructs were incubated with LGAC at 37°C at an MOI of 5 for 1 hr. After removal of virus and replacement of culture medium, LGAC were cultured another 16-18 hrs before analysis.

For assays analyzing release of syncollin-GFP, LGAC transduced with Ad-GFP or Ad-GFP-Myo5c-tail, both at an MOI of 1-5 were also transduced with Ad-Syncollin-GFP at a MOI of 5 resulting in LGAC doubly-transduced with Ad-GFP/ Ad-Syncollin-GFP or Ad-GFP-Myo5c-tail / Ad-Syncollin-GFP. Transduction efficiencies for Ad-GFP-Myo5c-tail, Ad-GFP, and Ad-GFP-Myo5c-full plus tet-on helper virus averaged >90%, in accord with previous studies (Wang *et al.*, 2003). Ad-Syncollin-GFP transduction efficiency was ~80%; however, due to the high efficiency of the other constructs, in dual transduction experiments essentially all LGAC expressing syncollin-GFP also expressed GFP or GFP-Myo5c-tail

Analysis of Myo5c-enriched Vesicle Diameter: LGAC were transduced with Ad encoding GFP-Myo5c-tail or GFP-Myo5c-full and tet-on helper virus as described and were fixed and processed for confocal fluorescence microscopy. Transduced GFP-Myo5c-tail or GFP-Myo5c-full expressing cells were blocked with 1% BSA and incubated with rhodamine phalloidin to label F-actin before mounting and analysis by confocal fluorescence microscopy. Only clearly defined vesicles enriched in either GFP-Myo5c-tail or GFP-Myo5c-full were evaluated with the measurement tool function using the Zeiss LSM 510 software. Vesicles were measured at their greatest diameter. Between 12-30 fields were evaluated for each condition, with 5-10 vesicles per field measured from n=8 separate experiments of Ad-GFP-Myo5c-tail transduced and Ad-GFP-Myo5c-full transduced LGAC.

SDS-PAGE and Western Blot analysis: LG homogenate was prepared by homogenizing one LG (0.39 gm) with three 30 second pulses on ice in 2 ml of RIPA buffer (50 mM Tris-HCl, pH 7.4, 150 mM NaCl, 1 mM EDTA, 1% Triton X-100, 1% sodium deoxycholate and 0.1% SDS) containing protease inhibitor cocktail (1 mM PMSF, 5 µg/ml aprotinin and 5 µg/ml leupeptin) using a PT-MR-2100 Polytron tissue homogenizer. Blots of LG lysate were probed with appropriate primary and HRP-conjugated donkey anti-rabbit secondary antibodies (Jackson ImmunoResearch Laboratories, Inc.). Immunoblots of LG lysate were developed using SuperSignal West Pico Chemiluminescent Substrate (Pierce, Rockford, IL), and films were scanned and imaged using Adobe Photoshop. LGAC lysate was prepared by 10 passes of 3.0×10^7 LGAC through a 23 gauge needle 3x on ice in 150 µl of RIPA buffer containing protease

inhibitor cocktail. LGAC lysate was resolved by SDS-PAGE and analyzed by Western blotting with appropriate primary and IR-conjugated secondary antibodies, and analyzed using the Odyssey infrared imaging system from Li-Cor (Lincoln, Nebraska).

Immunoreactive bands were quantified using the Odyssey imaging software version 2.1 (Lincoln, Nebraska).

Transmission EM: LGAC were isolated and cultured as described above in 150 mm Petri dishes before analysis, with and without transduction with Ad constructs before processing for EM analysis. Under resting conditions and after CCh-stimulation (100 μ M, 5-15 min), samples were pelleted and resuspended in buffered 4% paraformaldehyde and 0.5% glutaraldehyde fixative for two hrs. After fixation, all cells were pelleted and dehydrated with a graded ethanol series before embedding in LR white resin (London Resin Company Ltd, Berkshire, England). The resulting blocks were sectioned on nickel grids, glycine-reduced, blocked with donkey gold conjugate blocking solution (EMS, Hatfield, PA) and exposed to rabbit anti-human Myo5c antibody followed by 10 nm gold-conjugated donkey anti-rabbit secondary antibody (EMS, Hatfield, PA). In **Figure 1D**, LGAC were fixed with 3% glutaraldehyde in 0.1 M cacodylate buffer or Sorensen's phosphate buffer (0.75M) for two hours then post-fixed with 1% osmium tetroxide/ 0.8% Potassium ferricyanide (EMS, Hatfield, PA) in Sorensen's phosphate buffer (0.375M) for two hrs at room temperature. Where used, counterstaining was done with Sato's lead stain and 2% uranyl acetate.

Secretion Assays: Bulk protein release was measured in accordance with (Jerdeva *et al.*, 2005a; Jerdeva *et al.*, 2005b). Measurement of SC and Syncollin-GFP release from LGAC grown in 12-well plates was by collection of the culture medium bathing the cells under each condition (resting or CCh-stimulated) as previously described (Jerdeva *et al.*, 2005a; Jerdeva *et al.*, 2005b). The collected culture medium was then concentrated using YM-10 Microcon centrifugal filters (Millipore, Bedford, MA), samples were resolved by 12% SDS-PAGE, transferred to nitrocellulose membranes (Whatman, Dassel, Germany), and probed with the appropriate primary and IR-conjugated secondary antibodies. Band intensity from the resulting blot was quantified for resting and CCh-stimulated samples under each condition using the Odyssey infrared imaging system from Li-Cor (Lincoln, Nebraska) and the Odyssey imaging software version 2.1 (Lincoln, Nebraska). Band intensity was normalized to LGAC protein content per well as determined by protein assay using the micro-BCA kit from Pierce (Rockford IL). The resulting values were expressed as a percentage of release from unstimulated acini either in the absence of transduction (for SC release) or in acini co-transduced with syncollin-GFP and GFP (for syncollin-GFP release).

Statistics: For secretion assays (**Figure 2-4, 2-5, and 2-7, Table 2-1**), paired comparisons of differences in vesicle diameter (**Figure 2-10C**) or paired comparisons of the percentage of actin-coated vesicles with GFP label (**Figure 2-10D**), sample sets were compared using Student's paired two sample t-test for the means for each study with a criterion for significance of $p \leq 0.05$. For comparison of vesicle diameters (**Figure 2-10B**) under each experimental condition, assay means were compared using a one-way

ANOVA followed by post analysis using a Tukey's test. The criterion for significance was $p \leq 0.05$.

Results

Myo5c is enriched on large subapical vesicles in LGAC. LGAC are grouped into functional units called acini. Within acini, each individual acinar cell is organized around a central lumen bounded by apical plasma membrane (APM) underlaid with actin filaments (Figure 2-1A). Release of tear proteins is facilitated by exocytosis of mature secretory vesicles (mSVs) at these apical domains. Contents released into lumina drain into ducts, and these small ducts ultimately converge on the main excretory duct exiting the LG for release onto the ocular surface. As shown in Figure 2-1A, when Myo5c immunofluorescence was examined in frozen sections from rat LG, it is clear that the immunofluorescence associated with this protein was concentrated beneath the APM surrounding the lumina. The immunofluorescence also appeared to be associated around the periphery of large apparent vesicles (~ 0.5 – 1.0 μm), consistent with a possible association of Myo5c with mSVs. Figure 2-1A also shows Myo5c immunofluorescence in primary cultures of rabbit LGAC that have been grown under conditions which allow reassociation of the isolated cells into acinar-like structures (see Schematic for organization of apical and basolateral domains within the reconstituted acini). In these reconstituted acini, Myo5c immunofluorescence is also very clearly concentrated immediately beneath lumina that reform between the adjacent epithelial cells and that are delineated by the subapical actin cytoskeleton. Examination of high magnification images of LGAC labeled to detect Myo5c suggest that not all apparent large mSVs may be enriched in this protein (data not shown). This is consistent with EM analysis of SV morphology and composition, showing the presence of a heterogenous SV pool in LGAC

Figure 2-1. Localization of endogenous Myo5c and actin filaments in LG and LGAC. A. Top: Fluorescence micrograph of a frozen section from rat LG tissue illustrates the clear localization of Myo5c (arrows) in the subapical cytoplasm beneath the apical actin. **Middle:** Rabbit LGAC viewed by confocal/DIC overlay and presented schematically to indicate the cellular organization and cell polarity within the reconstituted acinus. Lumena surrounded by APM delineated by the intense actin filament labeling (red lines) are marked by (*) while basolateral membranes are delineated by the less intense actin filament labeling (black lines). **Bottom:** Confocal fluorescence microscopy image of reconstituted rabbit LGAC showing the localization of Myo5c (arrows) in the subapical cytoplasm beneath the apical actin. Overlay: DIC, Myo5c and Actin. **B.** Western blot showing expression of three class V Myosins in rabbit LG homogenate. **C.** Western blot showing Myo5c enrichment in insoluble (membrane + cytoskeleton) and soluble (cytoplasmic) fractions. LGAC lysate was concentrated and adjusted to the same volume and equal volumes were loaded. **D.** TEM micrograph of LGAC in culture organized around a central lumen (L) reveal a heterogeneous group of SVs of varying densities and sizes. All bars, ~5 μm .

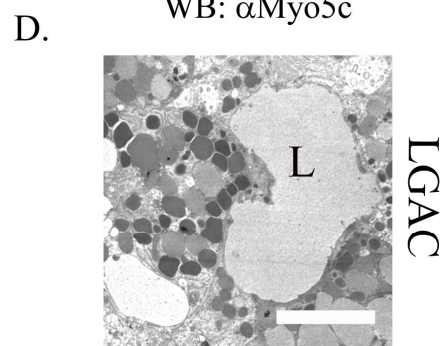
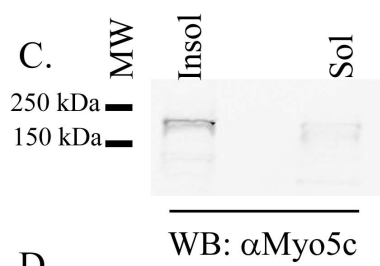
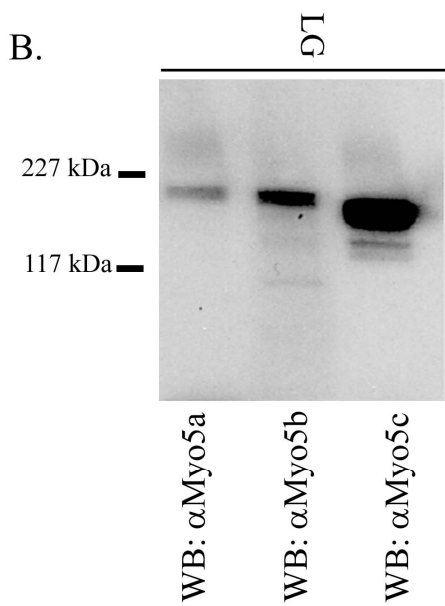
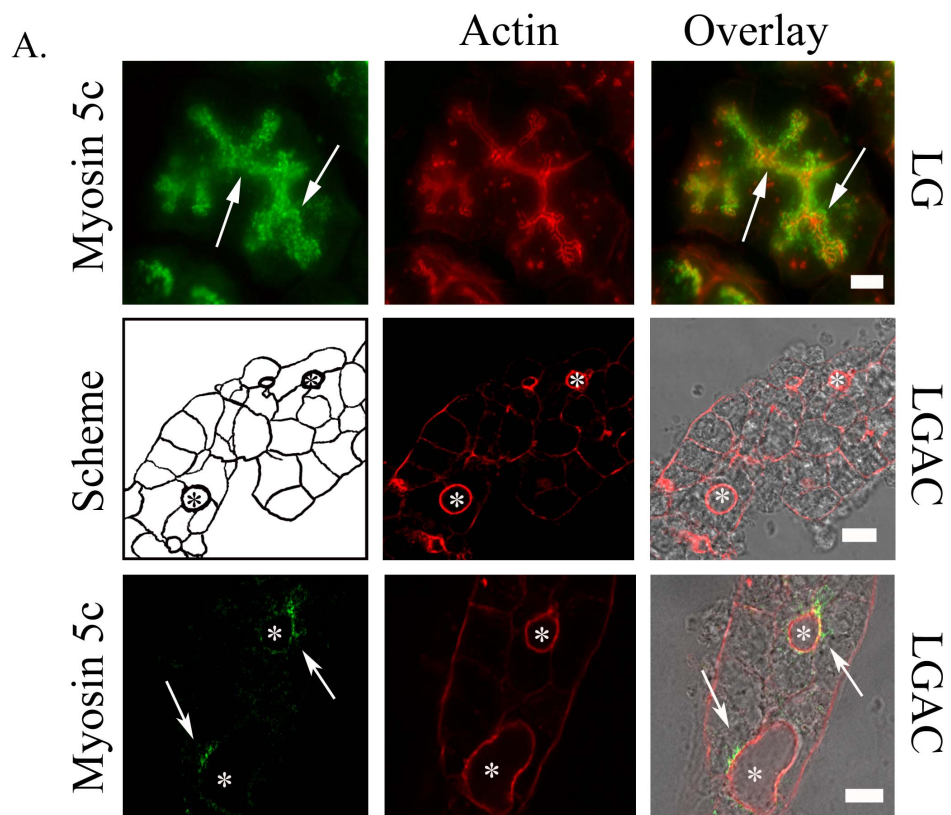
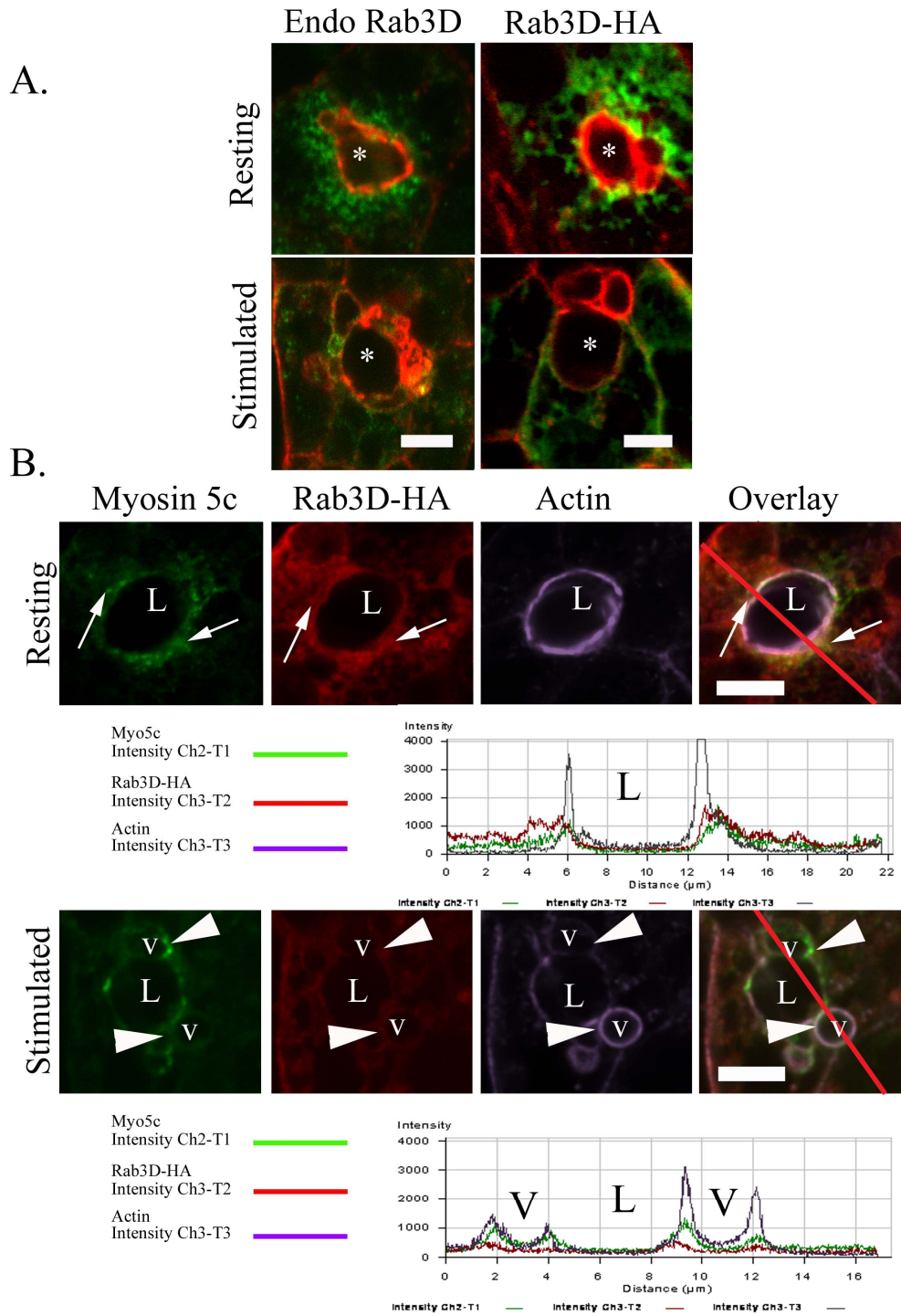


(**Figure 2-1D**). Note that the EM image shows that SVs occupy a significant amount of the cytoplasm, extending from the area immediately beneath the APM to the cell interior.

Western blot analysis of rabbit LG homogenate confirmed the abundant expression of Myo5c in this tissue (**Figure 2-1B**), although, Myo5a and Myo5b were also detected in LG. When extracts of LGAC homogenate were further divided into insoluble and soluble (supernatant) fractions, we found that Myo5c was largely concentrated with the insoluble fraction (e.g., membranes and cytoskeleton, **Figure 2-1C**).

Co-localization of Myo5c immunofluorescence with that of Rab3D suggests that this motor is associated with the most apically-enriched mSVs. Since the largely subapical and vesicular labeling pattern of Myo5c immunofluorescence occurred in a region enriched in mSVs in LGAC, we explored its co-localization with mSV markers. Rab3D is the best characterized marker for mSV in a variety of acinar cells including LGAC (Wang *et al.*, 2003), pancreatic acinar cells (Chen *et al.*, 2002) and parotid acinar cells (Riedel *et al.*, 2002). We transduced LGAC with an Ad construct encoding HA-tagged Rab3D to conduct this analysis, since the antibodies we had available to Rab3D and Myo5c were both from rabbit. As we demonstrate in **Figure 2-2A**, Rab3D-HA in transduced LGAC has a distribution comparable to that of endogenous rab3D in resting LGAC. Rab3D-HA also exhibits the shift from a largely subapical localization to a less subapical and more dispersed location in response to CCh stimulation that is characteristic of the endogenous protein (Wang *et al.*, 2003). However, in transduced LGAC, particularly after CCh-stimulation, Rab3D-HA can be more readily detected throughout the cytoplasm including the areas adjacent to the basolateral membrane. This

Figure 2-2: Myo5c and Rab3D co-localized in LGAC. **A:** Confocal fluorescence microscopy analysis of LGAC labeled with antibodies or affinity label to detect Rab3D (**green**) and actin filaments (**red**) without (Resting) or with CCh (100 μ M, 15 min) (Stimulated) for both endogenous Rab3D (Endo Rab3D) versus the Rab3D-HA introduced by Ad transduction. **B.** Higher magnification images of resting and CCh-stimulated LGAC transduced with Ad-Rab3D-HA and labeled to detect Rab3D-HA (**red**), Myo5c (**green**) and actin filaments (**purple**). Luminal area is indicated by asterisk (*). Line scan analysis (**red line**) using the LSM 510 co-localization software was conducted on the overlay image to confirm co-localization by coincident alignment of fluorescent peak intensities. These plots show the relative intensities of Myo5c (**green**), Rab3D-HA (**red**), and actin (**purple**) along the line. Areas devoid of fluorescence such as the luminal space (L) and the lumen of actin-rich vesicles (V) are indicated on the plot. All bars, \sim 5 μ m.



is not a basolateral enrichment, but rather reflects the high abundance of this overexpressed protein in transduced LGAC, and its concentration in spaces void of SVs, which occupy less space near the basolateral membrane.

Comparison of the distributions of Myo5c and Rab3D in **Figures 2-1** and **2-2** suggested that Myo5c might label the most apical pool of mSVs enriched in Rab3D. As shown in **Figure 2-2B**, high magnification images of the luminal regions of LGAC acini showed that Rab3D-HA immunofluorescence was associated with broad array of subapical SVs extending from the APM well into the cell interior. Myo5c immunofluorescence appeared to be consistently co-localized with the most apical pool of Rab3D-HA-enriched vesicles. This finding was verified by the comparison of the the fluorescent peaks associated with each marker along the line scan. When transduced cells were stimulated with CCh, there was an apparent decrease in co-localization between Myo5c and Rab3D. This change in co-localization appeared to be largely due to diminished intensity of Rab3D fluorescence adjacent to the APM. This observation was verified by comparison of the coincident peaks of fluorescence intensity associated with each marker along the line scan. The shift away from an apical Rab3D-HA enrichment is also supported by the reduction in peak intensity for this signal adjacent to the apical actin. We calculated that the extent of total Myo5c pixels (green) that were co-localized with total Rab3D-HA pixels (red) in resting acini was $42 \pm 3\%$; in contrast, there was a statistically significant 31 % decrease in the extent of total Myo5c pixels that were co-localized with Rab3D-HA pixels to $29 \pm 5\%$ in CCh-stimulated acini (results from N = 7 preparations). In addition to the co-localization analysis between total Myo5c pixels (green) and Rab3D-HA pixels (red), further co-localization analysis was done comparing

total Rab3D-HA (red) and total Myo5c (green) pixels. The percentage of total rab3D-HA pixels (red) co-localized with Myo5c pixels (green) was $30 \pm 2\%$ in resting acini (n=7). A small but not statistically significant reduction in total Rab3D-HA fluorescence pixels (red) co-localized with Myo5c pixels (green) in CCh-stimulated LGAC was seen ($26 \pm 4\%$, n=7). This lower percentage of co-localization of the total fluorescent Rab3D-HA signal with Myo5c may partially reflect the high Rab3D-HA fluorescent signal that results from overexpression, but is also consistent with our observation that not all the Rab3D-HA-enriched mSVs were enriched in Myo5c.

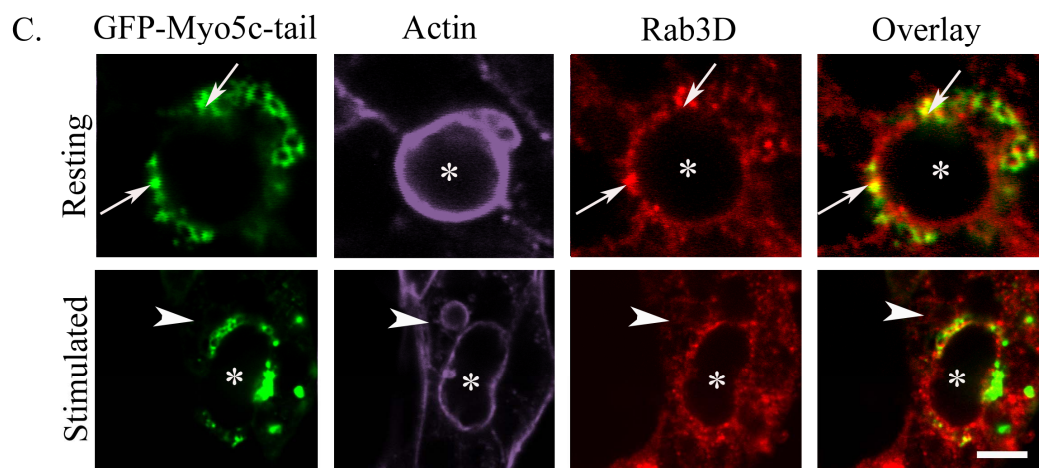
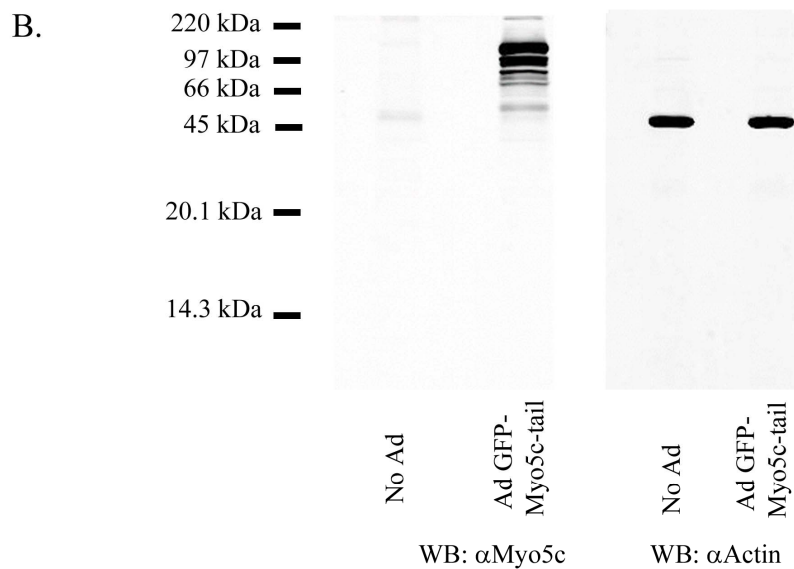
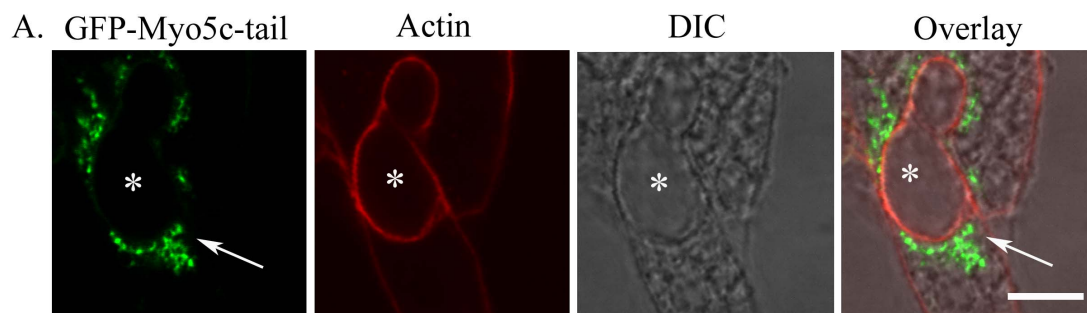
Another feature that was clearly evident in the CCh-stimulated LGAC was the formation of actin-coated structures at or adjacent to the APM. Our previous data suggest that these structures encompass fusion intermediates formed by multiple fusing mSVs; moreover, we have hypothesized that contraction of the actin coat facilitates extrusion of the contents of the vesicles at select regions within the APM (Jerdeva *et al.*, 2005b). Although Rab3D-HA was less concentrated on these actin-coated structures, the Myo5c remained highly enriched as verified by the coincidence of peaks associated with Myo5c and actin fluorescence along the line scan. We also noted that Myo5c distribution on vesicular structures beneath the APM was patchy, particularly in CCh-stimulated LGAC.

Although the use of Rab3D-HA to transduce LGAC suggested the association of Myo5c with subapical Rab3D-enriched vesicles, overexpression of Rab3D generated a higher background signal throughout the cytoplasm that was potentially problematic. We therefore utilized a sequential labeling technique using rabbit polyclonal antibodies against both Myo5c and endogenous Rab3D to verify the co-localization of these markers

in the resting LGAC and the apparent increase in Myo5c with actin-coated fusion intermediates in the CCh-stimulated LGAC. As shown in **Supplemental Figure 2-1**, this analysis was consistent with the findings in **Figure 2-2B**.

Dominant negative Myo5c fused to GFP is also co-localized with subapical mSVs in LGAC. Previous work has described the generation of a dominant negative (DN) Myo5c tail construct fused to GFP (Rodriguez and Cheney, 2002). The tail construct is thought to elicit its DN effect by competing with endogenous Myo5c for vesicle binding sites. To express this GFP-Myo5c-tail construct in LGAC, we cloned the construct in an Ad expression system for transduction of primary LGAC. Ad reproducibly elicits between an 80-95% transduction efficiency of LGAC, as previously reported (Wang *et al.*, 2003; Jerdeva *et al.*, 2005a; Jerdeva *et al.*, 2005b), and this construct behaved similarly to those we have previously characterized in generating high efficiency transduction. Confocal fluorescence microscopy indicated that the overexpressed fusion protein was associated with large subapical vesicles, likely mSVs (**Figure 2-3A**), which showed a distribution comparable to the endogenous protein (**Figures 2-1** and **2-2**). Analysis of LGAC lysates from cells transduced with the construct revealed the presence of the fusion protein at ~120 kD as well as some additional lower MW bands possibly representing partially degraded fusion protein (**Figure 2-3B**). The endogenous protein could still be detected at the top of each lane in transduced and non-transduced samples, but the signal was weak compared to the overexpression of the fusion protein construct. Stripping and reprobing

Figure 2-3: GFP-Myo5c-tail associates with mature SVs. **A.** Confocal fluorescence microscopy analysis of LGAC transduced with Ad-GFP-Myo5c-tail shows association with apparent mSVs (arrows) beneath the lumen (*). **B:** Western blot of LGAC lysates without (No Ad) or with (Ad-GFP-Myo5c-tail) transduction. The same blot was probed with anti-Myo5c antibody (left), prior to stripping and reprobing with an anti-actin antibody (right) to confirm equal protein loading. **C:** Confocal fluorescence micrographs of resting and CCh-stimulated LGAC transduced with GFP-Myo5c-tail (**green**) and fixed and labeled to detect Rab3D (**red**) and actin filaments (**purple**). Arrows, GFP-Myo5c-tail-enriched vesicles co-localized with endogenous Rab3D. Arrowhead, actin-coated structure with little GFP-Myo5c-tail. Overlay: GFP-Myo5c-tail and Rab3D only; Bars, ~5 μ m.

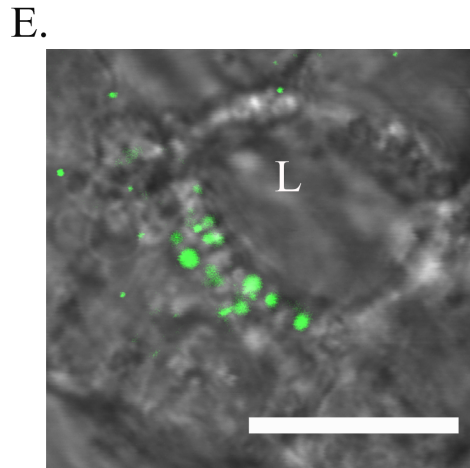
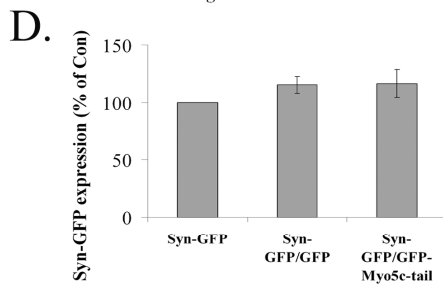
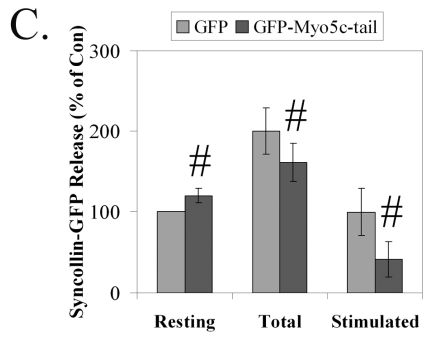
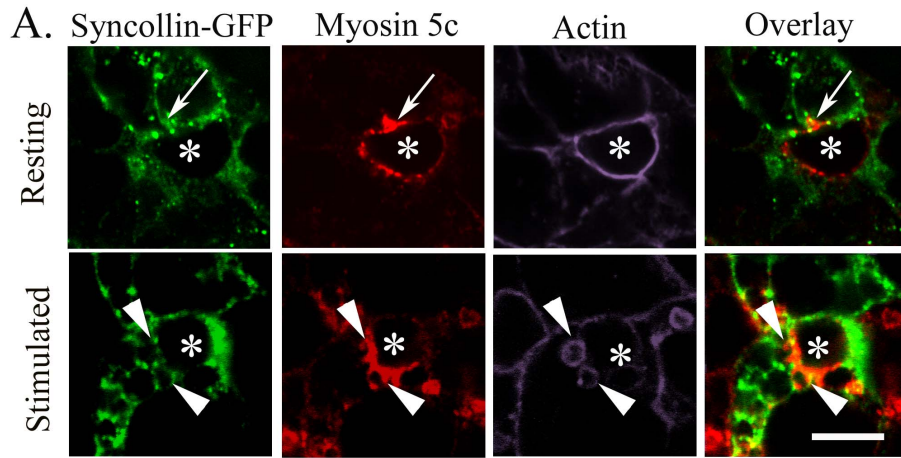


of the blot for actin content confirmed that equivalent protein was loaded from each lysate.

We investigated the changes in the distribution of the DN fusion protein in response to CCh. As shown in **Figure 2-3C**, there were no significant changes in the distribution of GFP-Myo5c-tail after CCh stimulation. Notably, we did detect the formation of actin-coated fusion intermediates in CCh-stimulated LGAC (arrowhead in **Figure 2-3C**) but, unlike the endogenous protein, which was associated with these actin coats in untransduced acini, the GFP-Myo5c-tail was not as frequently associated with these putative fusion intermediates.

GFP-Myo5c-tail expression selectively inhibits the CCh-stimulated release of secretory proteins from mSVs. In order to understand whether Myo5c function was essential for exocytosis, we examined the effect of the DN construct on release of different secretory products. Since both the endogenous Myo5c and the GFP-Myo5c-tail appeared to localize specifically to mSV, we focused on evaluating the effects of GFP-Myo5c-tail on specific mSV markers. We have established in previous work that syncollin, a protein originally identified in exocrine pancreas, can label a subpopulation of mSV in LGAC when introduced utilizing Ad-mediated expression. These SVs are most clearly seen in the confocal/DIC overlay image of live LGAC in **Figure 2-4E**, adjacent to the lumen. We have previously demonstrated in reconstituted acini that the lumina are open to the culture medium and that apical exocytosis of different content proteins can be measured in culture supernatant (Jerdeva *et al.*, 2005b). Syncollin secretion can be also followed biochemically by Western blotting of the culture medium; its release at the APM is

Figure 2-4: Expression of GFP-Myo5c-tail suppresses CCh-stimulated syncollin-GFP release in LGAC. **A.** Confocal fluorescence microscopy analysis of resting and CCh-stimulated (100 μ M, 15 min) LGAC transduced with Ad-syncollin-GFP (**green**) and then labeled with antibodies and affinity label to detect endogenous Myo5c (**red**) and actin filaments (**purple**). Arrows, syncollin-GFP co-localization with Myo5c in the subapical cytoplasm; Arrowheads, actin-coated structures containing Myo5c and syncollin-GFP. Overlay: Syncollin-GFP and Myo5c only; lumena, *; bar, \sim 5 μ m. **B.** and **C.** LGAC were doubly-transduced with Ad-Syncollin-GFP and Ad-GFP-Myo5c-tail (Syn-GFP/ GFP-Myo5c-tail) or Ad-Syncollin-GFP and Ad-GFP (Syn-GFP/ GFP) as described in **Methods**. Culture medium was collected in the resting state (Resting) and after CCh stimulation (Total, 100 μ M, 30 min) under each condition and concentrated and analyzed by Western blotting for syncollin-GFP content. **B.** shows a representative blot while **C.** depicts values from multiple experiments. Basal and total release were plotted directly, while the stimulated component was obtained by subtracting basal from total to yield the amount of release attributable to CCh. n= 11 assays and # indicates significance at $p \leq 0.05$. **D.** shows relative Syncollin-GFP expression in LGAC cell lysate transduced as in **C.** as analyzed from LGAC lysate by Western blotting (n=3). For **C.** and **D.**, band intensity values were measured and signal normalized to protein and averaged across assays (bars represent SEM). **E.** shows a live cell DIC/confocal fluorescence overlay of Syncollin-GFP in live LGAC. Lumen, (L) and bar, 5 μ m.



highly sensitive to CCh stimulation (Jerdeva *et al.*, 2005a; Jerdeva *et al.*, 2005b). When syncollin-GFP is expressed in LGAC, as shown in **Figure 2-4A**, there is considerable Myo5c associated with these mSVs in resting LGAC as well as recruited to actin-coated fusion intermediates containing syncollin-GFP in CCh-stimulated LGAC, confirming that this marker is of relevance to the Myo5c pathway in LGAC. The more diffuse syncollin-GFP below the basolateral membrane is likely Golgi and trans-Golgi network associated, since these compartments are located beneath the nucleus and towards the basolateral membrane in LGAC.

LGAC were co-transduced with syncollin-GFP and either GFP-Myo5c-tail or GFP alone, and the effects on CCh-stimulated release of syncollin-GFP assessed. **Figure 2-4B** shows a representative Western blot, indicating that LGAC transduced with GFP-Myo5c-tail had reduced syncollin-GFP released into the culture medium following CCh stimulation. **Figure 2-4C** plots the results of multiple assays showing that the total release (resting + stimulated) of syncollin-GFP in LGAC, as well as the release attributable to CCh stimulation, were both significantly reduced by GFP-Myo5c-tail expression. A slight but statistically significant increase in basal release of syncollin-GFP was also caused by GFP-Myo5c-tail. The reason for this small basal increase is unknown but might include a general efflux of overexpressed syncollin-GFP through constitutive pathways if defects in the capacity of the regulated secretory pathway were caused by with GFP-Myo5c-tail expression. It is also possible that Myo5c may act to tether resting SVs on subapical actin and somehow clutch or brake their movement. Alternatively this might be due to subtle functional changes in the subapical actin barrier in resting LGAC caused by the GFP-Myo5c-tail. **Figure 2-4D** shows that the decrease in

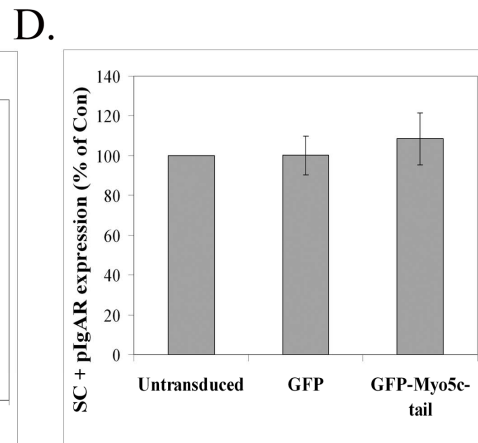
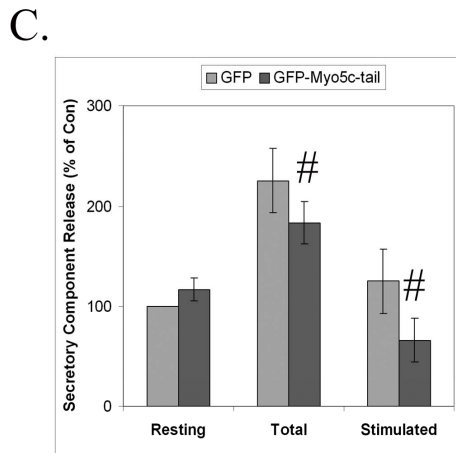
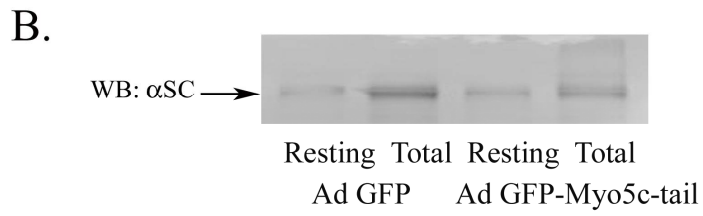
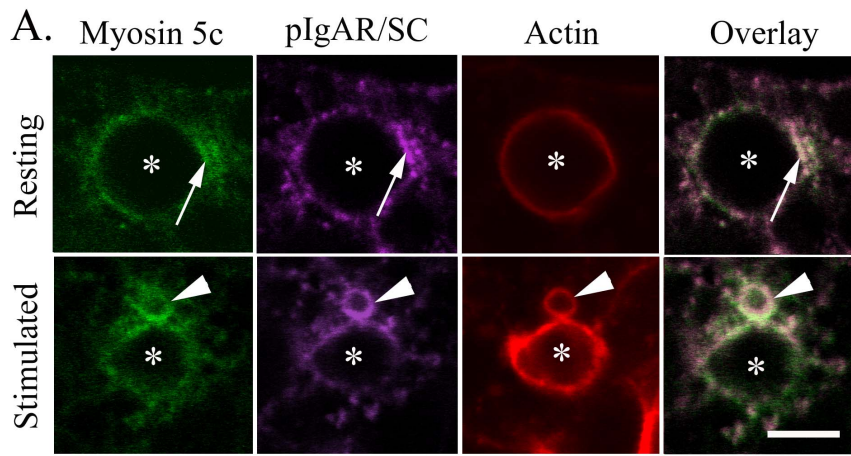
CCh-stimulated syncollin-GFP release is not due to changes in syncollin-GFP expression in cells expressing GFP-Myo5c-tail.

We wanted to assess an additional content marker of mSVs and chose to evaluate the release of SC from the subpopulation of pIgAR sequestered in mSVs. In polarized epithelial cells like MDCK cells, trafficking of pIgAR has largely been elucidated in the context of its movement within the transcytotic pathway, in a ligand-free form or bound to its ligand, dIgA. However, our recent work has established that this receptor is considerably enriched in mSV in LGAC (Jerdeva *et al.*, 2005a). pIgAR present in pre-formed vesicles is slowly cleaved to release free secretory component from the extracellular domain of this protein, which is released in a bolus following CCh-stimulated exocytosis of mSVs. This sorting occurs via a unique interaction of Rab3D with pIgAR to regulate its entry into and release from mSVs (Evans *et al.*, 2008).

Figure 2-5A shows the immunofluorescence signal associated with pIgAR/SC in LGAC. Since the antibody is to the extracellular domain of rabbit pIgAR (equivalent to SC), we cannot distinguish between the intact protein versus the cleaved SC fragment by immunofluorescence. Clearly, a considerable amount of pIgAR/SC immunofluorescence was detected in very large, mSV-sized vesicles immediately beneath the APM. We have established that these structures are enriched in rab3D (data not shown). Endogenous Myo5c is co-localized with pIgAR/SC in resting as well as CCh-stimulated LGAC. In particular, in the CCh-stimulated sample, both Myo5c and pIgAR/SC are detected within an actin-coated fusion intermediate. **Figures 2-5B** and **2-5C** indicate the results from a sample experiment and composite experiments, respectively. These data show that the total release of SC, as well as the release attributable to CCh stimulation were both

Figure 2-5: Expression of GFP-Myo5c-tail suppresses CCh-stimulated SC release in

LGAC. A. Confocal fluorescence microscopy analysis of resting and CCh-stimulated (100 μ m, 15 min) LGAC labeled with antibodies and affinity label to detect Myo5c (**green**), pIgAR/SC (**purple**) and actin filaments (**red**). Arrow, co-localization between Myo5c and pIgAR/SC; Arrowhead, co-localization of Myo5c and pIgAR/SC with an actin-coated structure. Lumena, *; bar, \sim 5 μ m. **B.** and **C.** LGAC were transduced with either Ad-GFP-Myo5c-tail or Ad-GFP as described in **Methods**. Culture medium was collected in the resting state (Resting) and after CCh stimulation (Total, 100 μ M, 30 min) under each condition, and concentrated and analyzed by Western blotting. **B.** shows a representative blot while **C.** depicts values from multiple experiments. Basal and total release were plotted directly, while the stimulated component was obtained by subtracting basal from total to yield the amount of release attributable to CCh. n= 10 assays and # indicates significance at $p \leq 0.05$. **D.** shows relative pIgAR/SC (summed) expression in LGAC without or with transduction with Ad-GFP (GFP) or Ad-GFP-Myo5c-tail (GFP-Myo5c-tail) as analyzed from LGAC lysate by Western blotting for pIgAR/SC content (n=5). Band intensity values were measured and signal normalized to protein and averaged across assays (bars represent SEM).



significantly reduced by the GFP-Myo5c-tail. **Figure 2-5D** shows that expression of GFP-Myo5c-tail does not affect cellular pIgAR and SC expression.

As shown in **Table 2-1**, overexpression of GFP-Myo5c-tail elicited no remarkable changes in the CCh-stimulated release of bulk protein, which reflects the secretagogue-enhanced trafficking of a variety of different vesicle populations including both mSV as well as vesicles trafficking through the transcytotic pathway. Combined with the finding that Myo5c and the GFP-Myo5c-tail appeared to label only a subset of the detectable large mSV in LGAC, these data suggest that the effect of GFP-Myo5c-tail is selective for certain mSV subpopulations.

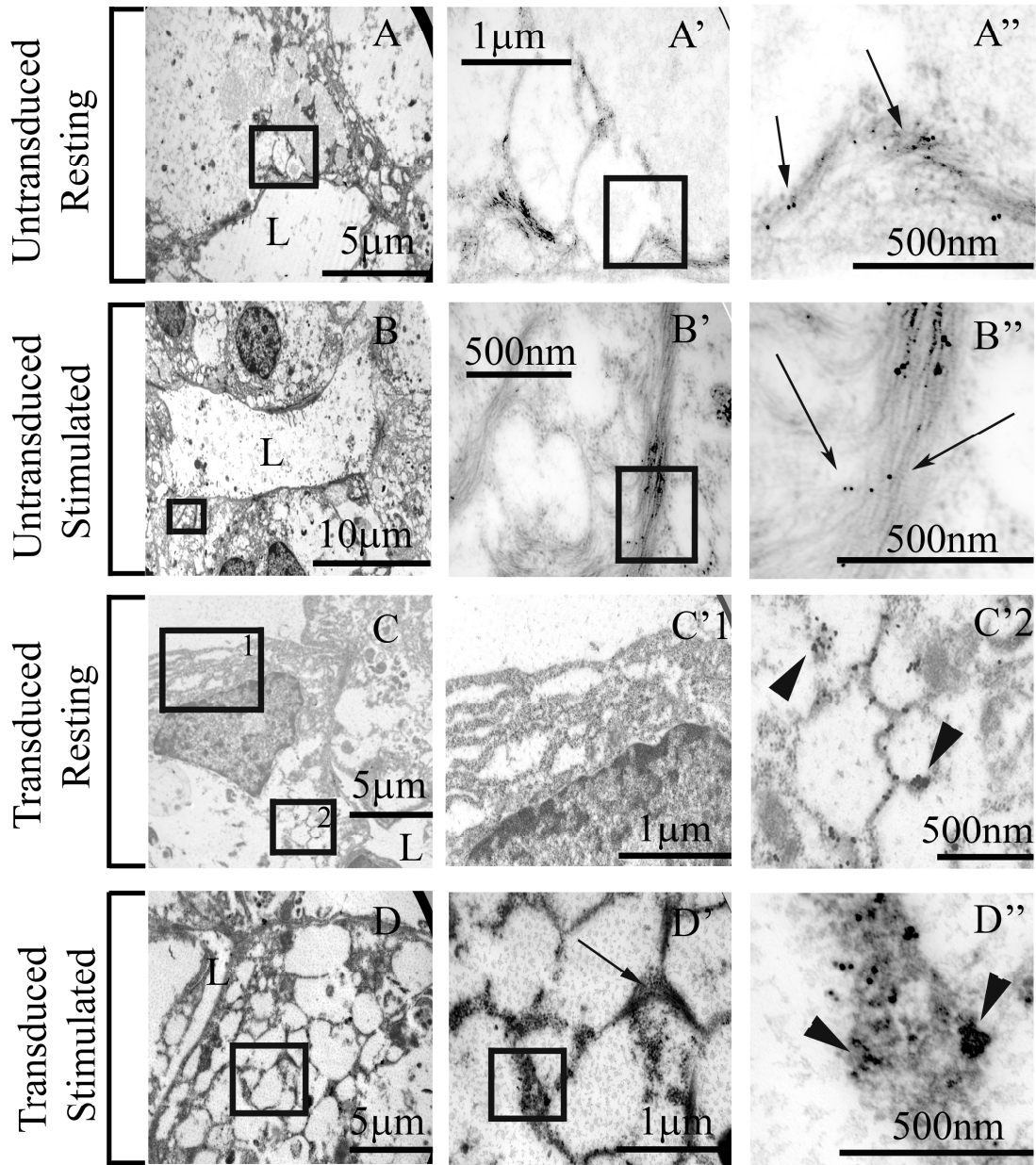
EM reveals Myo5c association with mSV and actin filaments underlying mSV. Here, we report for the first time, a successful attempt to observe Myo5c localization at the EM level. The results thus far suggested that Myo5c in LGAC was associated with mSVs and that it functioned in their exocytosis. To understand further the mechanisms of its involvement, we examined the cellular localization of endogenous Myo5c in resting and CCh-stimulated LGAC using immunogold labeling and EM. The panels in **Figure 2-6** reveal gold associated with endogenous Myo5c in regions surrounding the remnants of mSVs located beneath luminal regions. When the regions are expanded (see **A'**, **A''**), gold labeling is clearly localized to filament-enriched regions between the clustered mSV remnants. We note that the apparent actin filaments shown here by EM are not evident by confocal fluorescence microscopy in resting LGAC, suggesting that they are not highly abundant under these conditions and/or not readily accessible to added phalloidin. Examination of endogenous Myo5c in acini exposed to CCh revealed a more abundant

Table 2-1. Bulk Protein release in LGAC transduced with GFP or GFP-Myo5c-tail.

Treatment	Resting	Total	CCh-stimulated component
Ad-GFP	100%	462±85%	362±85%
Ad-GFP-Myo5c-tail	93 ± 9%	418 ± 79%	324 ± 81%

Resting values reflect release into culture medium over 30 minutes in the absence of stimulation. Total values reflect release over 30 minutes in the presence of 100 μ M CCh. The CCh-stimulated component reflects the Total minus the Resting Release. All values were normalized to protein content of the cell pellet before comparison. Results are from n=10 separate preparations and errors indicate S.E.M.

Figure 2-6: Electron Microscopy micrographs of Myo5c and GFP-Myo5c-tail enriched around mSV in resting and CCh-stimulated LGAC. TEM images at low and higher magnification of resting untransduced LGAC (Panel A and magnifications), CCh-stimulated (100 μ M CCh, 15 min) untransduced LGAC (Panel B and magnifications), resting Ad-GFP-Myo5c-tail-transduced LGAC (Panel C and magnifications), and CCh-stimulated (100 μ M CCh, 15 min) Ad-GFP-Myo5c-tail-transduced LGAC (Panel D and magnifications) were obtained from samples fixed and processed for immunogold labeling of Myo5c or GFP-Myo5c-tail as described in **Methods**. Selected regions (boxes) (from **Panels A, B, and D**) have been enlarged in **Panels A', B', and D'**. Further enlargements are shown in **Panels A'', B'' and D''**. Two different selected regions (boxes 1 and 2) in **C** are magnified to the right in **C'1 and C'2**. Immunogold label associated with actin are indicated by arrows. Immunogold label associated with apparent secretory vesicles are indicated with arrowheads.



filament network underlying mSVs, consistent with what we detect by confocal fluorescence microscopy as actin-coated fusion intermediates. Intriguingly, these actin filaments had clearly detectable Myo5c enrichment as evidenced by the increased abundance of gold particles associated within the filament network.

Figure 2-6 also shows gold labeling associated with overexpressed GFP-Myo5c-tail in transduced LGAC in the presence and absence of CCh. As is evident under each condition, a dense network of gold particles was detected in regions between adjacent mSVs. The addition of CCh did not elicit any changes in gold labeling patterns at the microscopic level, in contrast to the apparent redistribution to filament-rich regions seen in non-transduced, CCh-stimulated acini. Finally, magnification of regions of cytosol lacking mSV (**Figure 2-6, box C1**) at the basal cytoplasm did not show any evidence of significant gold labeling, suggesting that the overexpressed GFP-Myo5c-tail was specifically targeted to areas rich in mSV. Morphology in these specimens was not optimally preserved because the samples were not subjected to osmification.

LGAC overexpressing GFP-Myo5c-tail exhibit changes consistent with impaired compound fusion relative to LGAC expressing GFP-Myo5c-full. Although we saw evidence by confocal fluorescence microscopy (**Figures 2-3 thru 2-5**) and EM (**Figure 2-6**) that the relationship between actin coats assembled around putative fusion intermediates and SVs might be altered in LGAC overexpressing GFP-Myo5c-tail, it was difficult to come to firm conclusions because of some loss of morphology required to preserve antigen immunoreactivity in order to detect Myo5c by immunogold labeling. We therefore decided to compare SV parameters using confocal fluorescence

microscopy, by labeling SVs either with GFP-Myo5c-tail or with GFP-Myo5c-full length protein, which is functionally competent. We developed an Ad construct encoding GFP-Myo5c-full in a Tet-on system, to allow regulated expression of a large protein (~230 kD). This construct, plus the Ad-tet-on helper virus were used to transduce LGAC as described in **Methods**. **Figure 2-7A** shows the localization of GFP associated with GFP-Myo5c-full in structures resembling subapical mSVs, comparable to the labeling exhibited by GFP-Myo5c-tail. Like GFP-Myo5c-tail, GFP-Myo5c-full was co-localized with endogenous Rab3D in resting LGAC as shown in **Figure 2-7D**. Furthermore, GFP-Myo5c-full appears to be enriched in actin-coated fusion intermediates in CCh-stimulated LGAC, similar to endogenous Myo5c, and to have a patchy distribution, also as noted for the endogenous Myo5c. The Western blot in **Figure 2-7B** shows the relative expression of Myo5c in LGAC transduced with GFP-Myo5c-tail or GFP-Myo5c-full, relative to non-transduced LGAC, indicating the comparable overexpression of the GFP-fusion proteins under the conditions of our assays

To further validate that GFP-Myo5c-tail and GFP-Myo5c-full labeled the same SV population, we compared the co-localization of each of these proteins with the pIgAR; this protein and its soluble cleavage product, SC, are localized to Rab3D-enriched SVs in LGAC (Evans *et al.*, 2008). As shown in **Figure 2-8A**, GFP-Myo5c-full labels an array of apparent mSVs with fluorescence co-localized with that of pIgAR as shown by the line scan. In **Figure 2-8B**, the labeling of this pIgAR-enriched subapical SV population was similarly enriched with GFP-Myo5c-tail. These data reinforce the initial findings with Rab3D that both Myo5c constructs label comparable mSV populations.

Figure 2-7: GFP-Myo5c-full is localized to mSVs. **A.** Confocal fluorescence microscopy analysis of LGAC co-transduced with Ad-GFP-Myo5c-full and tet-on Ad helper virus and exposed to doxycycline as described in **Methods** shows its association (**green**, arrows) with apparent mature SVs around the lumen (*) identified by actin filament labeling (red). **B.** Western blotting of lysates from non-transduced (No Ad) and transduced LGAC with an antibody to Myo5c (upper blot). Equal sample loading (40 μ g lysate) was demonstrated by reprobing of blots with an anti-actin antibody (lower blot). **C.** LGAC were transduced with either Ad-GFP-Myo5c-full or Ad-GFP as described in **Methods**. Culture medium was collected in the resting state (Resting) and after CCh stimulation (Total, 100 μ M, 30 min) and concentrated and analyzed by Western blotting. Basal and total release were plotted directly, while the stimulated component was obtained by subtracting basal from total to yield the amount of release attributable to CCh. n= 15 assays. **D.** Subapical regions of LGAC expressing GFP-Myo5c-full (**green**) show GFP fluorescence on subapical vesicles co-localized (arrows) with Rab3D (**red**) beneath luminal regions (*) in resting LGAC. In CCh-stimulated LGAC (100 μ M, 15 min), GFP-Myo5c-full was co-localized with actin-coated structures (arrowhead). Overlay: GFP-Myo5c-full and Rab3D only; bars, \sim 5 μ m.

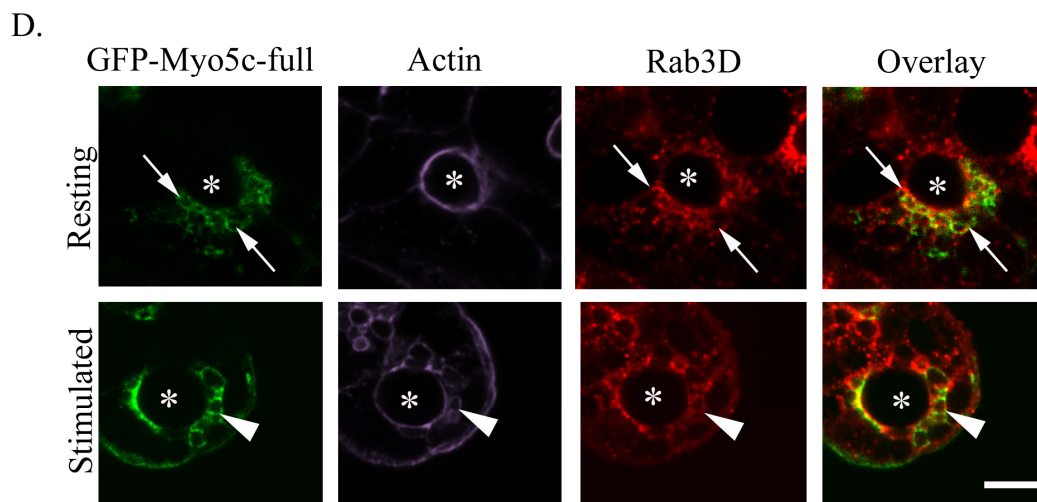
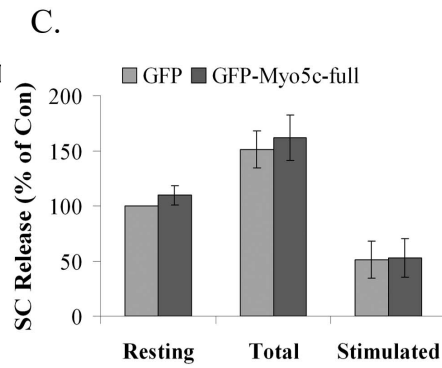
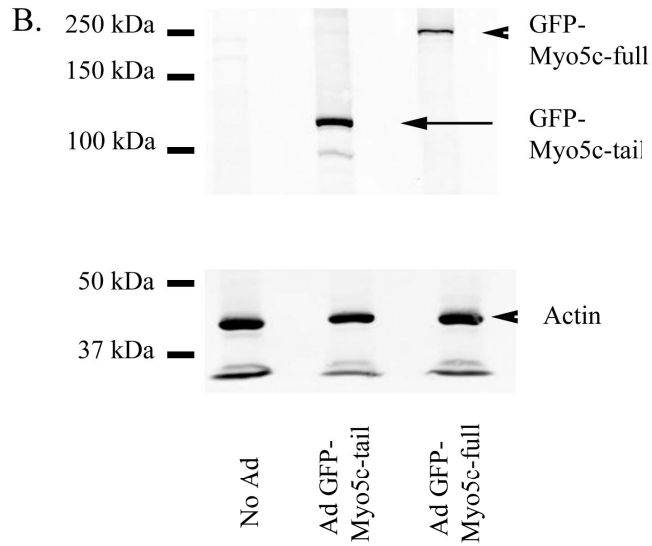
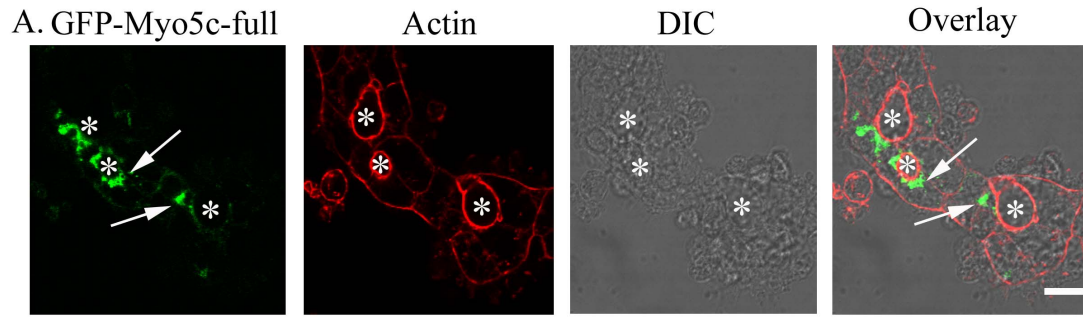
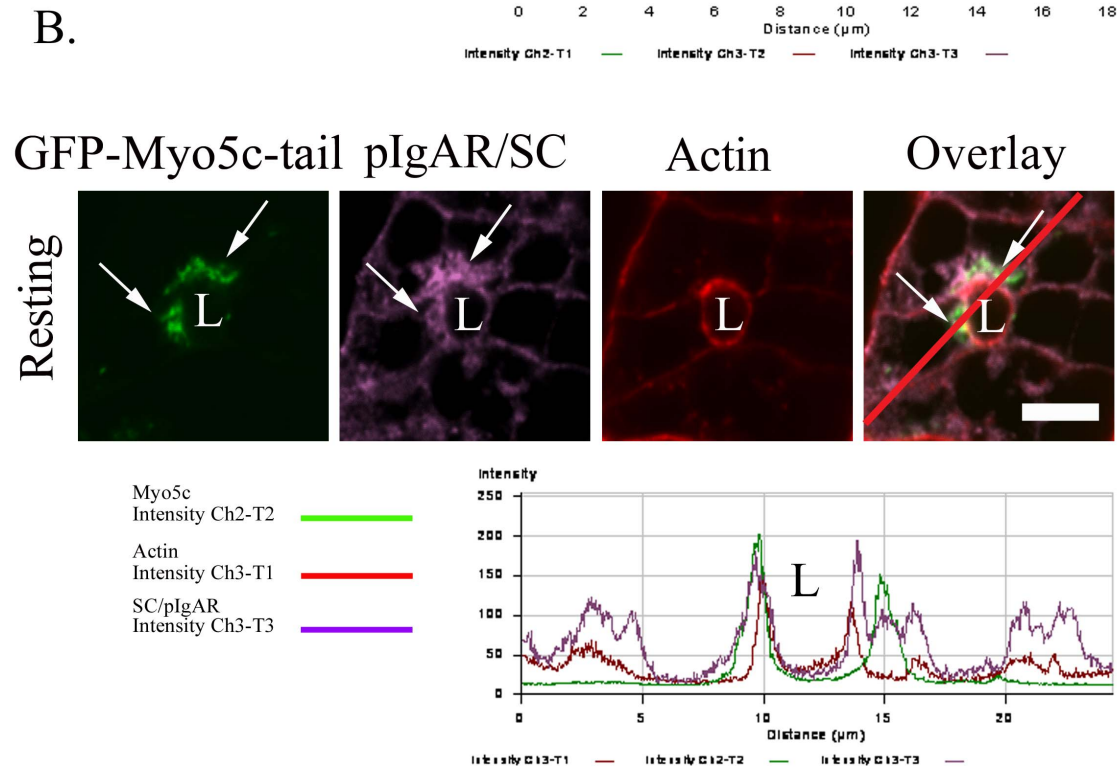
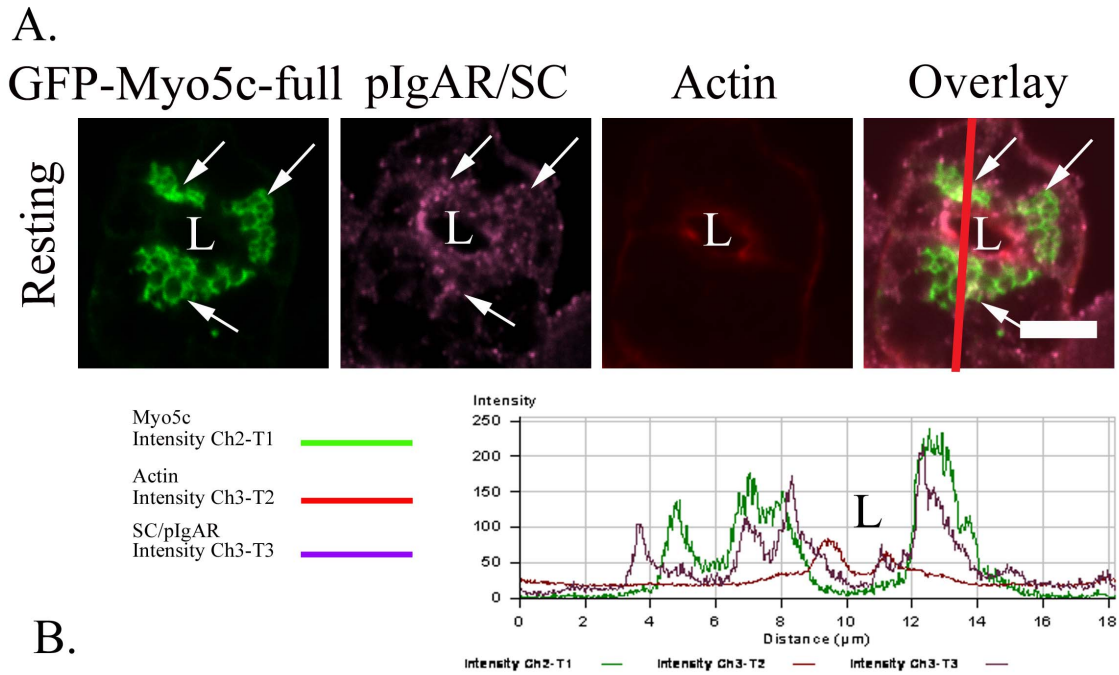


Figure 2-8: GFP-Myo5c-full and GFP-Myo5c-tail both localize to pIgAR/SC enriched mSVs beneath the APM. Confocal fluorescence microscopy analysis of resting LGAC transduced with Ad-GFP-Myo5c-full (**A, green**) or Ad-GFP-Myo5c-tail (**B, green**) and then labeled with antibodies and affinity label to detect endogenous pIgAR/SC (**purple**) and actin filaments (**red**). Co-localization of both Myo5c constructs with pIgAR/SC fluorescence is shown by **arrows**. Co-localization was confirmed using line scan analysis (**red line overlay**) and the fluorescence intensity plots for each marker are shown below the images. Areas devoid of fluorescence such as the lumena (L) and actin-coated vesicles (V) are marked on the line scan. Bars, $\sim 5\mu\text{m}$.



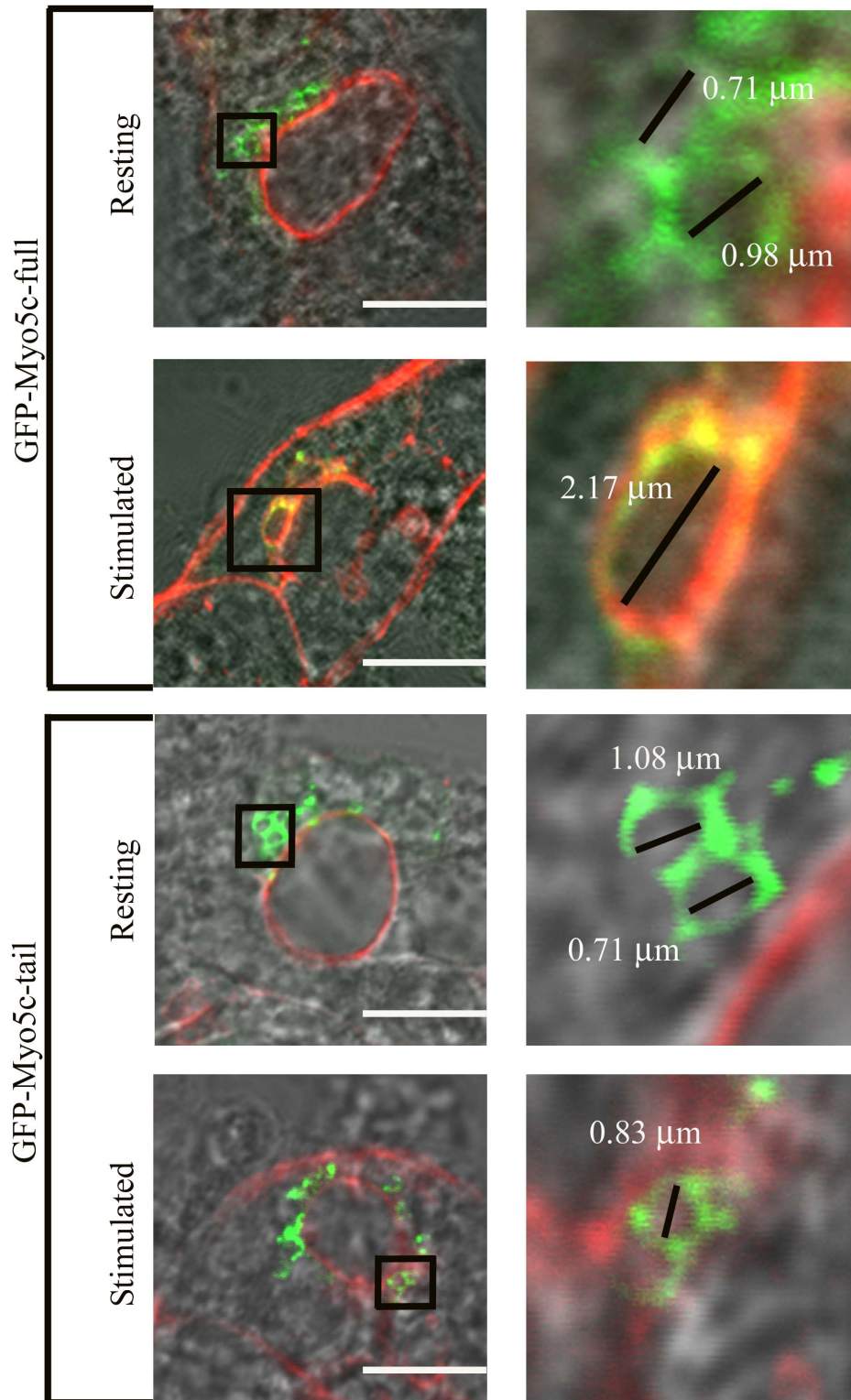
To confirm that the GFP-Myo5c-full did not adversely affect secretory functions in LGAC, we also measured SC release in LGAC transduced with this construct. As shown in **Figure 2-7C**, no effect was seen on basal or CCh-stimulated SC release, in contrast to the inhibitory effect elicited by GFP-Myo5c-tail (**Figure 2-5C**). We were unable to conduct comparable analyses of syncollin-GFP secretion with the GFP-Myo5c-full since the triple Ad transduction of LGAC that would be required is deleterious for cell viability.

We utilized confocal fluorescence microscopy to measure the diameter of mSVs labeled either with GFP-Myo5c-full or GFP-Myo5c-tail, in LGAC without or with CCh-stimulation. The results are shown in **Figures 2-9** and **2-10**. **Figure 2-9** illustrates the typical appearance of mSVs that are labeled with overexpressed GFP-Myo5c-full or GFP-Myo5c-tail under each condition. The diameter of mSVs enriched in GFP-Myo5c-full appears larger with CCh-stimulation relative to that in resting LGAC, consistent with our working model of compound fusion prior to exocytosis. However, such an increase was not readily apparent in mSV labeled with GFP-Myo5c-tail in LGAC stimulated with CCh, relative to resting LGAC. In addition, the actin coats frequently detected around subapical mSVs enriched in GFP-Myo5c-full in CCh-stimulated LGAC were infrequently detected with vesicles labeled with GFP-Myo5c-tail in CCh-stimulated LGAC.

The trends obtained from visual examination in **Figure 2-9** were reinforced by the quantitative analysis in **Figure 2-10**. Reinforcing the observations obtained from confocal and EM micrographs, we found that the percentage of actin-coated vesicles, as

observed by confocal as phalloidin-positive staining distinct from the cortical actin, that were

Figure 2-9: GFP-Myo5c-tail-enriched mSVs exhibit reduced diameter and infrequent association with actin-coated structures relative to GFP-Myo5c-full-enriched mSVs in stimulated LGAC. Confocal fluorescence/ DIC microscopy overlays are depicted showing Myo5c-enriched vesicles (**green**) labeled with either GFP-Myo5c-full or GFP-Myo5c-tail in resting and CCh-stimulated (100 μ M, 15 min) LGAC. Actin filaments (**red**) were used to identify lumena. Boxed regions in each image are magnified in the image to the right. Bars, \sim 5 μ m.



labeled with GFP in CCh-stimulated acini was significantly reduced in LGAC expressing GFP-Myo5c-tail relative to GFP-Myo5c-full (**Figure 2-10D**).

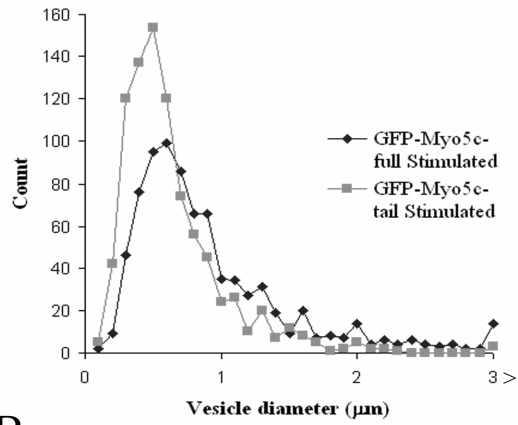
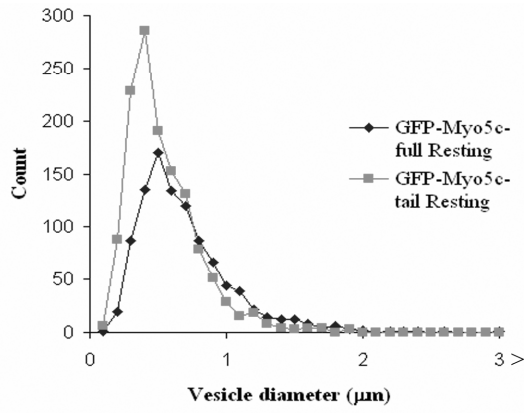
Other aspects of SV organization, although more subtle than the obvious lack of GFP-Myo5c-tail association with actin-coated granules, provided additional insights into Myo5c's role in exocytosis. The histogram plots shown in **Figure 2-10A** depict the number of vesicles of different diameter detected in resting and CCh-stimulated acini that were enriched in either GFP-Myo5c-full or GFP-Myo5c-tail. Our previous work (Jerdeva *et al.*, 2005b) had utilized EM to determine the range in diameter of individual mSVs, as well as dual and multiply-fused mSVs in LGAC. In this previous study, formation of dual and multiply-fused vesicles of greater diameter was stimulated by CCh, consistent with activation of compound fusion. In GFP-Myo5c-full and GFP-Myo5c-tail transduced and unstimulated LGAC, both motors were enriched on vesicle populations of diameter $<1 \mu\text{m}$. However, comparison of the histogram plots as well as the calculated mean diameter values (**Figure 2-10B**) in unstimulated LGAC revealed that the average diameter of vesicles labeled with GFP-Myo5c-tail was significantly less than those enriched in GFP-Myo5c-full.

Consistent with previous work, the analysis of diameter in vesicles labeled with GFP-Myo5c-full in CCh-stimulated LGAC relative to these vesicles in unstimulated LGAC revealed the appearance of vesicles of larger diameter. This apparent shift was verified by an increase in the average diameter of these vesicles relative to their diameter in unstimulated LGAC (**Figure 2-10B**). In contrast, fewer vesicles of diameter $>1 \mu\text{m}$ were labeled with GFP-Myo5c-tail in CCh-stimulated LGAC (**Figure 2-10A**). While a modest and still significant increase in diameter of GFP-Myo5c-tail-enriched vesicles

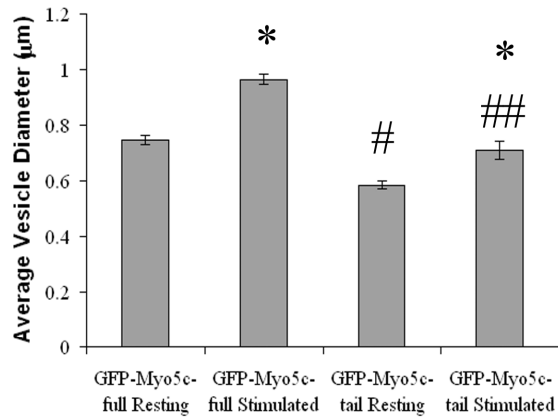
was seen in CCh-treated LGAC relative to unstimulated LGAC, the diameter of the GFP-Myo5c-tail-enriched vesicles in stimulated LGAC was significantly smaller than that for GFP-Myo5c-full-enriched vesicles in stimulated LGAC (**Figure 2-10B**). As shown in **Figure 2-10C**, the CCh-induced increase in vesicle diameter was significantly reduced by GFP-Myo5c-tail. These data, combined with the uncoupling of GFP-Myo5c-tail from actin coated vesicles, suggest that Myo5c participates in an aspect of compound fusion involving association of primed and fusing mSVs with actin coats.

Figure 2-10. GFP-Myo5c-tail-enriched mSVs exhibit reduced diameter in the presence and absence of CCh, and reduced association with actin-coated structures in CCh-stimulated LGAC. **A.** Diameters of GFP-Myo5c-full and GFP-Myo5c-tail-enriched vesicles in either resting or CCh-stimulated (100 μ m, 15 min) were measured using the LSM 510 confocal quantification software tool. The histogram plots shows the distribution of vesicle diameters in resting LGAC (upper) and CCh-stimulated LGAC (lower) for vesicles labeled with GFP-Myo5c-full (black) and GFP-Myo5c-tail (grey) quantified from n=8 preparations and 12-30 fields per preparation. The total vesicles counted include: GFP-Myo5c-full (resting), 983; GFP-Myo5c-full (CCh-stimulated), 704; GFP-Myo5c-tail (resting), 1295; GFP-Myo5c-tail (CCh-stimulated), 859. Vesicles greater than 3 μ m in diameter were pooled. Average vesicle diameter for all vesicles counted in **A.** were averaged by preparation (n=8) and changes in average values were compared for statistical significance using a one-way ANOVA and Tukey's post-test. *, significant increase from resting in the same category; #, significant decrease from GFP-Myo5c-full (resting); ##, significant decrease from GFP-Myo5c-full (CCh-stimulated), p<0.05. **C.** CCh-induced differences in vesicle diameter by treatment; # shows significance at p \leq 0.05. **D.** The percentage of actin-coated vesicles in stimulated LGAC that were labeled with GFP were quantified and plotted as a percentage of total actin-coated vesicles. Actin-coated vesicles were characterized by as phalloidin-positive vesicular structures that were distinct from cortical actin. # denotes the significant (p<0.05) decrease in GFP-Myo5c-tail-labeling of actin coats.

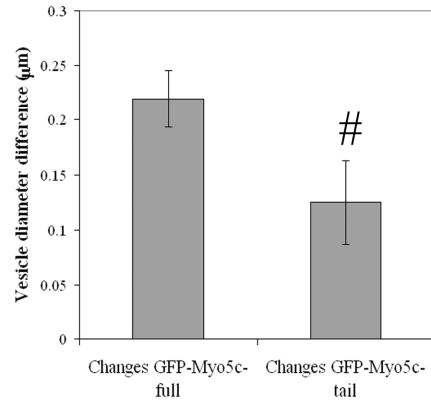
A.



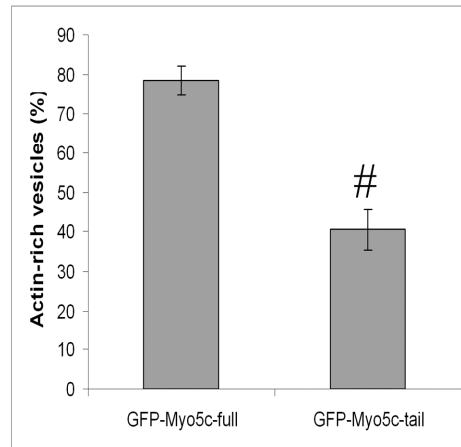
B.



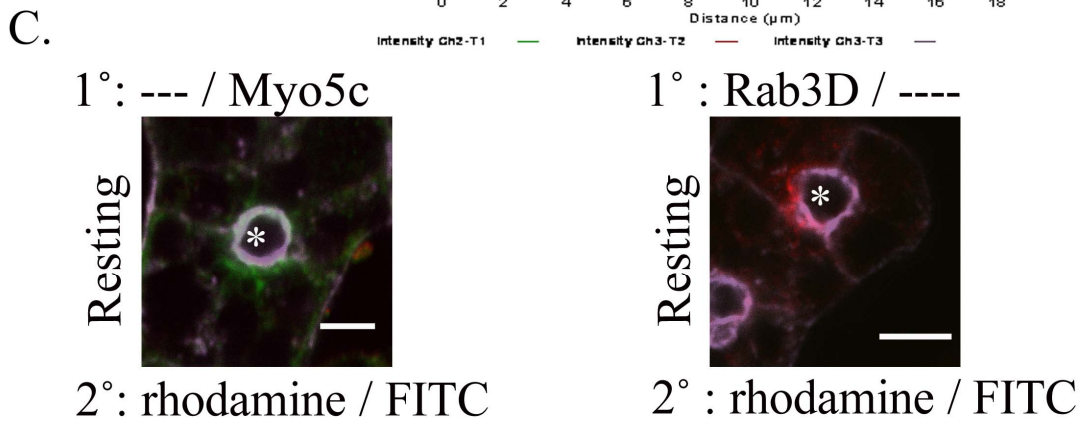
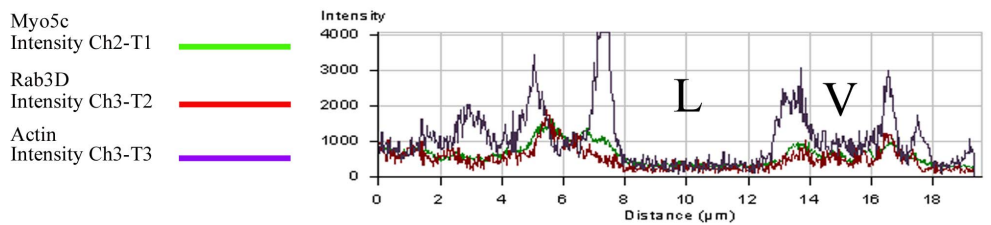
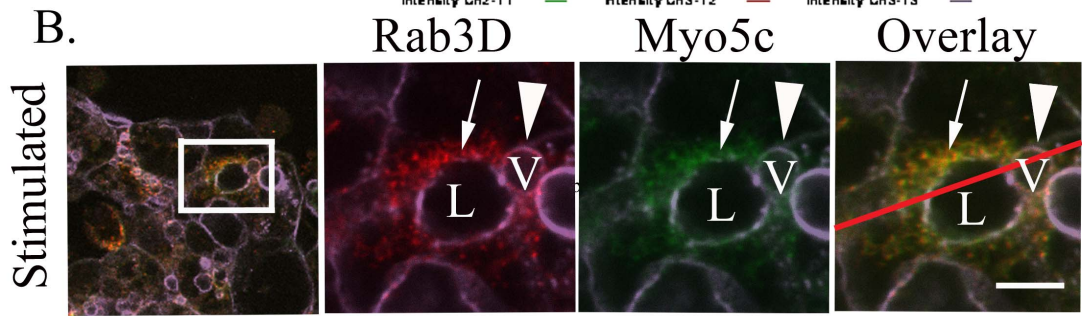
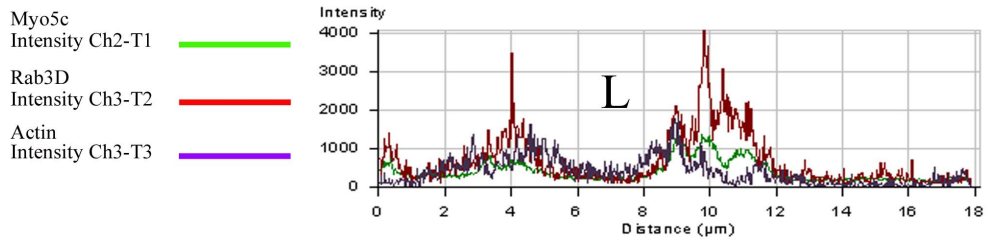
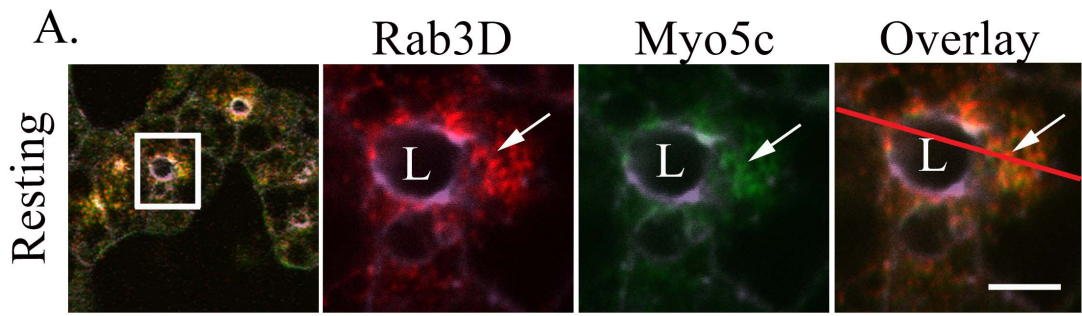
C.



D.



Supplemental Figure 2-1: Myo5c and endogenous Rab3D are co-localized on mSVs in LGAC. Resting (**A**) and CCh-stimulated (**B**, 100 μ M, 15 min) LGAC were processed using the sequential labeling procedure in **Methods** using rabbit polyclonal antibodies against Myo5c (**green**), endogenous Rab3D (**red**) and appropriate anti-rabbit secondary antibodies. Actin was affinity-labeled with fluorescent phalloidin (**purple**). The left most images show a lower magnification view while the boxed regions are magnified to the right. The line scan analysis was conducted comparably to that described in **Figure 2, Panel B**. When the rabbit polyclonal antibody to Rab3D was omitted and the sequential procedure was followed, no rhodamine fluorescence was detected (**Panel C, right**), and when the rabbit polyclonal antibody to Myo5c was omitted and the sequential procedure was followed, no FITC fluorescence was detected (**Panel C, left**). Bars = \sim 5 μ m.



Discussion

Our study is the first to test the function of Myo5c in secretion from acinar epithelial cells. Here we show that endogenous Myo5c is associated with LG mSVs. Evidence for this includes the finding that endogenous Myo5c is co-localized with Rab3D in vesicles of the very large diameter characteristic of mSVs. Rab3D has been well characterized as a constituent of mSVs in acinar cells from pancreas (Chen *et al.*, 2002), parotid gland (Nguyen *et al.*, 2003) and LG (Wang *et al.*, 2003), as well as within the lamellar bodies of type II alveolar cells (van Weeren *et al.*, 2004). In addition, Rab3D was co-localized with both GFP-Myo5c-tail and GFP-Myo5c-full in resting, transduced LGAC. Additional evidence that Myo5c is associated with mSV was provided by the demonstration of functional inhibition of CCh-stimulated SC and syncollin-GFP release from mSV by overexpression of GFP-Myo5c-tail. Finally, immunogold and EM shows clearly that Myo5c is associated with mSVs and their underlying actin cytoskeleton, particularly in stimulated LGAC. Our findings on the association of Myo5c with exocrine mSV in LGAC are consistent with a recent report utilizing organellar proteomics which identified Myo5c as a constituent of zymogen granules in pancreas (Chen, 2006).

In addition to the demonstration of Myo5c on mSV in resting LGAC, our study suggests a role for Myo5c in association of actin coats around fusing mSV during exocytosis. After stimulation of LGAC with CCh, actin-coated structures appear near the APM. These structures have previously been shown to contain several mSV enveloped with an actin coat that are in the process of undergoing compound fusion (Jerdeva *et al.*, 2005a; Jerdeva *et al.*, 2005b). We have hypothesized that this step precedes the

extrusion of vesicle contents from this intermediate at the APM. A role for non-muscle myosin II in contraction of the actin coat and subsequent compound fusion and extrusion of the contents within the actin-coated structure at the APM is supported by inhibitor studies. For instance, stabilization of actin coats by inhibition of non-muscle myosin II results in accumulation of multivesicular fusion intermediates as well as inhibition of protein secretion, suggesting that actin coat assembly precedes compound fusion and extrusion of vesicle contents (Jerdeva *et al.*, 2005b). In the current study, endogenous Myo5c was detected in association with actin-coated fusion intermediates in stimulated LGAC by both confocal fluorescence microscopy and immunogold and EM, suggesting that it may participate in an actin-dependent component of compound fusion.

When Myo5c-enriched vesicle association with actin-coated structures was examined in stimulated LGAC transduced either with GFP-Myo5c-tail versus GFP-Myo5c-full, changes indicative of altered association with actin coats were evident in LGAC expressing the DN construct. Although actin-coated structures were observed in CCh-stimulated LGAC transduced with GFP-Myo5c-tail and GFP-Myo5c-full, the extent of association of GFP-Myo5c-tail with actin coats was significantly reduced relative to GFP-Myo5c-full.

Additional analysis revealed that mSV labeled with GFP-Myo5c-full exhibited a significant increase in mean vesicle diameter in CCh-stimulated LGAC relative to resting acini, comparable to previous studies (Jerdeva *et al.*, 2005b). However, this increase in vesicle diameter was largely blunted in mSV labeled with GFP-Myo5c-tail in CCh-stimulated LGAC, suggesting that compound fusion was affected. In addition, the

histogram plot of vesicle diameters of vesicles labeled with GFP-Myo5c-tail indicated fewer large diameter vesicles, relative to vesicles labeled with GFP-Myo5c-full.

We suggest that Myo5c functions in pairing of primed mSV with actin coats as an initial step in the exocytotic process. EM data suggest that endogenous Myo5c is largely associated with the dense network of actin around SVs in CCh-stimulated LGAC. The distribution of Myo5c (both endogenous and GFP-Myo5c-full) in CCh-stimulated LGAC is patchy, consistent with enrichment on aggregates of actin filaments. Inhibition of Myo5c function by overexpression of the tail domain would have the consequence of inhibiting compound fusion by preventing actin coats from associating appropriately with primed mSVs. Intriguingly, recent biochemical studies of human Myo5c have suggested that it functions as a low duty ratio, non-processive motor protein (Li *et al.*, 2008; Takagi *et al.*, 2008). Myo5a has been well characterized as a highly processive motor which undergoes multiple enzymatic cycles while attached to the actin cytoskeleton; this profile is characteristic of a vesicle motor protein. Non-processive behavior by Myo5c means that this motor would require concerted action by multiple units to facilitate transport. This suggests that the function of Myo5c in cells may be quite different than its processive cousin; Myo5a.

Of interest in resting LGAC, when parameters of vesicles labeled with GFP-Myo5c-tail and GFP-Myo5c-full were compared, the vesicles labeled with GFP-Myo5c-tail were significantly smaller in diameter by ~15%, relative to vesicles labeled with GFP-Myo5c-full. Little is known about mSV biogenesis in LGAC but literature on maturation of mSV from immature SV in neuroendocrine and endocrine cells suggests a model of maturation by homotypic fusion (Arvan and Castle, 1998). If a similar model is

applicable in LGAC, a smaller diameter SV population might represent a preponderance of immature SVs. The role of Myo5c in vesicle maturation could be direct (e.g., plays a role in homotypic fusion) or indirect (e.g., plays a role in recruitment of other factors necessary for maturation).

Previous work has shown that expression of a GFP-Myo5c-tail construct in HeLa cells suggests that Myo5c participates in transferrin receptor recycling (Rodriguez and Cheney, 2002). This finding suggested a possible role for Myo5c in apical membrane recycling in LGAC, although it is important to note that HeLa cells are non-polarized and do not exhibit a regulated secretory pathway. Conceivably, Myo5c associated with mSV might be passively transported to the APM in association with exocytosing mSV, and it could then play an active role in the compensatory apical endocytosis of exocytosed mSV membrane to a recycling apical endosome. Inhibition of apical endocytosis might exert a negative feedback effect on apical exocytosis due to the distension of APM and/or the depletion of membranes available for regeneration of mSV, explaining the inhibition of SC and syncollin-GFP release exerted by the GFP-Myo5c-tail construct.

Interestingly, there is some disagreement in the literature about the precise point in acinar exocytosis at which actin-coated structures are formed. All results obtained thus far in LGAC indicate that these coats assemble prior to compound fusion and content extrusion (Jerdeva *et al.*, 2005b), but a few recent reports in pancreatic acini have suggested that the actin coat assembles on zymogen granules that have just undergone exocytosis (Nemoto *et al.*, 2004; Turvey and Thorn, 2004; Pickett and Edwardson, 2006). One explanation for the need for an actin coat just after initiation of exocytosis (e.g., formation of the fusion pore) is for stabilization of the opposing membranes and/or

content extrusion of the contents trapped in the large inclusion (Nemoto *et al.*, 2004). The dissection of the role of the actin coat in mSV exocytosis in exocrine tissues is complicated by the differing approaches used for analysis, as well as the existence of different modes of exocytosis utilized by these tissues; sequential (pancreatic acini) versus multivesicular (parotid acini and LGAC) (Pickett and Edwardson, 2006). However, if an actin coat forms after exocytosis is initiated in LGAC, it may in fact facilitate the rapid retrieval of mSV membrane to endosomal compartments via vesicle transport on subapical actin utilizing Myo5c. We feel that this scenario is less likely than our proposed model for Myo5c participation in compound fusion and exocytosis for several reasons. First, we saw no evidence for recovery of Myo5c with endosomal membranes in CCh-stimulated LGAC by immunogold/EM; rather the Myo5c appeared to become increasingly enriched in the apical actin meshwork that increased adjacent to fusing mSV. Second, we have previously shown that inhibition of actin-dependent apical endocytosis in CCh-stimulated LGAC resulted in accumulation of coated pits at the APM, an effect not seen in our studies (Da Costa *et al.*, 2003). Finally, our observation of the suppression of the normal increase in mSV diameter associated with CCh-stimulated compound exocytosis by expression of GFP-Myo5c-tail is more consistent with a role for Myo5c in promoting the formation of the actual compound fusion intermediate, rather than apical endocytosis.

It is important to note in any analysis of function of an individual protein member of a protein family, that findings can be complicated by expression of additional family members which may be able to partially substitute for a lost function exerted by expression of a DN construct. Such functional redundancy has been extensively reported

for rab proteins, including the members of the Rab3 family which are broadly expressed in a variety of secretory cells and which may substitute functionally for each other (Schluter *et al.*, 2002). Since Myo5a and Myo5b are also detected in LGAC, it is possible that some of the functional consequences of GFP-Myo5c-tail overexpression may be tempered by the ability of the other two class V myosins to compensate for some functions. Functional compensation of Myo5a and Myo5b may be responsible for the observed incomplete inhibition of exocytosis in LGAC expressing the GFP-Myo5c-tail. However, it is also possible that overexpression GFP-Myo5c-tail may not fully displace all of the endogenous Myo5c from SVs. It should also be noted that partial inhibition of secretion has been noted in situations where other essential effectors have been disrupted. Partial inhibition of secretion has been observed for 5-HT release in platelets from Rab27b knockout mice, for amylase release from mouse pancreatic acinar cells expressing dominant negative Rab3D and Rab27b, and for β -hexosaminidase release in mast cells from VAMP8 knockout mice (Chen *et al.*, 2002; Chen *et al.*, 2004; Tolmachova *et al.*, 2007; Puri and Roche, 2008).

Our data show evidence for a strong association of Myo5c with Rab3D-enriched mSV in particular. Since some myosins and kinesins have been shown to be tethered to vesicular cargo via rab binding (Wu *et al.*, 2001; Langford, 2002; Wu *et al.*, 2002; O'Connell C *et al.*, 2007), we considered whether Rab3D might actually bind directly to Myo5c. Co-immunoprecipitation studies from LGAC did not reveal any evidence for a strong protein-protein association between these effectors (unpublished data). As shown here, the co-localization of these two proteins was most extensive in resting LGAC. CCh-stimulation resulted in a decrease in Rab3D co-localization with Myo5c of 31%,

reflecting the release of Rab3D from primed fusing mSV that occurs prior to formation of the actin coat and subsequent compound exocytosis (Valentijn *et al.*, 1999; Valentijn *et al.*, 2000; Wang *et al.*, 2003). In contrast, the Myo5c was retained with the actin coat and mSVs in CCh-stimulated LGAC, suggesting that it does not require Rab3D to retain its association with mSV or their closely-associated actin filaments. Future studies will explore the likely receptors for Myo5c association with mSV including Rab27 family members.

To summarize, we have conclusively demonstrated for the first time that Myo5c is associated with mSV in LGAC, and the preponderance of evidence suggests that it functions in exocytosis of mSVs in this system. Our data suggests a model in which Myo5c on mSVs facilitates the pairing of primed mSVs with actin coats as the compound fusion intermediate is assembled, prior to exocytosis of mSV contents.

Text Footnotes

LG, lacrimal gland; LGAC, lacrimal gland acinar cells; secretory immunoglobulin A, sIgA; SC, secretory component; mSV, mature secretory vesicle; APM, apical plasma membrane; HA, hemagglutinin epitope; GFP, green fluorescent protein; pIgAR, polymeric immunoglobulin A receptor; SC, secretory component; BSA, bovine serum albumin; Ad, adenovirus; EM, electron microscopy; Myo5c, Myosin 5c; DN, dominant negative

Acknowledgements

The authors wish to acknowledge the support of NIH RO1 EY011386 and EY016985 to SHA, and NIH F31 EY015928 to RRM. JES was supported by NIH RO1 EY010550. REC was supported by NIH R01 DC03299 and DTJ was supported by a Porter Fellowship from the American Physiological Society. We also thank Limin Qian for his help with the Ad-GFP-Myo5c-tail construct preparation.

References

- Abu-Hamdah, R., Cho, W.J., Horber, J.K., and Jena, B.P. (2006). Secretory vesicles in live cells are not free-floating but tethered to filamentous structures: a study using photonic force microscopy. *Ultramicroscopy* 106, 670-673.
- Arvan, P., and Castle, D. (1998). Sorting and storage during secretory granule biogenesis: looking backward and looking forward. *The Biochemical journal* 332 (Pt 3), 593-610.
- Chen, L., Hodges, R.R., Funaki, C., Zoukhri, D., Gaivin, R.J., Perez, D.M., and Dartt, D.A. (2006). Effects of alpha1D-adrenergic receptors on shedding of biologically active EGF in freshly isolated lacrimal gland epithelial cells. *Am J Physiol Cell Physiol* 291, C946-956.
- Chen, X., Edwards, J.A., Logsdon, C.D., Ernst, S.A., and Williams, J.A. (2002). Dominant negative Rab3D inhibits amylase release from mouse pancreatic acini. *J Biol Chem* 277, 18002-18009.
- Chen, X., Li, C., Izumi, T., Ernst, S.A., Andrews, P.C., and Williams, J.A. (2004). Rab27b localizes to zymogen granules and regulates pancreatic acinar exocytosis. *Biochemical and biophysical research communications* 323, 1157-1162.
- Chen, X., Walker A.K., et al. (2006). Organellar proteomics: analysis of pancreatic zymogen granule membranes. *Mol Cell Proteomics* 5, 306-312.
- Da Costa, S.R., Andersson, S., Arber, F., Okamoto, C., and Hamm-Alvarez, S. (2002). Cytoskeletal participation in stimulated secretion and compensatory apical plasma membrane retrieval in lacrimal gland acinar cells. *Adv Exp Med Biol* 506, 199-205.
- Da Costa, S.R., Sou, E., Xie, J., Yarber, F.A., Okamoto, C.T., Pidgeon, M., Kessels, M.M., Mircheff, A.K., Schechter, J.E., Qualmann, B., and Hamm-Alvarez, S.F. (2003). Impairing actin filament or syndapin functions promotes accumulation of clathrin-coated vesicles at the apical plasma membrane of acinar epithelial cells. *Molecular biology of the cell* 14, 4397-4413.
- Evans, E., Zhang, W., Jerdeva, G., Chen, C.Y., Chen, X., Hamm-Alvarez, S.F., and Okamoto, C. (2008). Direct Interaction between Rab3d and the Polymeric Immunoglobulin Receptor and Trafficking through Regulated Secretory Vesicles in Lacrimal Gland Acinar Cells. *Am J Physiol Cell Physiol*.
- Fan, G.H., Lapierre, L.A., Goldenring, J.R., Sai, J., and Richmond, A. (2004). Rab11-family interacting protein 2 and myosin Vb are required for CXCR2 recycling and receptor-mediated chemotaxis. *Molecular biology of the cell* 15, 2456-2469.

Foth, B.J., Goedecke, M.C., and Soldati, D. (2006). New insights into myosin evolution and classification. *Proceedings of the National Academy of Sciences of the United States of America* *103*, 3681-3686.

Fox, R.I., and Stern, M. (2002). Sjogren's syndrome: mechanisms of pathogenesis involve interaction of immune and neurosecretory systems. *Scand J Rheumatol Suppl.* *31*, 3-13.

Imai, A., Yoshie, S., Nashida, T., Shimomura, H., and Fukuda, M. (2004). The small GTPase Rab27B regulates amylase release from rat parotid acinar cells. *J Cell Sci* *117*, 1945-1953.

Jerdeva, G.V., Wu, K., Yarber, F.A., Rhodes, C.J., Kalman, D., Schechter, J.E., and Hamm-Alvarez, S.F. (2005b). Actin and non-muscle myosin II facilitate apical exocytosis of tear proteins in rabbit lacrimal acinar epithelial cells. *J Cell Sci* *118*, 4797-4812.

Jerdeva, G.V., Yarber, F.A., Trousdale, M.D., Rhodes, C.J., Okamoto, C.T., Dartt, D.A., and Hamm-Alvarez, S.F. (2005a). Dominant-negative PKC-epsilon impairs apical actin remodeling in parallel with inhibition of carbachol-stimulated secretion in rabbit lacrimal acini. *Am J Physiol Cell Physiol* *289*, C1052-1068.

Johnston, G.C., Prendergast, J.A., and Singer, R.A. (1991). The *Saccharomyces cerevisiae* MYO2 gene encodes an essential myosin for vectorial transport of vesicles. *The Journal of cell biology* *113*, 539-551.

Karpova, T.S., Reck-Peterson, S.L., Elkind, N.B., Mooseker, M.S., Novick, P.J., and Cooper, J.A. (2000). Role of actin and Myo2p in polarized secretion and growth of *Saccharomyces cerevisiae*. *Molecular biology of the cell* *11*, 1727-1737.

Krendel, M., and Mooseker, M.S. (2005). Myosins: tails (and heads) of functional diversity. *Physiology (Bethesda)* *20*, 239-251.

Langford, G.M. (2002). Myosin-V, a versatile motor for short-range vesicle transport. *Traffic* *3*, 859-865.

Lapierre, L.A., Kumar, R., Hales, C.M., Navarre, J., Bhartur, S.G., Burnette, J.O., Provance, D.W., Jr., Mercer, J.A., Bahler, M., and Goldenring, J.R. (2001). Myosin vb is associated with plasma membrane recycling systems. *Molecular biology of the cell* *12*, 1843-1857.

Li, X.D., Jung, H.S., Wang, Q., Ikebe, R., Craig, R., and Ikebe, M. (2008). The globular tail domain puts on the brake to stop the ATPase cycle of myosin Va. *Proceedings of the National Academy of Sciences of the United States of America* *105*, 1140-1145.

- Lise, M.F., Wong, T.P., Trinh, A., Hines, R.M., Liu, L., Kang, R., Hines, D.J., Lu, J., Goldenring, J.R., Wang, Y.T., and El-Husseini, A. (2006). Involvement of myosin Vb in glutamate receptor trafficking. *J Biol Chem* *281*, 3669-3678.
- Ma, L., Bindokas, V.P., Kuznetsov, A., Rhodes, C., Hays, L., Edwardson, J.M., Ueda, K., Steiner, D.F., and Philipson, L.H. (2004). Direct imaging shows that insulin granule exocytosis occurs by complete vesicle fusion. *Proceedings of the National Academy of Sciences of the United States of America* *101*, 9266-9271.
- Nedvetsky, P.I., Stefan, E., Frische, S., Santamaria, K., Wiesner, B., Valenti, G., Hammer, J.A., 3rd, Nielsen, S., Goldenring, J.R., Rosenthal, W., and Klusmann, E. (2007). A Role of myosin Vb and Rab11-FIP2 in the aquaporin-2 shuttle. *Traffic* *8*, 110-123.
- Nemoto, T., Kojima, T., Oshima, A., Bito, H., and Kasai, H. (2004). Stabilization of exocytosis by dynamic F-actin coating of zymogen granules in pancreatic acini. *J Biol Chem* *279*, 37544-37550.
- Nguyen, D., Jones, A., Ojakian, G.K., and Raffaniello, R.D. (2003). Rab3D redistribution and function in rat parotid acini. *J Cell Physiol* *197*, 400-408.
- O'Connell C, B., Tyska, M.J., and Mooseker, M.S. (2007). Myosin at work: Motor adaptations for a variety of cellular functions. *Biochim Biophys Acta* *1773*, 615-630.
- Pickett, J.A., and Edwardson, J.M. (2006). Compound exocytosis: mechanisms and functional significance. *Traffic* *7*, 109-116.
- Provance, D.W., and Mercer, J.A. (1999). Myosin-V: head to tail. *Cell Mol Life Sci* *56*, 233-242.
- Pruyne, D.W., Schott, D.H., and Bretscher, A. (1998). Tropomyosin-containing actin cables direct the Myo2p-dependent polarized delivery of secretory vesicles in budding yeast. *The Journal of cell biology* *143*, 1931-1945.
- Puri, N., and Roche, P.A. (2008). Mast cells possess distinct secretory granule subsets whose exocytosis is regulated by different SNARE isoforms. *Proceedings of the National Academy of Sciences of the United States of America* *105*, 2580-2585.
- Reck-Peterson, S.L., Provance, D.W., Jr., Mooseker, M.S., and Mercer, J.A. (2000). Class V myosins. *Biochim Biophys Acta* *1496*, 36-51.
- Richards, T.A., and Cavalier-Smith, T. (2005). Myosin domain evolution and the primary divergence of eukaryotes. *Nature* *436*, 1113-1118.
- Riedel, D., Antonin, W., Fernandez-Chacon, R., Alvarez de Toledo, G., Jo, T., Geppert, M., Valentijn, J.A., Valentijn, K., Jamieson, J.D., Sudhof, T.C., and Jahn, R. (2002).

Rab3D is not required for exocrine exocytosis but for maintenance of normally sized secretory granules. *Mol Cell Biol* 22, 6487-6497.

Rodriguez, O.C., and Cheney, R.E. (2002). Human myosin-Vc is a novel class V myosin expressed in epithelial cells. *J Cell Sci* 115, 991-1004.

Schluter, O.M., Khvotchev, M., Jahn, R., and Sudhof, T.C. (2002). Localization versus function of Rab3 proteins. Evidence for a common regulatory role in controlling fusion. *J Biol Chem* 277, 40919-40929.

Schott, D.H., Collins, R.N., and Bretscher, A. (2002). Secretory vesicle transport velocity in living cells depends on the myosin-V lever arm length. *The Journal of cell biology* 156, 35-39.

Swiatecka-Urban, A., Talebian, L., Kanno, E., Moreau-Marquis, S., Coutermarsh, B., Hansen, K., Karlson, K.H., Barnaby, R., Cheney, R.E., Langford, G.M., Fukuda, M., and Stanton, B.A. (2007). Myosin VB is required for trafficking of CFTR in RAB11A-specific apical recycling endosomes in polarized human airway epithelial cells. *J Biol Chem*.

Takagi, Y., Yang, Y., Fujiwara, I., Jacobs, D., Cheney, R.E., Sellers, J.R., and Kovacs, M. (2008). Human myosin Vc is a low duty ratio, non-processive molecular motor. *J Biol Chem*.

Tolmachova, T., Abrink, M., Futter, C.E., Authi, K.S., and Seabra, M.C. (2007). Rab27b regulates number and secretion of platelet dense granules. *Proceedings of the National Academy of Sciences of the United States of America* 104, 5872-5877.

Turvey, M.R., and Thorn, P. (2004). Lysine-fixable dye tracing of exocytosis shows F-actin coating is a step that follows granule fusion in pancreatic acinar cells. *Pflugers Arch* 448, 552-555.

Valentijn, J.A., Valentijn, K., Pastore, L.M., and Jamieson, J.D. (2000). Actin coating of secretory granules during regulated exocytosis correlates with the release of rab3D. *Proceedings of the National Academy of Sciences of the United States of America* 97, 1091-1095.

Valentijn, K., Valentijn, J.A., and Jamieson, J.D. (1999). Role of actin in regulated exocytosis and compensatory membrane retrieval: insights from an old acquaintance. *Biochemical and biophysical research communications* 266, 652-661.

van Weeren, L., de Graaff, A.M., Jamieson, J.D., Batenburg, J.J., and Valentijn, J.A. (2004). Rab3D and actin reveal distinct lamellar body subpopulations in alveolar epithelial type II cells. *Am J Respir Cell Mol Biol* 30, 288-295.

Vilalta, P.M., Zhang, L., and Hamm-Alvarez, S.F. (1998). A novel taxol-induced vimentin phosphorylation and stabilization revealed by studies on stable microtubules and vimentin intermediate filaments. *J Cell Sci* *111* (Pt 13), 1841-1852.

Wakabayashi, Y., Dutt, P., Lippincott-Schwartz, J., and Arias, I.M. (2005). Rab11a and myosin Vb are required for bile canaliculi formation in WIF-B9 cells. *Proceedings of the National Academy of Sciences of the United States of America* *102*, 15087-15092.

Wang, Y., Jerdeva, G., Yarber, F.A., da Costa, S.R., Xie, J., Qian, L., Rose, C.M., Mazurek, C., Kasahara, N., Mircheff, A.K., and Hamm-Alvarez, S.F. (2003). Cytoplasmic dynein participates in apically targeted stimulated secretory traffic in primary rabbit lacrimal acinar epithelial cells. *J Cell Sci* *116*, 2051-2065.

Wang, Y., Xie, J., Yarber, F.A., Mazurek, C., Trousdale, M.D., Medina-Kauwe, L.K., Kasahara, N., and Hamm-Alvarez, S.F. (2004). Adenoviral capsid modulates secretory compartment organization and function in acinar epithelial cells from rabbit lacrimal gland. *Gene Ther* *11*, 970-981.

Waselle, L., Coppola, T., Fukuda, M., Iezzi, M., El-Amraoui, A., Petit, C., and Regazzi, R. (2003). Involvement of the Rab27 binding protein Slac2c/MyRIP in insulin exocytosis. *Molecular biology of the cell* *14*, 4103-4113.

Wu, K., Jerdeva, G.V., da Costa, S.R., Sou, E., Schechter, J.E., and Hamm-Alvarez, S.F. (2006). Molecular mechanisms of lacrimal acinar secretory vesicle exocytosis. *Exp Eye Res* *83*, 84-96.

Wu, X., Bowers, B., Wei, Q., Kocher, B., and Hammer, J.A., 3rd. (1997). Myosin V associates with melanosomes in mouse melanocytes: evidence that myosin V is an organelle motor. *J Cell Sci* *110* (Pt 7), 847-859.

Wu, X., Rao, K., Bowers, M.B., Copeland, N.G., Jenkins, N.A., and Hammer, J.A., 3rd. (2001). Rab27a enables myosin Va-dependent melanosome capture by recruiting the myosin to the organelle. *J Cell Sci* *114*, 1091-1100.

Wu, X., Wang, F., Rao, K., Sellers, J.R., and Hammer, J.A., 3rd. (2002). Rab27a is an essential component of melanosome receptor for myosin Va. *Molecular biology of the cell* *13*, 1735-1749.

Zhao, L.P., Koslovsky, J.S., Reinhard, J., Bahler, M., Witt, A.E., Provance, D.W., Jr., and Mercer, J.A. (1996). Cloning and characterization of myr 6, an unconventional myosin of the dilute/myosin-V family. *Proceedings of the National Academy of Sciences of the United States of America* *93*, 10826-10831.

**CHAPTER 3: MYOSIN VC IS A CLASS V MYOSIN THAT FUNCTIONS IN
SECRETORY GRANULE TRAFFICKING**

(Manuscript submitted to Molecular Biology of the Cell-currently in review; 4/09/2009)

Myosin Vc is a Molecular Motor that Functions in Secretory Granule Trafficking

Damon T. Jacobs*, Roberto Weigert†, Julie G. Donaldson‡, Richard E. Cheney*

*Medical Biomolecular Research Building rm 5314

Department of Cell and Molecular Physiology, School of Medicine

University of North Carolina at Chapel Hill, Chapel Hill, NC 27599

†National Institute of Dental and Craniofacial Research, National Institutes of Health

Bethesda, MD 20892

‡Laboratory of Cell Biology, National Heart, Lung, and Blood Institute, National

Institutes of Health, Bethesda, MD 20892

Address correspondence to: CheneyR@med.UNC.edu

running title: Myo5c localization and dynamics

Key words: Myo5c, Myosin V, Myosin 5c, exocrine secretion, exocytosis, secretory granule

Abstract

Class V myosins are actin-based motor proteins that have critical functions in organelle trafficking. Of the three class V myosins expressed in mammals, relatively little is known about Myo5c except that it is expressed at high levels in exocrine tissues. Here we use MCF-7 cells to identify organelles that Myo5c associates with, visualize the dynamics of Myo5c in living cells, and test the functions of Myo5c.

Immunofluorescence demonstrates that endogenous Myo5c localizes to small puncta and to slender tubules. In migrating cells, Myo5c exhibits a highly polarized distribution towards the leading edge. Live-cell imaging with GFP-Myo5c reveals that tubules move rapidly (~500 nm/s) and microtubule-dependently whereas puncta move slowly (~30 nm/s) and microtubule-independently. Most importantly, Myo5c puncta localize on granules containing markers for regulated secretion. TIRF imaging indicates that these granules can be triggered to undergo secretion. To test the functions of Myo5c, we expressed a dominant negative tail construct and found that it perturbed the distribution of secretory granule markers. These results provide the first high resolution studies of Myo5c localization and dynamics in a cell line and indicate that Myo5c functions in the trafficking of secretory granules.

Introduction

Class V myosins are an evolutionarily ancient group of molecular motors that mediate actin-dependent organelle trafficking (Provance and Mercer, 1999; Berg *et al.*, 2001; Trybus, 2008). In the yeast *Saccharomyces cerevisiae*, the class V myosin known as Myo2p localizes to secretory vesicles and functions as a molecular motor that transports vesicles along actin cables to sites of polarized secretion (Johnston *et al.*, 1991; Pruyne *et al.*, 1998; Karpova *et al.*, 2000). Myo2p is also required for proper trafficking of several other organelles, including vacuoles, peroxisomes, late golgi, and mitochondria (Pashkova *et al.*, 2006). In animal cells, organelles generally undergo long range movements using microtubule-based motors and the class V myosins appear to function primarily in the actin-rich cell cortex. Class V myosins in animal cells have thus been hypothesized to act as actin-based tethers and/or short-range transporters that function in organelle distribution and exocytosis (Wu *et al.*, 1998; Langford, 2002; Rose *et al.*, 2002; Nascimento *et al.*, 2003; Eichler *et al.*, 2006; Desnos *et al.*, 2007a). Although mammals express three different class V myosins, myosin-Va (Myo5a), myosin-Vb (Myo5b), and myosin-Vc (Myo5c) (Rodriguez and Cheney, 2002), little is known about the cellular localization and functions of Myo5c.

The class V myosins have been the subject of intensive study and have a generally conserved structure that can be divided into a head, neck and tail (Cheney *et al.*, 1993; Trybus, 2008). The head consists of a myosin motor domain that binds to actin filaments and hydrolyzes ATP to produce force, while the neck consists of 6 IQ motifs that provide binding sites for up to 6 calmodulin or calmodulin-like light chains (Espreafico *et al.*,

1992). The tail can be divided into a proximal region consisting largely of coiled coil and a distal region consisting of a globular domain important for organelle binding (Pashkova *et al.*, 2006). Biochemical studies with Myo5a indicate that its heavy chains dimerize via their coiled coil regions to form a two-headed molecule that moves processively along actin filaments at rates of 200-1000 nm/s (Cheney *et al.*, 1993; Wu *et al.*, 2006). Myo5b also forms dimers, is processive, and can power movement at ~200 nm/s (Watanabe *et al.*, 2006). Recent experiments show that micromolar Ca⁺⁺ regulates Myo5a activity by converting it from a compact inactive state to an extended active state that hydrolyzes ATP and moves along actin filaments (Krementsov *et al.*, 2004; Liu *et al.*, 2006; Thirumurugan *et al.*, 2006). Although the three class V myosins in mammals are predicted to have similar overall structures, their heavy chains share only 50-60% protein sequence identity and they appear to have distinct functions and patterns of expression (Rodriguez and Cheney, 2002).

Myo5a is expressed at relatively high levels in neurons and melanocytes and is involved in the transport and localization of several different organelles (Desnos *et al.*, 2007a). Myo5a mutations in mouse (*dilute-lethal*) and human (Griscelli syndrome) demonstrate that Myo5a has important functions in melanosome transport and in the localization of smooth ER within dendritic spines (Mercer *et al.*, 1991; Takagishi *et al.*, 1996; Pastural *et al.*, 1997). Myo5a is also expressed in endocrine cells, where it is involved in the localization of endocrine secretory granules (Rose *et al.*, 2002; Rudolf *et al.*, 2003; Varadi *et al.*, 2005). Myo5b is expressed in many different tissues (Zhao *et al.*, 1996) and expression of the Myo5b tail in HeLa cells leads to the formation of

perinuclear puncta that contain Myo5b tail, rab11a, and transferrin receptor (Lapierre *et al.*, 2001). Similar dominant negative experiments in other cell types implicate Myo5b and rab11a in the recycling of many proteins, including the M4 muscarinic receptor (Volpicelli *et al.*, 2002), CXCR2 chemokine receptor (Fan *et al.*, 2004), GluR1 glutamate receptor (Lise *et al.*, 2006), aquaporin-2 (Nedvetsky *et al.*, 2007), and the cystic fibrosis transmembrane receptor (CFTR)(Swiatecka-Urban *et al.*, 2007). These results indicate that Myo5b functions in the exocytic trafficking of receptors from a rab11a associated recycling compartment (Lapierre *et al.*, 2001).

Myo5c is the third and final member of the class V myosins to be identified in mammals and is expressed most abundantly in exocrine tissues such as pancreas, salivary gland, prostate gland, and mammary gland (Rodriguez and Cheney, 2002). Expression of the Myo5c tail in HeLa cells led to the formation of peripheral puncta that contain the Myo5c tail, rab8a, and transferrin receptor (Rodriguez and Cheney, 2002). This suggests that in HeLa cells, Myo5c is associated with a membrane compartment that is distinct from the Myo5b/rab11a recycling compartment. Unfortunately, the localization of endogenous Myo5c in cell lines remains unknown, in part due to low levels of expression in cell lines such as HeLa. Surprisingly, although baculovirus expressed Myo5c head-neck constructs can power movement at rates of 24-160 nm/s, Myo5c does not appear to be processive (Watanabe *et al.*, 2007; Takagi *et al.*, 2008). This suggests that several Myo5c molecules would be required to transport a single organelle. Tissue localization experiments show that Myo5c localizes to the actin-rich apical regions of epithelial cells in colon and exocrine pancreas, suggesting that Myo5c is a class V myosin that functions

in exocrine secretory cells (Rodriguez and Cheney, 2002). Consistent with a role in exocrine secretion, Myo5c is one of 101 proteins identified on zymogen granule membranes isolated from rat pancreas (Chen *et al.*, 2006). Importantly, recent experiments show that Myo5c is present on mature secretory granules in lacrimal gland acinar cells and that expressing the dominant negative Myo5c tail inhibits carbachol-induced secretion (Marchelletta *et al.*, 2008). The discovery of Myo5c and its association with exocrine secretion raises fundamental questions about the identity of the organelles Myo5c associates with, its dynamics, and its functions in cells. Here we use MCF-7 cells as a cellular model that allows high resolution imaging to investigate the localization, dynamics, and functions of Myo5c.

Materials and Methods

Cell culture: MCF-7 cells were grown in complete media consisting of Minimal Essential Medium (MEM; Gibco) supplemented with 10% fetal bovine serum (Sigma), 1% penicillin/streptomycin, 10 ug/ml insulin, 1% non-essential amino acids, 1% sodium-pyruvate. MCF-7 cells that stably express GFP-Myo5c (MCF-7 (DJ32)) were grown under the selection of 1.25 ug/ml Geneticin (Gibco) in complete media. HeLa cells were grown in MEM supplemented with 10% fetal bovine serum, and 1% penicillin/streptomycin. All cells were cultured at 37°C with 5% CO₂.

Antibodies and reagents: Affinity purified rabbit anti-Myo5c (#200) and affinity purified rabbit anti-Myo5a (clone 32a) were described previously (Rodriguez and Cheney, 2002). Antibodies used in this study are anti-lipase (Cortex Biochem, San Leandro, CA.), anti-transferrin receptor monoclonal (C2063, Sigma), anti-EEA1 monoclonal (BD Transduction Laboratories), anti-CD63 monoclonal and anti-LAMP1 monoclonal (H4A3; Developmental Studies Hybridoma Bank, University of Iowa), anti-GM130 monoclonal (BD Transduction Laboratories), anti-Golgin97 monoclonal (CDF4; Molecular Probes, Invitrogen Corp.), anti-TGN46 sheep polyclonal (ABD-Serotec), anti-Protein Disulfide Isomerase (PDI) monoclonal (S34200, Molecular Probes, Invitrogen Corp.), anti-HSC70 monoclonal (13D3; Affinity Bioreagents Inc.), anti-mannose-6-phosphate receptor monoclonal (2G11; Affinity Bioreagents Inc.), anti-exo70 polyclonal (kind gift from Dr. Patrick Brennwald) (Yeaman *et al.*, 2004), and anti-GFP monoclonal (JL-8; Clontech, Mountain View, CA.). Alexa-568 conjugated phalloidin was obtained from Molecular Probes (Invitrogen Corp.). For drug studies, nocodazole and ionomycin

were obtained from Calbiochem (EMD Chemicals Inc, Gibbstown, NJ) and were dissolved in DMSO at 1000x the working dilution.

Cloning and constructs: To generate the enhanced Green Fluorescent Protein (GFP) tagged full length myosin 5c, an N-terminal 4.0 kb fragment was obtained by PCR (Takara LA-Takara Bio, Madison, WI) from a human pancreas cDNA library (Clontech) using specific primer sequences (5'-tactcgagcatggcgggtggccgagctgtac-3' and 5'-gcggtcgacatcattgctttccaattgtctt-3'). An N-terminal ~3.4 kb fragment was then spliced into the existing GFP-Myo5c full tail construct (previously described in Rodriguez and Cheney, 2002) using an in frame XhoI site at the N-terminus and the SmaI site at nt 3411. mCherry-5.2 (empty vector), mCherry-Myo5c, mCherry-Myo5c full tail, and mCherry-Myo5b were constructed by inserting the mCherry coding sequence in frame and in place of the GFP coding sequence using the N-terminal AgeI restriction site and the XhoI restriction site within the pEGFP-C2 vector MCS or pEGFP-myosin expressing plasmid. The mCherry color cassette cDNA sequence was obtained by PCR from an mCherry-alpha tubulin plasmid (a kind gift from Dr. Roger Tsien) using specific primer sequences (5'-gctaccggtcgccaccatggtgagcaag-3' and 5'-gctcgagatcttgagtcggactgtac-3'). pEGFP-Myo5b (Myr6) was a gift from Dr Jim Goldenring (Lapierre *et al.*, 2001). The rat Myo5b full tail coding sequence (aa 912-1846) was obtained by PCR using specific primer sequences (5'-ataataagcttcgaggcccgttctgca-3' and 5'gcataggatccycagacttcattgaggaa-3') and using the pEGFP-Myo5b construct as the template. All PCR reactions were performed using PFU Ultra HF DNA polymerase (Stratagene, La Jolla, CA.). Constructs were verified by restriction enzyme digestion and sequencing. Chromogranin A-GFP

was obtained from Dr Ann Erickson (Taupenot *et al.*, 2002). NPY-mRFP and NPY-GFP were obtained from Dr. Francois Darchen and Dr. Jean-Pierre Henry (Desnos *et al.*, 2007b). Human Myo5a LT (full tail) was also obtained from Dr. Francois Darchen, (Desnos *et al.*, 2007b). All restriction enzymes were obtained from New England Biolabs (Ipswich, MA) (See Supplemental Figure 2 for a diagram of the myosin V constructs used in this manuscript).

Immunofluorescence: For immunofluorescence experiments cells were plated onto 12 mm round glass coverslips and allowed to adhere for 12-24 hours. Cells were then fixed using 2-4% para-formaldehyde in phosphate-buffered saline (PBS) for 10 minutes at 37°C, and then washed 3x for 10 minutes in PBS. For methanol fixation cells were incubated in 95% methanol (+ 5 mM EGTA) at -20°C for 20 minutes, then acetone (100%) extracted for 2 minutes at room temperature, before washing in PBS 3x for 10 minutes each. Cells were permeabilized using 0.2-0.5 % Triton X-100 in PBS for 10 minutes at room temperature, washed in PBS 3x for 10 minutes each. Cells were incubated in blocking solution (5% goat serum in PBS, pH 7.2, (G9023; Sigma) or 2% BSA (A4503; Sigma) in PBS) for 1 hour. Primary antibodies were used at 1ug/ml unless otherwise stated. Alexa-488 and Alexa-568 conjugated secondary antibodies made in goat directed against rabbit IgG and mouse IgG were obtained from Molecular Probes (Invitrogen Corp.). Alexa-568 secondary antibodies made in donkey against sheep IgG were also obtained from Molecular Probes. Secondary antibodies were used at 1 ug/ml. Alexa-568 conjugated phalloidin was obtained from Molecular Probes.

Coverslips were mounted onto glass slides for viewing and imaging using GelMount mounting media (Biomedica Corp., Foster City, CA.).

Transient transfections: For transient expression experiments, MCF-7 cells were plated onto glass coverslips (12 mm round or 22 mm square, #1.5) for 12-24 hours prior to transfection. Transient transfection of MCF-7 cells was achieved using PolyFect transfection reagent (Qiagen) according to manufacturer's recommendations for adherent HeLa cells in a 6-well plate. Depending on the expression construct being used, MCF-7 cells were allowed to express for 12-48 hours following the addition of transfection reagents to cells.

Generation of MCF-7 cells that stably express GFP-Myo5c: To generate an MCF-7 clonal cell line that stably expresses GFP-Myo5c (MCF-7 (DJ32)). MCF-7 cells were transfected with a full-length GFP-Myo5c construct as above. At 3 days post-transfection, cells were further cultured under the selection of 1.25 ug/ml Geneticin. Isolated clones were screened for GFP-Myo5c expression using fluorescence microscopy and by immunoblotting with antibodies to Myo5c and GFP.

Imaging: In live-cell imaging experiments, previously transfected MCF-7 cells were allowed to equilibrate in imaging media (Opti-MEM I, Gibco) for ≥ 2 hours prior to imaging. All live cell imaging was performed at 34-37°C. For drug perfusion experiments, cells were placed into an enclosed imaging chamber (Rose chamber) with Opti-MEM I. Perfusion of Opti-MEM I plus drugs was gravity induced at a rate of

approximately 2.0 ml/min. Cells were imaged on a Nikon TE2000U inverted microscope using wide-field epi-fluorescence illumination and/or Total Internal Reflection Fluorescence illumination (Nikon TIRF II system) equipped with a 60X (1.45 N.A.) DIC objective. Epi-fluorescence illumination was achieved using a 100 watt Hg lamp and TIRF illumination was achieved using a 488 nm line from a 300 mW Argon gas laser and/or a 568 nm line from a 120 mW mixed gas Argon/Krypton laser. (Dynamic Laser, Salt Lake City, UT). Laser lines were shuttered using an AOTF (NEOS 8 channel) controlled with a “Prairie AOTF” dropin in MetaMorph 6.0 (Molecular Devices Corporation, Downingtown, PA). In dual imaging mode (wide-field and TIRF), a 60%/40% (Laser/Hg illumination) mirror was placed into the light path to achieve fast, sequential illumination. Images were captured using an Orca-ER cooled CCD (Hamamatsu Corp.). TIRF illumination was obtained through a Nikon TIRF II illuminator and by adjustment of the angle of incidence of the laser beam with the glass/aqueous medium interface until total internal reflection was achieved. GFP and Alexa-488 were imaged using a GFP filter set Chroma 41001 (Chroma Technology Group, Rockingham, VT). For imaging in the red channel, a TRITC (Chroma 41002c) or Texas Red (Chroma 41004) filter set was used. For dual wavelength TIRF illumination, a 488 nm and 568 nm dual dichroic (Chroma 76653) (Z488/568 RDC) was used in conjunction with a green band pass (530 nm/35) and red band pass (630/60) emission filter (Chroma 83700) in a motorized filter wheel (Prior Scientific Inc. Rockland, MA). DIC images were obtained with brightfield illumination (100 watt Halogen bulb) and a DIC analyzer in the filter wheel. All hardware was controlled by MetaMorph 6.0 software. In fixed cell preparations, confocal images were obtained on a Zeiss LSM 510

NLO laser scanning confocal microscope in the UNC Neuroscience Center Confocal and Multi-Photon Imaging Facility. Images were obtained using a 63X (1.4 N.A.) objective in 12-bit mode. Laser illumination was achieved using a 30 mW Argon gas laser and a 1 mW HeNe mixed gas laser. Typically, for single image acquisition the pinhole was set to obtain an optical section of 1 μm using the 63x objective.

Image analysis: To obtain velocity measurements and track paths, individual puncta were tracked either by hand using “Track Points” or automatically by using the “Track Objects” function in MetaMorph 6.0. Velocities of Myo5c-labeled tubules were obtained by manually tracking the tip of the tubule, frame by frame using “Track Points” function in MetaMorph. Only clearly resolved tubules that were imaged using widefield epi-fluorescence were tracked. To obtain fluorescent intensity values along a trajectory across a secretory granule, a line, one pixel in width, was drawn and the MetaMorph function “Measure Linescan” was used to obtain the values and graph the intensities. TetraSpeck microspheres (0.1 μm) (Molecular Probes, Invitrogen Corp.) were used to obtain image registration on imaging systems used. Image registration was adjusted using color align function in MetaMorph 6.0. To quantify the level of secretory granule aggregation in MCF-7 cells, an “Aggregation Index” was generated by applying a weighted score of “0” = no aggregation; “1” = partial aggregation; “2” = full aggregation to cells that co-expressed a secretory granule marker and a dominant negative class V myosin. The same scoring method was used in control experiments performed simultaneously. Values reported are the mean \pm SEM. Statistical significance was determined using a two-tailed Students’ *t* test.

Immunoblot Analysis: To generate lysates of cultured cells, cells were trypsinized (0.25% trypsin + EDTA, Gibco) from the culture plate, collected in 1.5 ml microcentrifuge tubes, pelleted by low speed centrifugation (1000g), then resuspended in PBS with 5x Complete Protease Inhibitor Cocktail (Roche Diagnostics, Mannheim, Germany). Hot, 5x sample buffer (300 mM Tris-HCl, 10% SDS, 50% glycerol, 0.04% bromphenol blue, 50 mM DTT) was added directly to the cell suspension and then incubated at 90°C for 10 minutes. Samples were then flash frozen in liquid nitrogen and stored at -80°C until used. SDS PAGE was performed using 4-20 %, Tris-Glycine (Lonza) or 4-12% MOPS (Invitrogen Corp.) and molecular weight markers were from Bio-Rad Corporation (Catalog # 161-0318). Equal loading of gels was obtained by counting the cells/ml prior to generating lysates and Ponceau-S (0.2% in 3% trichloroacetic acid) staining confirmed transfer efficiency of the proteins to nitrocellulose. Following transfer, the nitrocellulose was blocked with 5% milk in Tris buffered saline plus 0.05% Tween 20 (TBST). Primary antibodies were used at 1 ug/ml in TBST. Blots were washed with TBST, 3x for 10 minutes following primary antibody incubation. Secondary antibodies were diluted 1:15,000 in TBST. Blots were washed 3x for 10 minutes following secondary antibody incubation. Secondary antibodies used were horse radish peroxidase conjugated donkey anti-rabbit (Jackson Immuno Research Laboratories Inc.). West Pico Super Signal Chemiluminescence (Pierce-Thermo Scientific, Rockford, IL) and Blue Devil x-ray film was used to visualize bands on blots. Quantitative analysis of immunoblotting was performed using Photoshop 6.0 and MetaMorph 6.0. Briefly, blots were scanned using an Epson 1680 scanner in the black

and white, 16-bit mode. Images were inverted, background subtracted, and the integrated intensity for each band was measured using MetaMorph 6.0 “Region Measurements” function.

Results

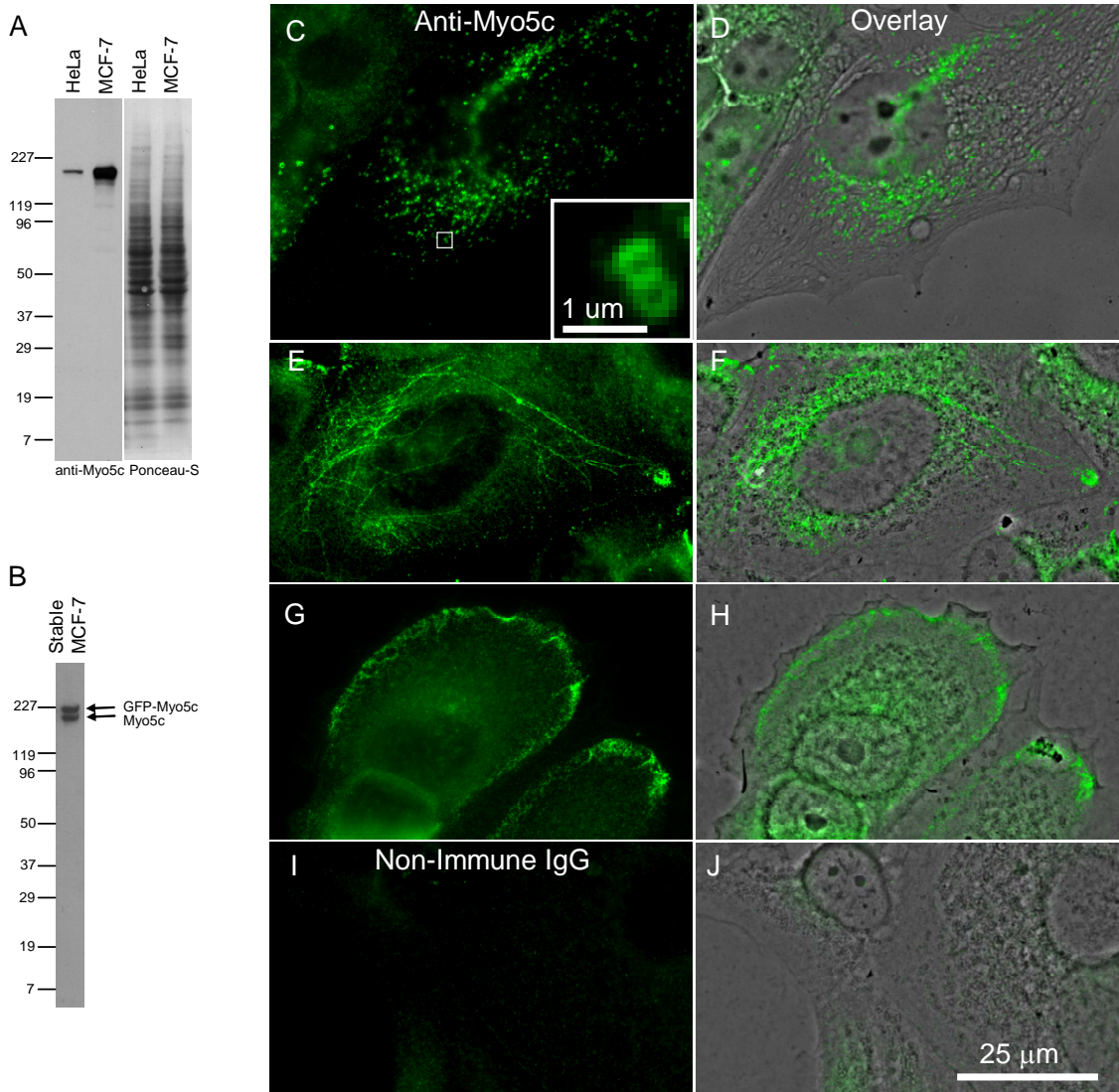
Myo5c is highly expressed in MCF-7 cells, an exocrine gland-derived cell line.

To identify the organelles that Myo5c associates with, we first sought to identify a cell line that would allow us to determine the localization of endogenous Myo5c. We thus screened rat tissues using immunoblotting and immunofluorescence to identify cell types that express high levels of Myo5c (Supplemental Figure 3-1). Consistent with previous results (Rodriguez and Cheney, 2002; Chen *et al.*, 2006), we observed specific Myo5c immuno-staining in the exocrine pancreas. Importantly, counter-staining with anti-lipase revealed that Myo5c is largely localized to acinar cells, the chief secretory cells of the exocrine pancreas. A similar pattern of localization was observed in the parotid and prostate glands, where the brightest Myo5c staining was found near the actin-rich region surrounding the secretory lumen. Together these results indicated that Myo5c was likely to be expressed at highest levels in cells derived from exocrine tissues. Consistent with this, we found that MCF-7 cells, a cell line derived from a human mammary gland adenocarcinoma, express relatively high levels of Myo5c (Figure 3-1A). Densitometry measurements of these immuno-blots revealed that MCF-7 cells express approximately 100-fold more Myo5c protein per cell than HeLa cells. These results suggested that MCF-7 cells would provide a useful system for high resolution studies on the localization, dynamics, and function of Myo5c.

Endogenous Myo5c localizes to puncta and tubules

Since Myo5c's localization in cultured cells was unknown, we performed immunofluorescence experiments in MCF-7 cells using a previously characterized

Figure 3-1. Endogenous Myo5c localizes to small puncta and slender tubules. (A) Immunoblot showing that MCF-7 cells express relatively high levels of Myo5c. SDS lysates of equal numbers of MCF-7 or HeLa cells were run on 4-20% SDS-PAGE gels and transferred to nitrocellulose, stained with Ponceau-S (right) to confirm equal protein loading, and then immunoblotted with Myo5c antibodies. (B) A similar immunoblot of MCF-7 cells that stably-express GFP-Myo5c (DJ32) illustrating the relative expression levels of GFP-Myo5c (upper band) and endogenous Myo5c (lower band). (C-H) Immunofluorescence images of MCF-7 cells stained with anti-Myo5c. (C, D) Endogenous Myo5c localizes to puncta that are distributed in the perinuclear region, the cell periphery, and the ventral surface. (C, inset) Higher magnification of boxed region showing that individual Myo5c puncta are often ring-like with a hollow center. (E, F) In some cells, endogenous Myo5c also localizes to slender tubules. (G, H) In spreading or migrating cells, Myo5c frequently exhibits a strikingly polarized localization toward the leading edge. Comparison of the fluorescence and phase contrast images shows that the Myo5c staining does not extend all the way to the leading edge, and is instead found in the transition zone behind the lamellipodium. (I, J) MCF-7 cells stained with control antibody shows little labeling. Left panels show fluorescence images alone and right panels show fluorescence images overlaid with the corresponding phase contrast images.



affinity-purified antibody against Myo5c (Rodriguez and Cheney, 2002). These experiments revealed that endogenous Myo5c localizes to small puncta in virtually all MCF-7 cells (Figure 3-1). There were tens to hundreds of puncta per MCF-7 cell and puncta had diameters that ranged from ~0.4-1.5 μm . The puncta were found in the perinuclear region, the cell periphery, and the ventral surface of the cell (Figure 3-1C-D). At high magnification, individual puncta of endogenous Myo5c often had a ring-like appearance, as would be expected if Myo5c was present on the cytoplasmic surface of a vesicle or granule (Figure 3-1C-inset).

In a subset of MCF-7 cells, endogenous Myo5c also localized on slender tubules. These tubules often spanned tens of micrometers and their morphology suggested that they corresponded to membranous structures (Figure 3-1E-F). Myo5c labeled tubules were detected in less than 5-10% of nonconfluent cells and in approximately 25% of confluent cells. Small puncta of Myo5c were often observed at different points along Myo5c labeled tubules. In methanol fixed cells, Myo5c exhibited a similar pattern of localization on puncta and tubules and the Myo5c labeled tubules exhibited only occasional sites of overlap with microtubules (not shown). Control antibodies showed only a diffuse background staining (Figure 3-1I-J).

In MCF-7 cells that were spreading or migrating, Myo5c puncta exhibited a strikingly polarized distribution to a region near the leading edge. Comparison of the fluorescence and phase contrast images indicates that Myo5c puncta in these cells were in fact largely excluded from the lamellipodium at the leading edge and instead localized to

the transition zone behind it. (Figure 3-1G-H). The transition zone is located at the interface between the microtubule-rich central region of the cell and the actin-rich periphery and is a region of active exocytosis and endocytosis that contains many membranous organelles (Bergmann *et al.*, 1983; Yvon and Wadsworth, 2000). The highly polarized localization of Myo5c puncta to the transition zone thus raises the possibility that Myo5c is associated with trafficking pathways involved in directed insertion near the leading edge (Hopkins *et al.*, 1994; Schmoranzer *et al.*, 2003).

Dynamics of Myo5c in living cells

To investigate the dynamics of Myo5c in living cells, we next generated a full length construct with GFP fused to the N-terminus of human Myo5c (GFP-Myo5c). N-terminally tagged class V myosins have been reported to retain their motor and cargo binding activities (Moore *et al.*, 1996; Zhang *et al.*, 2004) and N-terminally tagged myosins have been widely used to image myosin dynamics (Moore *et al.*, 1996; Berg and Cheney, 2002; Belyantseva *et al.*, 2005). When GFP-Myo5c was transiently expressed in MCF-7 cells, it exhibited a pattern of localization very similar to that of endogenous Myo5c. Like endogenous Myo5c, GFP-Myo5c localized to small puncta in all MCF-7 cells and to slender tubules in a subset of MCF-7 cells. Furthermore, in spreading or migrating cells, puncta of GFP-Myo5c exhibited a polarized distribution to the transition zone behind the leading edge (Figures 3-2 and 3-3).

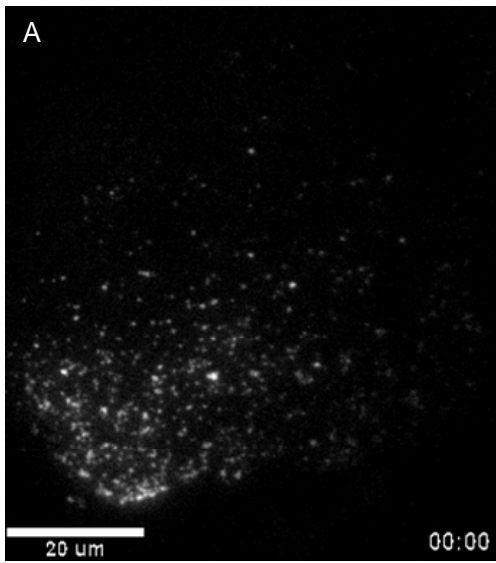
In addition to transiently transfecting MCF-7 cells with GFP-Myo5c, we also generated an MCF-7 cell line that stably expresses GFP-Myo5c. As expected,

immunoblots of the stable cell line revealed expression of a single additional band that was ~28 kDa larger than endogenous Myo5c (Figure 3-1B). Densitometry of these blots indicates that the stable line expresses GFP-Myo5c at approximately 1.3x the level of endogenous Myo5c. The stably expressed GFP-Myo5c yielded the same pattern of localization to puncta, slender tubules, and the transition zone that was observed with endogenous Myo5c (Figure 3-3 and 3-4). Together these results indicate that GFP-tagged Myo5c accurately recapitulates the localization of endogenous Myo5c.

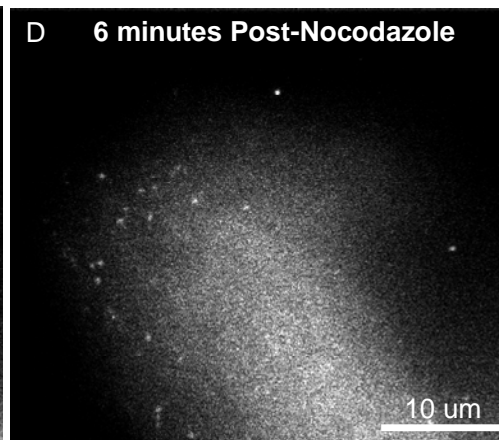
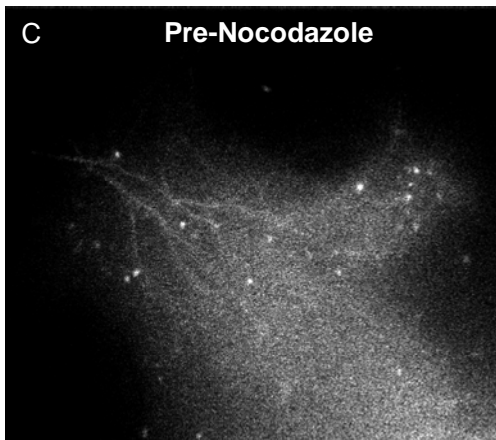
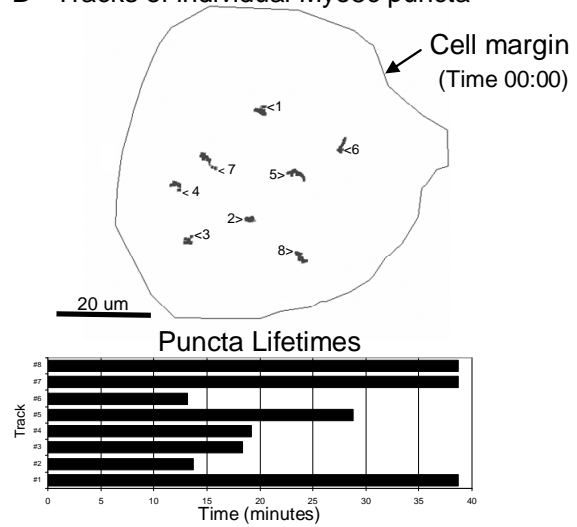
Live cell imaging of the GFP-Myo5c puncta revealed that they continuously undergo slow movements (~30 nm/s) that appear randomly directed (Figure 3-2A, 3-2E and Movie 3-1). Although puncta of GFP-Myo5c could be observed by either widefield or TIRF microscopy, TIRF yielded particularly clear images of Myo5c puncta. Since TIRF illumination only excites fluorophores within ~200 nm of coverslip surface, many of the Myo5c puncta are in extremely close proximity to the plasma membrane. Most Myo5c puncta remained within the TIRF field for several minutes and some could be tracked for the entire duration of a 38+ minute timelapse (Figure 3-2B). This indicates that the Myo5c labeled puncta are relatively long-lived under resting conditions. Addition of 5 μ M nocodazole, a microtubule depolymerizing agent, did not obviously perturb the velocity or distribution of the GFP-Myo5c puncta (Figure 3-2E-F, Movie 3-2).

Live-cell imaging of the GFP-Myo5c labeled tubules revealed that they are highly dynamic. Myo5c labeled tubules extended over tens of micrometers at an apparent rate of ~500 nm/s (Figure 2G and Movie 2). Most tubules appeared to extend toward the cell

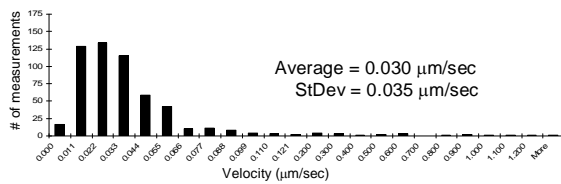
Figure 3-2. Dynamics of GFP-Myo5c associated puncta and tubules. (A) TIRF image from a time-lapse experiment showing the localization of GFP-Myo5c to numerous small puncta visible on the ventral surface of an MCF-7 cell. (B) Tracks of selected Myo5c puncta from the cell in (A) that were visible at the start of the timelapse. The starting positions of the puncta are indicated by the numbered arrowheads and the histogram shows the "lifetime" during which each puncta remained visible within the TIRF field. Note that the Myo5c puncta move in a slow and apparently random fashion and are relatively long lived (see also Movie 1). (C) Widefield image from a timelapse experiment showing localization of GFP-Myo5c to small puncta and slender tubules in an MCF-7 cell. (D) Widefield image of the same cell in (C) 6 minutes after treatment with 5 μ M nocodazole. Note that nocodazole leads to the disappearance of the Myo5c tubules, but not the Myo5c puncta. (see also Movie 2) (E) Histogram of the velocities of individual Myo5c puncta prior to addition of nocodazole. (F) Histogram of the velocities of individual Myo5c puncta after addition of nocodazole. Note that the Myo5c puncta move relatively slowly and continue to move in the presence of nocodazole. (G) Histogram showing the rapid extension rates of Myo5c tubules prior to addition of nocodazole. Since the Myo5c tubules disappeared after nocodazole addition, no measurements of tubule velocity were made after addition of nocodazole.



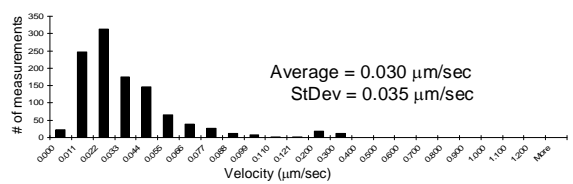
B Tracks of individual Myo5c puncta



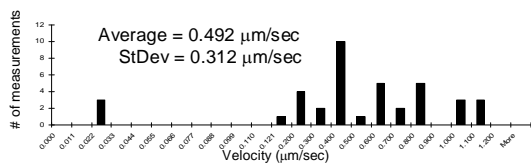
E Myo5c puncta velocity-Pre Nocodazole



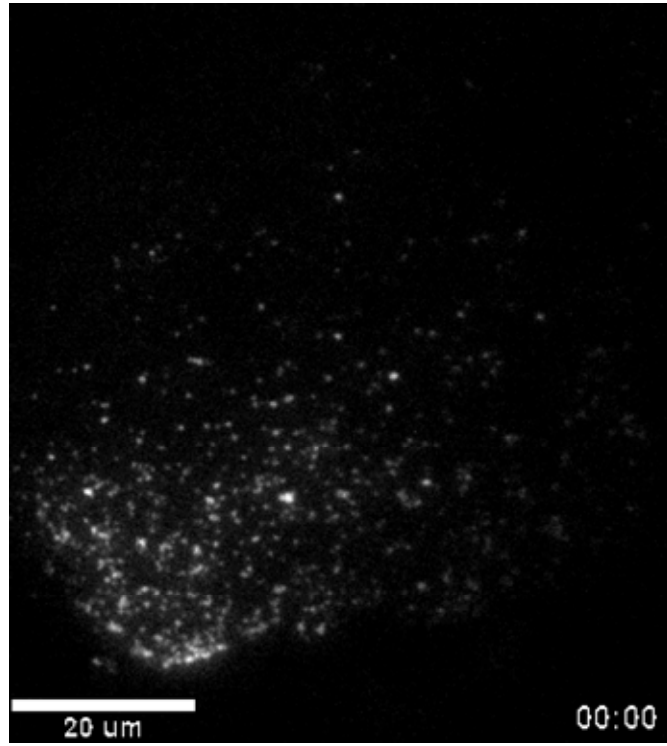
F Myo5c puncta velocity-Post Nocodazole



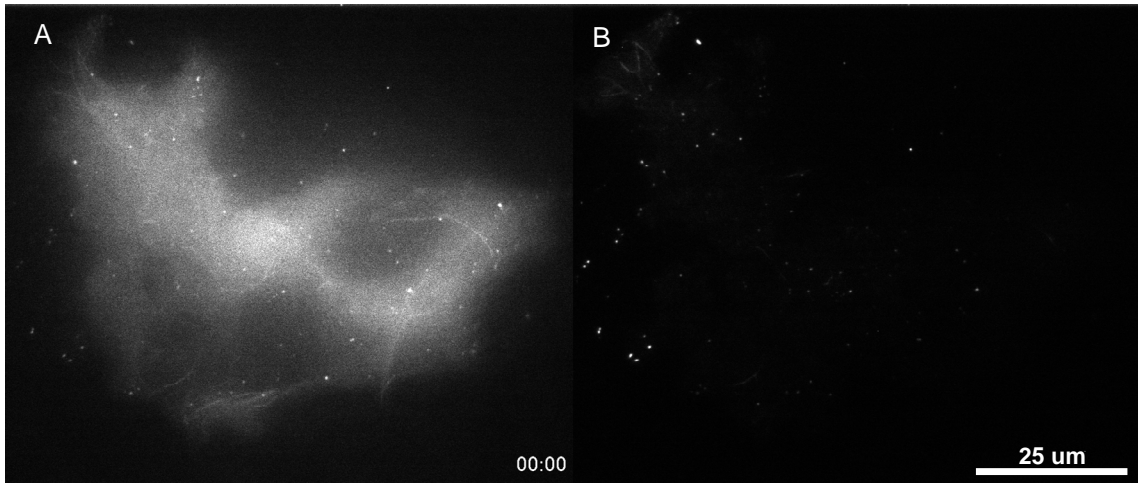
G Myo5c tubule velocity-Pre Nocodazole



Movie 3-1: Time lapse movie illustrating the dynamics of Myo5c puncta. The single cell illustrated here is moving towards the bottom of the frame and the Myo5c puncta are most abundant just behind the leading edge. Note that puncta of GFP-Myo5c move relatively slowly in an apparently random fashion and that some puncta remain visible within the TIRF field for the entire 38 minute timelapse. MCF-7 cells were transfected with GFP-Myo5c and imaged using TIRF, ~2 mW laser power (measured upon exit from the fiber optic cable), and 2x2 binning.



Movie 3-2: Timelapse movie demonstrating that Myo5c associated tubules move rapidly and microtubule-dependently whereas Myo5c puncta move slowly and microtubule-independently. (A) Widefield movie that highlights the rapid movements of the Myo5c tubules and their disappearance after addition of 5 uM nocodazole. (B) TIRF movie acquired at the same time shows that Myo5c puncta continue to move after the addition of 5 uM nocodazole. MCF-7 cells were transfected with GFP-Myo5c, incubated 16 hours, and then imaged by collecting widefield and TIRF images on a 6 second interval.



periphery. Addition of 5 μ M nocodazole led to a dramatic loss of the Myo5c tubules and appeared to induce their collapse towards the cell center (see Movie 3-2). These rapid and directed movements of the Myo5c labeled tubules, as well as their sensitivity to nocodazole, strongly suggest that Myo5c is associated with membranous tubules that undergo long range transport along microtubules.

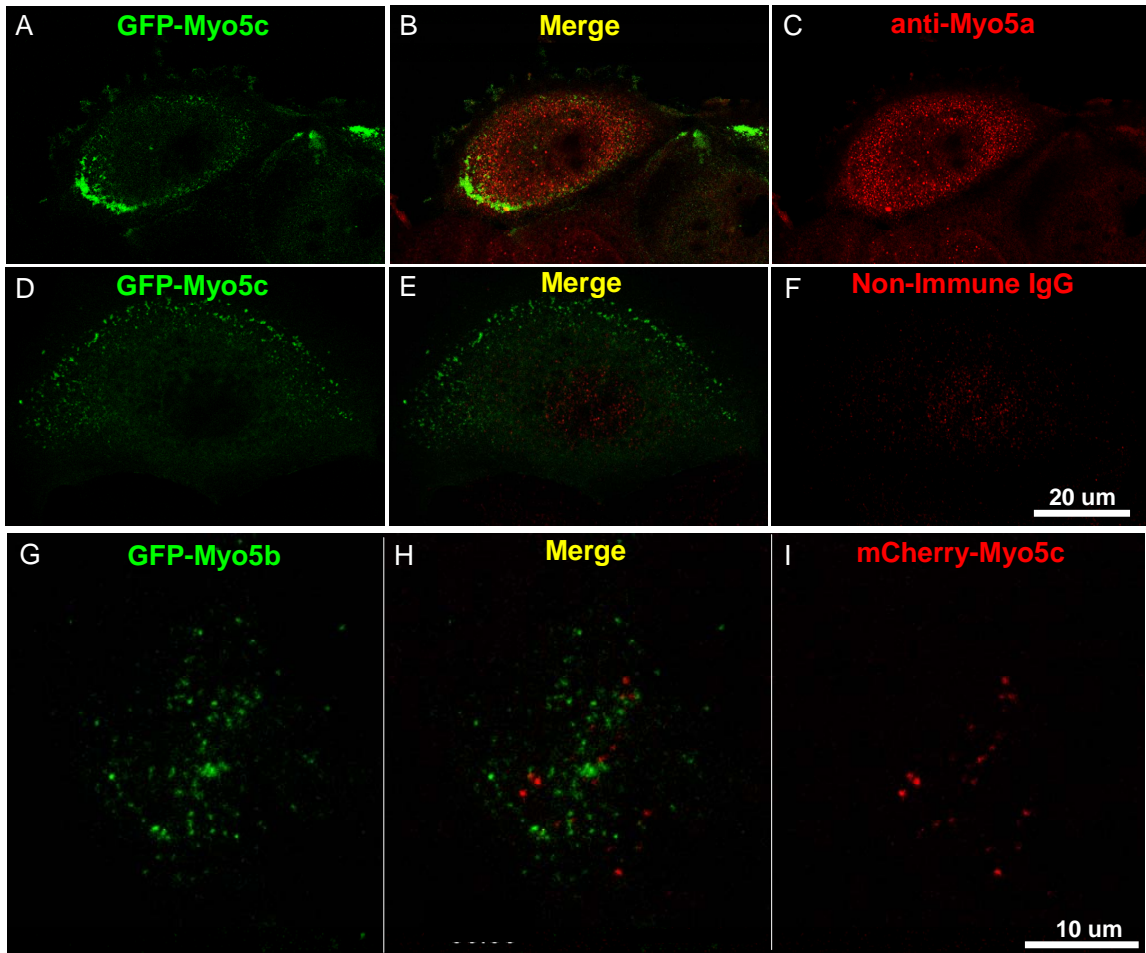
The localization of Myo5c is distinct from that of Myo5a or Myo5b

To test if the functions of Myo5c are distinct from those of the other two class V myosins, we first asked if the localization of Myo5c was distinct from that of Myo5a or Myo5b. Since our antibodies to Myo5a and Myo5c were both rabbit polyclonals, we immunolabeled MCF-7 cells that stably express GFP-Myo5c with antibodies to Myo5a (Figure 3-3A-C). Confocal images of endogenous Myo5a show that it localizes on bright puncta distributed throughout the cell and was thus similar to the Myo5a staining pattern we had observed in HeLa cells (Rodriguez and Cheney, 2002). Importantly, endogenous Myo5a exhibited little or no colocalization with the GFP-Myo5c labeled puncta, indicating that they associate with different organelles (Figure 3-3A-C). Immunolabeling with a rabbit non-immune IgG control shows that the Myo5a antibody staining is specific (Figure 3-3D-F).

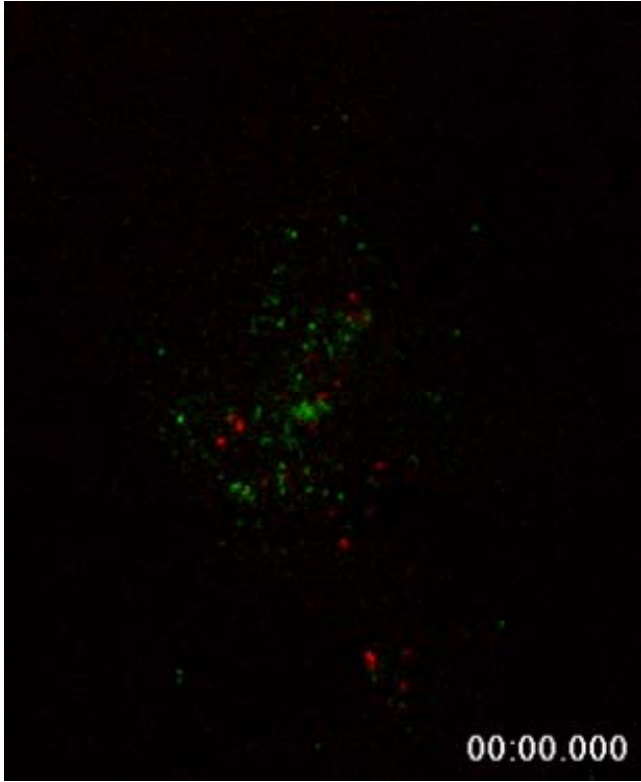
Since dominant negative experiments in HeLa cells had implicated both Myo5b and Myo5c in recycling pathways (Lapierre *et al.*, 2001; Rodriguez and Cheney, 2002), we next tested if the localization and dynamics of Myo5c were distinct from those of Myo5b. We thus performed live cell imaging experiments using MCF-7 cells cotransfected with a

Figure 3-3. The localization of Myo5c is distinct from that of Myo5a and Myo5b.

(A-C) MCF-7 cells stably expressing GFP-Myo5c were counterstained with Myo5a polyclonal antibodies. (D-F) Control antibody staining in MCF-7 cells stably expressing GFP-Myo5c, shows no significant signal above background. Confocal images were collected using a Zeiss LSM510. (G-I) MCF-7 cells were cotransfected with GFP-Myo5b and mCherry-Myo5c, incubated 12-16 hours, and then imaged using TIRF illumination. GFP-Myo5b (green) is shown in (G), mCherry-Myo5c (red) is shown in (I), and a merged image is shown in (H). The Myo5c labeled puncta are largely distinct from the Myo5b labeled puncta. (See also Movie 3)



Movie 3-3: The localization and dynamics of Myo5c are distinct from those of Myo5b. MCF-7 cells were transfected with GFP-Myo5b (green) and mCherry-Myo5c (red), incubated 12 hours, and imaged by TIRF. Note that the Myo5b puncta are generally smaller and faster than the Myo5c puncta. The Myo5b puncta also tend to disappear from the TIRF field within 10-60 seconds. Although the distributions of these two class V myosins are largely distinct, there are many examples of transient contacts being made between the Myo5c labeled and Myo5b labeled puncta. Images were acquired on a 6 second interval.



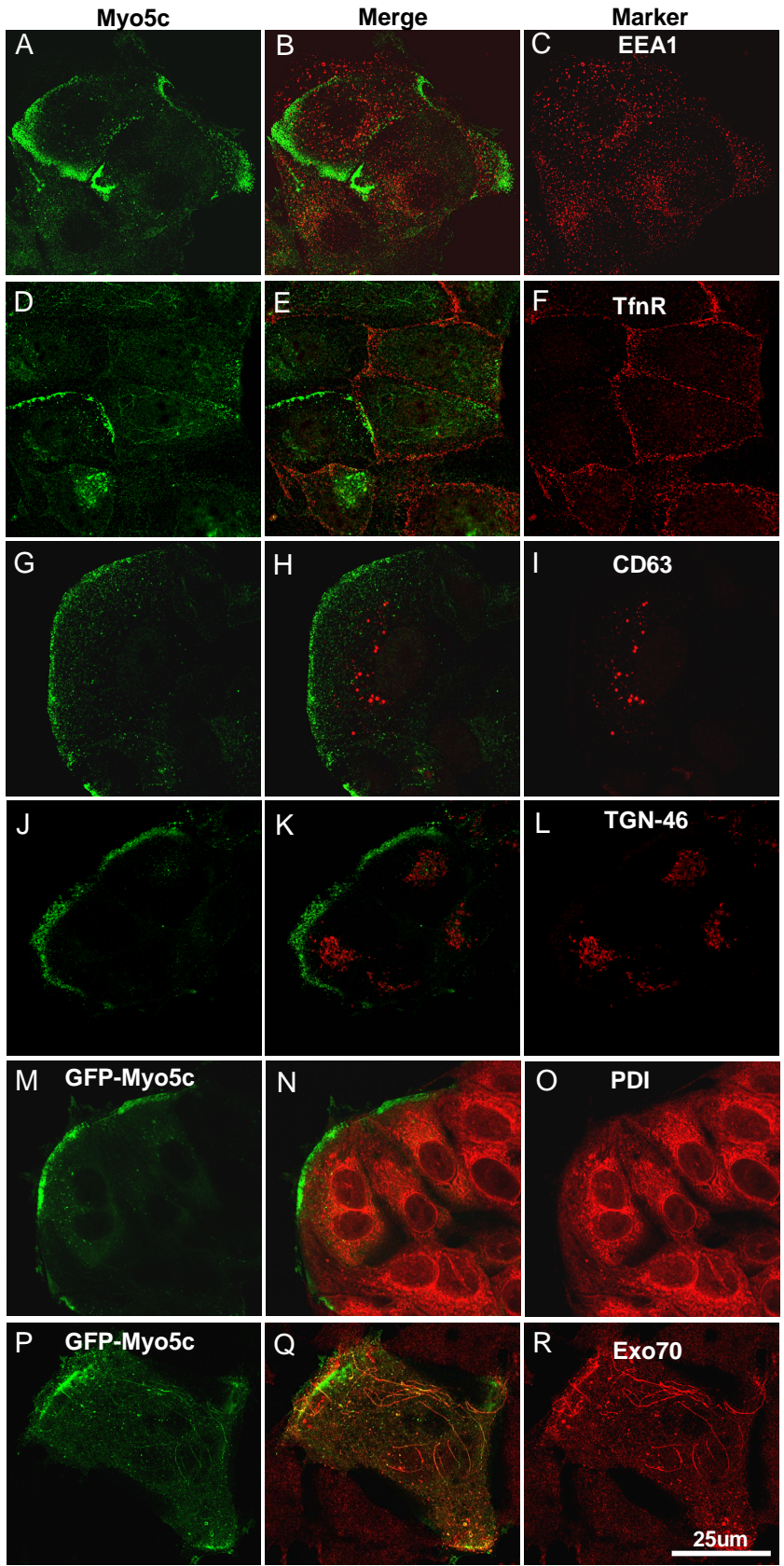
full length mCherry-Myo5c construct and a previously characterized full length GFP-Myo5b construct (Lapierre *et al.*, 2001). The mCherry-tagged Myo5c exhibited the same patterns of localization and dynamics we had observed for endogenous Myo5c and GFP-Myo5c (Figure 3-3G-I and Movie 3-3). Two-color TIRF imaging revealed that GFP-Myo5b localized to numerous small puncta that showed little overlap with Myo5c. On average, the Myo5b puncta also appeared smaller and moved more rapidly ($\sim 75 \pm 60$ nm/s) than the Myo5c puncta. In addition, the Myo5b puncta could typically only be tracked within the TIRF field for 10-60s before they disappeared. Although Myo5b puncta did sometimes appear to make contact with the larger and more stable Myo5c puncta, the localization and dynamics of Myo5c were clearly distinct from those of Myo5b.

What organelles does Myo5c associate with?

To identify the specific compartment(s) that Myo5c associates with and to gain an understanding of Myo5c's possible functions, we next performed double-labeling experiments with markers for several different membrane compartments (Figure 3-4). Confocal images showed little or no colocalization of endogenous Myo5c with markers for early endosomes (EEA1), the transferrin recycling pathway (transferrin receptor), multivesicular bodies (CD63), or the endoplasmic reticulum (protein disulfide isomerase; PDI) (Figure 3-4A-I). Myo5c also showed little colocalization with a marker for the trans-golgi network (TGN46), although it should be noted that faint Myo5c labeling was sometimes detected near the TGN (Figure 3-4J-K). We also observed little or no colocalization with markers for the Golgi apparatus (Golgin 97), late endosomes (mannose-6-phosphate receptor), or lysosomes (LAMP-1) (not shown).

Figure 3-4. Distribution of Myo5c relative to selected membrane compartments.

Endogenous Myo5c (A, D, G, J) and stably-expressed GFP-Myo5c (M, P) localize to puncta and to occasional tubules in MCF-7 cells. The middle panels are merged images of Myo5c and compartment markers (B, E, H, K, N, Q). Myo5c showed little or no overlap with known markers of endocytic compartments such as anti-EEA1 (C), or anti-transferrin receptor (F). Myo5c also showed little or no overlap with anti-CD63, a marker for late endosomes and multivesicular bodies (I). Anti-TGN46 (L), a marker of the trans-Golgi network, and protein disulfide isomerase (PDI; O), a marker of the ER, also showed little overlap with GFP-Myo5c. Antibodies to Exo70 do partially colocalize with GFP-Myo5c, especially along slender tubules. This colocalization with a component of the exocyst suggests that Myo5c is associated with compartment(s) involved in exocytic trafficking. These images are all single confocal planes.

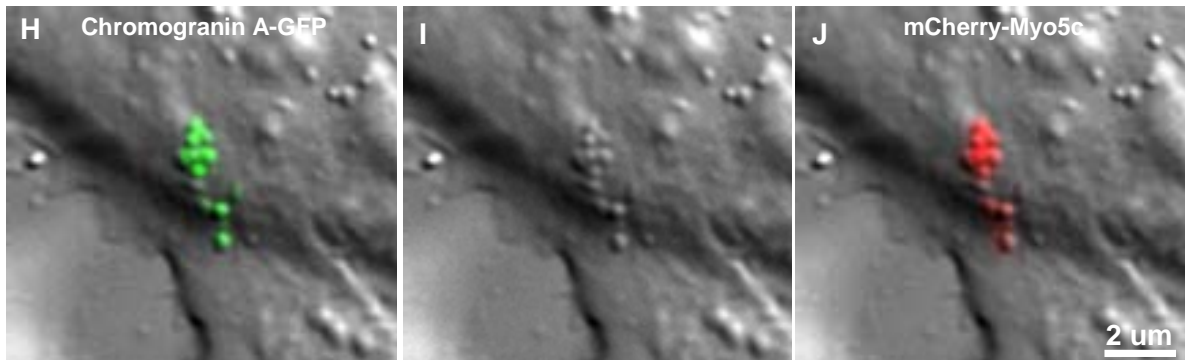
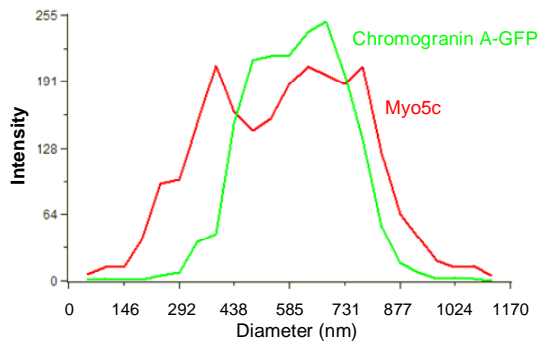
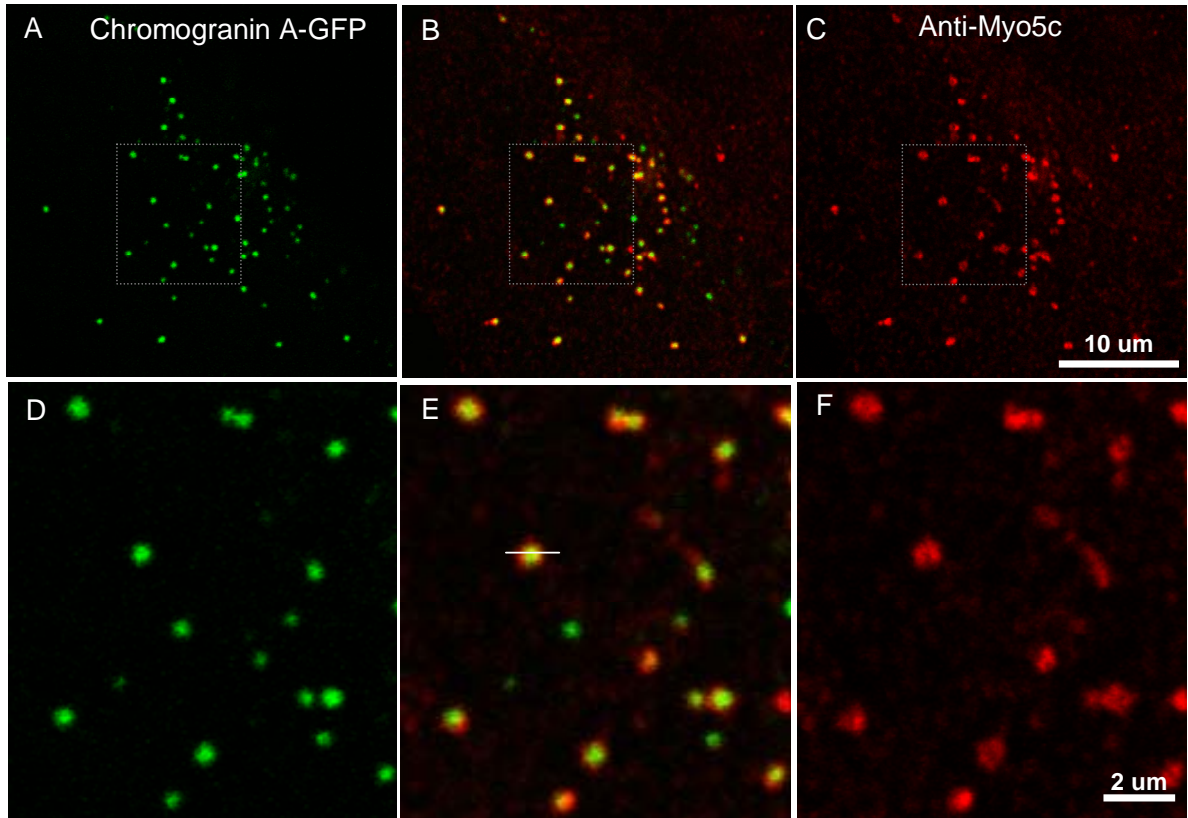


Interestingly, antibodies to Exo70 did partially colocalize with Myo5c on slender tubules and some puncta (Figure 3-4P-R). This colocalization with a component of the exocyst complex (Yeaman *et al.*, 2004) suggests that the Myo5c labeled tubules may function in an exocytic pathway.

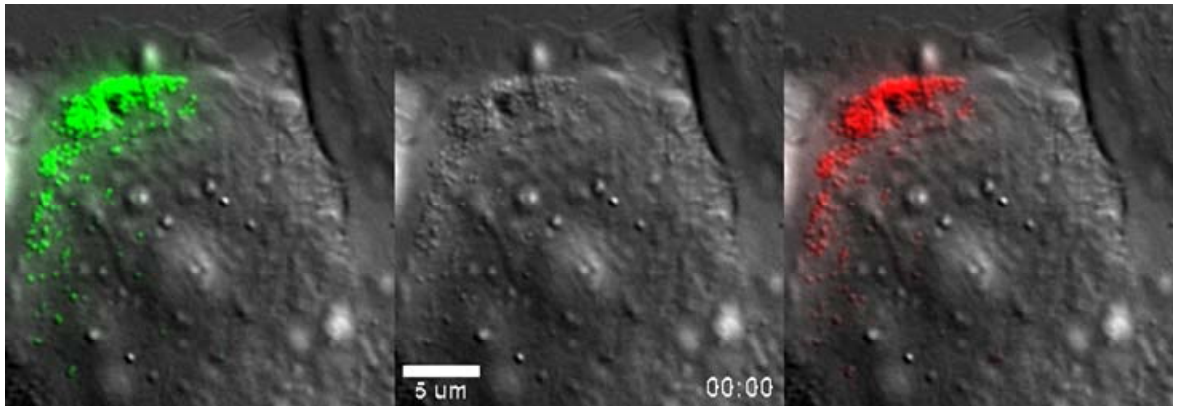
Myo5c localizes on secretory granules

Since EM studies have shown that MCF-7 cells contain secretory granules when cultured in the presence of the endogenous estrogens present in calf serum (Vic *et al.*, 1982), we next tested if endogenous Myo5c associates with secretory granules. Thus, we transfected MCF-7 cells with chromogranin A-GFP, a widely used marker protein that localizes to the lumen of granules that undergo regulated secretion (Taupenot *et al.*, 2002). Although chromogranins were originally characterized as secreted components of secretory granules in endocrine cells, they have also been detected in some exocrine cells (Kanno *et al.*, 1999; Hofslis *et al.*, 2002; Romeo *et al.*, 2002) and they are packaged within exocrine granules when expressed in exocrine cells (Natori *et al.*, 1998; Hofslis *et al.*, 2002). Confocal images revealed that chromogranin A-GFP localized to discrete granules that colocalize with puncta of endogenous Myo5c (Figure 3-5A-F). Although this colocalization is striking, it should be noted that some Myo5c puncta lack detectable chromogranin A and that some chromogranin A granules lack Myo5c. In puncta that do overlap, the ring-like puncta of endogenous Myo5c often appear to surround the chromogranin A labeled granules (Figure 3-5D-G). This relationship can also be seen in the linescan through an individual granule (Figure 3-5G). Since Myo5c is a cytoplasmic protein, these results indicate that Myo5c localizes to the cytoplasmic surface of secretory (or secretory-like) granules.

Figure 3-5. Myo5c localizes on secretory granules. (A-F) Endogenous Myo5c localizes on secretory granules labeled by chromogranin A-GFP. MCF-7 cells expressing the secretory granule marker chromogranin A-GFP (A, D; green) were immuno-labeled with anti-Myo5c antibodies (C, F; red). (D-F) Higher magnification views of the boxed region of the single confocal plane seen in panels A-C showing that each punctum of Myo5c often forms a ring-like structure that surrounds a chromogranin A-GFP labeled secretory granule. (G) Linescan analysis of a single chromogranin A-GFP/Myo5c punctum (indicated by the white line left of center in panel E) showing Myo5c staining surrounding a chromogranin A-GFP labeled granule. (H-J) Exogenously expressed mCherry-Myo5c also localizes on secretory granules labeled by chromogranin A-GFP. MCF-7 cells were cotransfected with chromogranin A-GFP (green) and mCherry-Myo5c (red) for ~1.5 days and then imaged by widefield fluorescence (H, J) and differential interference contrast microscopy (I). (See also Movie 4)



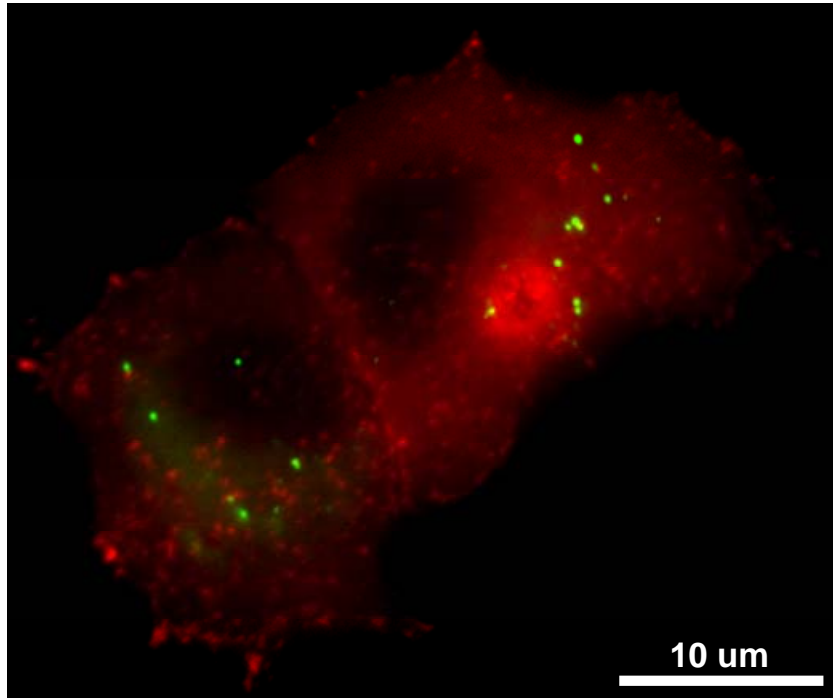
Movie 3-4: mCherry-Myo5c localizes on chromogranin A-GFP labeled secretory granules. MCF-7 cells were cotransfected with mCherry-Myo5c (red) and chromogranin A-GFP (green) for 16 hours. This two color TIRF/DIC timelapse movie was generated by collecting a TIRF image with a 488 nm laser and emission filter, a TIRF image with a 568 nm laser and emission filter, and a DIC image, with a new set of images collected every 6 seconds. Note that puncta of Myo5c clearly remain associated with chromogranin A labeled granules as they move throughout the cell. Although Myo5c puncta are enriched near the leading edge, they are excluded from the lamellipodium, which is demarcated by a region of clearly visible retrograde flow.



To confirm that Myo5c associates with secretory granules, we next tested whether exogenously expressed Myo5c also localizes to secretory granules. MCF-7 cells were thus cotransfected with chromogranin A-GFP and mCherry-Myo5c. Like endogenous Myo5c, mCherry-Myo5c localized to small puncta that showed striking colocalization with chromogranin A (Figure 3-5H-J). The puncta labeled by Myo5c and chromogranin A-GFP frequently colocalized with small granules detectable by Differential Interference Contrast (DIC) microscopy. The tight association between Myo5c and secretory granules was most clearly demonstrated by live cell imaging using two-color TIRF in conjunction with DIC. Movies from these experiments showed that mCherry-Myo5c and chromogranin A-GFP colocalize on moving granules (see Movie 3-4). This clear colocalization through time on moving granules provides extremely strong evidence that Myo5c associates with secretory granules in living MCF-7 cells.

To test whether the association of Myo5c with secretory granules was specific for Myo5c or was a general property of class V myosins, we cotransfected MCF-7 cells with chromogranin A-GFP and a mCherry-Myo5b construct. Time-lapse imaging illustrated that Myo5b showed little or no colocalization with chromogranin A labeled secretory granules (See Movie 3-5). As expected from our earlier data that showed that Myo5c and Myo5b had distinct patterns of localization and dynamics, the puncta labeled by the mCherry-Myo5b were smaller and moved faster than the chromogranin A labeled secretory granules. In addition, the chromogranin A-GFP labeled granules exhibited relatively long lifetimes and could be tracked for several minutes whereas most of the Myo5b puncta could only be tracked for 10-60 seconds. The dynamics of the

Movie 3-5: mCherry-Myo5b does not localize on chromogranin A-GFP labeled secretory granules. MCF-7 cells were cotransfected with chromogranin A-GFP (green) and mCherry-Myo5b (red) for 12 hours and then imaged using two-color, widefield fluorescence microscopy. Myo5b puncta generally appear smaller, faster, and shorter lived than the chromogranin A labeled secretory granules. Although Myo5b puncta do not localize on secretory granules, they occasionally appear to transiently make contact with them. Images were acquired on a 6 second interval.



chromogranin A-GFP labeled granules were very similar to those of Myo5c, as expected from the close association of Myo5c and secretory granules. Although Myo5b differed dramatically from Myo5c in showing little or no colocalization with chromogranin A labeled secretory granules, small puncta of Myo5b occasionally appeared to contact the secretory granules.

To show that Myo5c associates with secretory granules in the absence of transfection with chromogranin A, we also tested whether Myo5c colocalized with a second marker for secretory granules, Neuropeptide Y (NPY). (Lang *et al.*, 1997; Desnos *et al.*, 2003; Desnos *et al.*, 2007b). Fluorescently tagged NPY consists of the signal sequence and part of the propeptide from NPY fused to either GFP or mRFP. Since NPY-GFP is a small and relatively soluble marker that is packaged into secretion granules, it has been widely used as a non-perturbing probe to allow direct visualization of secretory granule exocytosis (Lang *et al.*, 1997; El Meskini *et al.*, 2001; Desnos *et al.*, 2007b). Thus, we imaged MCF-7 cells cotransfected with NPY-GFP and mCherry-Myo5c. As expected, many of the Myo5c puncta showed clear colocalization with secretory granules marked by NPY-GFP (See Movie 3-6). This clear colocalization of Myo5c with a second secretory granule marker provides strong additional evidence that Myo5c indeed associates with secretory granules in MCF-7 cells.

Myo5c associated granules can be triggered to undergo secretion

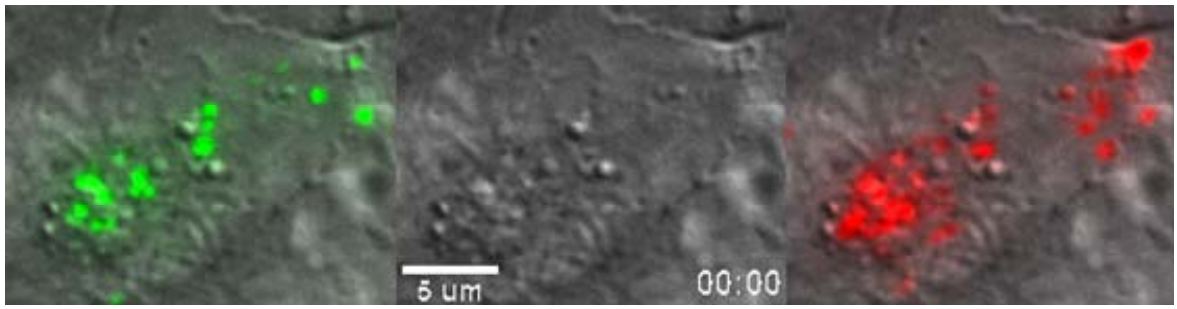
Given the clear association of Myo5c with two different secretory granule markers, we next tested if the granules labeled by Myo5c in MCF-7 cells were capable of undergoing secretion. We thus cotransfected MCF-7 cells with NPY-GFP and mCherry-

Myo5c, and then imaged them using two-color TIRF and DIC. To stimulate secretion, we added ionomycin, an ionophore that leads to increased intracellular Ca^{++} and that has been previously used to trigger secretion in MCF-7 cells (Flezar and Heisler, 1993; Vadlamudi *et al.*, 2000). Although exocytosis was not observed prior to addition of ionomycin, addition of 5 μM ionomycin triggered a series of exocytotic events over several minutes that could be recognized by the sudden discharge of an individual granule's NPY-GFP fluorescence (See Movie 3-6). Careful inspection revealed that at the same time the NPY fluorescence was lost from a given granule, a dimple-like structure detectable in DIC often appeared on the membrane. This simultaneous visualization of secretion events by DIC and by loss of NPY fluorescence provides strong evidence that ionomycin induced the secretory granules to undergo exocytosis. Although the NPY fluorescence associated with a given granule's exocytosis typically disappeared within the space of 3-6 s, the Myo5c fluorescence remained detectable for an additional 10-60 s.

To further confirm that Myo5c associated granules are capable of undergoing exocytosis, we performed similar experiments using cells stably expressing GFP-Myo5c and transiently transfecting them with NPY-mRFP to label the secretory granules (Figure 3-6 and Movie 3-7). The cell illustrated in this movie had relatively large granules (~ 1 μm diameter) and clearly demonstrates that individual granules are surrounded by a ring of Myo5c. Although ionomycin triggered the exocytosis of relatively few granules in this cell, several clear examples of granule secretion can be observed at different times

following ionomycin addition (Figure 3-6A-C). Note also that after ionomycin addition several secretory granules move into the TIRF field and eventually undergo exocytosis.

Movie 3-6: Myo5c associated secretory granules can be triggered to undergo secretion. MCF-7 cells were cotransfected with mCherry-Myo5c (red) and with NPY-GFP (green), a soluble marker of the secretory granule lumen. Cells were then imaged by two color TIRF plus DIC and 5 μ M ionomycin was perfused into the imaging chamber at 3:30 seconds (flash) to trigger secretion. Most Myo5c puncta localize on NPY-labeled granules, although some NPY-labeled granules lack detectable Myo5c and some Myo5c puncta lack detectable NPY. Within ~90 seconds of ionomycin addition, most of secretory granules in this cell had undergone exocytosis and disappeared. Individual fusion events are indicated by the sudden disappearance of NPY fluorescence. Puncta of Myo5c fluorescence often remain detectable for 30-60 seconds following fusion events. In some cases apparent fusion events also correlate with the appearance of dimple-like structures visible by DIC microscopy. The details of this process can be best appreciated by manually advancing and reversing the movie one frame at a time using the computer keyboard's arrow keys.



It is also important to note that the number and dynamics of Myo5c puncta appeared very similar in cells whether or not they expressed NPY-mRFP (See Movie 3-8).

Furthermore, adding ionomycin triggered Myo5c to undergo apparent fusion events both in cells that express granule markers and in cells that do not. Together these experiments demonstrate that 1) Myo5c associates with secretory granules in MCF-7 cells; 2) Myo5c associated granules can be triggered to undergo exocytosis; and 3) Myo5c can remain associated with the granule membrane for tens of seconds following fusion.

Although the colocalization between Myo5c puncta and secretory granule markers is striking, it should be noted that it is not perfect and that some secretory granules lacked detectable Myo5c staining. The granules that lack Myo5c may represent immature secretory granules since granule markers showed little colocalization with Myo5c puncta in the first 5-10 hours after transfection and instead exhibited a diffuse localization near the golgi (not shown). It should also be noted that some Myo5c puncta lack detectable secretory granule markers, which indicates that, in addition to secretory granules, Myo5c is likely to associate with as yet unidentified organelles.

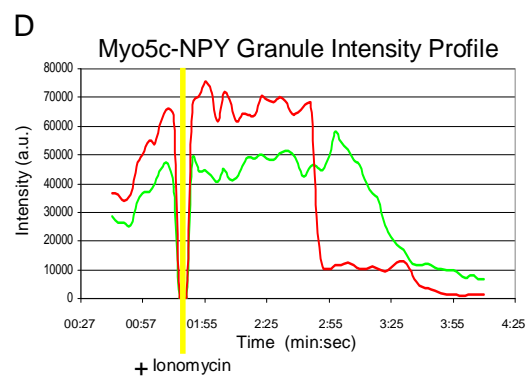
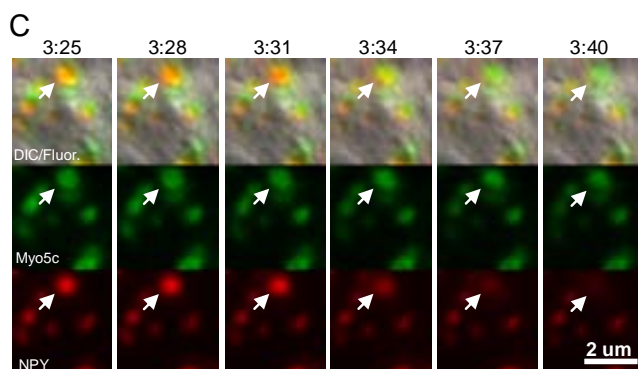
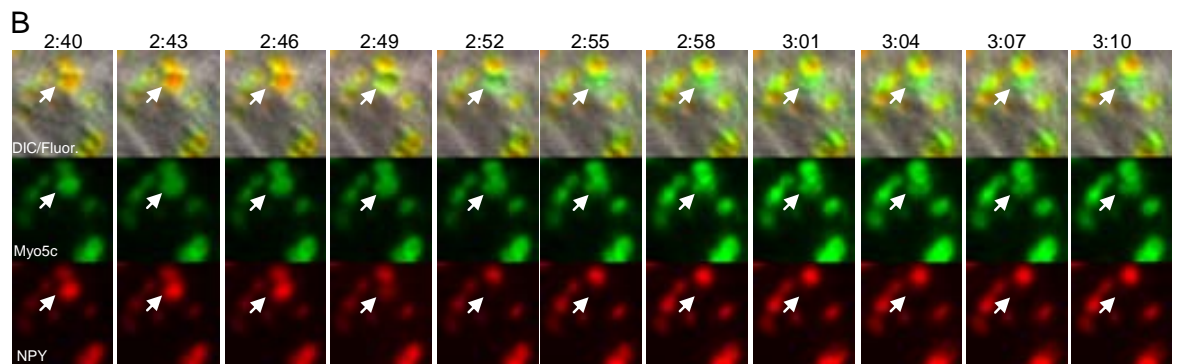
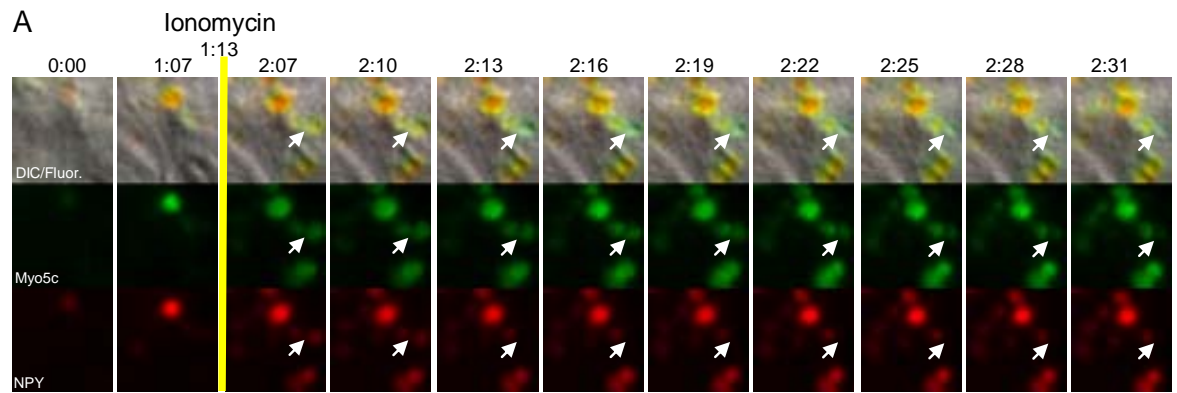
Dominant-negative Myo5c perturbs the distribution of secretory granules

Given the clear association of both endogenous and exogenous Myo5c with secretory granules, we next investigated whether Myo5c functions in secretory granule trafficking. The tail domains of class V myosins have been widely used as dominant negatives and have been reported to yield phenotypes similar to those of genetic knock-outs (Catlett and Weisman, 1998; Wu *et al.*, 1998; Reck-Peterson *et al.*, 1999; Schott *et*

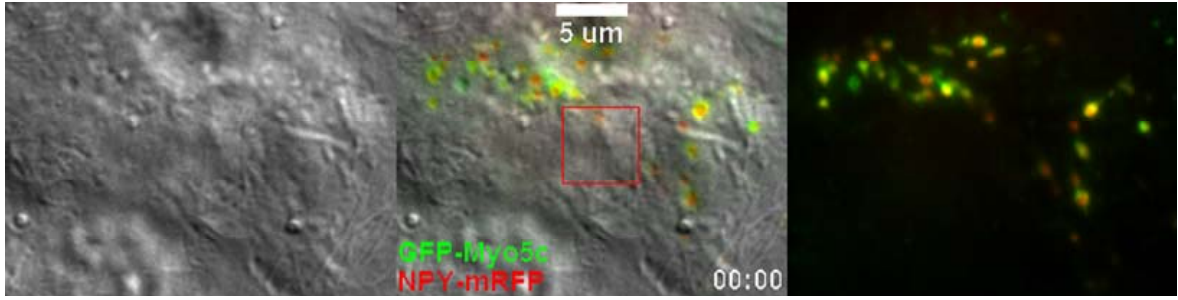
al., 1999; Jones *et al.*, 2000). We previously used the Myo5c full tail as a dominant negative in HeLa cells, where it formed large puncta that specifically colocalized with and perturbed the distribution of rab8a and transferrin receptor but not the golgi, late endosomes, lysosomes, or rab11a positive recycling endosomes (Rodriguez and Cheney, 2002). We thus tested if a dominant negative Myo5c full tail construct labeled with mCherry would perturb the distribution of secretory granules labeled by chromogranin A-GFP. In control cells transfected with an empty mCherry vector, mCherry exhibited a diffuse localization throughout the cytoplasm and chromogranin A-labeled secretory granules exhibited their usual pattern of localization (Figure 3-7A-C). In the cells transfected with the dominant negative mCherry-Myo5c full tail, however, chromogranin A localization was dramatically perturbed and it formed large aggregates that partially colocalized with the Myo5c tail (Figure 3-7D-F). To quantitate the level of perturbation induced by the expression of the dominant negative tail, an aggregation index was generated by applying a weighted score (0, 1, or 2) to cells exhibiting varying degrees of granule aggregation (See Materials and Methods for details). The aggregation index for cells expressing chromogranin A-GFP and mCherry empty vector exhibited a background level of aggregation (0.15 ± 0.21), whereas expression of mCherry-Myo5c full tail induced a significantly higher aggregation index (1.71 ± 0.30) ($p < 0.008$) (Figure 3-7M). Values are expressed as mean \pm SEM.

As an additional test to determine if Myo5c functions in secretory granule trafficking, we also asked if expression of the Myo5c dominant negative tail perturbed the distribution of a second secretory granule marker, NPY-GFP. As shown in

Figure 3-6: Myo5c-labeled secretory granules can be triggered to undergo secretion. MCF-7 cells stably expressing GFP-Myo5c were transiently transfected with NPY-mRFP to label secretory granules and were stimulated to secrete with Ionomycin (5 μ M). (A-C) Image sequences from same movie showing several secretory events (arrows). Upper, middle, and lower panels of each sequence correspond to DIC-fluorescence overlay, GFP-Myo5c, and NPY-mRFP, respectively. (D) Fluorescence intensity profile of secretory event in (B), showing Myo5c fluorescence remaining at site of secretion after granule contents were secreted. Secretory granule was tracked with a 1 μ m x 1 μ m region to obtain integrated intensity values. In A-C, the DIC images (upper panels) show the formation of granule “dimples” during secretory events. Fluorescence image sequences were acquired using TIRF illumination. Note the appearance of many secretory granules into the TIRF field following ionomycin treatment. See also Movie 7 to view the entire cell used in this analysis.



Movie 3-7: Myo5c remains associated with secretory granule membranes following exocytosis. MCF-7 (DJ32) cells, that stably expressed GFP-Myo5c, were transiently transfected with NPY-mRFP and imaged using two color TIRF illumination and Differential Interference Contrast (DIC) to visualize Myo5c-associated granule dynamics during exocytosis. Ionomycin (5uM) was perfused onto cells to induce granule exocytosis at the 1:13 timepoint. Within 1 minute, several secretory granules move into the TIRF illumination field and undergo secretory events that correlate strongly with, 1) a dramatic loss of NPY fluorescence (red) over a 6 second interval, and 2) the formation of dimple-like structures in the DIC channel. Strikingly, the GFP-Myo5c remains associated with the secretory granule membrane for 30-45 seconds following loss of NPY fluorescence. The red box is the area used in Figure 6. Similar results were observed in 3 separate experiments.



Movie 3-8: Myo5c labeled secretory granules are not perturbed by exogenous markers of secretory granules. MCF-7 cells stably expressing GFP-Myo5c were transfected with NPY-mRFP and imaged using two color, widefield epi-fluorescence at 3 second intervals. The size, morphology, and dynamics of the GFP-Myo5c ring-like structures are highly similar in cells expressing and not expressing the exogenous granule marker. Treatment with ionomycin (5 uM) induced many secretory granules to undergo secretion in both NPY-expressing and non-NPY-expressing cells within the same field of view.

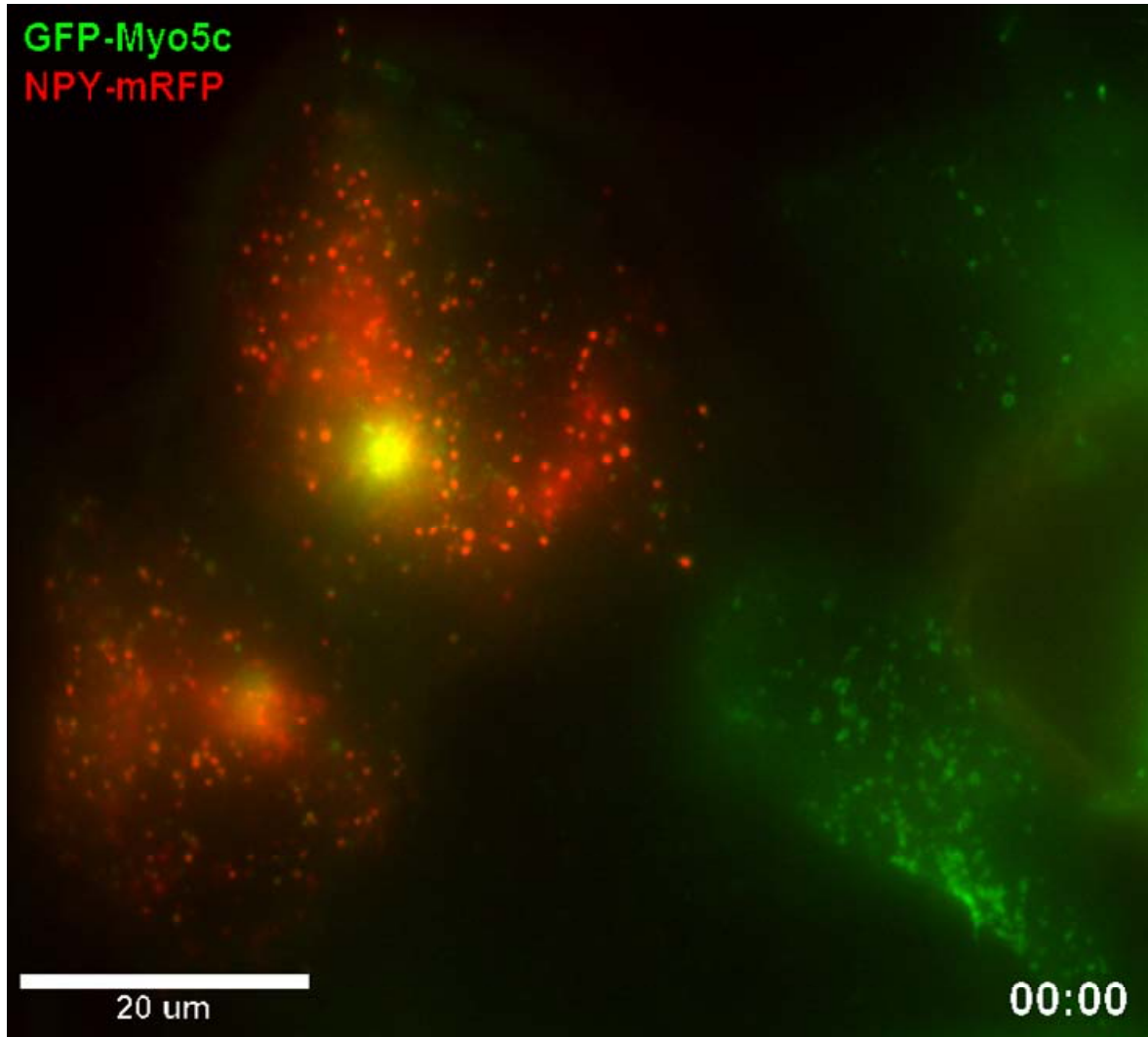
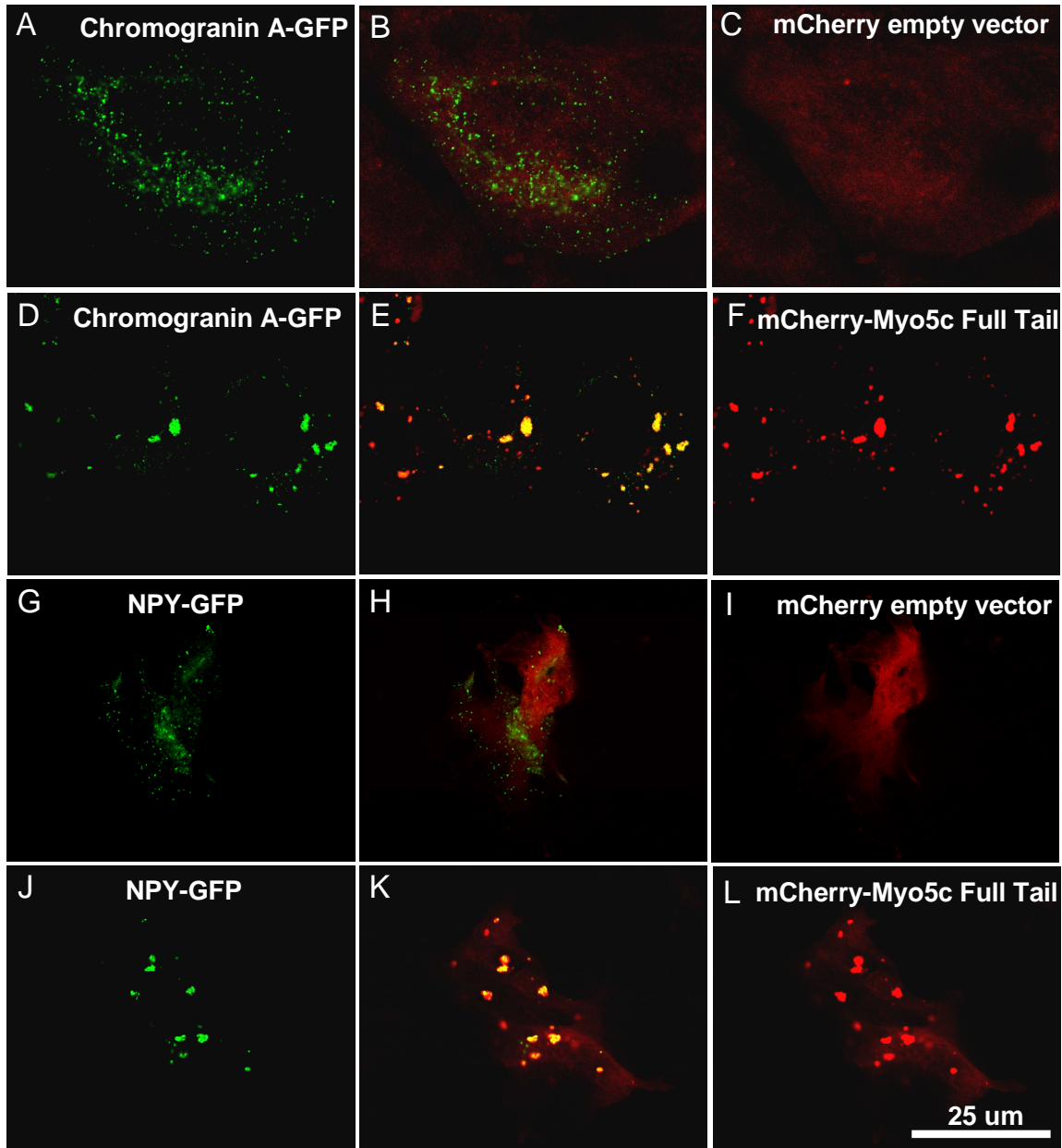


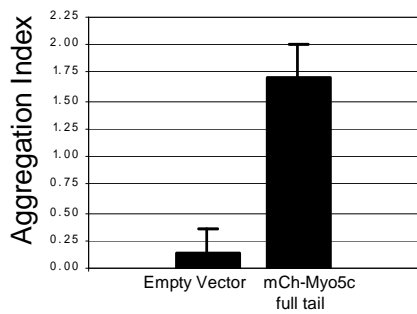
Figure 3-7G-L, transfection with mCherry-Myo5c dramatically perturbed the distribution of NPY-GFP. The NPY-GFP in these cells also formed large aggregates that partially colocalized with the Myo5c tail. The aggregation index for cells expressing NPY-GFP and mCherry empty vector exhibited a background level of granule aggregation (0.06 ± 0.10) (N=3 expts.; 21 cells), whereas expression of mCherry-Myo5c full tail induced a significantly higher aggregation index (1.35 ± 0.45) (n=4 expts.; 39 cells) ($p < 0.005$) (Figure 3-7N). Values are expressed as mean \pm SEM. These experiments thus show that the dominant negative mCherry-Myo5c tail perturbs the distribution of two different markers of secretory granules.

As a final test of the function of Myo5c in secretory granule distribution, we switched fluorescent tags and performed similar experiments using NPY-mRFP to label secretory granules and a dominant negative GFP-Myo5c full tail construct (See Supplemental Figure 3-3). As observed above with the mCherry-Myo5c full tail construct, expression of GFP-Myo5c full tail induced the formation of large NPY puncta that partially colocalized with the Myo5c tail. These effects appear to be specific to the GFP-Myo5c full tail construct since transfection with equivalent full tail constructs from Myo5a (GFP-Myo5a full tail) or Myo5b (GFP-Myo5b full tail) did not grossly perturb the distribution of the NPY-mRFP granule marker and showed little colocalization with them. Together these experiments indicate that the Myo5c tail domain is sufficient for targeting to secretory granules in MCF-7 cells and that dominant negative Myo5c perturbs the distribution of secretory granule markers.

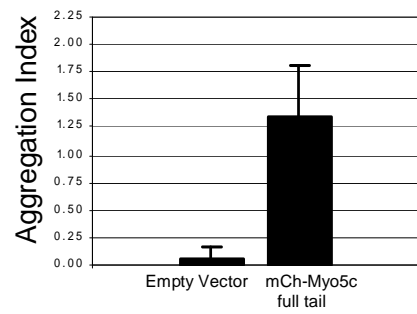
Figure 3-7. Dominant negative Myo5c disrupts the distribution of secretory granules. MCF-7 cells transiently expressing chromogranin A-GFP (A,D) and mCherry-Empty Vector (C) or mCherry-Myo5c full tail (F) show that dominant negative Myo5c dramatically induces aggregation of secretory granules (E,F). (G-L) Transient co-expression of a second marker of secretory granules, NPY-GFP (G, J) and mCherry empty vector (I) or mCherry-Myo5c full tail (L). The center panels (B, E, H, K) show the merged images. (M, N) Bar graphs indicating the “Aggregation Index” of chromogranin A-labeled (M) and NPY-labeled (N) secretory granules in the presence of dominant negative Myo5c. (M) mCherry-Myo5c full tail induced a statistically significant increase in the “aggregation index” ($p < 0.008$). (N) mCherry-Myo5c full tail induced a statistically significant increase in the “aggregation index” ($p < 0.005$) (See Materials and Methods for scoring method) Cells were fixed ~24 hours (A-F, M) and ~36 hours (G-L, N) post-transfection and imaged on Zeiss LSM510 confocal microscope. (N=3 experiments).



M Chromogranin A Granule Aggregation



N NPY Granule Aggregation



Discussion

Although class V myosins play critical roles in organelle trafficking and have been the subject of intensive research, relatively little is known about Myo5c, one of the three class V myosins expressed in mammals. Here we have used MCF-7 cells as a model system to provide the first immunolocalization of endogenous Myo5c in a cell line and the first visualization of the dynamics of GFP-Myo5c in living cells. These experiments showed that Myo5c associates with at least two compartments: small puncta present in all MFC-7 cells and slender tubules detected in a subset of the cells. We also show that the localization and dynamics of Myo5c are distinct from those of Myo5b, that Myo5c localizes on secretory granules, and that dominant negative Myo5c perturbs the distribution of secretory granule markers. As discussed below, these results help define the basic cell biology of Myo5c and indicate that Myo5c functions as a molecular motor in the trafficking of exocrine secretory granules.

Myo5c associates with slender tubules that move rapidly and microtubule-dependently

The morphology, dynamics, and microtubule-dependence of the Myo5c associated tubules strongly suggest they correspond to membranous tubules. Since Myo5c is an actin-dependent motor, it is likely to function as a passenger on membrane tubules undergoing rapid microtubule-dependent transport (Figure 3-8). Although the precise identity and functions of these tubules are not yet clear, there is precedent for an association of Myo5c with membranous tubules. We previously reported that the GFP-Myo5c tail localized to slender tubules in a subset of HeLa cells (Rodriguez and Cheney,

2002). Membranous tubules have been implicated in many different trafficking pathways, including exocytic recycling pathways such as those utilized by the transferrin receptor (Hopkins *et al.*, 1994) or MHC1 (Weigert *et al.*, 2004). A recent study reported that Myo5c binds to rab8a and that rab8a localizes to slender tubules in ~10% of HeLa cells (Roland *et al.*, 2007), which is consistent with previous data showing that rab8a colocalizes with the Myo5c tail in HeLa cells (Rodriguez and Cheney, 2002). In addition, rab8a functions in secretory trafficking (Peranen *et al.*, 1996; Desnos *et al.*, 2003; Sato *et al.*, 2007; Henry and Sheff, 2008) and has recently been associated with secretory granules (Faust *et al.*, 2008). An association between the Myo5c tubules and exocytic trafficking is also supported by our observation that Myo5c tubules partially colocalize with antibodies to Exo70. It should also be noted that EM studies have reported that post-golgi tubules appear to emanate towards immature secretory granules in acinar cells (Hand and Oliver, 1977a, 1977b). Importantly, we detected Myo5c tubules in only a subset of MCF-7 cells, even under live cell imaging conditions. This indicates that Myo5c tubules are associated with membrane trafficking events that are either transient or induced only in a subset of cells.

Myo5c puncta move slowly and microtubule-independently

Endogenous Myo5c and GFP-Myo5c both localized primarily to numerous small puncta. Since many GFP-Myo5c puncta could be imaged by TIRF, these puncta must be located at the cell cortex, where Myo5c could potentially interact with cortical actin filaments. Individual puncta often remained within the ~200 nm depth of the TIRF field for hundreds or thousands of seconds, and thus are relatively long lived structures under

Figure 3-8: Summary Diagram: Myo5c is associated with dynamic tubules and regulated secretory granules. (A) In MCF-7 cells, endogenous Myo5c labels long, slender tubules that exhibit dependence upon microtubules. (A) Endogenous Myo5c localizes to punctate structures that exhibit a polarized distribution at the leading edge and also on the ventral surface of migrating MCF-7 cells. (B) High magnification schematic illustration of endogenous Myo5c is in a ring-like distribution on the periphery of large (0.5-1.5 μm diameter) secretory granules that are distributed near the leading edge and on the ventral surface of MCF-7 cells. (B) Schematic illustration of Myo5c remaining associated with secretory granules before, during, and post-exocytosis.

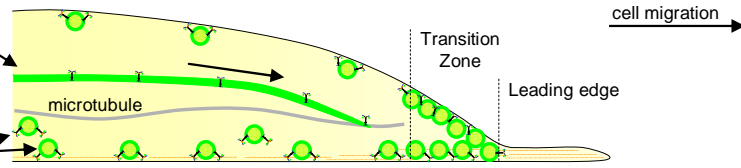
A Myo5c associates with tubules and puncta in MCF-7 cells

Myo5c tubules

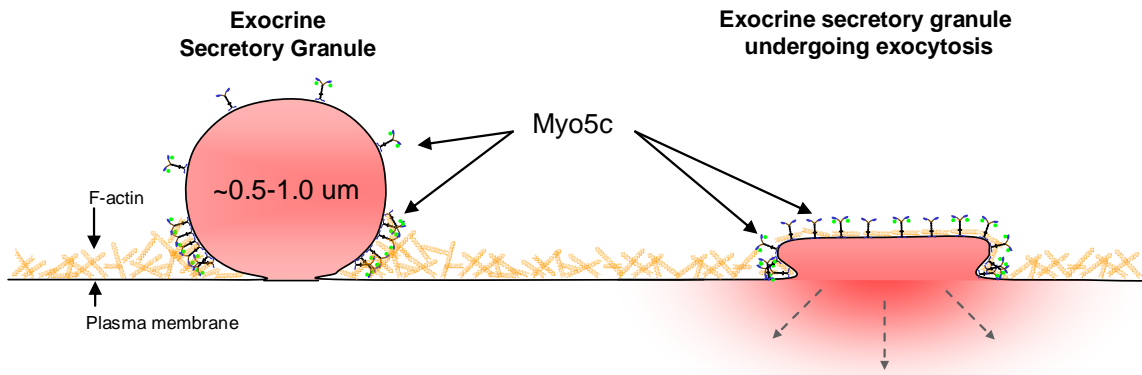
- Move rapidly (~ 500 nm/s)
- Extend toward periphery
- Microtubule-dependent
- Exo70 (+)

Myo5c puncta

- Move slowly (~30 nm/s)
- Randomly directed
- Microtubule-independent
- Polarized distribution
- Undergo regulated secretion



B Myo5c is associated with secretory granules



resting conditions. Although the Myo5c puncta exhibited little movement in the Z-axis, they moved constantly in the X-Y plane in a slow (~30 nm/s) and apparently random fashion. These slow movements in the plane of the membrane are presumably due either to some form of tethered diffusion or to Myo5c motor activity. Since the slow movements continued in the presence of nocodazole, they are not dependent on microtubules. The slow movements are also unlikely to be driven by actin-based rocketing since we did not detect comet tails on Myo5c puncta when cells were stained with phalloidin (not shown). It is possible that the slow movements are driven by myosins moving on randomly oriented cortical actin filaments, but it should be noted that the ~30 nm/s velocity of the puncta is at the lower end of the 24-160 nm/s range of *in vitro* motility velocities reported for Myo5c (Watanabe *et al.*, 2007; Takagi *et al.*, 2008).

Do the different class V myosins have distinct or overlapping functions?

An important result from this work was the demonstration that the localization of Myo5c is distinct from that of Myo5a or Myo5b. This indicates that Myo5c associates with distinct organelles and suggests that the different class V myosins have distinct functions in MCF-7 cells. An important difference between Myo5c and the other class V myosins in mammals is that Myo5c appears to be non-processive (Watanabe *et al.*, 2007; Takagi *et al.*, 2008). Although processivity in myosins was first discovered in Myo5a (Mehta *et al.*, 1999), it is now known that several other class V myosins, including *Drosophila* myosin V (Toth *et al.*, 2005), Myo2p (Reck-Peterson *et al.*, 2001), and Myo4p (Reck-Peterson *et al.*, 2001; Dunn *et al.*, 2007) are not processive. While processivity provides the potential advantage that a single motor molecule would be

sufficient to transport an organelle, non-processive motors can also transport organelles as long as enough motors are present. Since biochemical studies with baculovirus expressed Myo5c constructs indicate a duty ratio of 0.10 (Takagi *et al.*, 2008) and 0.33 (Watanabe *et al.*, 2007), as few as 3-10 Myo5c molecules might be sufficient to transport an organelle processively. Even fewer Myo5c molecules would be needed if other proteins or cytoplasmic factors such as intracellular ADP increase the processivity of Myo5c within cells. Given the 36 nm step size of myosin V (Mehta *et al.*, 1999), it should also be noted that even a few steps could be sufficient to span the entire depth of the TIRF field or actin rich cortex.

Myo5c associates with secretory granules and functions in secretory granule trafficking

Myo5c puncta exhibited striking colocalization with two independent markers of secretory granules, chromogranin A-GFP and fluorescently tagged NPY. Individual secretory granules were often surrounded by a ring of Myo5c, as would be expected from association of Myo5c with the cytoplasmic surface of the granule. Importantly, puncta of endogenous Myo5c often had a ring-like appearance even in MCF-7 cells that had not been transfected with granule markers. This, plus previous EM evidence showing that MCF-7 cells contain secretory granules (Vic *et al.*, 1982), suggests that Myo5c associates with secretory granules even in MCF-7 cells that have not been transfected with secretory granule markers. Live cell imaging with TIRF demonstrated that Myo5c labeled granules can be triggered to undergo secretion and also provided the first high resolution imaging of the dynamics of Myo5c during exocytosis. Interestingly, individual Myo5c

puncta generally remained detectable for 10-60 s after loss of a granule's contents, which indicates that Myo5c remains at least transiently associated with granule membranes following exocytosis. To test if Myo5c functions in granule trafficking, we expressed the dominant negative Myo5c tail and found that it induced the formation of large puncta that partially colocalized with secretory granule markers and dramatically perturbed their distribution. These effects appear to be specific to Myo5c since equivalent tail constructs from Myo5a and Myo5b did not grossly perturb the distribution of secretory granules and showed little colocalization with secretory granule markers. Together these experiments provide strong evidence that Myo5c associates with secretory granules and is required for normal secretory granule trafficking.

Myo5c and exocrine secretion

Although MCF-7 cells provide a model system that is ideal for high resolution imaging and investigation of the basic cell biology of Myo5c, it is also important to consider the functions of Myo5c in actual exocrine secretory tissues. In recent collaborative studies, we showed that Myo5c localizes on mature exocrine secretory granules in rabbit lacrimal gland acinar cells (Marchelletta *et al.*, 2008). Most importantly, expression of the Myo5c tail partially inhibited carbachol stimulated secretion, indicating that Myo5c is required for normal secretion in actual exocrine secretory cells. The combination of the data from lacrimal gland acinar cells, the proteomics data identifying Myo5c as one of the proteins present in membranes from exocrine secretory granules (Chen *et al.*, 2006), and the imaging data presented here with

MCF-7 cells provide extremely strong evidence that Myo5c is a class V myosin that functions in the trafficking of exocrine secretory granules.

A key goal for future research will thus be to identify the precise step or steps where Myo5c functions in secretory granule trafficking. A myosin on secretory granules could potentially act at several different steps in granule trafficking, including termination of microtubule-dependent transport at the cell cortex (Wu *et al.*, 1998), tethering of granules to cortical actin (Wu *et al.*, 1998; Desnos *et al.*, 2003; Desnos *et al.*, 2007a), transport and distribution of granules within the plane of the cortex (Desnos *et al.*, 2003; Rudolf *et al.*, 2003; Varadi *et al.*, 2005), recruitment of granules to the cortex in response to signals for secretion (Nascimento *et al.*, 2003), transport of granules through the actin cortex to the plasma membrane during secretion (Valentijn *et al.*, 2000; Desnos *et al.*, 2007b), contraction of the granule membrane to facilitate expulsion of granule contents (Valentijn *et al.*, 1999; Jerdeva *et al.*, 2005; Yu and Bement, 2007), and recycling of granule membranes following exocytosis (Valentijn *et al.*, 1999; Bement *et al.*, 2000; Thorn *et al.*, 2004; Sokac *et al.*, 2006; Larina *et al.*, 2007). Importantly, there are now several reports demonstrating that Myo5a localizes to endocrine secretory granules and that perturbing Myo5a function perturbs endocrine granule distribution (for recent reviews see (Eichler *et al.*, 2006; Desnos *et al.*, 2007a). The functions of Myo5c on exocrine granules may thus be similar to the functions of Myo5a on endocrine granules. This being said, there are a number of major differences between endocrine and exocrine secretion. Exocrine secretion is polarized to the apical rather than the basolateral surface, exocrine granules are typically larger than endocrine granules, and

exocrine secretion often occurs with a relatively slow time course (Lang *et al.*, 1997; Steyer *et al.*, 1997; Oheim *et al.*, 1998; Thorn *et al.*, 2004; Thorn and Parker, 2005; Sokac and Bement, 2006). In addition, exocrine cells often exhibit compound exocytosis and exocrine granule membranes can persist as empty vesicles or "ghosts" for tens to hundreds of seconds after fusion (Thorn and Parker, 2005).

It will also be important to determine how Myo5c is attached to exocrine granules. An obvious question is whether the Myo5c tail is linked to exocrine granules via a specific docking complex analogous to the rab27-melanophilin complex that links the Myo5a tail to melanosomes (Wu *et al.*, 2002). In this regard, it should be noted that the Myo5c tail interacts with rab8a (Rodriguez and Cheney, 2002; Roland *et al.*, 2007), and that several rab proteins, including rab3d (Valentijn *et al.*, 1996; Chen *et al.*, 2006; Marchelletta *et al.*, 2008), rab8a (Chen *et al.*, 2006; Faust *et al.*, 2008), and rab27b (Chen *et al.*, 2004; Imai *et al.*, 2004; Chen *et al.*, 2006) have been identified on exocrine granules. Finally, since we have shown that Myo5c associates both with secretory granules and with other organelles such as the slender tubules, it will be important to identify these other organelles and to determine if Myo5c functions in their trafficking.

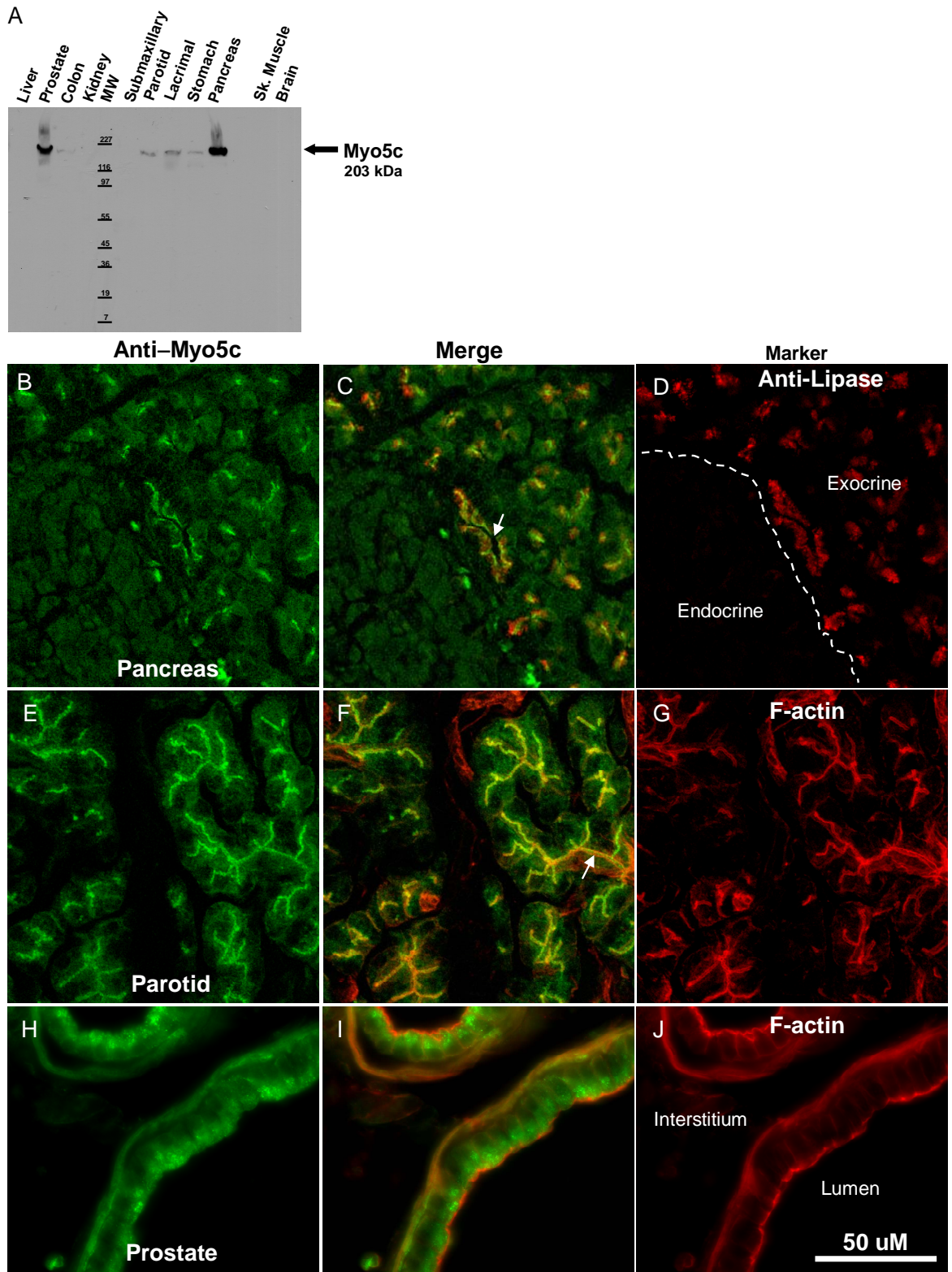
Acknowledgements

The authors thank Dr. Sarah Hamm-Alvarez and Dr. Ron Marchelletta (University of Southern California) for helpful comments and suggestions. We also thank Dr. Roger Tsien (University of California San Diego/Howard Hughes Medical Institute Investigator) for providing mCherry-alpha tubulin; Dr. Francois Darchen and Dr. Clare Desnos for the GFP-tagged human Myo5a tail construct (Institut de Biologie Physico-Chimique, Paris, France); Drs. John Mercer (McLaughlin Research Institute), James Goldenring (Vanderbilt University), and Joseph Roland (Vanderbilt University) for the Myo5b (Myr6) construct; Dr. Laurent Taupenot for chromogranin A-GFP (University of California San Diego); Dr. Wolfhard Almers for generating NPY-GFP (Vollum Institute-Oregon Health Sciences University); Dr. Patrick Brennwald (UNC Chapel Hill) for antibodies to exo70; and Dr. Ann Erickson (UNC Chapel Hill) for assistance with organelle markers. We also wish to acknowledge the UNC Neuroscience Center Confocal and Multi-Photon Imaging Facility for confocal imaging and the assistance of Kirk McNaughton of the UNC Cell and Molecular Physiology Histology Facility. DTJ was supported by a Porter Fellowship from the American Physiological Society and a UNC Sequoyah Dissertation Completion Fellowship. This research was supported by National Institutes of Health/National Institute on Deafness and Other Communicative Disorders grant DC03299 to REC.

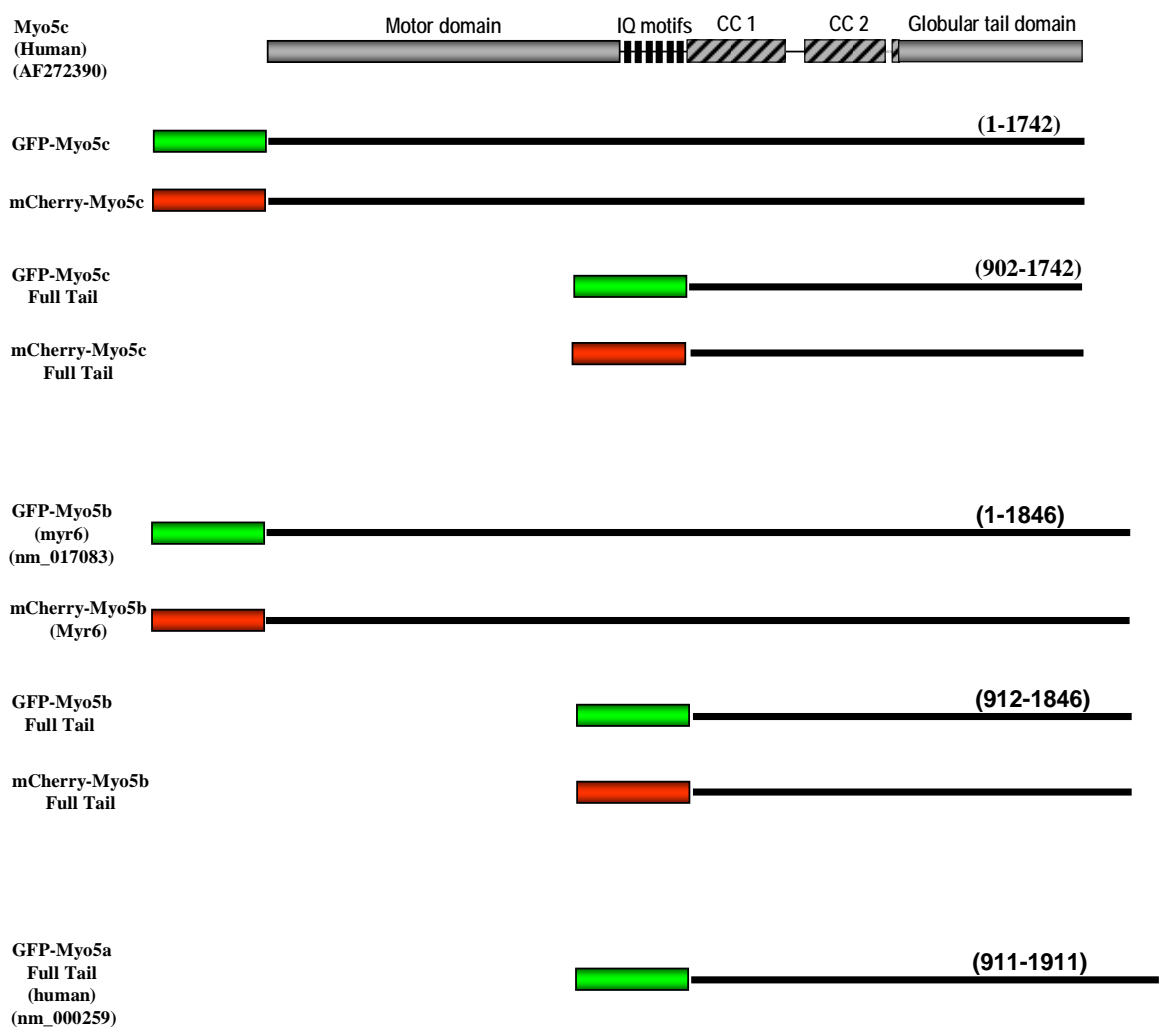
Supplemental Figure 3-1. Myo5c is expressed in exocrine secretory tissues. (A)

Immunoblot of rat tissues showing high levels of Myo5c expression in exocrine tissues such as pancreas and prostate and low levels of expression in liver, kidney, skeletal muscle, and brain. In the salivary glands, Myo5c appears to be more abundant in the parotid gland, which secretes a protein-rich fluid, than in the submaxillary gland, which secretes a mucous-rich fluid. SDS lysates of equal weights of the indicated tissues were run on a 4-20% SDS-PAGE gel and subjected to immunoblotting. (B-D)

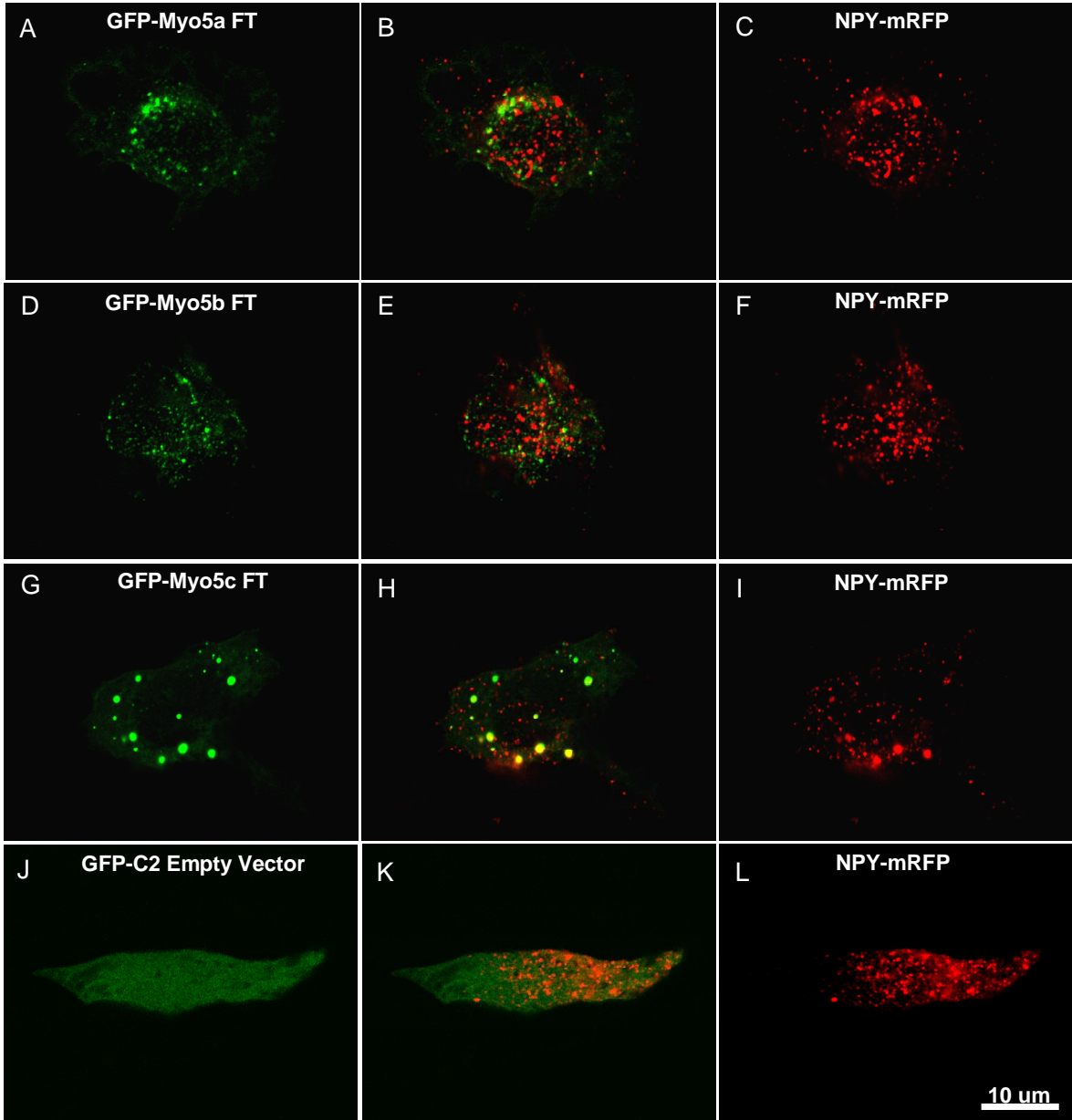
Immunolocalization of Myo5c in the pancreas. Note that the brightest Myo5c staining is present in cells labeled with anti-lipase, a marker for the acinar cells of the exocrine pancreas. The dashed line indicates the boundary between the exocrine and endocrine portions of the pancreas and the arrow indicates one of the relatively small luminal spaces into which acinar cells secrete. (E-G) Immunolocalization of Myo5c in the parotid gland. Myo5c is expressed in the parotid acinar cells and is again most abundant in the actin-rich apical region that surrounds the lumen of each secretory acinus (see arrow). (H-J) Immunolocalization of Myo5c in the prostate gland. The brightest Myo5c staining is present in the apical region of the principal prostate cells and is thus located near the very large lumen into which these cells secrete. Immuno-localization experiments were performed using rat tissues that had been fixed, frozen, and cut into 10 um sections. The images of the pancreas and parotid are single confocal planes and the images of the prostate were obtained using widefield fluorescence microscopy. Control sections stained with non-immune IgG showed only a faint background signal similar to that observed with anti-Myo5c in the exocrine pancreas (not shown). F-actin was labeled with Alexa-568 phalloidin.



Supplemental Figure 3-2: Class V myosin constructs used to investigate the cellular functions of Myo5c. Class V myosins are ~50-60% identical and each family member contains a motor domain, a neck region, and a tail consisting of a region of coiled-coil and a cargo binding domain. Full length and full tail constructs for each class V myosin were tagged with GFP and/or mCherry. Empty vectors that express only GFP or mCherry were generated and used as control vectors. The accession numbers for each class V myosin are indicated on the figure.



Supplemental Figure 3-3: Dominant-negative Myo5c specifically associates with secretory granules and disrupts their distribution in MCF-7 cells. MCF-7 cells were cotransfected with the secretory granule marker NPY-mRFP (red) and dominant negative tail constructs (green) of Myo5a (A), Myo5b (D), or Myo5c (G) to test if the ability of the Myo5c tail to perturb secretory granules in MCF-7 cells is specific to Myo5c or shared by other class V myosins. (A-C) Cell transfected with GFP-Myo5a full tail. (D-F) Cell transfected with GFP-Myo5b full tail. (G-I) Cell transfected with GFP-Myo5c tail. Note that the Myo5c tail perturbs the distribution of the secretory granule marker, while exhibiting significant colocalization in large puncta while the Myo5a tail and Myo5b tail constructs did not grossly perturb the distribution of the secretory granules and show relatively little colocalization with the granule marker. Cells were fixed 36 hours post transfection and images are single confocal planes. Similar results were obtained in 3 separate experiments.



Supplemental Methods

For immunoblotting, tissues were homogenized 1:10 (w:v) in homogenization buffer (40 mM Hepes, 10 mM EDTA-K, 5mM ATP, 2mM DTT, 1mM Pefabloc) prior to SDS-PAGE. For tissue immunofluorescence, paraformaldehyde (2% in PBS) fixed tissues were perfused with sucrose (15% in PBS), embedded in Tissue-Tek OCT embedding compound (#4583-Sakura Finetek, Torrance, CA.) and serially sectioned to 10 um each. Sections were then stained using standard immunofluorescence protocols (see Materials and Methods section). Stained sections were imaged using either a Zeiss Axiovert TV100 with a 63x (1.4 N.A.) objective and a Hamamatsu Orca II cooled CCD digital camera or a Leica SP1 laser scanning confocal microscope using a 40x (1.25 N.A.) objective. Tissues from adult Sprague-Dawley rats were harvested in accordance with IACUC rules/regulations and approved laboratory protocols.

References

- Belyantseva, I.A., Boger, E.T., Naz, S., Frolenkov, G.I., Sellers, J.R., Ahmed, Z.M., Griffith, A.J., and Friedman, T.B. (2005). Myosin-XVa is required for tip localization of whirlin and differential elongation of hair-cell stereocilia. *Nat Cell Biol* 7, 148-156.
- Bement, W.M., Benink, H., Mandato, C.A., and Swelstad, B.B. (2000). Evidence for direct membrane retrieval following cortical granule exocytosis in *Xenopus* oocytes and eggs. *J Exp Zool* 286, 767-775.
- Berg, J.S., and Cheney, R.E. (2002). Myosin-X is an unconventional myosin that undergoes intrafilopodial motility. *Nat Cell Biol* 4, 246-250.
- Berg, J.S., Powell, B.C., and Cheney, R.E. (2001). A millennial myosin census. *Mol Biol Cell* 12, 780-794.
- Bergmann, J.E., Kupfer, A., and Singer, S.J. (1983). Membrane insertion at the leading edge of motile fibroblasts. *Proc Natl Acad Sci U S A* 80, 1367-1371.
- Catlett, N.L., and Weisman, L.S. (1998). The terminal tail region of a yeast myosin-V mediates its attachment to vacuole membranes and sites of polarized growth. *Proc Natl Acad Sci U S A* 95, 14799-14804.
- Chen, X., Li, C., Izumi, T., Ernst, S.A., Andrews, P.C., and Williams, J.A. (2004). Rab27b localizes to zymogen granules and regulates pancreatic acinar exocytosis. *Biochem Biophys Res Commun* 323, 1157-1162.
- Chen, X., Walker, A.K., Strahler, J.R., Simon, E.S., Tomanicek-Volk, S.L., Nelson, B.B., Hurley, M.C., Ernst, S.A., Williams, J.A., and Andrews, P.C. (2006). Organellar proteomics: analysis of pancreatic zymogen granule membranes. *Mol Cell Proteomics* 5, 306-312.
- Cheney, R.E., O'Shea, M.K., Heuser, J.E., Coelho, M.V., Wolenski, J.S., Espreafico, E.M., Forscher, P., Larson, R.E., and Mooseker, M.S. (1993). Brain myosin-V is a two-headed unconventional myosin with motor activity. *Cell* 75, 13-23.
- Desnos, C., Huet, S., and Darchen, F. (2007a). 'Should I stay or should I go?' myosin V function in organelle trafficking. *Biol Cell* 99, 411-423.
- Desnos, C., Huet, S., Fanget, I., Chapuis, C., Bottiger, C., Racine, V., Sibarita, J.B., Henry, J.P., and Darchen, F. (2007b). Myosin va mediates docking of secretory granules at the plasma membrane. *J Neurosci* 27, 10636-10645.
- Desnos, C., Schonn, J.S., Huet, S., Tran, V.S., El-Amraoui, A., Raposo, G., Fanget, I., Chapuis, C., Menasche, G., de Saint Basile, G., Petit, C., Cribier, S., Henry, J.P., and

Darchen, F. (2003). Rab27A and its effector MyRIP link secretory granules to F-actin and control their motion towards release sites. *J Cell Biol* 163, 559-570.

Dunn, B.D., Sakamoto, T., Hong, M.S., Sellers, J.R., and Takizawa, P.A. (2007). Myo4p is a monomeric myosin with motility uniquely adapted to transport mRNA. *J Cell Biol* 178, 1193-1206.

Eichler, T.W., Kogel, T., Bukoreshtliev, N.V., and Gerdes, H.H. (2006). The role of myosin Va in secretory granule trafficking and exocytosis. *Biochem Soc Trans* 34, 671-674.

El Meskini, R., Jin, L., Marx, R., Bruzzaniti, A., Lee, J., Emeson, R., and Mains, R. (2001). A signal sequence is sufficient for green fluorescent protein to be routed to regulated secretory granules. *Endocrinology* 142, 864-873.

Espreafico, E.M., Cheney, R.E., Matteoli, M., Nascimento, A.A., De Camilli, P.V., Larson, R.E., and Mooseker, M.S. (1992). Primary structure and cellular localization of chicken brain myosin-V (p190), an unconventional myosin with calmodulin light chains. *J Cell Biol* 119, 1541-1557.

Fan, G.H., Lapierre, L.A., Goldenring, J.R., Sai, J., and Richmond, A. (2004). Rab11-family interacting protein 2 and myosin Vb are required for CXCR2 recycling and receptor-mediated chemotaxis. *Mol Biol Cell* 15, 2456-2469.

Faust, F., Gomez-Lazaro, M., Borta, H., Agricola, B., and Schrader, M. (2008). Rab8 is involved in zymogen granule formation in pancreatic acinar AR42J cells. *Traffic* 9, 964-979.

Flezar, M., and Heisler, S. (1993). P2-purinergic receptors in human breast tumor cells: coupling of intracellular calcium signaling to anion secretion. *J Pharmacol Exp Ther* 265, 1499-1510.

Hand, A.R., and Oliver, C. (1977a). Cytochemical studies of GERL and its role in secretory granule formation in exocrine cells. *Histochem J* 9, 375-392.

Hand, A.R., and Oliver, C. (1977b). Relationship between the Golgi apparatus, GERL, and secretory granules in acinar cells of the rat exorbital lacrimal gland. *J Cell Biol* 74, 399-413.

Henry, L., and Sheff, D.R. (2008). Rab8 regulates basolateral secretory, but not recycling, traffic at the recycling endosome. *Mol Biol Cell* 19, 2059-2068.

Hofslis, E., Thommesen, L., Norsett, K., Falkmer, S., Syversen, U., Sandvik, A., and Laegreid, A. (2002). Expression of chromogranin A and somatostatin receptors in pancreatic AR42J cells. *Mol Cell Endocrinol* 194, 165-173.

- Hopkins, C.R., Gibson, A., Shipman, M., Strickland, D.K., and Trowbridge, I.S. (1994). In migrating fibroblasts, recycling receptors are concentrated in narrow tubules in the pericentriolar area, and then routed to the plasma membrane of the leading lamella. *J Cell Biol* 125, 1265-1274.
- Imai, A., Yoshie, S., Nashida, T., Shimomura, H., and Fukuda, M. (2004). The small GTPase Rab27B regulates amylase release from rat parotid acinar cells. *J Cell Sci* 117, 1945-1953.
- Jerdeva, G.V., Wu, K., Yarber, F.A., Rhodes, C.J., Kalman, D., Schechter, J.E., and Hamm-Alvarez, S.F. (2005). Actin and non-muscle myosin II facilitate apical exocytosis of tear proteins in rabbit lacrimal acinar epithelial cells. *J Cell Sci* 118, 4797-4812.
- Johnston, G.C., Prendergast, J.A., and Singer, R.A. (1991). The *Saccharomyces cerevisiae* MYO2 gene encodes an essential myosin for vectorial transport of vesicles. *J Cell Biol* 113, 539-551.
- Jones, J.M., Huang, J.D., Mermall, V., Hamilton, B.A., Mooseker, M.S., Escayg, A., Copeland, N.G., Jenkins, N.A., and Meisler, M.H. (2000). The mouse neurological mutant flailer expresses a novel hybrid gene derived by exon shuffling between *Gnb5* and *Myo5a*. *Hum Mol Genet* 9, 821-828.
- Kanno, T., Asada, N., Yanase, H., Iwanaga, T., Ozaki, T., Nishikawa, Y., Iguchi, K., Mochizuki, T., Hoshino, M., and Yanaihara, N. (1999). Salivary secretion of highly concentrated chromogranin a in response to noradrenaline and acetylcholine in isolated and perfused rat submandibular glands. *Exp Physiol* 84, 1073-1083.
- Karpova, T.S., Reck-Peterson, S.L., Elkind, N.B., Mooseker, M.S., Novick, P.J., and Cooper, J.A. (2000). Role of actin and Myo2p in polarized secretion and growth of *Saccharomyces cerevisiae*. *Mol Biol Cell* 11, 1727-1737.
- Krementsov, D.N., Krementsova, E.B., and Trybus, K.M. (2004). Myosin V: regulation by calcium, calmodulin, and the tail domain. *J Cell Biol* 164, 877-886.
- Lang, T., Wacker, I., Steyer, J., Kaether, C., Wunderlich, I., Soldati, T., Gerdes, H.H., and Almers, W. (1997). Ca²⁺-triggered peptide secretion in single cells imaged with green fluorescent protein and evanescent-wave microscopy. *Neuron* 18, 857-863.
- Langford, G.M. (2002). Myosin-V, a versatile motor for short-range vesicle transport. *Traffic* 3, 859-865.
- Lapierre, L.A., Kumar, R., Hales, C.M., Navarre, J., Bhartur, S.G., Burnette, J.O., Provance, D.W., Jr., Mercer, J.A., Bahler, M., and Goldenring, J.R. (2001). Myosin vb is associated with plasma membrane recycling systems. *Mol Biol Cell* 12, 1843-1857.

- Larina, O., Bhat, P., Pickett, J.A., Launikonis, B.S., Shah, A., Kruger, W.A., Edwardson, J.M., and Thorn, P. (2007). Dynamic regulation of the large exocytotic fusion pore in pancreatic acinar cells. *Mol Biol Cell* 18, 3502-3511.
- Lise, M.F., Wong, T.P., Trinh, A., Hines, R.M., Liu, L., Kang, R., Hines, D.J., Lu, J., Goldenring, J.R., Wang, Y.T., and El-Husseini, A. (2006). Involvement of myosin Vb in glutamate receptor trafficking. *J Biol Chem* 281, 3669-3678.
- Liu, J., Taylor, D.W., Krementsova, E.B., Trybus, K.M., and Taylor, K.A. (2006). Three-dimensional structure of the myosin V inhibited state by cryoelectron tomography. *Nature* 442, 208-211.
- Marchelletta, R.R., Jacobs, D.T., Schechter, J.E., Cheney, R.E., and Hamm-Alvarez, S.F. (2008). The Class V Myosin Motor, Myosin 5c, Localizes to Mature Secretory Vesicles and Facilitates Exocytosis in Lacrimal Acini. *Am J Physiol Cell Physiol*.
- Mehta, A.D., Rock, R.S., Rief, M., Spudich, J.A., Mooseker, M.S., and Cheney, R.E. (1999). Myosin-V is a processive actin-based motor. *Nature* 400, 590-593.
- Mercer, J.A., Seperack, P.K., Strobel, M.C., Copeland, N.G., and Jenkins, N.A. (1991). Novel myosin heavy chain encoded by murine dilute coat colour locus. *Nature* 349, 709-713.
- Moores, S.L., Sabry, J.H., and Spudich, J.A. (1996). Myosin dynamics in live Dictyostelium cells. *Proc Natl Acad Sci U S A* 93, 443-446.
- Nascimento, A.A., Roland, J.T., and Gelfand, V.I. (2003). Pigment cells: a model for the study of organelle transport. *Annu Rev Cell Dev Biol* 19, 469-491.
- Natori, S., King, A., Hellwig, A., Weiss, U., Iguchi, H., Tsuchiya, B., Kameya, T., Takayanagi, R., Nawata, H., and Huttner, W.B. (1998). Chromogranin B (secretogranin I), a neuroendocrine-regulated secretory protein, is sorted to exocrine secretory granules in transgenic mice. *Embo J* 17, 3277-3289.
- Nedvetsky, P.I., Stefan, E., Frische, S., Santamaria, K., Wiesner, B., Valenti, G., Hammer, J.A., 3rd, Nielsen, S., Goldenring, J.R., Rosenthal, W., and Klussmann, E. (2007). A Role of myosin Vb and Rab11-FIP2 in the aquaporin-2 shuttle. *Traffic* 8, 110-123.
- Oheim, M., Loerke, D., Stuhmer, W., and Chow, R.H. (1998). The last few milliseconds in the life of a secretory granule. Docking, dynamics and fusion visualized by total internal reflection fluorescence microscopy (TIRFM). *Eur Biophys J* 27, 83-98.
- Pashkova, N., Jin, Y., Ramaswamy, S., and Weisman, L.S. (2006). Structural basis for myosin V discrimination between distinct cargoes. *Embo J* 25, 693-700.

Pastural, E., Barrat, F.J., Dufourcq-Lagelouse, R., Certain, S., Sanal, O., Jabado, N., Seger, R., Griscelli, C., Fischer, A., and de Saint Basile, G. (1997). Griscelli disease maps to chromosome 15q21 and is associated with mutations in the myosin-Va gene. *Nat Genet* 16, 289-292.

Peranen, J., Auvinen, P., Virta, H., Wepf, R., and Simons, K. (1996). Rab8 promotes polarized membrane transport through reorganization of actin and microtubules in fibroblasts. *J Cell Biol* 135, 153-167.

Provance, D.W., and Mercer, J.A. (1999). Myosin-V: head to tail. *Cell Mol Life Sci* 56, 233-242.

Pruyne, D.W., Schott, D.H., and Bretscher, A. (1998). Tropomyosin-containing actin cables direct the Myo2p-dependent polarized delivery of secretory vesicles in budding yeast. *J Cell Biol* 143, 1931-1945.

Reck-Peterson, S.L., Novick, P.J., and Mooseker, M.S. (1999). The tail of a yeast class V myosin, myo2p, functions as a localization domain. *Mol Biol Cell* 10, 1001-1017.

Reck-Peterson, S.L., Tyska, M.J., Novick, P.J., and Mooseker, M.S. (2001). The yeast class V myosins, Myo2p and Myo4p, are nonprocessive actin-based motors. *J Cell Biol* 153, 1121-1126.

Rodriguez, O.C., and Cheney, R.E. (2002). Human myosin-Vc is a novel class V myosin expressed in epithelial cells. *J Cell Sci* 115, 991-1004.

Roland, J.T., Kenworthy, A.K., Peranen, J., Caplan, S., and Goldenring, J.R. (2007). Myosin Vb interacts with Rab8a on a tubular network containing EHD1 and EHD3. *Mol Biol Cell* 18, 2828-2837.

Romeo, R., Pellitteri, R., Mazzone, V., and Marcello, M.F. (2002). Chromogranin A expression in human colonic adenocarcinoma. *Ital J Anat Embryol* 107, 177-183.

Rose, S.D., Lejen, T., Casaletti, L., Larson, R.E., Pene, T.D., and Trifaro, J.M. (2002). Molecular motors involved in chromaffin cell secretion. *Ann N Y Acad Sci* 971, 222-231.

Rudolf, R., Kogel, T., Kuznetsov, S.A., Salm, T., Schlicker, O., Hellwig, A., Hammer, J.A., 3rd, and Gerdes, H.H. (2003). Myosin Va facilitates the distribution of secretory granules in the F-actin rich cortex of PC12 cells. *J Cell Sci* 116, 1339-1348.

Sato, T., Mushiake, S., Kato, Y., Sato, K., Sato, M., Takeda, N., Ozono, K., Miki, K., Kubo, Y., Tsuji, A., Harada, R., and Harada, A. (2007). The Rab8 GTPase regulates apical protein localization in intestinal cells. *Nature* 448, 366-369.

- Schmoranzner, J., Kreitzer, G., and Simon, S.M. (2003). Migrating fibroblasts perform polarized, microtubule-dependent exocytosis towards the leading edge. *J Cell Sci* *116*, 4513-4519.
- Schott, D., Ho, J., Pruyne, D., and Bretscher, A. (1999). The COOH-terminal domain of Myo2p, a yeast myosin V, has a direct role in secretory vesicle targeting. *J Cell Biol* *147*, 791-808.
- Sokac, A.M., and Bement, W.M. (2006). Kiss-and-coat and compartment mixing: coupling exocytosis to signal generation and local actin assembly. *Mol Biol Cell* *17*, 1495-1502.
- Sokac, A.M., Schietroma, C., Gundersen, C.B., and Bement, W.M. (2006). Myosin-1c couples assembling actin to membranes to drive compensatory endocytosis. *Dev Cell* *11*, 629-640.
- Steyer, J.A., Horstmann, H., and Almers, W. (1997). Transport, docking and exocytosis of single secretory granules in live chromaffin cells. *Nature* *388*, 474-478.
- Swiatecka-Urban, A., Talebian, L., Kanno, E., Moreau-Marquis, S., Coutermarsh, B., Hansen, K., Karlson, K.H., Barnaby, R., Cheney, R.E., Langford, G.M., Fukuda, M., and Stanton, B.A. (2007). Myosin Vb is required for trafficking of the cystic fibrosis transmembrane conductance regulator in Rab11a-specific apical recycling endosomes in polarized human airway epithelial cells. *J Biol Chem* *282*, 23725-23736.
- Takagi, Y., Yang, Y., Fujiwara, I., Jacobs, D., Cheney, R.E., Sellers, J.R., and Kovacs, M. (2008). Human myosin Vc is a low duty ratio, non-processive molecular motor. *J Biol Chem*.
- Takagishi, Y., Oda, S., Hayasaka, S., Dekker-Ohno, K., Shikata, T., Inouye, M., and Yamamura, H. (1996). The dilute-lethal (dl) gene attacks a Ca²⁺ store in the dendritic spine of Purkinje cells in mice. *Neurosci Lett* *215*, 169-172.
- Taupenot, L., Harper, K.L., Mahapatra, N.R., Parmer, R.J., Mahata, S.K., and O'Connor, D.T. (2002). Identification of a novel sorting determinant for the regulated pathway in the secretory protein chromogranin A. *J Cell Sci* *115*, 4827-4841.
- Thirumurugan, K., Sakamoto, T., Hammer, J.A., 3rd, Sellers, J.R., and Knight, P.J. (2006). The cargo-binding domain regulates structure and activity of myosin 5. *Nature* *442*, 212-215.
- Thorn, P., Fogarty, K.E., and Parker, I. (2004). Zymogen granule exocytosis is characterized by long fusion pore openings and preservation of vesicle lipid identity. *Proc Natl Acad Sci U S A* *101*, 6774-6779.

- Thorn, P., and Parker, I. (2005). Two phases of zymogen granule lifetime in mouse pancreas: ghost granules linger after exocytosis of contents. *J Physiol* 563, 433-442.
- Toth, J., Kovacs, M., Wang, F., Nyitray, L., and Sellers, J.R. (2005). Myosin V from *Drosophila* reveals diversity of motor mechanisms within the myosin V family. *J Biol Chem* 280, 30594-30603.
- Trybus, K.M. (2008). Myosin V from head to tail. *Cell Mol Life Sci*.
- Vadlamudi, R.K., Wang, R.A., Talukder, A.H., Adam, L., Johnson, R., and Kumar, R. (2000). Evidence of Rab3A expression, regulation of vesicle trafficking, and cellular secretion in response to heregulin in mammary epithelial cells. *Mol Cell Biol* 20, 9092-9101.
- Valentijn, J.A., Sengupta, D., Gumkowski, F.D., Tang, L.H., Konieczko, E.M., and Jamieson, J.D. (1996). Rab3D localizes to secretory granules in rat pancreatic acinar cells. *Eur J Cell Biol* 70, 33-41.
- Valentijn, J.A., Valentijn, K., Pastore, L.M., and Jamieson, J.D. (2000). Actin coating of secretory granules during regulated exocytosis correlates with the release of rab3D. *Proc Natl Acad Sci U S A* 97, 1091-1095.
- Valentijn, K.M., Gumkowski, F.D., and Jamieson, J.D. (1999). The subapical actin cytoskeleton regulates secretion and membrane retrieval in pancreatic acinar cells. *J Cell Sci* 112 (Pt 1), 81-96.
- Varadi, A., Tsuboi, T., and Rutter, G.A. (2005). Myosin Va transports dense core secretory vesicles in pancreatic MIN6 beta-cells. *Mol Biol Cell* 16, 2670-2680.
- Vic, P., Vignon, F., Derocq, D., and Rochefort, H. (1982). Effect of estradiol on the ultrastructure of the MCF7 human breast cancer cells in culture. *Cancer Res* 42, 667-673.
- Volpicelli, L.A., Lah, J.J., Fang, G., Goldenring, J.R., and Levey, A.I. (2002). Rab11a and myosin Vb regulate recycling of the M4 muscarinic acetylcholine receptor. *J Neurosci* 22, 9776-9784.
- Watanabe, S., Mabuchi, K., Ikebe, R., and Ikebe, M. (2006). Mechanoenzymatic characterization of human myosin Vb. *Biochemistry* 45, 2729-2738.
- Watanabe, S., Watanabe, T., Sato, O., Awata, J., Homma, K., Umeki, N., Higuchi, H., Ikebe, R., and Ikebe, M. (2007). Human myosin Vc is a low duty ratio non-processive motor. *J Biol Chem*.
- Weigert, R., Yeung, A.C., Li, J., and Donaldson, J.G. (2004). Rab22a regulates the recycling of membrane proteins internalized independently of clathrin. *Mol Biol Cell* 15, 3758-3770.

Wu, X., Bowers, B., Rao, K., Wei, Q., and Hammer, J.A., 3rd. (1998). Visualization of melanosome dynamics within wild-type and dilute melanocytes suggests a paradigm for myosin V function *In vivo*. *J Cell Biol* *143*, 1899-1918.

Wu, X., Sakamoto, T., Zhang, F., Sellers, J.R., and Hammer, J.A., 3rd. (2006). *In vitro* reconstitution of a transport complex containing Rab27a, melanophilin and myosin Va. *FEBS Lett* *580*, 5863-5868.

Wu, X.S., Rao, K., Zhang, H., Wang, F., Sellers, J.R., Matesic, L.E., Copeland, N.G., Jenkins, N.A., and Hammer, J.A., 3rd. (2002). Identification of an organelle receptor for myosin-Va. *Nat Cell Biol* *4*, 271-278.

Yeaman, C., Grindstaff, K.K., and Nelson, W.J. (2004). Mechanism of recruiting Sec6/8 (exocyst) complex to the apical junctional complex during polarization of epithelial cells. *J Cell Sci* *117*, 559-570.

Yu, H.Y., and Bement, W.M. (2007). Multiple myosins are required to coordinate actin assembly with coat compression during compensatory endocytosis. *Mol Biol Cell* *18*, 4096-4105.

Yvon, A.M., and Wadsworth, P. (2000). Region-specific microtubule transport in motile cells. *J Cell Biol* *151*, 1003-1012.

Zhang, H., Berg, J.S., Li, Z., Wang, Y., Lang, P., Sousa, A.D., Bhaskar, A., Cheney, R.E., and Stromblad, S. (2004). Myosin-X provides a motor-based link between integrins and the cytoskeleton. *Nat Cell Biol* *6*, 523-531.

Zhao, L.P., Koslovsky, J.S., Reinhard, J., Bahler, M., Witt, A.E., Provance, D.W., Jr., and Mercer, J.A. (1996). Cloning and characterization of myr 6, an unconventional myosin of the dilute/myosin-V family. *Proc Natl Acad Sci U S A* *93*, 10826-10831.

CHAPTER 4: CONCLUSIONS AND FUTURE DIRECTIONS

Class V myosins are actin-based molecular motors that transport organelles

There is now overwhelming evidence that class V myosins associate with membranous organelles and provide a link to the actin cytoskeleton. Studies in yeast show that class V myosins transport cellular organelles, vesicles, and mRNA along actin cables (Valiathan and Weisman, 2008). These studies highlight that class V myosins associate with multiple cargoes in the same cell and provide a structural basis for these associations (Pashkova *et al.*, 2006; Valiathan and Weisman, 2008). In vertebrates, studies of class V myosins have revealed fundamental properties of motor function (Trybus, 2008), membrane trafficking (Wu *et al.*, 1998), and organelle association (Wu *et al.*, 2002b). Class V myosins have a broad tissue distribution and levels of expression appear to vary depending on cell type (Rodriguez and Cheney, 2002). Of the three class V myosins in vertebrates (Myo5a, Myo5b, and Myo5c), Myo5a has received the most attention. Through studies of Myo5a and trafficking of melanosomes a general paradigm for organelle trafficking that utilizes microtubules for long-range transport and actin filaments for short-range transport or tethering has emerged (Wu *et al.*, 1998). Although class V myosins in yeast power long-range, actin-based organelle movement, class V myosins in vertebrates appear to be short-range transporters or tethers.

How is organelle specificity achieved?

Class V myosins associate with several organelles through organelle association complexes. In yeast and in vertebrate systems several such complexes have been described. The first “docking complex” to be elucidated was the association of Myo5a with melanosomes. Myo5a was shown to associate with melanosomes through an

interaction with melanophilin which also binds to Rab27a (Wu *et al.*, 2002b). Through this and several other studies, a general model of a docking complex has emerged. This complex utilizes an actin-based motor, a rab protein, and a “linker” protein. There is good evidence that suggests this tripartite docking complex can be regulated at three or more levels.

Regulation at the level of the tail domain

In yeast, a single class V myosin can transport several organelles and recent structural and biochemical data has provided structural and temporal mechanisms to regulate those interactions (Ishikawa *et al.*, 2003; Tang *et al.*, 2003; Pashkova *et al.*, 2006). As discussed in the introduction, the globular tail of Myo2p has distinct domains, termed subdomain I and subdomain II, that specifically interact with the vacuole and secretory vesicles, respectively (Catlett *et al.*, 2000). Although it is not known how the globular tail determines which subdomain to use at a given time, it likely involves the availability of accessory “linker” proteins. In Myo5a the tail domain undergoes alternative splicing of three of the six exons (exon A-exon F) to regulate the interactions with specific cargoes (Wu *et al.*, 2002a; Wu *et al.*, 2002b). Myo5a containing exon F is a melanocyte-specific isoform that binds to melanosomes through exon F-dependent binding partners. In neurons exon B is expressed in the absence of exon F, and appears to provide a binding site for a dynein light chain (Hodi *et al.*, 2006; Wagner *et al.*, 2006). Recent studies demonstrated that alternative splicing of exon D in Myo5a and Myo5b may regulate interactions with rab proteins and endocytic organelles in HeLa cells (Roland *et al.*, 2008). These studies indicate that the tail domains and alternative splicing within them can provide a level of specificity for cargo association.

Regulation through linker proteins

Melanophilin/Slac2-a provides a linkage between the globular tail of Myo5a and Rab27a, which is on the surface of the organelle to form an organelle attachment complex (Wu *et al.*, 2002b). Melanophilin/Slac2-a is one member of a family of Rab27 effector proteins and appears to be expressed specifically in melanocytes (Izumi, 2007). In retinal pigment epithelial cells (RPE), Myo5a is expressed but does not associate with Rab27a on melanosomes. Instead, MyRIP/Slac2-c, a different Rab27 effector protein, forms a complex on melanosomes with myosin VIIa and Rab27a (Lopes *et al.*, 2007) in RPE cells. An additional family of linker proteins is the Rab11-Family of Interacting Proteins (Rab11-FIPs). Rab11-FIP2 functions as a linker protein for Myo5b and rab11a on recycling endosomes (Hales *et al.*, 2002). Although the functions of three additional Rab11-FIP proteins are unknown, they may mediate associations between Rab11a and other myosin motors (Hales *et al.*, 2001). In yeast, Vac17p links Myo2p with Vac8p on vacuolar membranes to form a transport complex during cell division (Tang *et al.*, 2003). Interestingly, the expression of Vac17p was shown to be regulated in cell cycle-dependent manner, which implies that the association of Myo2p with vacuolar membranes is a regulated process. These examples indicate that cargo specificity and association can be regulated through linker proteins.

Regulation through rab proteins

Rab proteins associate directly with organelle membranes and appear to provide the final link between class V myosins and the organelles they transport (Hales *et al.*, 2002; Wu *et*

al., 2002a). There are ~60 members of the rab family in humans and generally each labels a distinct membrane compartment (Zerial and McBride, 2001; Grosshans *et al.*, 2006). Although the mechanism of how a given rab protein distinguishes between the multitude of different compartments in a cell is not clear, this organelle specificity allows rab proteins to be used as markers for distinct compartments. In most instances, a rab protein appears to be the organelle “specificity factor” and provides the final link between the motor protein and the cargo, thus completing the tripartite docking complex on the surface of the organelle. Since rab proteins are thought to associate organelles via geranylgeranyl groups, other unidentified proteins may act to stabilize the association and increase specificity. Although it is clear that rab proteins are key components for attaching a class V myosin to an organelle, both direct and indirect interactions have been reported.

There appear to be at least three levels of regulation involved in organelle association. These include the class V myosin tail domain, the linker protein, and the rab protein. Although additional determinants may exist for transporting the organelle, the tail, the linker, and the rab appear to represent the minimal components of organelle association. Hammer and colleagues have demonstrated both *in vivo* (Wu *et al.*, 2002b) and *in vitro* that Myo5a, melanophilin, and Rab27a are the minimal essential components of a transport complex (Wu *et al.*, 2006b). Since more than one protein appears to exist at each tier of regulation this likely reflects an increased number of organelles associated with a particular member of a motor family and/or linker protein.

Myo5c is a class V myosin for exocrine secretion

Our initial characterization of Myo5c showed that it was abundantly expressed in exocrine glands and initial immunofluorescence studies suggested that it was localized to the apical plasma membrane of epithelial cells. Subsequent localization in rat exocrine tissues definitively showed that Myo5c localizes to the apical domain of the acinar cells and surrounded granule-like structures (Marchelletta *et al.*, 2008). These results suggested that Myo5c is associated with secretory granules and may play a role in regulated secretion in exocrine tissues.

The biosynthetic secretory pathway was first described in acinar cells of the exocrine pancreas. George E. Palade (1912-2008) was awarded the 1974 Nobel Prize in Physiology and Medicine for these studies. It was clear at that time that this process is highly complex and involves several cellular organelles that function in an integrated fashion (Palade, 1975). The climactic goal of the biosynthetic process is secretion of proteins from the apical plasma membrane. Secretion in the exocrine system occurs in a highly regulated series of events, rather than in a constitutive manner. Secretory organelles emerge from the trans-Golgi network containing processed proteins that have been packaged for transport to the apical domain where they undergo maturation. A large pool of mature secretory granules is stored in the apical cytoplasm and can undergo fusion with the plasma membrane following stimulation. The life cycle of a post-golgi secretory granule can be described in 5 distinct steps:

1) Transport to the cell periphery involves microtubules and microtubule-based motors and it is during this time that maturation of the secretory organelle occurs through homotypic fusion and subsequent concentration of contents (Rudolf *et al.*, 2001).

2) Tethering of the secretory granule in the cell periphery acts to oppose the microtubule-mediated inward trafficking of organelles. Granules that are tethered are considered to comprise the reserve pool of secretory organelles. Tethering is F-actin dependent and likely involves myosin motor proteins (Loubery and Coudrier, 2008).

3) Docking of the granule to a fusion site immediately precedes fusion. This process is known to involve both v-snare and t-snare proteins and brings the membranes into very close apposition (Cai *et al.*, 2007). Docked granules exhibit greatly reduced mobility and comprise the ready releasable pool (Rose *et al.*, 2002).

4) Fusion of the granule with the plasma membrane is regulated by free [calcium]. Fusion proteins such as the snares and synaptotagmin are thought to provide the force for membrane fusion in a process that is not fully understood (Brunger, 2005; Lang and Jahn, 2008). Following fusion the contents of the granule undergo exocytosis to the extracellular space. F-actin in the apical domain undergoes a dramatic rearrangement and F-actin “coats” appear to form around the secretory granule following secretory stimulation (Valentijn *et al.*, 1999a; Sokac *et al.*, 2006).

5) Retrieval of granule membranes following exocytosis is an important and often overlooked step during the process of secretion. Although little data is available on how retrieval occurs or how it is regulated, initial studies have indicated that F-actin is required for granule structural integrity and possibly for retrieval of membranes

(Valentijn *et al.*, 1999a; Valentijn *et al.*, 1999b; Sokac *et al.*, 2006; Yu and Bement, 2007a).

The role of the cytoskeleton in facilitating directed transport of secretory organelles is an area of research that has received much attention (Wu *et al.*, 1998; Rudolf *et al.*, 2001; Wu *et al.*, 2006a). It has been established that microtubules and microtubule-based motors mediate the trafficking of secretory organelles toward the plasma membrane, but the roles of actin and actin-based motors are less clear. In cell types that undergo regulated secretion, such as acinar cells of the exocrine secretory system or neuroendocrine cells of the endocrine secretory system, F-actin is highly concentrated near sites of secretion (Rose *et al.*, 2002). There are at least two hypotheses concerning the role of the actin cytoskeleton during secretion: 1) F-actin creates a barrier to the movement of vesicles to the plasma membrane, thus inhibiting random fusion events, and 2) F-actin serves as a facilitator of vesicle movement and the process of secretion. There is good evidence to support both hypotheses and it should be noted that they are not mutually exclusive (Valentijn *et al.*, 1999a; Valentijn *et al.*, 1999b; Valentijn *et al.*, 2000; Neco *et al.*, 2003; Ehre *et al.*, 2005).

Our results have established that Myo5c localizes to the apical domain of secretory acinar cells and that overexpression of a dominant-negative Myo5c tail partially inhibits regulated secretion (Marchelletta *et al.*, 2008). In support of a role in granule secretion, a proteomics study identified Myo5c as a component of isolated zymogen granule membranes from rat exocrine pancreas (Chen *et al.*, 2006). Our recent data

shows that in living, exocrine-derived MCF-7 cells, Myo5c is tightly associated with secretory granules and remains associated with the granules during fusion with the plasma membrane. Myo5c also remained associated with the granule for up to one minute following exocytosis (Jacobs et al., manuscript in revision-Chapter 3 results). In this study, TIRF microscopy was used in conjunction with DIC to visualize fluorescently-labeled secretory granule markers undergoing exocytosis to the extracellular medium. Exocytosis of granule contents clearly coincided with a loss of fluorescently-labeled contents and formation of a DIC-visible “dimple-like” structure on the plasma membrane. Although the precise step at which Myo5c functions is not known, together these results convincingly demonstrate that Myo5c is associated with secretory granules in exocrine acinar cells and functions in granule trafficking.

Myo5c and secretory granule transport

Our results do not support a role for Myo5c during the initial post-Golgi transport step. Our observations that Myo5c exhibited little colocalization with small (diffraction-limited) vesicles containing granule markers (unpublished), or with secretory granule markers at early time points following transfection, argues that Myo5c associates with mature secretory granules (Jacobs et al., manuscript in revision-Chapter 3 results). Results obtained in lacrimal gland acinar cells suggested that Myo5c may be required for late stages of secretory granule maturation (Marchelletta *et al.*, 2008). It has been shown that immature secretory granules undergo rapid microtubule-based transport from the cell center to the periphery (Rudolf *et al.*, 2001), we were unable to detect Myo5c associated with these transport vesicles. It is possible that Myo5c does associate with immature secretory organelles, but at levels below our detection threshold. If Myo5c were

associated with these immature structures, it would likely be as a passenger, since the movements have been shown to be microtubule mediated (Rudolf *et al.*, 2001). These observations support our hypothesis that Myo5c functions primarily in the actin-rich cell periphery.

Myo5c and tethering of secretory granules

We also asked if Myo5c was involved in tethering of secretory granules in the cortical F-actin. To test this, a dominant-negative Myo5c tail was overexpressed in MCF-7 cells. These experiments showed that secretory granules were highly aggregated and colocalized with Myo5c tail, and the distribution was dramatically disrupted. Consistent with this, the addition of F-actin destabilizers also disrupted the Myo5c-associated secretory granule distribution and increased the level of aggregation (not shown). In melanocytes and neuroendocrine cells, Myo5a appears to function as a tether for secretory organelles in the actin-rich cell periphery (Wu *et al.*, 1998; Desnos *et al.*, 2007). The tethering function of Myo5a appears to oppose microtubule-based transport back to the cell center. Expression of a dominant-negative Myo5a tail increased the cortical clustering of secretory granules in MIN-6 beta cells (Varadi *et al.*, 2005), which also decreased the secretory response. The disrupted distribution caused by the dominant-negative tail may have had secondary effects on secretion. These results support the hypothesis that Myo5c is required to maintain the wild-type distribution of secretory organelles through tethering to the cortical F-actin.

Myo5c and docking of secretory granules

Although our studies did not address whether Myo5c was required for docking of secretory granules, it is a possible function for Myo5c. Our live cell imaging of MCF-7 cells show secretory granules moving into the TIRF field (within ~150-200 nm of the plasma membrane) following stimulation to secrete. This region of the cell is dominated by actin filaments and directed movement of a secretory granule though it likely requires an actin-based motor(s). Apparent docking was evident when the secretory granules became less mobile just prior to fusion (Movie 3-6). Myo5c is clearly coupled to the secretory granule at this time, however the activity of Myo5c is unknown. In neuroendocrine cells, Myo5a has been shown to associate with and regulate the distribution of secretory granules, and appears to facilitate docking of granules at the plasma membrane (Rose *et al.*, 2002; Rudolf *et al.*, 2003; Varadi *et al.*, 2005; Desnos *et al.*, 2007). Additionally, an *in vitro* study suggested that Myo5a in neuronal cells can interact with syntaxin 1a, which is a t-snare in the plasma membrane, and suggested that docking is mediated through this interaction (Watanabe *et al.*, 2005). At this time there is insufficient data to support such an interaction *in vivo*. In neuroendocrine cells, following stimulation to secrete, a granule undergoes a 20 nm step toward the plasma membrane (Karatekin *et al.*, 2008). This change in z-axis position is hypothesized to represent a tethered granule becoming docked. This change in z-axis position also corresponded tightly with a suppression of mobility in the x, y, and z axis. Together, these results indicate that Myo5a is likely to bring secretory granules into close apposition with the plasma membrane and therefore increase the chances that secretory granules will become docked. It will be extremely interesting to know if Myo5c motor activity is required for: 1) moving secretory granules through the cortical F-actin toward

the plasma membrane, and/or 2) docking the secretory granule to a site of exocrine secretion.

Myo5c and fusion of secretory granules

We showed that Myo5c remained associated with the secretory granules during the fusion step in MCF-7 cells. Our live-cell imaging showed that the granule contents were lost over an ~6 second time course (Jacobs et al., manuscript in revision-Chapter 3 results), but Myo5c could be detected for up to 60 seconds. Interestingly, Myo5a in neuroendocrine cells is reported to dissociate from secretory granules during fusion (Rose *et al.*, 2002). In collaborative studies carried out in lacrimal gland acinar cells, electron micrographs of post-fusion granules appeared to retain Myo5c on or near the granule membrane (Marchelletta *et al.*, 2008). Despite the extremely high resolution obtained with thin section EM, the lacrimal gland model system lacks spatial distinction between cellular organelles. Since secretory organelles occupy much of the space in the apical cytoplasm, it would be hard to detect a change in distribution if Myo5c were to dissociate from the granule membrane. In MCF-7 cells we visualized individual granules with high spatial resolution in living cells following secretory stimulation and monitored the dynamics of Myo5c. Our results indicate that Myo5c remained associated with the granule throughout the secretory event. Since exocrine secretory granules are known to acquire an F-actin coat following secretory stimulus (Valentijn *et al.*, 1999a; Valentijn *et al.*, 1999b; Valentijn *et al.*, 2000; Nemoto *et al.*, 2004; Yu and Bement, 2007b), Myo5c may facilitate an actin-based function on the surface of the organelle. Non-muscle myosin II also associates with secretory organelles in exocrine secretory cells (Jerdeva *et al.*, 2005) and existing data indicates that it may function to: 1) maintain the structure of

the secretory granule, 2) provide contractile forces for content extrusion, and/or 3) retain the fusion pore opening during content extrusion, which are all actin-dependent processes (Bement *et al.*, 2000; Jerdeva *et al.*, 2005; Sokac and Bement, 2006; Sokac *et al.*, 2006; Larina *et al.*, 2007; Yu and Bement, 2007b). Since myosin II forms bipolar filaments that provide contractile forces and is not predicted to interact directly with membranes, Myo5c may carry out one or several of the actin-based functions on the surface of the secretory granule during fusion.

Myo5c and retrieval of secretory granule membranes

The retrieval of membranes following exocytosis is an important step in secretory physiology, however; few studies have addressed this fundamental process. Acinar cells undergo compound exocytosis and do not engage in “kiss and collapse” or “kiss and run” fusion strategies. A kiss and collapse strategy requires an endocytic re-uptake of secretory membranes for recycling (Sokac and Bement, 2006), whereas the kiss and run strategy retains an intact secretory organelle for recycling (Thorn *et al.*, 2004). The fusion and content extrusion event in pancreatic acinar cells has a relatively slow time course of ~6 seconds, and the empty, “granule ghost” can remain for up to ~12 minutes (Nemoto *et al.*, 2001; Thorn *et al.*, 2004). A fusion pore is retained between the ghost and the plasma membrane during this time (Larina *et al.*, 2007), and is thought to be a mechanism to promote compound exocytosis. Since lipid exchange is thought to be inhibited by unknown mechanisms, Thorn *et al.* (Thorn *et al.*, 2004) suggest that pancreatic granule ghosts are recycled through a piecemeal retrieval mechanism, thus retaining the integrity of the granule membrane and the plasma membrane. In *Xenopus* oocytes, following fertilization, a cortical granule fusion intermediate is captured by the

formation of a CDC42 and N-WASP-dependent actin coat (Yu and Bement, 2007a). Myosins provide a linkage between the actin coat and the granule membrane and also provide compressive forces that facilitate membrane retrieval (Sokac *et al.*, 2006). This model strongly supports a role for actin-based motor(s) during membrane retrieval. Our live-cell imaging of secretory granule exocytosis showed that Myo5c fluorescence remained for up to one minute following content extrusion. (Movie 3-7) This is likely to represent an association with a granule “ghost”. Intriguingly, we can also observe what appear to be Myo5c-labeled vesicles and tubules emanating from a ghost granule following exocytosis. Although these observations are preliminary, it is tempting to speculate that Myo5c may function during a granule membrane retrieval step.

Myo5c, non-processivity, and exocrine secretion

Myo5c, in contrast to Myo5a or Myo5b, has been shown to be non-processive (Takagi *et al.*, 2008). This raises questions concerning the advantage(s) of being a non-processive motor. As discussed briefly in the introduction, processivity is the ability of a motor molecule to undergo multiple steps along an actin filament before dissociating. A main determinant of processivity is the duty ratio, which is a measure of the amount of time a motor spends in a tight, actin-bound state. Low duty ratio motors are generally non-processive, however; multiple low duty ratio motors can form processive ensembles. In yeast, Myo2p and Myo4p are non-processive motors, but are capable of providing long-range transport of vesicles, organelles, and mRNA (Reck-Peterson *et al.*, 2001). Similarly, in *Drosophila*, the single class V myosin is non-processive (Toth *et al.*, 2005). The presence of *only* a non-processive myosin to mediate all organelle trafficking

functions argues that processivity is not an essential characteristic for actin-based motor function. Processivity (and a high duty ratio!) may be a specialized adaptation for motors that have evolved to perform low motility and/or tethering functions. Since secretory granules are tightly packed in the apical cytoplasm of acinar cells, a processive actin-based motor may not be required to maintain their positions. However, secretory processes such as docking, fusion, extrusion and membrane retrieval likely require high activity of motor proteins. As can be appreciated in skeletal muscle, the intricate regulation of force production is an advantage to having many low duty ratio motors working in a coordinated effort to attain constant force production. In acinar cells, this fundamental property of Myo5c may be advantageous as an inherent and tightly modulated mechanism of transport, docking, fusion, extrusion, and/or retrieval.

Future Directions

We and others have shown that Myo5c is associated with exocrine secretory granules and participates in granule trafficking (Chen *et al.*, 2006; Marchelletta *et al.*, 2008) (Jacobs *et al.*, manuscript in revision-Chapter 3 results). Despite this clear association, there are still many unanswered questions concerning the role(s) of Myo5c in exocrine secretion. Through additional exploratory studies, I have identified several other avenues of research that potentially are important to understanding Myo5c function(s). My generation of an extensive set of vertebrate class V myosin constructs (Myo5a, Myo5b, and Myo5c) in different fluorescent protein vectors and the generation of an MCF-7 clonal line that stably expresses full length Myo5c can be highly useful tools to answer many questions concerning the fundamental cell biology of Myo5c. Below is a brief summary of preliminary results that implicate Myo5c in various processes.

What is the role of Myo5c in secretory granule trafficking?

Although the presence of Myo5c on secretory granules is well established, the precise step at which Myo5c functions is still vague. As discussed in chapter 3, Myo5c has the potential to function at several steps during the secretory process including tethering of granules to cortical actin (Wu *et al.*, 1998; Desnos *et al.*, 2003; Desnos *et al.*, 2007), transport and distribution of granules within the plane of the cortex (Desnos *et al.*, 2003; Rudolf *et al.*, 2003; Varadi *et al.*, 2005), recruitment of granules to the cortex in response to signals for secretion (Nascimento *et al.*, 2003), transport of granules through the actin cortex to the plasma membrane during secretion (Valentijn *et al.*, 2000; Desnos *et al.*, 2007), contraction of the granule membrane to facilitate exocytosis (Valentijn *et al.*,

1999a; Jerdeva *et al.*, 2005; Yu and Bement, 2007b), and recycling of granule membranes following exocytosis (Valentijn *et al.*, 1999b; Bement *et al.*, 2000; Thorn *et al.*, 2004; Sokac *et al.*, 2006; Larina *et al.*, 2007). Identifying the functions of Myo5c in granule trafficking may be greatly facilitate by the development of knock-down strategies. Recently, I have worked out a siRNA protocol that appears to decrease the endogenous Myo5c protein level by >90%. I have also been able to transfect into “knock-down cells”, cDNA’s encoding fluorescently-labeled granule markers. These knock-down/transfected MCF-7 cells provide a model system in which to answer fundamental questions of Myo5c functions during secretion. Quite likely several steps of the secretory granule trafficking will require functional Myo5c protein.

Is Myo5c associated with an organelle docking complex?

Since Myo5a and Myo5b both appear to associate with organelles through multi-protein “docking complexes”, it is likely that one exists for Myo5c as well. Sequence alignments of the class V myosins indicate that the tail domains are ~50% identical and are predicted to have similar structures. Strikingly, a threading alignment of the Myo5c globular tail protein sequence using the Phyre software algorithm indicates that an extremely high structural homology (E-value = 2.57×10^{-38}) with the Myo2p globular tail structure (PDB model 2f6h). This suggests that Myo5c may associate with several organelles, thus there may be several proteins that facilitate attachment of Myo5c to the cargo. The association with secretory granules in acinar cells and also in MCF-7 cells presents an ideal system to probe for a Myo5c-specific docking complex. Williams and colleagues have developed a proteomics screen that has identified several rab proteins on zymogen granule membranes, including Rab3d, Rab8a, Rab11a, and Rab27b (Chen *et al.*, 2006). Studies

in exocrine tissues have shown that, following secretory stimulation, Rab3d dissociates from the granule membrane just prior to fusion and correlates precisely with the formation of an F-actin coat (Valentijn *et al.*, 2000). Since our results have shown that Myo5c remains associated with the secretory granule throughout fusion and exocytosis, Rab3d is unlikely to form a Myo5c-specific docking complex with the secretory granule. In yeast, Myo2p transports secretory vesicles and associates with them through the rab protein, Ypt31/32, which is the yeast homolog to Rab11a (Lipatova *et al.*, 2008). However a different rab protein, Sec4p, which is the yeast homolog to Rab8a, localizes in a Myo2p dependent manner, exhibits synthetic lethality with Myo2p, and is required for vesicle fusion (Pruyne *et al.*, 1998; Schott *et al.*, 1999). If yeast can be used as an analogous trafficking system, both Rab11a and Rab8a may be likely candidates to form an organelle docking complex with Myo5c. Yeast two-hybrid studies have shown that Myo5c tail can interact with Rab8a in nucleotide dependent manner, but does not appear to interact with Rab11a (Roland *et al.*, 2007). Initial studies of Myo5c in HeLa cells also showed that GFP-Myo5c tail colocalized with Rab8a, and not Rab11a (Rodriguez and Cheney, 2002). These studies suggest that a Myo5c-specific docking complex may likely be formed with Rab8a, and less likely with Rab11a. Rab27b localizes on secretory granules in rat parotid acinar cells and controls the release of amylase secretion (Imai *et al.*, 2004). Interestingly, Rab27b also forms a complex with two different members of the Rab27 family of effector proteins, MyRip/Slac2-c and Slp4-a, to regulate exocytosis. These results provide a basis to begin a systematic analysis of Myo5c interactions with various rab proteins. One possibility is that a Myo5c organelle docking complex may change with time or stage of trafficking. Another possibility is that a different Myo5c:rab

interaction or “rab transition” may be required for each step (ie. transport (Rab11a), tethering (Rab3d), docking (rab27b), fusion (Rab8a), extrusion (?), and retrieval (Rab5??)).

Myo5c associates with vacuole-like structures

In addition to secretory granules, in a subset of MCF-7 cells, Myo5c also localized on large circular structures resembling vacuoles. These structures were present in ~30% of cells and measure ~5 um in diameter. Strikingly, the association of Myo5c with these structures appeared to be temporally regulated. In preliminary live cell imaging experiments, Myo5c fluorescence increased dramatically on the periphery of these structures. After Myo5c associated with a vacuole, small vesicles and tubules were seen emanating from the periphery as the vacuole decreased in size. (See Movie 4-1) These observations indicate that Myo5c associates with a vacuole-like structure and may function to transport the emanating vesicles and tubules. One hypothesis is that these structures are macropinocytic vacuoles containing membranes derived from the plasma membrane that undergo a regulated redistribution. This can be tested by incubating MCF-7 cells in fluid phase markers (ie. fluorescent dextran) and determining whether these vacuoles become filled with the dextran. Fluid phase markers can also be used in live cell assays that potentially will allow the tracking of the Myo5c-associated vesicles and tubules. The use of the siRNA protocol I have developed should allow us to test if Myo5c is involved in macropinocytosis.

Myo5c localizes to the leading edge

The highly polarized distribution pattern of Myo5c at the leading edge of MCF-7 cells suggests that Myo5c may function in transport to the leading edge. The leading edge of a migrating cell is an area of high cytoskeletal dynamics. The microtubules are oriented toward the leading edge and the actin cytoskeleton is highly dynamic. Although actin dynamics have been shown to be the driving force behind cellular protrusion (Forscher *et al.*, 1992), membrane insertion also plays a role in directed migration (Schmidt *et al.*, 1993; Hopkins *et al.*, 1994; Prigozhina and Waterman-Storer, 2004). I hypothesize that Myo5c regulates membrane insertion and uptake at the leading edge, and contributes to cellular protrusions and retraction. Preliminary data shows that the intensity of Myo5c fluorescence correlates with protrusive activity. (Figure 4-1) Use of siRNA and dominant negative strategies should allow us to determine if Myo5c is playing a role in directed cell migration.

Knock out mouse

Generating a Myo5c knock-out mouse would be an ideal method of determining physiological function. For Myo5a, the discovery of the *dilute-lethal* mouse and its subsequent characterization has led to the determination of important insights into the Myo5a physiological function and mechanism of action at the level of the cell. There are many strategies for generating a targeting construct. Using a Cre-lox strategy allows the selective deletion of the targeted region of the gene at any time point. At least two regions of Myo5c could be targeted for deletion such as the actin-binding and ATP-binding sites in the motor domain. The globular tail domain may also be an attractive target for deletion. Since the tail domain is required for localization and cargo

association (Reck-Peterson *et al.*, 1999; Schott *et al.*, 1999), this is an ideal method to inhibit function of Myo5c. Another strategy will be to target an exon for deletion that can disrupt the coding sequence. This strategy will generate highly truncated Myo5c protein and will inhibit Myo5c function. From our studies one would expect a Myo5c knock-out mouse to exhibit defects in membrane trafficking and exocrine function. Since defects in Myo5a lead to Griscelli Syndrome type I (Mercer *et al.*, 1991) and defects in Myo5b lead to microvillar inclusion disease (Erickson *et al.*, 2008; Muller *et al.*, 2008), it will be important to know if defects in Myo5c also lead to human disease.

Movie 4-1: Myo5c localizes to vacuole-like structures in a temporally-regulated manner. MCF-7 cells stably expressing GFP-Myo5c were imaged under DIC and wide-field fluorescence. The arrows point toward vacuole-like structures during the movie. Strikingly, Myo5c fluorescence suddenly appears on the periphery of the vacuole. Small vesicles and tubules emanate radially from the vacuole as the vacuole shrinks in size. Myo5c may be budding vesicles and tubules from the vacuole-like structure.

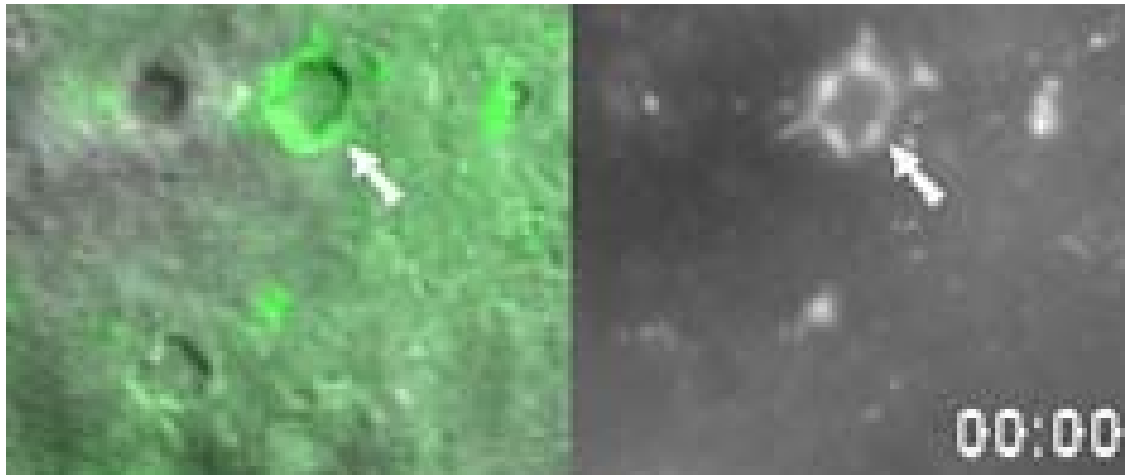
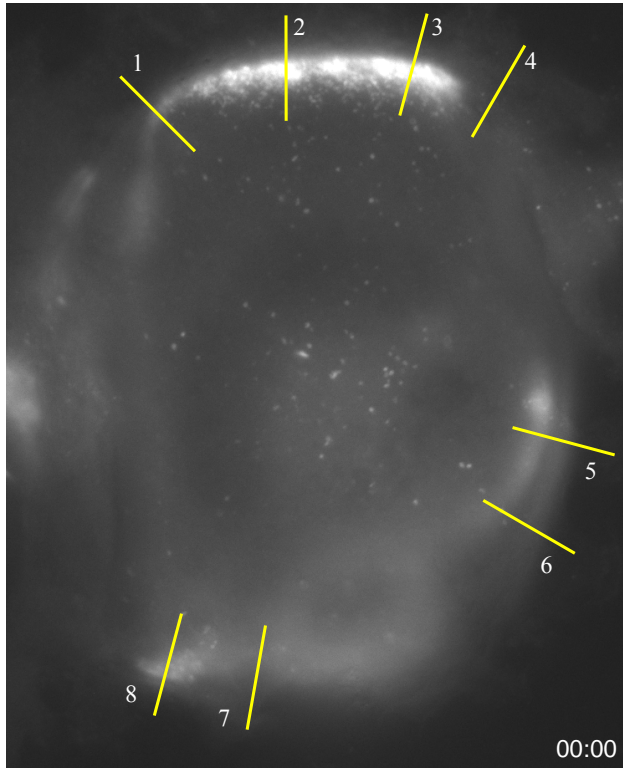
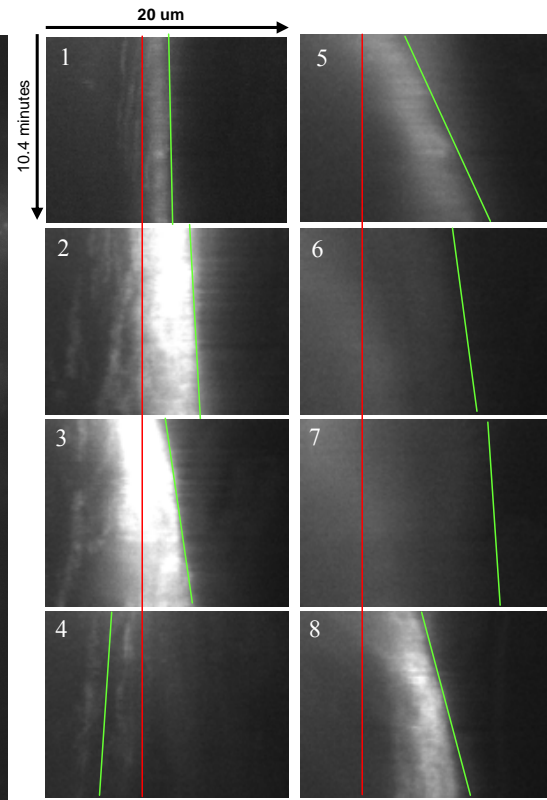


Figure 4-1: Myo5c is enriched in regions of protrusive activity in MCF-7 cells.

(A) Still image taken from frame 1 of a 10.4 minute time-lapse movie of one cell. The numbered regions (yellow lines) correspond to individual kymographs shown in (B).

(B). Kymographs of regions positioned perpendicular to the plasma membrane to highlight membrane protrusion. The green lines correspond to the observed slope of the leading edge over time. The red line corresponds to “0” slope (baseline) over time, indicating no protrusive activity. The X-axis of each kymograph corresponds to 20 μm . The Y-axis corresponds to 10.4 minutes.

A**B**

References

- Bement, W.M., Benink, H., Mandato, C.A., and Swelstad, B.B. (2000). Evidence for direct membrane retrieval following cortical granule exocytosis in *Xenopus* oocytes and eggs. *J Exp Zool* 286, 767-775.
- Brunger, A.T. (2005). Structure and function of SNARE and SNARE-interacting proteins. *Q Rev Biophys* 38, 1-47.
- Cai, H., Reinisch, K., and Ferro-Novick, S. (2007). Coats, tethers, Rabs, and SNAREs work together to mediate the intracellular destination of a transport vesicle. *Dev Cell* 12, 671-682.
- Catlett, N.L., Duex, J.E., Tang, F., and Weisman, L.S. (2000). Two distinct regions in a yeast myosin-V tail domain are required for the movement of different cargoes. *J Cell Biol* 150, 513-526.
- Chen, X., Walker, A.K., Strahler, J.R., Simon, E.S., Tomanicek-Volk, S.L., Nelson, B.B., Hurley, M.C., Ernst, S.A., Williams, J.A., and Andrews, P.C. (2006). Organellar proteomics: analysis of pancreatic zymogen granule membranes. *Mol Cell Proteomics* 5, 306-312.
- Desnos, C., Huet, S., Fanget, I., Chapuis, C., Bottiger, C., Racine, V., Sibarita, J.B., Henry, J.P., and Darchen, F. (2007). Myosin va mediates docking of secretory granules at the plasma membrane. *J Neurosci* 27, 10636-10645.
- Desnos, C., Schonn, J.S., Huet, S., Tran, V.S., El-Amraoui, A., Raposo, G., Fanget, I., Chapuis, C., Menasche, G., de Saint Basile, G., Petit, C., Cribier, S., Henry, J.P., and Darchen, F. (2003). Rab27A and its effector MyRIP link secretory granules to F-actin and control their motion towards release sites. *J Cell Biol* 163, 559-570.
- Ehre, C., Rossi, A.H., Abdullah, L.H., De Pestel, K., Hill, S., Olsen, J.C., and Davis, C.W. (2005). Barrier role of actin filaments in regulated mucin secretion from airway goblet cells. *Am J Physiol Cell Physiol* 288, C46-56.
- Erickson, R.P., Larson-Thome, K., Valenzuela, R.K., Whitaker, S.E., and Shub, M.D. (2008). Navajo microvillous inclusion disease is due to a mutation in MYO5B. *Am J Med Genet A*.
- Forscher, P., Lin, C.H., and Thompson, C. (1992). Novel form of growth cone motility involving site-directed actin filament assembly. *Nature* 357, 515-518.
- Grosshans, B.L., Ortiz, D., and Novick, P. (2006). Rabs and their effectors: achieving specificity in membrane traffic. *Proc Natl Acad Sci U S A* 103, 11821-11827.

- Hales, C.M., Griner, R., Hobdy-Henderson, K.C., Dorn, M.C., Hardy, D., Kumar, R., Navarre, J., Chan, E.K., Lapierre, L.A., and Goldenring, J.R. (2001). Identification and characterization of a family of Rab11-interacting proteins. *J Biol Chem* 276, 39067-39075.
- Hales, C.M., Vaerman, J.P., and Goldenring, J.R. (2002). Rab11 family interacting protein 2 associates with Myosin Vb and regulates plasma membrane recycling. *J Biol Chem* 277, 50415-50421.
- Hodi, Z., Nemeth, A.L., Radnai, L., Hetenyi, C., Schlett, K., Bodor, A., Perczel, A., and Nyitray, L. (2006). Alternatively spliced exon B of myosin Va is essential for binding the tail-associated light chain shared by dynein. *Biochemistry* 45, 12582-12595.
- Hopkins, C.R., Gibson, A., Shipman, M., Strickland, D.K., and Trowbridge, I.S. (1994). In migrating fibroblasts, recycling receptors are concentrated in narrow tubules in the pericentriolar area, and then routed to the plasma membrane of the leading lamella. *J Cell Biol* 125, 1265-1274.
- Imai, A., Yoshie, S., Nashida, T., Shimomura, H., and Fukuda, M. (2004). The small GTPase Rab27B regulates amylase release from rat parotid acinar cells. *J Cell Sci* 117, 1945-1953.
- Ishikawa, K., Catlett, N.L., Novak, J.L., Tang, F., Nau, J.J., and Weisman, L.S. (2003). Identification of an organelle-specific myosin V receptor. *J Cell Biol* 160, 887-897.
- Izumi, T. (2007). Physiological roles of Rab27 effectors in regulated exocytosis. *Endocr J* 54, 649-657.
- Jerdeva, G.V., Wu, K., Yarber, F.A., Rhodes, C.J., Kalman, D., Schechter, J.E., and Hamm-Alvarez, S.F. (2005). Actin and non-muscle myosin II facilitate apical exocytosis of tear proteins in rabbit lacrimal acinar epithelial cells. *J Cell Sci* 118, 4797-4812.
- Karatekin, E., Tran, V.S., Huet, S., Fanget, I., Cribier, S., and Henry, J.P. (2008). A 20-nm step toward the cell membrane preceding exocytosis may correspond to docking of tethered granules. *Biophys J* 94, 2891-2905.
- Lang, T., and Jahn, R. (2008). Core proteins of the secretory machinery. *Handb Exp Pharmacol*, 107-127.
- Larina, O., Bhat, P., Pickett, J.A., Launikonis, B.S., Shah, A., Kruger, W.A., Edwardson, J.M., and Thorn, P. (2007). Dynamic regulation of the large exocytotic fusion pore in pancreatic acinar cells. *Mol Biol Cell* 18, 3502-3511.
- Lipatova, Z., Tokarev, A.A., Jin, Y., Mulholland, J., Weisman, L.S., and Segev, N. (2008). Direct interaction between a myosin V motor and the Rab GTPases Ypt31/32 is required for polarized secretion. *Mol Biol Cell* 19, 4177-4187.

- Lopes, V.S., Ramalho, J.S., Owen, D.M., Karl, M.O., Strauss, O., Futter, C.E., and Seabra, M.C. (2007). The ternary Rab27a-Myrip-Myosin VIIa complex regulates melanosome motility in the retinal pigment epithelium. *Traffic* 8, 486-499.
- Loubery, S., and Coudrier, E. (2008). Myosins in the secretory pathway: tethers or transporters? *Cell Mol Life Sci* 65, 2790-2800.
- Marchelletta, R.R., Jacobs, D.T., Schechter, J.E., Cheney, R.E., and Hamm-Alvarez, S.F. (2008). The Class V Myosin Motor, Myosin 5c, Localizes to Mature Secretory Vesicles and Facilitates Exocytosis in Lacrimal Acini. *Am J Physiol Cell Physiol*.
- Mercer, J.A., Seperack, P.K., Strobel, M.C., Copeland, N.G., and Jenkins, N.A. (1991). Novel myosin heavy chain encoded by murine dilute coat colour locus. *Nature* 349, 709-713.
- Muller, T., Hess, M.W., Schiefermeier, N., Pfaller, K., Ebner, H.L., Heinz-Erian, P., Ponstingl, H., Partsch, J., Rollingshoff, B., Kohler, H., Berger, T., Lenhartz, H., Schlenck, B., Houwen, R.J., Taylor, C.J., Zoller, H., Lechner, S., Goulet, O., Utermann, G., Ruemmele, F.M., Huber, L.A., and Janecke, A.R. (2008). MYO5B mutations cause microvillus inclusion disease and disrupt epithelial cell polarity. *Nat Genet* 40, 1163-1165.
- Nascimento, A.A., Roland, J.T., and Gelfand, V.I. (2003). Pigment cells: a model for the study of organelle transport. *Annu Rev Cell Dev Biol* 19, 469-491.
- Neco, P., Giner, D., del Mar Frances, M., Viniegra, S., and Gutierrez, L.M. (2003). Differential participation of actin- and tubulin-based vesicle transport systems during secretion in bovine chromaffin cells. *Eur J Neurosci* 18, 733-742.
- Nemoto, T., Kimura, R., Ito, K., Tachikawa, A., Miyashita, Y., Iino, M., and Kasai, H. (2001). Sequential-replenishment mechanism of exocytosis in pancreatic acini. *Nat Cell Biol* 3, 253-258.
- Nemoto, T., Kojima, T., Oshima, A., Bito, H., and Kasai, H. (2004). Stabilization of exocytosis by dynamic F-actin coating of zymogen granules in pancreatic acini. *J Biol Chem* 279, 37544-37550.
- Palade, G. (1975). Intracellular aspects of the process of protein synthesis. *Science* 189, 347-358.
- Pashkova, N., Jin, Y., Ramaswamy, S., and Weisman, L.S. (2006). Structural basis for myosin V discrimination between distinct cargoes. *Embo J* 25, 693-700.
- Prigozhina, N.L., and Waterman-Storer, C.M. (2004). Protein kinase D-mediated anterograde membrane trafficking is required for fibroblast motility. *Curr Biol* 14, 88-98.

- Pruyne, D.W., Schott, D.H., and Bretscher, A. (1998). Tropomyosin-containing actin cables direct the Myo2p-dependent polarized delivery of secretory vesicles in budding yeast. *J Cell Biol* *143*, 1931-1945.
- Reck-Peterson, S.L., Novick, P.J., and Mooseker, M.S. (1999). The tail of a yeast class V myosin, myo2p, functions as a localization domain. *Mol Biol Cell* *10*, 1001-1017.
- Reck-Peterson, S.L., Tyska, M.J., Novick, P.J., and Mooseker, M.S. (2001). The yeast class V myosins, Myo2p and Myo4p, are nonprocessive actin-based motors. *J Cell Biol* *153*, 1121-1126.
- Rodriguez, O.C., and Cheney, R.E. (2002). Human myosin-Vc is a novel class V myosin expressed in epithelial cells. *J Cell Sci* *115*, 991-1004.
- Roland, J.T., Kenworthy, A.K., Peranen, J., Caplan, S., and Goldenring, J.R. (2007). Myosin Vb interacts with Rab8a on a tubular network containing EHD1 and EHD3. *Mol Biol Cell* *18*, 2828-2837.
- Roland, J.T., Lapierre, L.A., and Goldenring, J.R. (2008). Alternative splicing in class V myosins determines association with RAB10. *J Biol Chem*.
- Rose, S.D., Lejen, T., Casaletti, L., Larson, R.E., Pene, T.D., and Trifaro, J.M. (2002). Molecular motors involved in chromaffin cell secretion. *Ann N Y Acad Sci* *971*, 222-231.
- Rudolf, R., Kogel, T., Kuznetsov, S.A., Salm, T., Schlicker, O., Hellwig, A., Hammer, J.A., 3rd, and Gerdes, H.H. (2003). Myosin Va facilitates the distribution of secretory granules in the F-actin rich cortex of PC12 cells. *J Cell Sci* *116*, 1339-1348.
- Rudolf, R., Salm, T., Rustom, A., and Gerdes, H.H. (2001). Dynamics of immature secretory granules: role of cytoskeletal elements during transport, cortical restriction, and F-actin-dependent tethering. *Mol Biol Cell* *12*, 1353-1365.
- Schmidt, C.E., Horwitz, A.F., Lauffenburger, D.A., and Sheetz, M.P. (1993). Integrin-cytoskeletal interactions in migrating fibroblasts are dynamic, asymmetric, and regulated. *J Cell Biol* *123*, 977-991.
- Schott, D., Ho, J., Pruyne, D., and Bretscher, A. (1999). The COOH-terminal domain of Myo2p, a yeast myosin V, has a direct role in secretory vesicle targeting. *J Cell Biol* *147*, 791-808.
- Sokac, A.M., and Bement, W.M. (2006). Kiss-and-coat and compartment mixing: coupling exocytosis to signal generation and local actin assembly. *Mol Biol Cell* *17*, 1495-1502.

- Sokac, A.M., Schietroma, C., Gundersen, C.B., and Bement, W.M. (2006). Myosin-1c couples assembling actin to membranes to drive compensatory endocytosis. *Dev Cell* *11*, 629-640.
- Takagi, Y., Yang, Y., Fujiwara, I., Jacobs, D., Cheney, R.E., Sellers, J.R., and Kovacs, M. (2008). Human myosin Vc is a low duty ratio, non-processive molecular motor. *J Biol Chem*.
- Tang, F., Kauffman, E.J., Novak, J.L., Nau, J.J., Catlett, N.L., and Weisman, L.S. (2003). Regulated degradation of a class V myosin receptor directs movement of the yeast vacuole. *Nature* *422*, 87-92.
- Thorn, P., Fogarty, K.E., and Parker, I. (2004). Zymogen granule exocytosis is characterized by long fusion pore openings and preservation of vesicle lipid identity. *Proc Natl Acad Sci U S A* *101*, 6774-6779.
- Toth, J., Kovacs, M., Wang, F., Nyitray, L., and Sellers, J.R. (2005). Myosin V from *Drosophila* reveals diversity of motor mechanisms within the myosin V family. *J Biol Chem* *280*, 30594-30603.
- Trybus, K.M. (2008). Myosin V from head to tail. *Cell Mol Life Sci*.
- Valentijn, J.A., Valentijn, K., Pastore, L.M., and Jamieson, J.D. (2000). Actin coating of secretory granules during regulated exocytosis correlates with the release of rab3D. *Proc Natl Acad Sci U S A* *97*, 1091-1095.
- Valentijn, K., Valentijn, J.A., and Jamieson, J.D. (1999a). Role of actin in regulated exocytosis and compensatory membrane retrieval: insights from an old acquaintance. *Biochem Biophys Res Commun* *266*, 652-661.
- Valentijn, K.M., Gumkowski, F.D., and Jamieson, J.D. (1999b). The subapical actin cytoskeleton regulates secretion and membrane retrieval in pancreatic acinar cells. *J Cell Sci* *112 (Pt 1)*, 81-96.
- Valiathan, R.R., and Weisman, L.S. (2008). Pushing for answers: is myosin V directly involved in moving mitochondria? *J Cell Biol* *181*, 15-18.
- Varadi, A., Tsuboi, T., and Rutter, G.A. (2005). Myosin Va transports dense core secretory vesicles in pancreatic MIN6 beta-cells. *Mol Biol Cell* *16*, 2670-2680.
- Wagner, W., Fodor, E., Ginsburg, A., and Hammer, J.A., 3rd. (2006). The binding of DYNLL2 to myosin Va requires alternatively spliced exon B and stabilizes a portion of the myosin's coiled-coil domain. *Biochemistry* *45*, 11564-11577.

- Watanabe, M., Nomura, K., Ohyama, A., Ishikawa, R., Komiya, Y., Hosaka, K., Yamauchi, E., Taniguchi, H., Sasakawa, N., Kumakura, K., Ushiki, T., Sato, O., Ikebe, M., and Igarashi, M. (2005). Myosin-Va regulates exocytosis through the submicromolar Ca²⁺-dependent binding of syntaxin-1A. *Mol Biol Cell* *16*, 4519-4530.
- Wu, K., Jerdeva, G.V., da Costa, S.R., Sou, E., Schechter, J.E., and Hamm-Alvarez, S.F. (2006a). Molecular mechanisms of lacrimal acinar secretory vesicle exocytosis. *Exp Eye Res* *83*, 84-96.
- Wu, X., Bowers, B., Rao, K., Wei, Q., and Hammer, J.A., 3rd. (1998). Visualization of melanosome dynamics within wild-type and dilute melanocytes suggests a paradigm for myosin V function *In vivo*. *J Cell Biol* *143*, 1899-1918.
- Wu, X., Sakamoto, T., Zhang, F., Sellers, J.R., and Hammer, J.A., 3rd. (2006b). *In vitro* reconstitution of a transport complex containing Rab27a, melanophilin and myosin Va. *FEBS Lett* *580*, 5863-5868.
- Wu, X., Wang, F., Rao, K., Sellers, J.R., and Hammer, J.A., 3rd. (2002a). Rab27a is an essential component of melanosome receptor for myosin Va. *Mol Biol Cell* *13*, 1735-1749.
- Wu, X.S., Rao, K., Zhang, H., Wang, F., Sellers, J.R., Matesic, L.E., Copeland, N.G., Jenkins, N.A., and Hammer, J.A., 3rd. (2002b). Identification of an organelle receptor for myosin-Va. *Nat Cell Biol* *4*, 271-278.
- Yu, H.Y., and Bement, W.M. (2007a). Control of local actin assembly by membrane fusion-dependent compartment mixing. *Nat Cell Biol* *9*, 149-159.
- Yu, H.Y., and Bement, W.M. (2007b). Multiple myosins are required to coordinate actin assembly with coat compression during compensatory endocytosis. *Mol Biol Cell* *18*, 4096-4105.
- Zerial, M., and McBride, H. (2001). Rab proteins as membrane organizers. *Nat Rev Mol Cell Biol* *2*, 107-117.

APPENDICES

**APPENDIX 1: MYOSIN VC IS A LOW DUTY RATIO, NON-PROGRESSIVE
MOLECULAR MOTOR**

Human Myosin Vc is a Low Duty Ratio, Non-Processive Molecular Motor

Yasuharu Takagi¹, Yi Yang¹, Ikuko Fujiwara², Damon Jacobs³, Richard E. Cheney³,
James R. Sellers^{1*} and Mihály Kovács^{4*}

¹Laboratory of Molecular Physiology, National Heart, Lung, and Blood Institute,
National Institutes of Health, Bethesda, MD 20892-8015; ²Laboratory of Cell Biology,
National Heart, Lung, and Blood Institute, National Institutes of Health, Bethesda, MD
20892-8017; ³Cell and Molecular Physiology, University of North Carolina - Chapel Hill,
School of Medicine, Chapel Hill, NC 27599-7545; ⁴Department of Biochemistry, Eötvös
University, H-1117 Budapest, Pázmány P. sétány 1/C, Hungary

*Address correspondences to: James R. Sellers, Ph.D., Laboratory of Molecular
Physiology, National Heart, Lung, and Blood Institute, Building 50 Room 3523, National
Institutes of Health, Bethesda, MD 20892-8015; Tel: (301) 496-6887; Fax: (301) 402-
1542; E-mail: sellersj@mail.nih.gov, and Mihály Kovács, Ph.D. Department of
Biochemistry, Eötvös University, H-1117 Budapest, Pázmány P. sétány 1/C, Hungary;
Tel: +36-1-209-0555/8401; Fax: +36-1-381-2172; E-mail: stocil@gmail.com

Abstract

Myosin Vc is the product of one of the three genes of the class V myosin found in vertebrates. It is widely found in secretory and glandular tissues, with a possible involvement in transferrin trafficking. Transient and steady-state kinetic studies of human myosin Vc were performed using a truncated, single-headed construct. Steady-state actin activated ATPase measurements revealed a V_{max} of $1.8 \pm 0.3 \text{ s}^{-1}$ and a K_{ATPase} of $43 \pm 11 \text{ }\mu\text{M}$. Unlike previously studied vertebrate myosin-Vs, the rate-limiting step in the acto-myosin Vc ATPase pathway is the release of inorganic phosphate ($\sim 1.5 \text{ s}^{-1}$), rather than the ADP release step ($\sim 12.0 - 16.0 \text{ s}^{-1}$). Nevertheless, the ADP affinity of acto-myosin Vc ($K_d = 0.25 \pm 0.02 \text{ }\mu\text{M}$) reflects a higher ADP affinity than seen in other myosin V isoforms. Using the measured kinetic rates, the calculated duty ratio of myosin Vc was $\sim 10 \%$, indicating that myosin Vc spends the majority of the actomyosin ATPase cycle in weak actin-binding states, unlike the other vertebrate myosin V isoforms. Consistent with this a fluorescently-labeled double-headed heavy meromyosin form showed no processive movements along actin filaments in a single molecule assay, but did move actin filaments at a velocity of $\sim 24 \text{ nm/s}$ in ensemble assays. Kinetic simulations reveal that the high ADP affinity of acto-myosin Vc may lead to elevations of the duty ratio of MVc to as high as 64% under possible physiological ADP concentrations. This, in turn, may possibly imply a regulatory mechanism that may be sensitive to moderate changes in ADP concentration.

Introduction

Class V myosins are part of the myosin super-family, currently composed of as many as 37 types of myosins (Richards and Cavalier-Smith, 2005). This diverse superfamily is constituted with proteins that have been identified from conserved sequences in the catalytic domain (motor), which are needed for actin binding and ATP hydrolysis (Sellers, 1999;Sellers, 2000). Within this actin-based molecular motor superfamily, class V myosins are one of the most ancient and widely distributed forms (Berg et al., 2001). Myosin Vs have been implicated in actin-dependent organelle transport (DePina and Langford, 1999;Krendel and Mooseker, 2005) and membrane trafficking (Brown, 1999;Reck-Peterson et al., 2000). In recent years, various studies using assorted scientific techniques including both *in vitro* single molecule/ensemble biochemical and biophysical assays, as well as cell biological assays, have contributed to our current understanding of the mechanisms used by myosin V family members (Wu et al., 2002;Sweeney and Houdusse, 2004;Sellers and Veigel, 2006).

Within vertebrates, three genes of the class V myosin (Va, Vb and Vc) have been discovered (Espreafico et al., 1992;Zhao et al., 1996;Rodriguez and Cheney, 2002). Of these gene products, myosin Va (Espreafico et al., 1992;Cheney et al., 1993), has been the focus of attention. Myosin Va is expressed at high levels in neurons and melanocytes (Mercer et al., 1991;Espindola et al., 1992;Provance, Jr. et al., 1996;Wu et al., 1998;DePina and Langford, 1999;Tuxworth and Titus, 2000;Westbroek et al., 2003). The lack of myosin Va in mouse can result in neurological seizures and critical defects in the transport of melanosomes (Mercer et al., 1991;Wilson et al., 2000;Matesic et al., 2001;Libby et al., 2004). Thus, studying this myosin at the molecular level may provide

insights in human pathology. Myosin Vb is expressed in many tissue types, but Northern blot hybridization has shown that this protein is found primarily in the testes, kidney, liver, lung and the heart (Zhao et al., 1996). *In vivo* studies have shown that myosin Vb is associated with recycling of numerous receptors, including the transferrin receptor (Lapierre et al., 2001), muscarinic acetyl choline receptor (Volpicelli et al., 2002) and the cystic fibrosis conductance regulator ((Swiatecka-Urban et al., 2007)). Myosin Vc is expressed chiefly in epithelial cells in the pancreas, prostate, mammary, stomach, colon, and the lung (Rodriguez and Cheney, 2002). It has been suggested that one role of myosin Vc *in vivo* is membrane trafficking, specifically that of the transferrin receptor, where myosin Vb is also implicated. However, myosin Vc appears to be partially distinct with the same myosin Vb associated membrane compartments (Rodriguez and Cheney, 2002).

The structure of myosin Va has been thoroughly studied (Cheney et al., 1993;Espreafico et al., 1992;Walker et al., 2000;Burgess et al., 2002) (Coureux et al., 2004;Sweeney and Houdusse, 2004). Myosin Va is an oligomeric protein, which is composed of a dimerized heavy chain, each containing a motor domain, a lever-arm containing six IQ motifs which bind a total of six light chains (mostly or entirely calmodulins) per heavy chain, followed by a coiled-coil region and a carboxy-terminal globular tail. The sequence alignment of the three vertebrate myosin V isoforms showed that throughout the class, there is approximately 50 % amino acid identity. Myosin Vc, for example, shares ~62 % identity to the myosin Va and Vb motor domains, approximately 20 – 30 % identity in the coiled-coil region, and some differences in the globular tail region, such as the absence of the PEST site, found in myosin Va and Vb

(Rodriguez and Cheney, 2002). The structure of myosin Vb (Watanabe et al., 2006) and Vc have not been studied as thoroughly as myosin Va, however, the predicted structures from the amino acid sequence analysis exhibited that three isoforms are comparatively similar. The lack of the PEST domain for the myosin Vc reduces its size to approximately 12 kDa smaller than the other myosin Vs.

To characterize the molecular mechanism of these vertebrate myosin V isoforms, steady-state and transient solution kinetic studies have been performed using both myosin Va (Nascimento et al., 1996; Trybus et al., 1999; De La Cruz et al., 1999; De La Cruz et al., 2000; Wang et al., 2000; Yengo et al., 2002; Yengo and Sweeney, 2004) and myosin Vb (Watanabe et al., 2006). The enzymatic properties of myosin Vc have not yet been characterized. Ensemble solution kinetics is a powerful technique that can be used to elucidate the fundamental kinetic properties of the different types of myosin, and a detailed kinetic analysis can furthermore be used to gain insights into the chemo-mechanical coupling of the molecular motor, as done for myosin Va (De La Cruz et al., 1999; De La Cruz et al., 2000). One of the unique properties that distinguished the kinetic mechanism of myosin Va from the other previously studied myosins (Sellers, 1999; Sellers, 2000; De La Cruz and Ostap, 2004) is that it spends most of its kinetic cycle strongly bound to actin during steady-state ATPase cycling (>70%) and that the rate limiting step of the acto-myosin Va ATPase cycle is ADP release. These kinetic properties are consistent with this myosin being a *processive* motor, *i.e.* a protein that undergoes multiple enzymatic cycles while at least one of the motor domains of the molecule is attached to the filamentous actin, such that it can take multiple steps (Mehta et al., 1999; Sakamoto et al., 2000; Forkey et al., 2003; Yildiz et al., 2003). The kinetic

mechanism of myosin Vb has been studied (Watanabe et al., 2006) and showed indications that also this molecule is processive, however, direct observations that the dimerized form of this molecule is processive have not been shown. The kinetic mechanism of myosin Vc has not yet been studied in detail, and a detailed kinetic mechanism may be needed to understand its physiological function *in vivo*. Furthermore, the question whether myosin Vc isoform is processive or not, would be of interest to unravel, since *Drosophila* myosin V was recently determined as a low duty-ratio motor (*i.e.* a myosin head that spends only a small fraction of the catalytic cycle strongly bound to actin) that is presumably non-processive (Toth et al., 2005).

In this present study, we report a full biochemical kinetic characterization of the *Homo sapiens* myosin Vc subfragment-1 (MVc-S1) protein. Steady-state and transient solution kinetic characterizations were performed using a recombinant single-headed MVc-S1 construct, bound with a single calmodulin. Additionally, to directly investigate if the recombinant form of the *Homo sapiens* myosin Vc translocates actin in an *in vitro* actin gliding assay, and furthermore, in an attempt to visualize processive motion of single molecules of *Homo sapiens* myosin Vc, a heavy meromyosin form (HMM) of the double headed construct, intact with six IQ motifs and an enhanced green fluorescent protein (eGFP) attached to each motor domain (eGFP-MVc-HMM) on the N-terminal end was expressed and purified from the Sf9-baculovirus system. The biochemical kinetic characterization revealed that MVc-S1 is a low duty ratio motor, which spends most of its time during the actomyosin ATPase cycle residing in the states weakly bound to actin. Unlike the other two vertebrate myosins, Va and Vb, myosin Vc's kinetic cycle is not rate limited by its ADP release, but by the inorganic phosphate (P_i) release, which

is biochemically closer resemblance to myosins that form ensemble structures to function in physiological conditions, such as skeletal muscle myosin II.

We conclude that myosin Vc is a non-processive motor protein and therefore employs a different mechano-chemical mechanism to perform its tasks in the cytoskeleton compared to both myosin Va and Vb. Acto-MVc has a relatively high ADP affinity and this unusual kinetic difference may possibly make the mechanical activity sensitive to ADP concentration; *i.e.* the duty ratio of this motor may increase at even the moderate ADP concentrations in an *in vivo* environment, consistent with our kinetic simulation results, as well as reported for non-muscle myosin IIB (Kovacs et al., 2003).

Materials and Methods

Expression and Purification of the Myosin Vc-S1 and HMM Proteins — Using a cDNA clone of the *Homo sapiens* myosin Vc encoding the 2930 amino acids fused with an N-terminally fused enhanced GFP (D. Jacobs and R.E. Cheney, *unpublished*), we engineered a cDNA fragment which encodes the first 777 amino acids, containing the motor domain plus the first predicted light-chain binding IQ motifs (myosin Vc subfragment-1; MVc-S1). In addition to the subfragment-1 like construct, a heavy meromyosin-like myosin Vc construct with a N-terminally fused enhanced GFP (eGFP-MVc-HMM) was also engineered by encoding the first 1108 amino acids, containing the motor domain, the six predicted IQ motifs and the predicted coiled-coil region. These amplified clones were sub-cloned into the pFastBac1 baculovirus transfer vector (Invitrogen) designed with a FLAG epitope tag (DYKDDDDK) fused C-terminally to aid

in purification (Yang et al., 2005). Double-stranded DNA sequencing was performed to confirm the complete nucleotide sequencing from both engineered vectors.

Both constructs were coexpressed with *Xenopus* calmodulin in the Sf9-baculovirus system and purified essentially as previously described (Yang et al., 2005). (The amino acid sequence of *Xenopus* calmodulin is identical to that of the human protein.)

Actin and Reagents — Rabbit skeletal muscle actin was prepared as previously described (Spudich and Watt, 1971). Pyrene-iodoacetamide labeled actin was prepared by labeling Cys-374 with pyrenelyiodoacetamide (Invitrogen Corp., Carlsbad, CA) (Pollard, 1984). Pyrene labeled actin was depolymerized by dialysis against G-buffer (1 mM Tris (pH 8.0), 0.1 mM ATP, 0.1 mM CaCl₂, 0.5 mM DTT and 1mM NaN₃), centrifuged and gel filtered using a PD-10 column (Amersham Biosciences, Buckinghamshire, U.K.) to remove free dye. Actin concentration was determined using the extinction coefficient as follows: Unlabeled actin: $A_{290} = 26,600 \text{ M}^{-1}\text{cm}^{-1}$ (Houk, Jr. and Ue, 1974). Pyrene-actin: $(A_{290}-A_{344} \cdot 0.127)/26,600 \text{ M}^{-1}\text{cm}^{-1}$. Pyrene dye: $A_{344} = 22000 \text{ M}^{-1}\text{cm}^{-1}$.

Tetramethylrhodamine phalloidin (TMR-Phalloidin) (Invitrogen Corp., Carlsbad, CA) labeled filamentous actin and 10% biotinylated filamentous actin was prepared essentially as described by Ishijima *et al.* (Ishijima et al., 1998) and Takagi *et al.* (Takagi et al., 2006). Labeled filaments lacking biotinylated globular actin were used for the *in vitro* actin gliding assay, and biotinylated filaments only for the single molecule TIRF assays.

MANT-ATP and MANT-ADP were purchased from Molecular Probes (Invitrogen Corp., Carlsbad, CA) and stored at -20 °C. MDCC labeled, phosphate-binding

protein (MDCC-PBP) (Brune et al., 1994) was generously provided by Dr. Howard D. White (Eastern Virginia Medical School, Norfolk, VA). All other reagents used in this study were from Sigma (St. Louis, MO).

Steady-state ATPase Experiments — Steady-state ATPase measurements of myosin Vc, both in the presence and absence of filamentous actin, were measured using an NADH-coupled assay as previously described by Trentham *et al.* (Trentham et al., 1972), De La Cruz *et al.* (De La Cruz et al., 2000) and Wang *et al.* (Wang et al., 2003). The solutions used for these measurements included the following reagents: 10 mM MOPS (pH 7.2); 2 mM MgCl₂; 0.15 mM EGTA; 2 mM ATP and 50 mM KCl, 40 units/ml lactate dehydrogenase, 200 units/ml pyruvate kinase, 1 mM phosphoenolpyruvate, and 200 μM NADH. Changes in A₃₄₀ were monitored using a Beckman DU640 spectrophotometer and stored for further data analysis.

Stopped-flow Experiments — All measurements were performed using a SF-2001 stopped-flow apparatus (KinTek Corp., Austin, TX) at 25 °C. For constancy, all stopped-flow experiments were performed using buffer (SF buffer) having the same contents. The SF buffer contained the following reagents: 20 mM MOPS (pH 7.0); 5 mM MgCl₂; 0.05 mM EGTA; and 50 mM KCl. To determine the kinetic parameters for P_i release, double-mixing stopped-flow experiments using MDCC-PBP (Brune et al., 2001b) were performed as in (Wang et al., 2003). Only for the P_i release experiment, 10 mM KCl was used. MVc-S1 and acto-MVc-S1 were pre-incubated with 0.02 units/ml of apyrase for at least 30 minutes at 25 °C to deplete any nucleotide in the sample when required. The optical setups of the apparatus are described in depth elsewhere (Kovacs et al., 2005; Toth et al., 2005; Wang et al., 2003).

Post-mix concentrations of proteins and reagents are indicated throughout the text, unless stated otherwise.

Quenched-flow Experiments — Quenched-flow experiments were also performed at 25°C in SF buffer. Quenched-flow experiments were performed using a KinTek RQF-3 apparatus as described previously (Wang et al., 2003) except that 1 M HCl was used as a quench.

Data Analysis — Data analyses of the steady-state and transient solution kinetic measurements were performed using either SigmaPlot 8.0 (Systat Software, San Jose, CA), OriginLab 7.5 (Microcal Corp. Northampton, MA), or the KinTek SF-2004 data analysis software. The means \pm standard deviations (S.D.) cited in this study are mostly averages of two to seven rounds of experiments performed using protein from different preparations.

In Vitro Actin Gliding Motility and Single Molecule Total Internal Reflection Fluorescence (TIRF) Microscopy Assay — Both light microscopy assays were performed using an apparatus previously described by Sakamoto *et al.* (2003 and 2005) (REF) with some minor modifications. Motility assays were performed in buffer containing the following reagents: 20 mM MOPS (pH 7.4); 5 mM MgCl₂; 0.1 mM EGTA; 50 mM KCl; 1 mM ATP; 5 μ M calmodulin; 25 μ g/ml glucose oxidase, 45 μ g/ml catalase; 2.5 mg/ml glucose and 20 mM DTT (final concentrations listed). Experiments were performed at 25 °C. Additionally, to determine if ionic strength alters the motility of eGFP-MVc-HMM, single molecule motility assays were performed in the range varying from 0 to 250 mM KCl as shown previously for myosin Va (Sakamoto et al., 2000).

Observation chambers were also prepared from coverslips (Corning Inc., Corning, NY) using a protocol described previously (Sakamoto et al., 2003).

Data analysis of the *in vitro* actin gliding assay was performed using the ImageJ image analysis software (U. S. National Institutes of Health, Bethesda, Maryland, USA; <http://rsb.info.nih.gov/ij/>) with a data analysis algorithm described in (Kuhn and Pollard, 2005) to track the leading ends of the labeled actin filaments.

Kinetic simulation of the acto-myosin Vc ATPase cycle — Kinetic simulations of the acto-MVc-S1 ATPase cycle were performed using Gepasi v3.30 (Pedro Mendes, Virginia Bioinformatics Institute, www.gepasi.org) based on SCHEME 1 and the experimentally determined rate constants listed in TABLE ONE.

Results

Construct Design, Protein Expression and Purification — Both the MVc-S1 and EGFP-MVc-HMM constructs were purified using FLAG affinity chromatography (Fig. 1). The single-headed subfragment-1 (S1) construct was used for the kinetic characterization, whereas the double-headed HMM construct was used to study its mechanical properties via *in vitro* actin gliding and single molecule TIRF assays. As described previously, the S1 construct only contained the motor domain and the first IQ motif, whereas the HMM construct contained the motor domain, the six (predicted) IQ binding motifs, and the >200 amino acid stretch of the coiled-coil region to promote dimerization of the two heavy chains.

Protein expression was performed using the baculovirus expression system with the Sf9 insect cells, co-expressed with *Xenopus* calmodulin, at 27 °C using shaken cultures. Optimum expression of the protein was reached at approximately 3 to 3.5 days. Both constructs showed reasonable levels of expression, generally yielding ~1 mg of protein purified from $\sim 1 \times 10^9$ cells for the single headed S1 construct, and ~0.5 – 0.7 mg of protein for the double headed HMM construct.

Actin Activation of the Steady-State ATPase Activity — The steady-state ATPase activity of MVc-S1 was activated by actin to a maximal rate of $1.8 \pm 0.3 \text{ s}^{-1}$ (V_{max}), and half-maximal activation was achieved at $42.5 \pm 10.6 \text{ }\mu\text{M}$ (K_{ATPase}) (Fig. 2A and TABLE ONE). Furthermore, in the absence of actin, the basal steady-state activity of MVc-S1 was $0.05 \pm 0.01 \text{ s}^{-1}$. Association of MVc with actin therefore activates the steady-state activity of MVc-S1 by approximately 30-fold. Similarly to MVc-S1, steady-state ATPase

Figure A1-1: SDS polyacrylamide electrophoretogram of MVc-S1. Samples were run on a 4-20% gradient polyacrylamide-SDS gel. *Lane 1*, FLAG-affinity purified MVc-S1 consisting of a 89.5-kDa heavy chain and a 15.7-kDa *Xenopus* calmodulin light chain. (CaM) *Lane 2*, FLAG-affinity purified eGFP-MVc-HMM consisting of a 157.9-kDa heavy chain and a 15.7-kDa *Xenopus* calmodulin light chain (CaM).

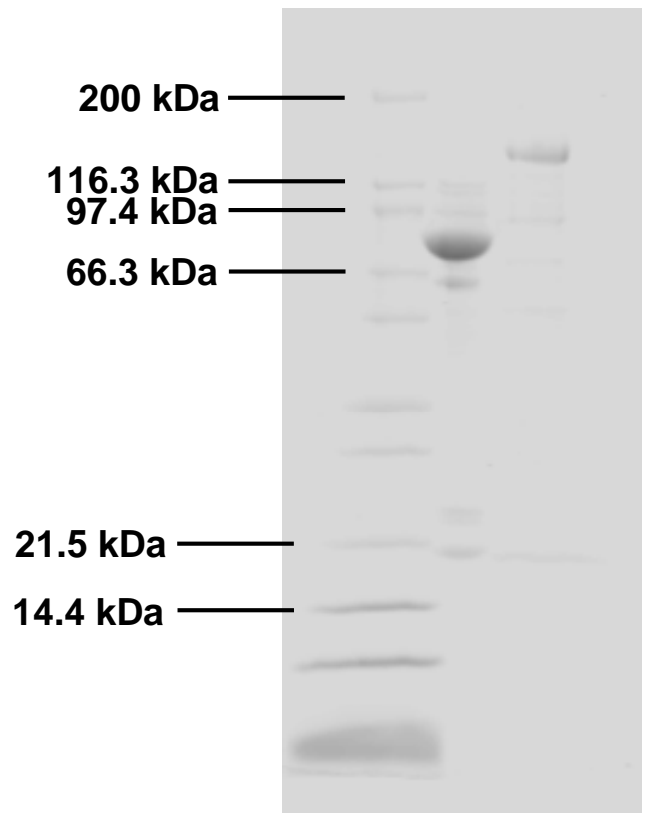


Figure A1-2: Steady-state actin-activated ATPase activity of MVc-S1. The ATPase activity of acto-MVc-S1 depended hyperbolically on actin concentration. This example data set shows a V_{max} of $1.7 \pm 0.1 \text{ s}^{-1}$ and a K_{ATPase} of $45.0 \pm 6.8 \text{ }\mu\text{M}$. Average values taken from seven NADH-coupled assays from seven different protein purifications were: $1.8 \pm 0.3 \text{ s}^{-1}$ (V_{max}) and half-maximal activation was achieved at $42.5 \pm 10.6 \text{ }\mu\text{M}$ (K_{ATPase}). The activity shown in the figure is expressed in terms of heads. Conditions: Temperature = 25 °C; 10 mM MOPS (pH 7.0); 2 mM MgCl_2 ; 0.15 mM EGTA; 2 mM ATP; 50 mM KCl.

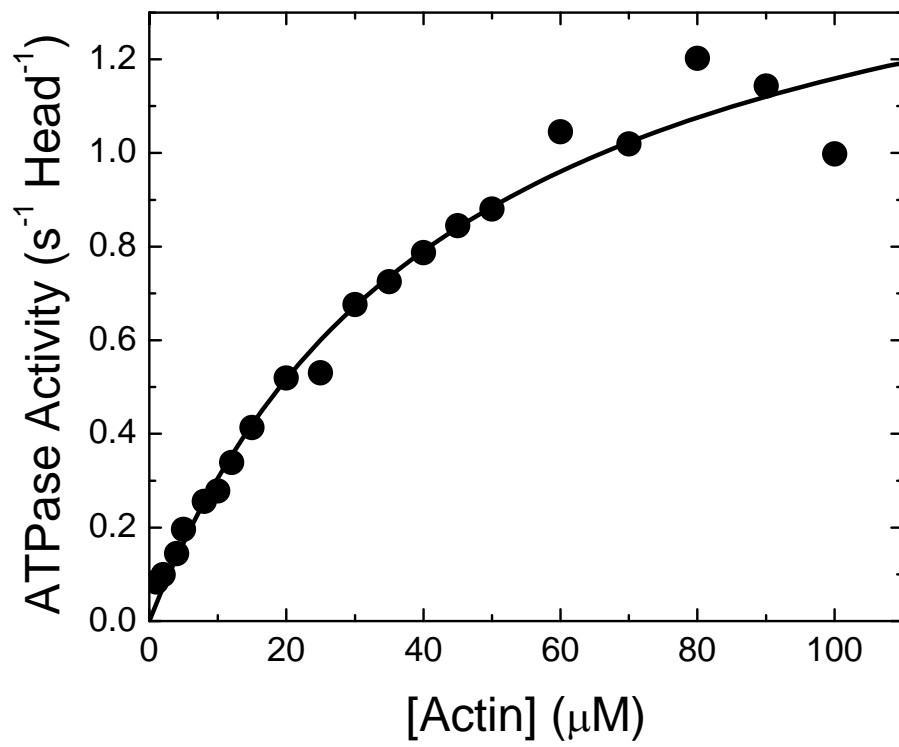


Table A1-1: Kinetic parameters of the MVc-S1 ATPase cycle with corresponding values for myosins Va, Vb and Drosophila myosin V. Numbering of the kinetic rates and equilibrium constants correspond to SCHEME 1.

	Signal or Calculation	Myosin Vc-S1 ^a	Myosin Va ^b	Myosin Vb ^d	Drosophila Myosin V ^e
Steady-state ATPase activity					
k_{basal} (s ⁻¹)	NADH assay	0.05±0.01	0.03	0.09±0.04	0.07±0.013
V_{max} (s ⁻¹)	NADH assay	1.8±0.3	15	9.7±0.4	12.5±0.8
K_{ATPase} (μM)	NADH assay	42.5±10.6	1.4	28.1±5.9	9.9±0.6
Actin binding					
k_{-6} (μM ⁻¹ s ⁻¹)	Pyrene-actin	0.66±0.02	73		2.5±0.29
k_6 (s ⁻¹)	Pyrene-actin	0.019	0.0036		0.04±0.001
K_6 (μM)	k_6/k_{-6}	0.029	4.9 x 10 ⁻⁶		0.016
k_{-10} (μM ⁻¹ s ⁻¹)	Pyrene-actin	1.17±0.03	4.2		2.3±0.14
k_{10} (s ⁻¹)	Pyrene-actin	0.051	0.032		0.43±0.01
K_{10} (μM)	k_{10}/k_{-10}	0.044	0.0076		0.19
K_9 (μM)	MDCC-PBP	14	9±2 ^c		70±10
ATP binding					
$K_1'k_2'$ (μM ⁻¹ s ⁻¹)	Pyrene-actin	0.82±0.03	0.9		0.36±0.006
	MANT-ATP			0.31±0.02	
k_2' (s ⁻¹)	Pyrene-actin	287	771±70 ^c		>180
	Tryptophan		≥750		
ATP hydrolysis					
$k_3 + k_{-3}$ (s ⁻¹)	Quenched-flow	90			
	Tryptophan		750		68±4.7
	MDCC-PBP		>250		
K_3	Quenched-flow calculation	0.54			
	Quenched-flow		5.3		0.39±0.22
P_i release					
k_4 (s ⁻¹)	MDCC-PBP	0.16			
	$K_{\text{basal}}(1 + K_3)/K_3$		0.03		
k_4' (s ⁻¹)	MDCC-PBP	1.5	110±10 ^c		177±18
k_4'/K_9 (μM ⁻¹ s ⁻¹)	MDCC-PBP (Calculated)	0.11	12		
ADP binding					
k_5' (s ⁻¹)	MANT-ADP chase	15.6±0.6	12	11.1±2.1	150
	Pyrene-actin	15.8±0.8			
	Pyrene-actin (Simulated)		16		
K_5' (μM)	Pyrene-actin	0.25±0.02			
	MANT-ADP amplitude				32±5.4
	k_5'/k_{-5}' (MANT-ADP data)		0.8		
k_{-5}' (μM ⁻¹ s ⁻¹)	k_5'/K_5' (Calculated)	~56–72			
k_{-5} (μM ⁻¹ s ⁻¹)	MANT-ADP		4.6		2.2±0.3
Actin-ADP coupling					
K_{10}/K_6	Pyrene-actin (Calculated)	~1.5	~1550		~4.8

^a Data refer to this study.

^b Data refer to Ref. (De La Cruz et al., 1999) (De La Cruz *et al.*, PNAS, 1999), unless otherwise stated.

^c Data refer to Ref. (Yengo and Sweeney, 2004) (Yengo and Sweeney, Biochemistry, 2004).

^d Data refer to Ref. (Watanabe et al., 2006) (Watanabe *et al.*, Biochemistry, 2006).

^e Data refer to Ref. (Toth et al., 2005) (Tóth *et al.*, JBC, 2005).

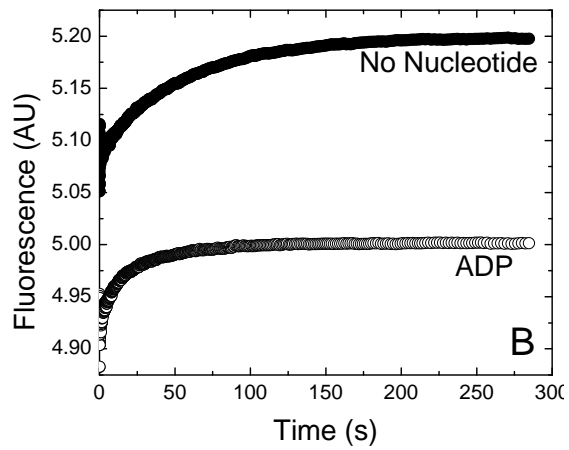
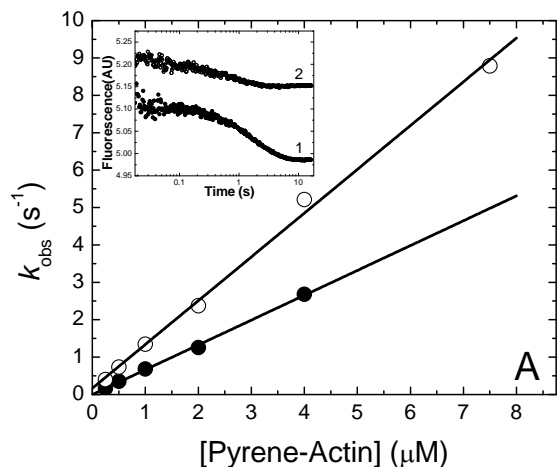
activity of eGFP-MVc-HMM was activated by actin and yielded similar V_{max} and K_{ATPase} (data not shown).

Association and Dissociation of MVc-S1 with Actin in the Absence of Nucleotide and in ADP—Pyrene-labeled filamentous actin has been used extensively to monitor the strong binding of myosin to actin in many myosins (Ostap and Pollard, 1996). Pyrene fluorescence is quenched on mixing of MVc-S1 or MVc-S1·ADP with pyrene-actin in the stopped-flow, and the fluorescence decreases indicate the strong binding of MVc-S1 with pyrene-labeled actin. Fig. 3A shows the dependence of the k_{obs} (observed rate constant) of the observed fluorescence decreases on pyrene-actin concentration. The k_{obs} versus [pyrene-actin] plots were linear, and their slopes represent the second-order actin binding rate constants of $0.66 \pm 0.02 \mu\text{M}^{-1}\cdot\text{s}^{-1}$ and $1.17 \pm 0.03 \mu\text{M}^{-1}\cdot\text{s}^{-1}$ in the absence of nucleotide ($k_{.6}$) and in ADP ($k_{.10}$), respectively.

The dissociation rates of MVc-S1 from pyrene-actin in the absence and presence of ADP were made using stopped-flow spectrophotometry chase experiments. The pyrene-acto-MVc-S1 rigor complex or the pyrene-acto-MVc-S1·ADP ternary complex was rapidly mixed with excess unlabeled filamentous actin in the stopped-flow apparatus. Pyrene fluorescence increases occur during dissociation of MVc-S1 or MVc-S1·ADP from the pyrene-actin, and the rebinding reaction is inhibited by the excess unlabeled filamentous actin. Single exponentials were fitted to the average transients, and the corresponding dissociation rate constants in the absence of nucleotide and in ADP were determined as 0.019 s^{-1} ($k_{.6}$) and 0.051 s^{-1} ($k_{.10}$), respectively.

The equilibrium constants in the absence ($K_{.6}$) and presence of nucleotide ($K_{.10}$), were also calculated using the determined second-order actin binding rate constants and

Figure A1-3: Interaction of MVc-S1 with actin in the absence of nucleotide and in the presence of ADP. A, dependence of the k_{obs} values of the recorded pyrene fluorescence transients via mixing 0.3 μM MVc-S1 with various pyrene-actin concentrations (0.25 – 7.5 μM ; post-mix concentration), as indicated. Transients were recorded in the absence of any nucleotide (*solid symbols*) and in the presence of 20 μM ADP (*open symbols*). The second-order binding rate constants were determined by fitting a linear curve to the k_{obs} values, which yielded the second order binding rate constants, $0.66 \pm 0.02 \mu\text{M}^{-1}\cdot\text{s}^{-1}$ (k_{-6}) and $1.17 \pm 0.03 \mu\text{M}^{-1}\cdot\text{s}^{-1}$ (k_{-10}) in the absence of nucleotide and in ADP, respectively. *Inset* shows an example of pyrene fluorescence transients recorded at 1 μM pyrene-actin (*Trace 1, solid symbols*, No nucleotide trace, $k_{\text{obs}} = 0.68 \text{ s}^{-1}$; *Trace 2, open symbols*, in ADP trace, $k_{\text{obs}} = 1.34 \text{ s}^{-1}$). Traces were offset for clarity. The transients were fitted using a single-exponential curve fit. B, pyrene-fluorescence transients to determine dissociation rates of MVc-S1 from pyrene-actin, both in the absence of nucleotide and in ADP. Chase experiments where a pre-mixture of the pyrene-acto-MVc-S1 rigor complex or the pyrene-acto-MVc-S1·ADP ternary complex (0.3 μM MVc-S1 and 0.5 μM pyrene-actin, in the absence of nucleotide (*solid symbols*) or 20 μM ADP (*solid symbols*)) was rapidly mixed with excess unlabeled 20 μM actin in the stopped-flow apparatus. Averaged transients were fitted to a single exponential curve. Corresponding dissociation rates in the absence of nucleotide and 20 μM ADP were 0.019 s^{-1} and 0.051 s^{-1} , respectively.

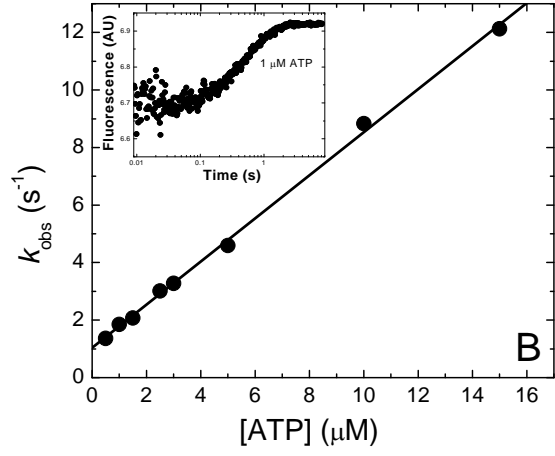
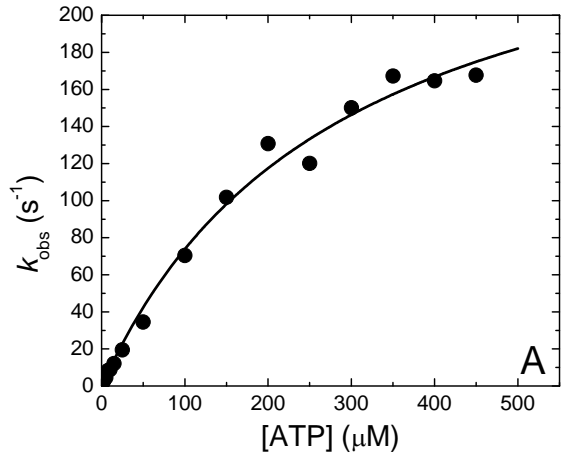


the dissociation rate constants. The corresponding equilibrium constants in the absence of nucleotide and in ADP were determined as 0.029 μM (K_6) and 0.044 μM (K_{10}), respectively.

Interaction of ATP with Acto-MVc-S1 — We measured the binding of ATP to acto-MVc-S1 by monitoring the ATP-induced dissociation of the pyrene-acto-MVc-S1 complex using the stopped-flow apparatus. Pyrene-acto-MVc-S1 (0.5 μM MVc-S1 and 1.0 μM pyrene-actin) incubated with apyrase was rapidly mixed with increasing concentrations of ATP (0 – 450 μM) under pseudo-first order conditions. Pyrene fluorescence increases after MVc-S1 dissociates from actin and this fluorescence change can be fitted by a single-exponential curve. k_{obs} increased hyperbolically with ATP concentration, approaching a maximal rate constant (k_2) of 287 s^{-1} with a half-maximum (K_1) at 288 μM ATP (K_1') (Fig. 4A). At low ATP concentrations, the data sets of the observed rate constants increased linearly with ATP concentration and the apparent second order rate constant ($K_1 k_2'$) was $0.75 \pm 0.03 \mu\text{M}^{-1}\cdot\text{s}^{-1}$ (Fig. 4B), for this particular example. $K_1 k_2'$ determined from the average of multiple experiments yielded an apparent second order rate constant of $0.82 \pm 0.03 \mu\text{M}^{-1}\cdot\text{s}^{-1}$ (TABLE ONE).

Interaction of ADP with Acto-MVc-S1 — To determine the ADP dissociation rate constant from acto-MVc-S1 (k_5') we monitored the decrease in fluorescence upon dissociation of MANT-ADP from acto-MVc-S1. 1 μM MVc-S1 was incubated with 20 μM filamentous actin and 50 μM MANT-ADP (pre-mix concentrations). This ternary complex was mixed rapidly with excess ATP (1 mM; pre-mix concentration). Upon mixing, decrease in the MANT-ADP fluorescence was recorded and the transients were

Figure A1-4: Interaction of ATP with acto-MVc-S1. *A*, binding of ATP to pyrene-acto-MVc-S1 was monitored to observe the ATP-induced dissociation of the pyrene-actomyosin complex. A pre-incubated pyrene-acto-MVc-S1 complex (0.5 μM MVc-S1 and 1.0 μM pyrene-actin) was mixed with increasing concentrations of ATP (0 – 450 μM). Pyrene fluorescence increase was observed due to MVc-S1 dissociation from actin. Fluorescence transients were fitted to single-exponential curves. The k_{obs} increased with increasing ATP concentration. The maximal observed rate constant was $k_2' = 287 \text{ s}^{-1}$ with a half-saturation (K_I) at 288 μM ATP. At low [ATP] concentrations, k_{obs} grew linearly with ATP concentration. A linear fit at low [ATP], yielded an apparent second-rate constant, $K_I'k_2' = 0.75 \mu\text{M}^{-1}\cdot\text{s}^{-1}$. *B*, Same data as *A*, but graph only shows data at low ATP concentrations (0.5 – 15 μM). A linear curve fit to the plot of k_{obs} versus [ATP] gave an apparent second-order rate constant of $1.20 \pm 0.01 \mu\text{M}^{-1}\cdot\text{s}^{-1}$. *Inset* shows an example of a pyrene-actin fluorescence transient recorded at 1 μM ATP ($k_{\text{obs}} = 1.86 \text{ s}^{-1}$).



fitted by single exponential curves. Fig. 5 shows an example of these averaged transients. The fits yielded rate constants of $15.6 \pm 0.6 \text{ s}^{-1}$ ($= k_5'$).

To measure the ADP affinity of acto-MVc-S1, 1.0 μM pyrene-labeled actin was incubated with 0.5 μM MVc-S1 and various concentrations of ADP, then rapidly mixed with 150 μM ATP (pre-mixing concentrations). The transient of the pyrene fluorescence increases as the pyrene-actin dissociates from the MVc-S1. Fig. 6A shows an example of these transients, whereby pyrene-acto-MVc-S1 was incubated with 3 μM ADP (pre-mixing concentrations). The fluorescence increase was fitted by a double exponential, whereby the fast phase ($\sim 100 \text{ s}^{-1}$) corresponded to the ATP-induced dissociation of the ADP-free actomyosin complex, and the relative amplitude of this phase reports the fraction of acto-MVc-S1 free of bound nucleotide. The slower phase of the transient at low ADP concentrations, $15.8 \pm 0.8 \text{ s}^{-1}$, reflects the kinetics of ADP dissociation from the actomyosin complex (k_5') (which must occur before ATP can bind and dissociate pyrene-acto-MVc-S1), and therefore the relative amplitude of this phase reports the fraction of acto-MVc-S1 bound with ADP. This ADP dissociation rate constant determined from the pyrene-actin fluorescence signal agree well with the MANT-ADP fluorescence decrease upon dissociation from the acto-MVc-S1 ($15.6 \pm 0.6 \text{ s}^{-1}$) (Fig. 5 and TABLE ONE).

A hyperbolic fit to the plot of the percent amplitudes of the slow phase (*i.e.* 100% $\cdot [A_{\text{slow}}/(A_{\text{slow}} + A_{\text{fast}})]$) versus ADP concentration allowed for the determination of the acto-MVc-S1 ADP dissociation constant (K_5') of $0.25 \pm 0.02 \mu\text{M}$ (Fig. 6B and TABLE ONE). Thus, the ADP affinity of MVc-S1, in the presence of actin, is high, approximately 3-fold greater than that of chicken myosin Va (De La Cruz et al., 1999).

Figure A1-5: MANT-ADP release from acto-MVc-S1. Average time course of the MANT-ADP fluorescence decrease as MANT-ADP was displaced from MVc-S1. Initially, 50 μM MANT-ADP, 1 μM MVc-S1 and 20 μM filamentous actin were mixed and this mixture was subsequently mixed with 1 mM ATP (pre-mixing concentrations). The *solid line* is the best single exponential fit, whereby the observed rate constant (k_5) was $16.0 \pm 0.6 \text{ s}^{-1}$.

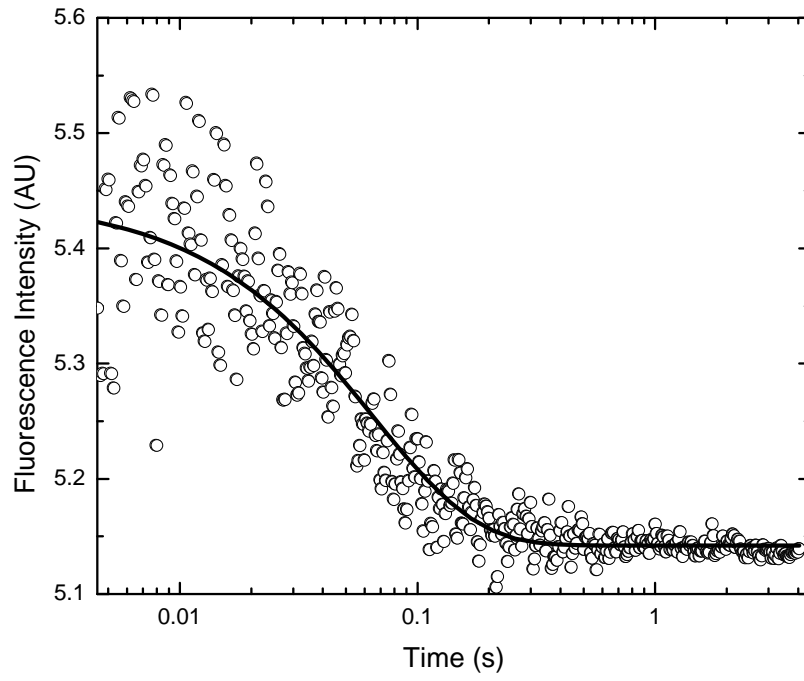
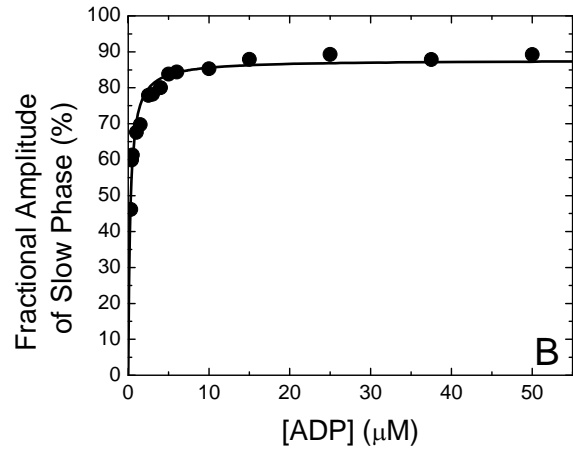
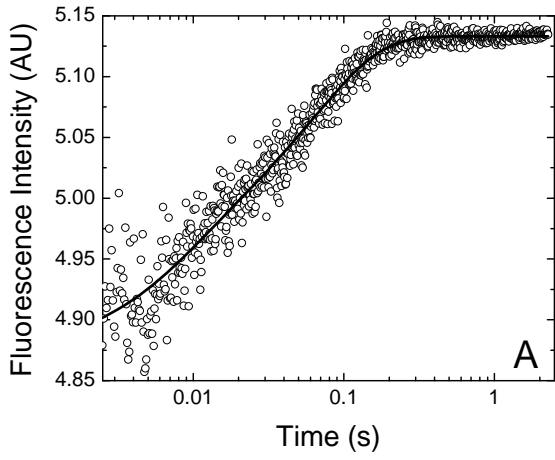


Figure A1-6: Acto-MVc-S1 ADP affinity. *A*, 1.0 μM pyrene-labeled actin was initially incubated with 0.5 μM MVc-S1 and various concentrations of ADP. This pre-incubated mixture was then mixed with 150 μM ATP (pre-mixing concentrations). Shown is an averaged time course of the pyrene fluorescence increase due to dissociation of the MVc-S1 from the pyrene-labeled actin. In this particular example, 3 μM ADP was used in the pre-incubated mixture. *Solid line* is the best double exponential fit to the data. The observed rate constant of the slow phase (k_5) in this case was $15.1 \pm 0.6 \text{ s}^{-1}$. *B*, Shown is the ADP dependence of the relative amplitude of the slower phase of the double exponential fit to the averaged time course of the pyrene fluorescence increase (*i.e.* $100\% \cdot [A_{\text{slow}} / (A_{\text{slow}} + A_{\text{fast}})]$). Fitting the data with a quadratic equation yielded a K_d value $0.25 \pm 0.02 \mu\text{M}$ ($= K_5$).

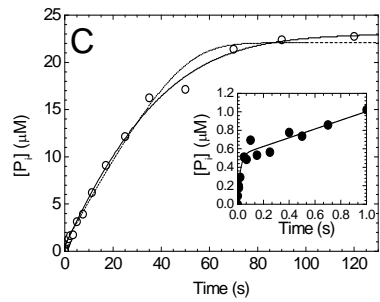
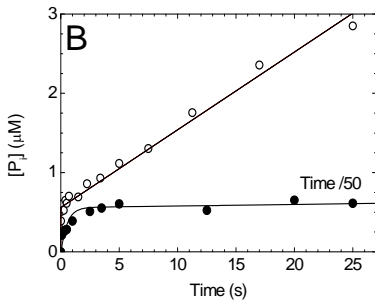
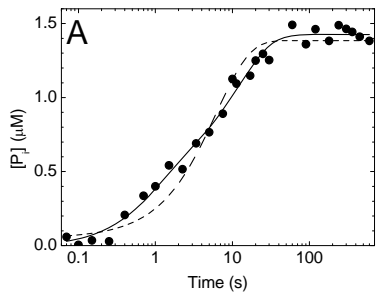


Transient kinetics of ATP hydrolysis by MVc-S1 — The ATP hydrolysis kinetics of MVc-S1 was measured using the quenched flow technique. MVc-S1 or acto-MVc-S1 was rapidly mixed with γ - 32 P-ATP and the time course of P_i liberation was monitored over time. When MVc-S1 was mixed with ATP in single turnover conditions (1.5 μ M protein and 1.5 μ M nucleotide post-mix), the time course of the reaction consisted of two phases (Fig. 7A). The first phase had an amplitude of 0.49 μ M P_i (corresponding to a fractional amplitude of 0.34) and a k_{obs} of 1.1 s^{-1} , which is likely limited by ATP binding. The slower second phase had a k_{obs} of 0.083 s^{-1} , in agreement with the basal steady-state activity of MVc-S1 (measured as 0.062 s^{-1} under the same reactant conditions in the NADH-linked assay).

When mixed with excess ATP in the quenched-flow, MVc-S1 produced a P_i burst with an amplitude of 0.40 mol P_i /mol MVc-S1 (Fig. 7B). The burst was followed by a linear steady-state phase of P_i production characterized by a turnover rate of 0.064 s^{-1} , again in agreement with the results of the above quenched-flow and steady-state measurements. When the same experiment was performed in the presence of 15 μ M actin (post-mix), the steady-state rate was accelerated to 5-fold to 0.32 s^{-1} (in line with NADH-linked steady state ATPase measurements (Fig. 2)), but the burst amplitude was not markedly affected (0.35 mol P_i /mol MVc-S1) (Fig. 7C). Using these burst amplitudes (B), the hydrolysis equilibrium constant (K_3) can be estimated by the following equation $B = K_3/(1 + K_3)$. K_3 therefore is ~ 0.54 . ATP hydrolysis for MVc-S1 is therefore reversible.

By following the time course of the reaction until near-complete exhaustion of ATP, we detected signs of weak product inhibition by ADP (Fig. 7C). As expected from

Figure A1-7: Transient kinetics of ATP hydrolysis by MVc-S1 monitored by quenched-flow. *A*, time course of P_i liberation upon rapidly mixing 1.5 μM MVc-S1 with 1.5 μM $\gamma\text{-}^{32}\text{P}\text{-ATP}$. The *solid line* indicates the best double exponential fit to the data with rate constants of 1.1 s^{-1} (fractional amplitude: 0.34) and 0.083 s^{-1} . The best single exponential fit (*dashed line*) showed systematic deviation from the data points. *B-C*, P_i liberation upon mixing 1.5 μM MVc-S1 with 25 μM $\gamma\text{-}^{32}\text{P}\text{-ATP}$, in the absence (*B*) and presence (*C*) of 15 μM actin. *B*, in the absence of actin, an exponential burst phase having an amplitude of 0.59 μM P_i (corresponding to 0.40 mol P_i /mol MVc-S1) and a rate constant of 90 s^{-1} was followed by a linear steady-state phase indicating a turnover rate of 0.064 s^{-1} . *Open symbols* show all the data obtained in this experiment. *Closed symbols* show the initial phase (i.e. Time/50) of the data. *C*, a similar burst phase was observed in the presence of 15 μM actin (amplitude: 0.35 mol P_i /mol MVc-S1, $k_{\text{obs}} = 50 \text{ s}^{-1}$), but the steady-state turnover rate was accelerated to 0.32 s^{-1} . The time course of ATP hydrolysis was followed until quasi-complete exhaustion of the substrate to monitor product inhibition by ADP. The *solid line* in the *main panel* is a simulated progress curve of P_i liberation resulting from a global fitting procedure using the kinetic parameters of TABLE 1 and leaving the ADP binding rate constant of actomyosin (k_{-5}) as a floating parameter. The best fit was obtained at $k_{-5}' = 18 \mu\text{M}^{-1}\cdot\text{s}^{-1}$. The *dashed line* is a progress curve with a fixed $k_{-5}' = 5 \mu\text{M}^{-1}\cdot\text{s}^{-1}$. *Inset* shows the data points from the initial period (i.e. Time 0 – 1 s) of this burst phase with the fit.

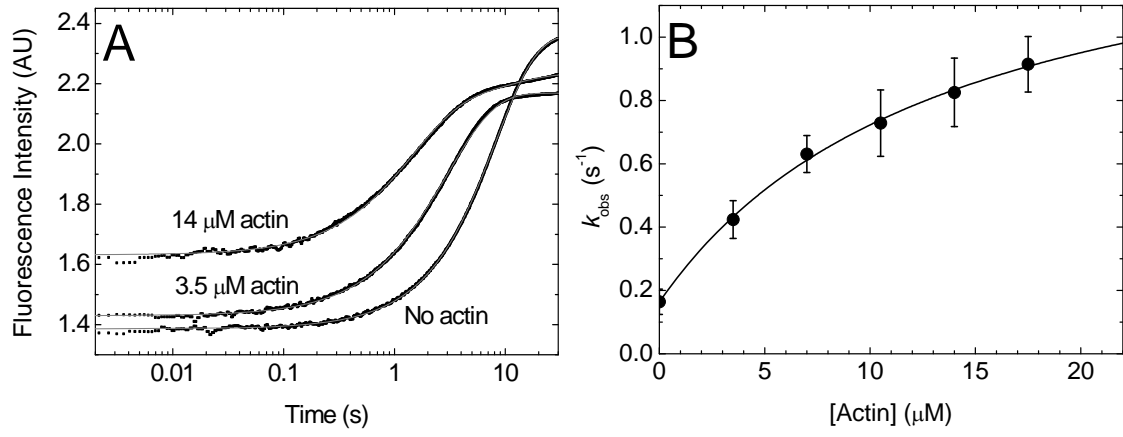


the kinetic parameters in TABLE ONE, the ADP inhibition was much less pronounced in acto-MVc-S1 than in acto-mVa-S1 where ADP release is rate-limiting (De La Cruz et al., 1999; De La Cruz et al., 2000).

Kinetics of the P_i release step — We monitored the time course of P_i release from MVc-S1.ADP.P_i and acto-MVc-S1.ADP.P_i using MDCC-PBP, a fluorescently-labeled P_i binding protein (White et al., 1997; Brune et al., 2001a). In double-mixing stopped-flow experiments, MVc-S1 was first mixed with ATP under single turnover conditions (5.2 μM MVc-S1 and 4 μM ATP after the first mix), incubated for 3 s so that ATP binding and hydrolysis can occur, and then rapidly mixed with actin (0 – 17.5 μM after the second mix) to monitor basal and actin-activated P_i release. Time courses of P_i release were best fit with single exponentials. Fig. 8A shows examples of transients, including their curve-fits. The fitted k_{obs} values depended hyperbolically on actin concentration, starting from 0.16 s⁻¹ in the absence of actin (k_4) and delineating a maximal P_i release rate constant of 1.5 s⁻¹ (k_4^{\wedge}) reaching half-saturation at 14 μM actin (K_9) (Fig. 8B).

In Vitro Actin Gliding Assay — *In vitro* actin gliding assays were performed to measure the velocity (v) at which the eGFP-MVc-HMM translocates TMR-Phalloidin labeled filamentous actin filaments using a TIRF microscope setup equipped with a shutter to illuminate the field briefly every 10 or 20 seconds, to minimize photo-bleaching of the labeled actin filaments. Actin filaments more than 5 μm in length were tracked for more than 3 minutes. Time lapse images were collected digitally and analysis of the leading edge of the actin filaments in the direction of translocation was performed by tracking the actin filaments over sequential images using the ImageJ image analysis software. The velocity (v) distribution of actin filaments gliding over eGFP-MVc-HMM

Figure A1-8: Pi release from M_{Vc}-S1 and acto-M_{Vc}-S1 monitored by MDCC-PBP fluorescence. *A*, MDCC-PBP fluorescence traces obtained in double-mixing stopped-flow experiments where m_{5c}-S1 was first mixed with ATP (5.2 μM M_{Vc}-S1 and 4 μM ATP after the first mix), aged for 3 s, and then rapidly mixed with different concentrations of actin (as indicated). Single exponential fits to the traces are shown ($k_{\text{obs}} = 0.082 \text{ s}^{-1}$ (no actin), 0.34 s^{-1} (3.5 μM actin post-mix concentration), 0.67 s^{-1} (14 μM actin post-mix concentration)). *B*, dependence of the k_{obs} values on actin concentration. The best hyperbolic fit to the data yielded a maximum of 1.5 s^{-1} , with half-saturation at 14 μM actin and a *y*-intercept of 0.16 s^{-1} .

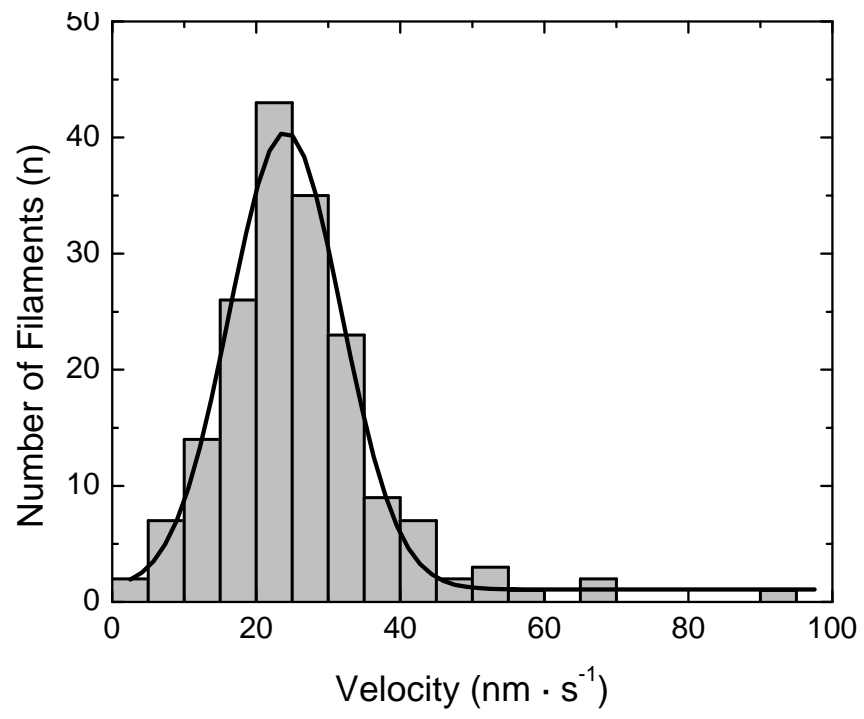


at saturating ATP concentration (1 mM) was $24.1 \pm 7.8 \text{ nm}\cdot\text{s}^{-1}$ (mean \pm standard deviation) (Fig. 9). A Gaussian fit to the velocity distribution histogram was used to determine the mean and standard deviations.

Single Molecule Motility Assay — Single molecule Total Internal Reflection Fluorescence (TIRF) microscopy assay (Yildiz et al., 2003) was performed as previously reported from our laboratory (Snyder et al., 2004; Sakamoto et al., 2005). The single molecule TIRF microscopy assay is a direct indication of whether or not the myosin is processive *in vitro*. TIRF microscopy experiments were performed using the recombinant heavy meromyosin like myosin Vc construct encoding the first 1108 amino acids, containing the motor domain, the six predicted IQ motifs and the coiled-coil region with an N-terminally fused enhanced GFP (eGFP-MVc-HMM). The assay was performed over a range of KCl concentrations (0 – 300 mM) to determine if KCl affects the single molecule processivity of eGFP-MVc-HMM, as previously reported for myosin Va (Sakamoto et al., 2000). The images recorded did not show any processive motion of the eGFP-MVc-HMM over the range of KCl or ATP concentrations (1 μM – 1 mM) whereby the experiments were performed (*data not shown*), even though the eGFP-MVc-HMM does bind to and detach from actin filaments. This non-processive behavior is expected of single molecules of eGFP-MVc-HMM from the transient kinetic rates, *i.e.* specifically the P_i release limitation of the ATPase cycle, determined using the MVc-S1 in this study.

We conclude that the recombinant double-headed myosin Vc construct, eGFP-MVc-HMM, under unloaded *in vitro* conditions, is not processive as a single molecule.

Figure A1-9: in vitro actin gliding assay of eGFP-MVc-HMM. Actin gliding velocity (v) distribution of eGFP-MVc-HMM in 1 mM ATP ($v = 24.1 \pm 7.8 \text{ nm}\cdot\text{s}^{-1}$, $n = 175$). Actin gliding assays were performed in the following conditions: Buffer: 20 mM MOPS (pH 7.4); 5 mM MgCl_2 ; 0.1 mM EGTA; 50 mM KCl; 1 mM ATP; 5 μM calmodulin; 25 $\mu\text{g/ml}$ glucose oxidase, 45 $\mu\text{g/ml}$ catalase; 2.5 mg/ml glucose and 20 mM DTT (final concentrations listed). Temperature = 25 °C.



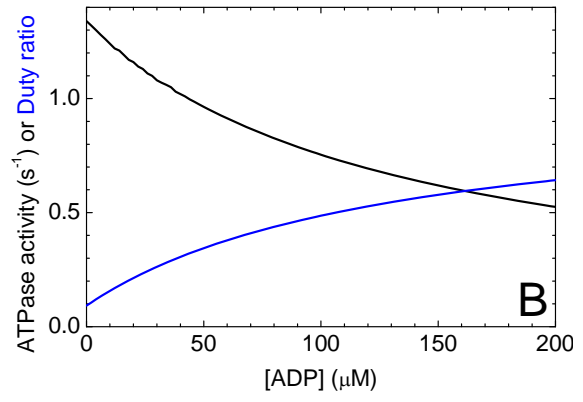
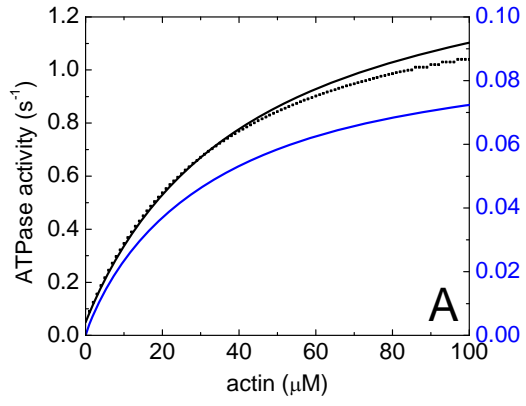
Kinetic Simulations — Kinetic simulations of the acto-MVc-S1 ATPase cycle were performed based on SCHEME 1 and the experimentally determined rate constants listed in TABLE ONE. Steps K_1 , K_2 and K_7 (ATP binding to m5c-S1 detached from actin) were omitted from the simulations, since their parameters are unknown and the flux through these steps is negligible. Parameters used in the simulations but not listed in TABLE ONE were: $k_9 = 1400 \text{ s}^{-1}$, $k_{-9} = 100 \text{ }\mu\text{M}^{-1}\text{s}^{-1}$ (to yield a rapid step with the measured $K_9 = 14 \text{ }\mu\text{M}$); $k_3 = 31.6 \text{ s}^{-1}$, $k_{-3} = 58.4 \text{ s}^{-1}$ (calculated from K_3 and $(k_3 + k_{-3})$ in TABLE ONE); $k_{5'} = 14.7 \text{ s}^{-1}$ (average of $k_{5'}$ values listed in TABLE ONE); $k_{-5'} = 64 \text{ }\mu\text{M}^{-1}\text{s}^{-1}$.

First, we performed a global fit of the mechanism to attain the measured actin concentration dependence of the steady-state ATPase activity. In this fit, we floated the parameters of the experimentally inaccessible steps K_8 and $K_{3'}$ as well as the k_4' rate constant, which might not precisely equal the maximal observed P_i release rate constant of the MDCC-PBP measurements (Fig. 7).

The [actin] dependence of the partitioning between the weak-binding MVc-ATP, MVc-ADP- P_i and acto-MVc-ADP- P_i (and acto-MVc-ATP, if relevant) states is dictated by the reversible K_3 and K_9 equilibria, with possible contributions from K_8 and/or $K_{3'}$. The fact that $K_9 \cdot (1 + K_3) / K_3 (= 40 \text{ }\mu\text{M})$ nearly equals $K_{ATPase} (= 42.5 \text{ }\mu\text{M})$ caused the fits to produce nearly complete dissociation of MT from actin following ATP binding (i.e. in the well-fitting models K_8 was $\geq 1 \text{ mM}$). The presence or absence of actin-attached hydrolysis ($K_{3'}$) did not affect the outcome of the steady-state parameters (ATPase activity and duty ratio) at the experimentally applied actin concentrations. Therefore, in further simulations we used two extremes of the adequately-fitting parameter sets to calculate the dependence of the ATPase activity and the duty ratio on actin and ADP

concentration. Importantly, these two sets of parameters (see Figs. 10 A and B) yielded similar ATPase activity and duty ratio values due to the same maximal effective rate of P_i release from acto-MVc (around 1.5 s^{-1}). Set #1 represented a mechanism in which actin-attached ATP hydrolysis does not occur ($k_3' = 0$, $k_{-3}' = 0$, $K_8 = 1 \text{ mM}$ (rapid step), $k_4' = 1.618 \text{ s}^{-1}$), whereas set #2 contained a rapid and favorable actin-attached ATP hydrolysis step ($k_3' = 100 \text{ s}^{-1}$, $k_{-3}' = 3 \text{ s}^{-1}$, $K_8 = 1 \text{ mM}$ (rapid step), $k_4' = 1.508 \text{ s}^{-1}$). In both conditions, the duty ratio of MVc-S1 depended hyperbolically on actin concentration, yielding a maximum value of 0.095 (reaching half-saturation at $31 \text{ }\mu\text{M}$ actin) in the absence of background ADP ($[\text{ATP}] = 1 \text{ mM}$, $[\text{ADP}] = 0$, $[\text{actin}]$ scanned between $0\text{-}100 \text{ }\mu\text{M}$; Fig. 10A). At saturating actin concentration (using set #1), the increase of background $[\text{ADP}]$ from 0 to $200 \text{ }\mu\text{M}$ caused the ATPase activity of MVc to decrease to 39 % of its original value (from 1.34 s^{-1} to 0.53 s^{-1}), whereas the duty ratio increased nearly 7-fold (from 0.093 to 0.64) ($[\text{actin}] = 1 \text{ mM}$, $[\text{ATP}] = 1 \text{ mM}$, $[\text{ADP}]$ scanned between $0\text{-}200 \text{ }\mu\text{M}$; Fig. 10B).

Figure A1-10: Dependence of steady-state parameters (ATPase activity, duty ratio) of MVc-S1 on (A) actin and (B) background ADP concentration. *A*, dependence of the ATPase activity (left axis; solid black line: target for global fit ($V_{max} = 1.5 \text{ s}^{-1}$, $K_{ATPase} = 43.5 \text{ }\mu\text{M}$); black dots: best-fit simulation) and duty ratio (right axis; blue line) of MVc-S1 on actin concentration in the absence of ADP background. Parameter sets #1 and #2 described in the text yielded similar ATPase and duty ratio values. *B*, dependence of the ATPase activity (black) and duty ratio (blue) of MVc-S1 at saturating [actin] (1 mM) on ADP concentration. Parameter set #1 was used in panel B. ATP concentration was kept constant at 1 mM in all simulations.



Discussion

The kinetic characterization of the MVc-S1 and the *in vitro* motility assays performed using the eGFP-MVc-HMM revealed that the biochemistry of the vertebrate myosin Vc actomyosin ATPase cycle is fundamentally different from the other vertebrate myosin V isoforms, as well as the invertebrate *Drosophila* myosin V. We discuss hereafter these differences and the implications of these unique characteristics of myosin Vc.

Hum-MVc-S1 Exhibits a Low Duty Ratio — Kinetic analysis of MVc-S1 demonstrated that the rate-limiting step in the acto-MVc-S1 ATPase cycle is the P_i release step ($k_4' = 1.5 \text{ s}^{-1}$), which is close to the maximal steady-state ATPase rate ($V_{max} = 1.8 \pm 0.3 \text{ s}^{-1}$) and approximately 10 times slower than the ADP release rate. Myosin Vc's rate limitation by the P_i release step in the actomyosin ATPase cycle contrasts to other vertebrate myosin Vs (Va and Vb) whose ADP dissociation rate constant (k_5') is rate limiting (De La Cruz et al., 1999);(Wang et al., 2000); (Watanabe et al., 2006). It has been shown that the rate limiting P_i release is a common feature of ensemble myosins such as skeletal muscle myosin II (Geeves, 1991), non muscle myosin IIA (Kovacs et al., 2003) and some myosin Is (Ostap and Pollard, 1996);(Coluccio and Geeves, 1999);(El Mezgueldi et al., 2002). Ensemble myosins' duty ratios are generally known to be small (i.e. $\leq 10 \%$).

Assuming a very simplified cycle in which only two states alternate: a strong and a weak actin-binding one, which the ADP release rate constant ($k_5' = 12 - 16 \text{ s}^{-1}$) is the exit rate from the strong binding state, and the P_i release rate constant ($k_4' = 1.5 \text{ s}^{-1}$) is the exit rate from the weak binding state, we can estimate the duty ratio of MVc-S1 by using the equation $k_4' / (k_4' + k_5')$ (De La Cruz et al., 1999;De La Cruz and Ostap, 2004). This

yields a duty ratio within the range of 6 – 13 % for MVc-S1, which is dramatically lower compared to some other high duty ratio motors such as myosin Va and VI (De La Cruz et al., 1999;De La Cruz et al., 2001), but quite comparable to the low duty ratio myosins as aforementioned.

To calculate the duty ratio under different conditions, we performed global kinetic simulations using the parameters determined from the biochemically observed rates in this study. The simulations generated a duty ratio in line with the above simple calculations (around 10 %), and an increase of this duty ratio by approximately 7-fold to more than 60 % in the presence of moderate background levels of [ADP] (Fig. 10). Simulations were performed for ADP concentrations from 0 – 200 μM , which has been suggested as physiological concentrations, for example in muscle at rest and during work (Dawson et al., 1978;Kushmerick et al., 1992;Radda, 1986). This increase in duty ratio due to increased [ADP] may be a regulatory mechanism *in vivo* to modulate the intracellular function of myosin Vc in the cell, perhaps as a tension generating, or anchoring, myosin.

Furthermore, the estimated low duty ratio of the MVc-S1 is consistent with our observations that single molecules of eGFP-MVc-HMM exhibit non-processive movements in the single molecule TIRF microscopy assays. Thus, the biochemical rates obtained from the steady-state and transient kinetic solution experiments provided a satisfactory basis for its mechano-chemical behavior.

Bio-chemical and Mechanical Implications of Human Myosin Vc as a Cytoskeletal Cargo Transporter — The duty ratio, discussed in the previous section, captures the essence of how different myosin Vc is compared to myosins Va and Vb.

However, a number of unique details of the kinetic mechanism provide insights on the functional role of the myosin Vc *in vivo*. In this section, we will discuss about these different kinetic features.

The maximal steady-state ATPase rate of MVc-S1 (1.8 s^{-1}) is markedly lower than that of chicken myosin Va (12 s^{-1}) (De La Cruz et al., 1999) and *Homo sapiens* myosin Vb ($9.7 \pm 0.4 \text{ s}^{-1}$) (Watanabe et al., 2006). Moreover, the apparent affinity of MVc-S1 to actin filaments (K_{ATPase}) is approximately 30-fold lower than chicken myosin Va (De La Cruz et al., 1999) and 1.5-fold higher than that of myosin Vb (See TABLE ONE). This lower actin affinity of MVc, may be in part due to the difference in the loop 2 region, which has been shown to affect the K_{ATPase} of chicken myosin Va (Swiatecka-Urban et al., 2007). Comparing the loop 2 of *Homo sapiens* MVc to that of the *Homo sapiens* myosin Va, the overall charge of MVc in this region is approximately half that of myosin Va (Toth et al., 2005). The *in vitro* actin gliding assays also reflected this phenomenon, whereby the velocity of filamentous actin translocation by eGFP-MVc-HMM was approximately an order of magnitude slower ($v_{Average} \sim 24 \text{ nm}\cdot\text{s}^{-1}$) than myosin Va ($v_{Average} \sim 320 \text{ nm}\cdot\text{s}^{-1}$; (Homma et al., 2000) or myosin Vb ($v_{Average} \sim 220 \text{ nm}\cdot\text{s}^{-1}$; (Watanabe et al., 2006). The *in vitro* actin gliding assays was also performed using the creatine phosphate/creatine phosphokinase ATP regeneration system, to determine if the levels of ADP contamination accounts for this slow velocity of actin filaments. Using the ATP regeneration system, the velocity of the actin filaments increased by approximately a factor of two (*data not shown*), still reporting actin filaments velocity an order of magnitude slower than both myosins Va and Vb. From the ADP release rate constant reported our transient kinetic measurements, we expected that the results from the *in vitro*

actin gliding assays would be closer to that the actin filament velocities of myosin Va and Vb. The slower actin filament velocity may be accounted for by the hindrance due to weakly actin-bound heads of the eGFP-MVc-HMM.

Another possible reason of the slower *in vitro* actin gliding velocity of MVc may be due to the structure of the MVc lever arm, or IQ motifs. The IQ motifs assembling the myosin Va lever, have been shown to be separated by a repetition of 23 and 25 amino acid residues. However, the first two IQ motifs assembling the MVc lever seems to be separated by 23 and 28 amino acid residues (De La Cruz et al., 1999). This structural difference in the separation of IQ motifs assembling the MVc lever, may in part a factor of the slow *in vitro* actin gliding velocity reported here, as shown with a myosin Va construct with altered spacing between the third and fourth IQ motifs by artificially inserting two alanine residues (Watanabe et al., 2006). Both ensemble and single molecule studies of this myosin Va chimera showed slower velocity and smaller single displacements compared to the wild type construct without the additional alanines.

We note that the unexpectedly low *in vitro* actin gliding velocity of eGFP-MVc-HMM might possibly be due to a slow, rate-limiting isomerization between two actomyosin.ADP states that could occur after P_i release and precede ADP release. Such a step might remain undetected in the ADP release stopped-flow experiments if the “starting” state of the isomerization is an energetically unfavorable state that does not become populated upon ADP addition. However, the inability of eGFP-MVc-HMM to perform processive movement implies that its duty ratio is low and thus, the low actin gliding velocity results from hindrance by weakly actin-bound heads rather than an undetected strong actin-binding state.

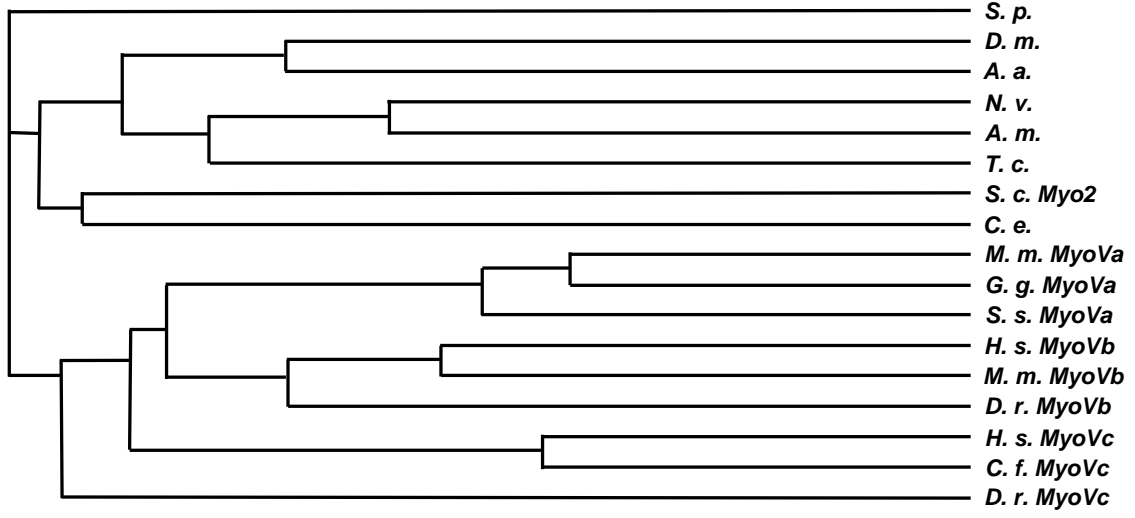
Furthermore, both in the presence of nucleotide, as well as in the absence of nucleotide, myosin Vc seems to have a lower affinity to actin than myosin Va. The binding rate of MVc-S1 to actin in the absence of nucleotide is approximately 100-fold slower as compared to chicken myosin Va ($= 73 \mu\text{M}^{-1}\cdot\text{s}^{-1}$; (De La Cruz et al., 1999)). These rigor and nucleotide bound on-rate constants may not be directly related to single-molecule processivity. However, it may indirectly bear implications on the actin on-rate constant in the weak actin-binding states, which parameter indeed is an important factor in processivity (e.g. a common factor determining strong and weak-binding on-rate constants may be surface charge distribution). These implications may suggest that myosin Vc is inadequate for a single-molecule cargo transporter.

Thus, for myosin Vc to function as a cargo transporter motor protein *in vivo*, it may function collectively as an ensemble of low duty ratio motors that can become a processive cargo transporter. However, myosin Vc may be useful for other cellular processes, such as budding, tethering or fusion within the membrane trafficking system which myosin Vc has been implicated to (Rodriguez and Cheney, 2002; Krendel and Mooseker, 2005). The high affinity of myosin Vc for ADP, may allow myosin Vc to have long-lived, non-moving attached states, that may be a useful feature for a tension-generating, or anchoring, myosin *in vivo*.

Phylogenetic analysis of Homo sapiens myosin Vc — A consensus tree of the *Homo sapiens* myosin V isoforms (Va, Vb and Vc) and *Drosophila* myosin V, was reported recently (Toth et al., 2005) which indicated that the motor domain of the *Homo sapiens* myosin Vc had closer resemblance to the *Drosophila* myosin V than the other *Homo sapiens* myosin V isoforms' motor domains. Both *Drosophila* myosin V and the

Figure A1- 11: Phylogenetic analysis of various myosin Vs from different organisms.

The consensus tree was generated using the ClustalW multiple sequence alignment program (<http://www.ebi.ac.uk/Tools/clustalw/index.html>). Abbreviations as follows: *S. p.*, *Strongylocentrotus purpuratus*; *D. m.*, *Drosophila melanogaster*; *A. a.*, *Aedes aegypti*; *N. v.*, *Nagoni vetripennis*; *A. m.*, *Apis mellifera*; *T. c.*, *Triboleum castaneum*; *S. c.*, *Saccharomyces cerevisiae*; *C. e.*, *Caenorhabditis elegans*; *M. m.*, *Mus musculus*; *G. g.*, *Gallus gallus*; *S. s.*, *Sus serofa*; *H. s.*, *Homo sapiens*; *D. r.*, *Danio rerio*; *C. f.*, *Canis familiaris*.



Homo sapiens myosin Vc, as characterized in this study, are low duty ratio motors, however the kinetic mechanisms of these two myosins are quite different. We therefore performed a more extensive phylogenetic analysis of the motor domain of myosin Vs from different organisms (Fig. 11). The result of the analysis indicated that the alignment of vertebrate myosin Vc in the consensus tree is separate from those of vertebrate myosin Va and Vb. Furthermore, all the vertebrate myosin Vs were located far from the *Drosophila* myosin V too. This result implies that the *Homo sapiens* myosin Vc, even with the general dissimilarity of the kinetic cycle with its vertebrate myosin V counterparts, it is closer to these isoforms than the *Drosophila* myosin V, which has a closer kinetic property to the *Homo sapiens* myosin Vc. Perhaps evolution had evolved other vertebrate myosin V isoforms, Va and Vb, to become processive molecular motors.

High ADP Affinity of Myosin Vc – One unusual and intriguing aspect of the MVc-S1 actomyosin ATPase cycle is its high affinity for ADP. The ADP affinities were measured using the pyrene-actin fluorescence signal and the MANT-ADP signal, and independent experiments indicated similar results, suggesting that the ADP affinity (K_5) is higher for MVc-S1 (0.25 – 0.4 μM) than myosin Va (0.8 μM ; (De La Cruz et al., 1999)), but not as high as the non-muscle myosin IIB (0.15 μM ; (Wang et al., 2003)). It may be that the myosin Vc is sensitive to ADP concentration changes, and increases the duty ratio at high, or even at moderate, [ADP] as previously hypothesized for non-muscle myosin IIB (Wang et al., 2003). This unique feature may enhance the function of myosin Vc as a possible tension-generating molecular motor inside of a cell.

Future experiments are required to reveal if this is a plausible mechanism, however, this could be a novel *in vivo* process to alter a naturally occurring low duty ratio

motor into a high duty ratio motor by functionally adapting to the physical environment they encounter, and also may be a form of regulation for this molecular motor.

Acknowledgments

We thank Dr. Howard D. White for his generous gift of the MDCC-PBP; Dr. Takeshi Sakamoto for training to use the Olympus IX70 TIRF microscope system; Antoine F. Smith for rabbit muscle actin purification; Dr. J.R. Kuhn for the ImageJ plugin; Dr. Fang Zhang for expert technical assistance; Ms. Rachel E. Farrow, Dr. Earl E. Homsher and Dr. Attila Nagy for critical reading of the manuscript; and the members of the Laboratory of Molecular Physiology and Laboratory of Molecular Cardiology for support and critical advice. MK is supported by NIH Research Grant #D43 TW006230 (1 R01 TW007241-01) funded by the Fogarty International Center and the National Heart, Lung and Blood Institute, an EMBO-HHMI Startup Grant, and the Bolyai Fellowship of the Hungarian Academy of Sciences. JRS is supported by funds from the intramural NHLBI program.

References

Berg, J.S., B.C.Powell, and R.E.Cheney. (2001). A millennial myosin census. *Mol. Biol. Cell* 12:780-794.

Brown, S.S. (1999). Cooperation between microtubule- and actin-based motor proteins. *Annu. Rev. Cell Dev. Biol.* 15:63-80.

Brune, M., J.E.Corrie, and M.R.Webb. (2001a). A fluorescent sensor of the phosphorylation state of nucleoside diphosphate kinase and its use to monitor nucleoside diphosphate concentrations in real time. *Biochemistry* 40:5087-5094.

Brune, M., J.E.Corrie, and M.R.Webb. (2001b). A fluorescent sensor of the phosphorylation state of nucleoside diphosphate kinase and its use to monitor nucleoside diphosphate concentrations in real time. *Biochemistry* 40:5087-5094.

Brune, M., J.L.Hunter, J.E.T.Corrie, and M.R.Webb. (1994). Direct, real-time measurement of rapid inorganic phosphate release using a novel fluorescent probe and its application to actomyosin subfragment 1 ATPase. *Biochemistry* 33:8262-8271.

Burgess, S., M.Walker, F.Wang, J.R.Sellers, H.D.White, P.J.Knight, and J.Trinick. (2002). The prepower stroke conformation of myosin V. *J. Cell Biol.* 159:983-991.

Cheney, R.E., M.K.O'Shea, J.E.Heuser, M.V.Coelho, J.S.Wolenski, E.M.Espreafico, P.Forscher, R.E.Larson, and M.S.Mooseker. (1993). Brain myosin-V is a two-headed unconventional myosin with motor activity. *Cell* 75:13-23.

Coluccio, L.M. and M.A.Geeves. (1999). Transient kinetic analysis of the 130-kDa myosin I (MYR-1 gene product) from rat liver. A myosin I designed for maintenance of tension? *J. Biol. Chem* 274:21575-21580.

Coureux, P.D., H.L.Sweeney, and A.Houdusse. (2004). Three myosin V structures delineate essential features of chemo-mechanical transduction. *EMBO J.* 23:4527-4537.

Dawson, M.J., D.G.Gadian, and D.R.Wilkie. (1978). Muscular fatigue investigated by phosphorus nuclear magnetic resonance. *Nature* 274:861-866.

De La Cruz, E.M. and E.M.Ostap. (2004). Relating biochemistry and function in the myosin superfamily. *Curr. Opin. Cell Biol.* 16:61-67.

De La Cruz, E.M., E.M.Ostap, and H.L.Sweeney. (2001). Kinetic mechanism and regulation of myosin VI. *J. Biol. Chem* 276:32373-32381.

De La Cruz, E.M., H.L.Sweeney, and E.M.Ostap. (2000). ADP inhibition of myosin V ATPase activity. *Biophys. J.* 79:1524-1529.

De La Cruz, E.M., A.L.Wells, S.S.Rosenfeld, E.M.Ostap, and H.L.Sweeney. (1999). The kinetic mechanism of myosin V. *Proc. Natl. Acad. Sci. U. S. A* 96:13726-13731.

DePina, A.S. and G.M.Langford. (1999). Vesicle transport: the role of actin filaments and myosin motors. *Microsc. Res. Tech.* 47:93-106.

El Mezgueldi, M., N.Tang, S.S.Rosenfeld, and E.M.Ostap. (2002). The kinetic mechanism of Myo1e (human myosin-1C). *J. Biol. Chem.* 277:21514-21521.

Espindola, F.S., E.M.Espreafico, M.V.Coelho, A.R.Martins, F.R.C.Costa, M.S.Mooseker, and R.E.Larson. (1992). Biochemical and immunological characterization of p190-calmodulin complex from vertebrate brain: A novel calmodulin-binding myosin. *J. Cell Biol.* 118:359-368.

Espreafico, E.M., R.E.Cheney, M.Matteoli, A.A.C.Nascimento, P.V.De Camilli, R.E.Larson, and M.S.Mooseker. (1992). Primary structure and cellular localization of chicken brain myosin-V (p190), an unconventional myosin with calmodulin light chains. *J. Cell Biol.* 119:1541-1557.

Forkey, J.N., M.E.Quinlan, M.A.Shaw, J.E.Corrie, and Y.E.Goldman. (2003). Three-dimensional structural dynamics of myosin V by single-molecule fluorescence polarization. *Nature* 422:399-404.

Geeves, M.A. (1991). The dynamics of actin and myosin association and the crossbridge model of muscle contraction. *Biochem. J.* 274:1-14.

Homma, K., J.Saito, R.Ikebe, and M.Ikebe. (2000). Ca²⁺-dependent regulation of the motor activity of myosin V. *J. Biol. Chem.* 275:34766-34771.

Houk, T.W., Jr. and K.Ue. (1974). The measurement of actin concentration in solution: a comparison of methods. *Anal. Biochem.* 62:66-74.

Ishijima, A., H.Kojima, T.Funatsu, M.Tokunaga, H.Higuchi, H.Tanaka, and T.Yanagida. (1998). Simultaneous observation of individual ATPase and mechanical events by a single myosin molecule during interaction with actin. *Cell* 92:161-171.

Kovacs, M., F.Wang, A.Hu, Y.Zhang, and J.R.Sellers. (2003). Functional divergence of human cytoplasmic myosin II: kinetic characterization of the non-muscle IIA isoform. *J. Biol. Chem* 278:38132-38140.

Kovacs, M., F.Wang, and J.R.Sellers. (2005). Mechanism of action of myosin X, a membrane-associated molecular motor. *J. Biol. Chem.* 280:15071-15083.

Krendel, M. and M.S.Mooseker. (2005). Myosins: tails (and heads) of functional diversity. *Physiology.* (Bethesda.) 20:239-251.

Kuhn, J.R. and T.D.Pollard. (2005). Real-time measurements of actin filament polymerization by total internal reflection fluorescence microscopy. *Biophys. J.* 88:1387-1402.

Kushmerick, M.J., T.S.Moerland, and R.W.Wiseman. (1992). Mammalian skeletal muscle fibers distinguished by contents of phosphocreatine, ATP, and Pi. *Proc. Natl. Acad. Sci. U. S. A* 89:7521-7525.

Lapierre, L.A., R.Kumar, C.M.Hales, J.Navarre, S.G.Bhartur, J.O.Burnette, D.W.Provance, Jr., J.A.Mercer, M.Bahler, and J.R.Goldenring. (2001). Myosin vb is associated with plasma membrane recycling systems. *Mol. Biol. Cell* 12:1843-1857.

Libby, R.T., C.Lillo, J.Kitamoto, D.S.Williams, and K.P.Steel. (2004). Myosin Va is required for normal photoreceptor synaptic activity. *J. Cell Sci.* 117:4509-4515.

Matesic, L.E., R.Yip, A.E.Reuss, D.A.Swing, T.N.O'Sullivan, C.F.Fletcher, N.G.Copeland, and N.A.Jenkins. (2001). Mutations in *Mlph*, encoding a member of the Rab effector family, cause the melanosome transport defects observed in leaden mice. *Proc. Natl. Acad. Sci. U. S. A* 98:10238-10243.

Mehta, A.D., R.S.Rock, M.Ridf, J.A.Spudich, M.S.Mooseker, and R.E.Cheney. (1999). Myosin-V is a processive actin-based motor. *Nature* 400:590-593.

Mercer, J.A., P.K.Seperack, M.C.Strobel, N.G.Copeland, and N.A.Jenkins. (1991). Novel myosin heavy chain encoded by murine dilute coat colour locus. *Nature* 349:709-713.

Nascimento, A.A., R.E.Cheney, S.B.Tauhata, R.E.Larson, and M.S.Mooseker. (1996). Enzymatic characterization and functional domain mapping of brain myosin-V. *J. Biol. Chem* 271:17561-17569.

Ostap, E.M. and T.D.Pollard. (1996). Biochemical kinetic characterization of the *Acanthamoeba* myosin-I ATPase. *J. Cell Biol.* 132:1053-1060.

Pollard, T.D. (1984) Polymerization of ADP-actin. *J. Cell Biol.* 99:769-777.

Provance, D.W., Jr., M.Wei, V.Ipe, and J.A.Mercer. (1996). Cultured melanocytes from dilute mutant mice exhibit dendritic morphology and altered melanosome distribution. *Proc. Natl. Acad. Sci. USA* 93:14554-14558.

Radda, G.K. (1986). The use of NMR spectroscopy for the understanding of disease. *Science* 233:640-645.

Reck-Peterson, S.L., D.W.Provance, M.S.Mooseker, and J.A.Mercer. (2000). Class V myosins [In Process Citation]. *Biochim. Biophys. Acta* 1496:36-51.

Richards, T.A. and T.Cavalier-Smith. (2005). Myosin domain evolution and the primary divergence of eukaryotes. *Nature* 436:1113-1118.

Rodriguez, O.C. and R.E.Cheney. (2002). Human myosin-Vc is a novel class V myosin expressed in epithelial cells. *J. Cell Sci.* 115:991-1004.

Sakamoto, T., I.Amitani, E.Yokota, and T.Ando. (2000). Direct observation of processive movement by individual myosin V molecules. *Biochem. Biophys. Res. Commun.* 272:586-590.

Sakamoto, T., F.Wang, S.Schmitz, Y.H.Xu, Q.Xu, J.E.Molloy, C.Veigel, and J.R.Sellers. (2003). Neck length and processivity of myosin V. *J. Biol. Chem.* 278:29201-29207.

Sakamoto, T., A.Yildiz, P.R.Selvin, and J.R.Sellers. (2005). Step-size is determined by neck length in myosin V. *Biochemistry* 44:16203-16210.

Sellers, J.R. (1999). *Myosins*. Oxford University Press, Oxford.

Sellers, J.R. (2000). Myosins: a diverse superfamily. *Biochim. Biophys. Acta* 1496:3-22.

Sellers, J.R. and C.Veigel. (2006). Walking with myosin V. *Curr. Opin. Cell Biol.* 18:68-73.

Snyder, G.E., T.Sakamoto, J.A.Hammer, III, J.R.Sellers, and P.R.Selvin. (2004). Nanometer localization of single green fluorescent proteins: evidence that myosin V walks hand-over-hand via telemark configuration. *Biophys. J.* 87:1776-1783.

Spudich, J.A. and S.Watt. (1971). The regulation of rabbit skeletal muscle contraction. *J. Biol. Chem.* 246:4866-4871.

Sweeney, H.L. and A.Houdusse. (2004). The motor mechanism of myosin V: insights for muscle contraction. *Philos. Trans. R. Soc. Lond B Biol. Sci.* 359:1829-1841.

Swiatecka-Urban, A., L.Talebian, E.Kanno, S.Moreau-Marquis, B.Coutermarsh, K.Hansen, K.H.Karlson, R.Barnaby, R.E.Cheney, G.M.Langford, M.Fukuda, and B.A.Stanton. (2007). Myosin Vb Is Required for Trafficking of the Cystic Fibrosis Transmembrane Conductance Regulator in Rab11a-specific Apical Recycling Endosomes in Polarized Human Airway Epithelial Cells. *J. Biol. Chem.* 282:23725-23736.

Takagi, Y., E.E.Homsher, Y.E.Goldman, and H.Shuman. (2006). Force generation in single conventional actomyosin complexes under high dynamic load. *Biophys. J.* 90:1295-1307.

Toth, J., M.Kovacs, F.Wang, L.Nyitray, and J.R.Sellers. (2005). Myosin V from *Drosophila* Reveals Diversity of Motor Mechanisms within the Myosin V Family. *J. Biol. Chem.* 280:30594-30603.

Trentham, D.R., R.G.Bardsley, J.F.Eccleston, and A.G.Weeds. (1972). Elementary processes of the magnesium ion-dependent adenosine triphosphatase activity of heavy meromyosin. A transient kinetic approach to the study of kinases and adenosine triphosphatases and a colorimetric inorganic phosphate assay in situ. *Biochem. J.* 126:635-644.

Trybus, K.M., E.Krementsova, and Y.Freyzon. (1999). Kinetic characterization of a monomeric unconventional myosin V construct. *J. Biol. Chem* 274:27448-27456.

Tuxworth, R.I. and M.A.Titus. (2000). Unconventional myosins: anchors in the membrane traffic relay. *Traffic*. 1:11-18.

Volpicelli, L.A., J.J.Lah, G.Fang, J.R.Goldenring, and A.I.Levey. (2002). Rab11a and myosin Vb regulate recycling of the M4 muscarinic acetylcholine receptor. *J. Neurosci*. 22:9776-9784.

Walker, M.L., S.A.Burgess, J.R.Sellers, F.Wang, J.A.Hammer, III, J.Trinick, and P.J.Knight. (2000). Two-headed binding of a processive myosin to F-actin. *Nature* 405:804-807.

Wang, F., L.Chen, O.Arcucci, E.V.Harvey, B.Bowers, Y.Xu, J.A.Hammer, III, and J.R.Sellers. (2000). Effect of ADP and ionic strength on the kinetic and motile properties of recombinant mouse myosin V. *J. Biol. Chem*. 275:4329-4335.

Wang, F., M.Kovacs, A.H.Hu, J.Limouze, E.V.Harvey, and J.R.Sellers. (2003). Kinetic mechanism of non-muscle myosin IIB - Functional adaptations for tension generation and maintenance. *J. Biol. Chem*. 278:27439-27448.

Watanabe, S., K.Mabuchi, R.Ikebe, and M.Ikebe. (2006). Mechanoenzymatic characterization of human myosin Vb. *Biochemistry* 45:2729-2738.

Westbroek, W., J.Lambert, P.Bahadoran, R.Busca, M.C.Herteleer, N.Smit, M.Mommaas, R.Ballotti, and J.M.Naeyaert. (2003). Interactions of human Myosin Va isoforms, endogenously expressed in human melanocytes, are tightly regulated by the tail domain. *J. Invest Dermatol*. 120:465-475.

White, H.D., B.Belknap, and M.R.Webb. (1997). Kinetics of nucleoside triphosphate cleavage and phosphate release steps by associated rabbit skeletal actomyosin, measured using a novel fluorescent probe for phosphate. *Biochemistry* 36:11828-11836.

Wilson, S.M., R.Yip, D.A.Swing, T.N.O'Sullivan, Y.Zhang, E.K.Novak, R.T.Swank, L.B.Russell, N.G.Copeland, and N.A.Jenkins. (2000). A mutation in Rab27a causes the vesicle transport defects observed in ashen mice. *Proc. Natl. Acad. Sci. U. S. A* 97:7933-7938.

Wu, X., B.Bowers, K.Rao, Q.Weil, and J.A.Hammer, III. (1998). Visualization of melanosome dynamics within wild-type and dilute melanocytes suggests a paradigm for myosin V function in vivo. *J. Cell Biol*. 143:1-20.

Wu, X.S., K.Rao, H.Zhang, F.Wang, J.R.Sellers, L.E.Matesic, N.G.Copeland, N.A.Jenkins, and J.A.Hammer, III. (2002). Identification of an organelle receptor for myosin-Va. *Nat. Cell Biol.* 4:271-278.

Yang, Y., M.Kovacs, E.Xu, J.B.Anderson, and J.R.Sellers. (2005). Myosin VIIB from *Drosophila* is a high duty ratio motor. *J. Biol. Chem.* 280:32061-32068.

Yengo, C.M., E.M.De La Cruz, D.Safer, E.M.Ostap, and H.L.Sweeney. (2002). Kinetic characterization of the weak binding states of myosin V. *Biochemistry* 41:8508-8517.

Yengo, C.M. and H.L.Sweeney. (2004). Functional role of loop 2 in myosin V. *Biochemistry* 43:2605-2612.

Yildiz, A., J.N.Forkey, S.A.McKinney, T.Ha, Y.E.Goldman, and P.R.Selvin. (2003). Myosin V walks hand-over-hand: single fluorophore imaging with 1.5-nm localization. *Science* 300:2061-2065.

Zhao, L.P., J.S.Koslovsky, J.Reinhard, M.Bahler, A.E.Witt, D.W.Provance, Jr., and J.A.Mercer. (1996). Cloning and characterization of myr 6, an unconventional myosin of the dilute/myosin-V family. *Proc. Natl. Acad. Sci. U. S. A* 93:10826-10831.

**APPENDIX 2: SINGLE MOLECULE IMAGING OF MYOSIN-X REVEALS A
NOVEL FORM OF MOTILITY IN FILOPODIA**

Single-Molecule Imaging of Myosin-X Reveals a Novel Form of Motility in Filopodia

Michael L. Kerber*, Damon T. Jacobs*, Luke Campagnola, Brian D. Dunn, Taofei Yin,
Aurea D. Sousa, Omar A. Quintero, and Richard E. Cheney

Department of Cell and Molecular Physiology, School of Medicine
University of North Carolina at Chapel Hill, Chapel Hill, NC 27599

Correspondence should be directed to Richard E. Cheney at the above address
email: CheneyR@Med.UNC.edu phone: 919-966-0331 fax: 919-966-6927

Dr. Quintero's current address is:

Biology Department, Mount Holyoke College
50 College Street, South Hadley, MA 01075

Dr. Sousa's current address is:

National Institutes of Health, NIDCD, Bethesda, MD 20892

*The first two authors contributed equally to this work

Abstract

Myosin-X (Myo10) is an actin-based molecular motor hypothesized to use its motor activity to move forward along actin filaments to the tips of filopodia. Here we use total internal reflection fluorescence (TIRF) microscopy to track the movements of GFP-Myo10 at the single-molecule level in living cells. This reveals a novel form of motility in which extremely faint particles of Myo10 move in a rapid and directed fashion towards the filopodial tip at ~600 nm/s. These fast forward movements require Myo10 motor activity and actin filaments, but are independent of microtubules. Remarkably, faint particles of GFP-Myo5a also move towards the filopodial tip, but at a slower velocity of ~250 nm/s. Similar movements are not detected with GFP-Myo1a, indicating that not all myosins are capable of this intrafilopodial motility. These data indicate the existence of a novel system for forward transport based on the rapid movement of myosin molecules along filopodial actin filaments.

Introduction

Filopodia are slender, actin-based extensions thought to function as cellular sensors in processes such as nerve growth and blood vessel formation (Mattila and Lappalainen, 2008). Although it has been known since the 1970s that filopodia can transport particles rearward towards the cell body in a process now known as retrograde flow (Albrecht-Buehler and Goldman, 1976), the mechanisms by which molecules move forward towards the tips of filopodia are much less clear. The discovery of myosin-X (Myo10), an unconventional myosin that localizes to the tips of filopodia (Berg *et al.*, 2000), led to the hypothesis that Myo10 may function as a molecular motor for forward transport in filopodia (Berg and Cheney, 2002).

Filopodia have a relatively simple structure consisting of a bundle of parallel actin filaments surrounded by the plasma membrane (Mattila and Lappalainen, 2008). Each actin filament has its barbed end oriented towards the tip, and actin monomers are constantly added to the filament at its barbed end. The actin in filopodia typically moves rearward at rates of 10-100 nm/s. Many cytoskeletal proteins, cell surface proteins, and viruses can couple to retrograde flow (Felsenfeld *et al.*, 1996; Lidke *et al.*, 2005; Hu *et al.*, 2007; Sherer *et al.*, 2007). Current evidence indicates that retrograde flow in filopodia is powered by a combination of actin polymerization at the tip and myosin-II-mediated contraction from deeper in the cell (Medeiros *et al.*, 2006). Since microtubules and membranous vesicles are generally absent from filopodia, forward movement in filopodia is likely to depend either on diffusion or an actin-based mechanism.

Myo10 is one of four MyTH4-FERM myosins expressed in mammals and has potent filopodia-inducing activity (Sousa and Cheney, 2005; Bohil *et al.*, 2006). The Myo10 heavy chain consists of a myosin head domain responsible for binding to actin and generating force, a neck domain with 3 IQ motifs that provide binding sites for calmodulin or calmodulin-like light chains (Rogers and Strehler, 2001), and a large tail domain. The tail includes a segment that was initially predicted to form a coiled coil (Berg *et al.*, 2000), 3 PH domains that can bind to inositol phospholipids such as PIP₃ (Mashanov *et al.*, 2004), a MyTH4 domain that can bind to microtubules (Weber *et al.*, 2004), and a FERM domain that can bind to candidate cargoes including β -integrins (Zhang *et al.*, 2004) and netrin receptors (Zhu *et al.*, 2007).

Standard epifluorescence imaging in living cells revealed that the bright puncta of GFP-Myo10 at the tips of filopodia occasionally released from the tip and moved slowly rearward at 10-20 nm/s. This suggested that Myo10 can move rearward by binding in a rigor-like state to actin filaments undergoing retrograde flow (Berg and Cheney, 2002). Bright puncta of GFP-Myo10 also occasionally moved forward at ~100 nm/s, leading to the hypothesis that Myo10 uses its barbed-end motor activity to move forward to the tips of filopodia. Consistent with this, a Myo10 construct comprised of the head, neck, and coiled coil (Myo10-HMM) was sufficient for tip localization (Berg and Cheney, 2002). Interestingly, although forced dimerization of Myo10 head-neck constructs leads to tip localization *in vivo* (Tokuo *et al.*, 2007), Myo10-HMM appears largely monomeric *in vitro* (Knight *et al.*, 2005). Kinetic analyses of Myo10 head-neck constructs indicate they have duty ratios intermediate between those of highly processive motors, such as Myo5a, and non-

processive motors, such as muscle myosin (Homma and Ikebe, 2005; Kovacs *et al.*, 2005).

Importantly, recent work using TIRF in *in vitro* assays demonstrates that a HMM-like Myo10 forced-dimer moves rapidly and processively on actin bundles at 340-780 nm/s (Nagy *et al.*, 2008).

Although single-molecule imaging has been widely used for *in vitro* experiments, tracking the movements of individual motor molecules in living cells has remained a major challenge. Using TIRF to image substrate-attached filopodia provides several important advantages for this. First, the low background provided by TIRF is ideal for single-molecule studies both *in vitro* and *in vivo*. Second, the $\sim 0.1 \mu\text{m}$ thickness of filopodia means that all or most of a substrate-attached filopodium will be within the $\sim 0.1 \mu\text{m}$ penetration depth of the TIRF field. Third, although filopodia are part of a living cell, their linear organization and defined polarity greatly simplifies imaging, interpretation, and analysis. Imaging filopodia with TIRF thus provides a system that has much of the simplicity of *in vitro* motility assays, but in the context of a living cell.

Materials and Methods

Constructs. Bovine GFP-Myo10 (aa 1-2052), GFP-Myo10-HMM (aa 1-947), and GFP-Myo10-head-neck (aa 1-811) in pEGFP-C2 have been described previously (Berg and Cheney, 2002). The GFP-Myo10 E456K motor domain point mutant (GAG>AAG, nt 1588-1590) was generated by PCR in pEGFP-C2 and corresponds to a weak actin-binding mutant (Friedman *et al.*, 1998). The GFP-Myo10-head-neck-GCN4 forced dimer was generated by fusing the 29 aa leucine zipper (VKQLEDKVEELASKNYHLENEVARLKKLV) from yeast GCN4 to aa 811 of the bovine Myo10-head-neck construct and cloning this into the BglII-HindIII sites of pEGFP-C2. The GFP-Myo10-head-neck-34 construct consists of aa 1-845 of bovine Myo10 inserted into the BglII-HindIII sites pEGFP-C2. The GFP-Myo10-head-neck-34-GCN4 construct was identical except that the GCN4 leucine zipper sequence was added after aa 845. Myo10 constructs were verified by sequencing and their numbering is based on GenBank sequence NM_174394. Mouse GFP-Myo1a in pEGFP-C (Tyska and Mooseker, 2002) was a generous gift from Dr. Matthew Tyska, mouse brain GFP-Myo5a in pEGFP-C1 ("BR MV") (Wu *et al.*, 2002) was a generous gift of Dr. John Hammer, and pEGFP-C2 was used as a GFP control.

Cells. HeLa cells were transfected with Polyfect (Qiagen) unless indicated otherwise. To obtain the relatively low levels of expression required to facilitate single-molecule imaging, HeLa cells were generally transfected for no more than 6-12 hours. Cells were replated onto #1.5 glass coverslips that had been precoated with fibronectin to facilitate formation of substrate-attached filopodia. Coverslips were precoated by incubating acid-washed coverslips for 20 minutes in 10 µg/ml fibronectin in PBS and then washed at least 3x in PBS

over 10 minutes prior to plating. To minimize background from cellular debris, cells were usually plated onto coverslips at <10% confluence, with best results obtained with less than one cell per camera field. Cells were allowed to attach to the coverslip for 1-2 hours and the coverslip was mounted in a Rose chamber with a 3 mm spacer and a #1.5 coverslip for the roof. The chamber was completely filled with Optimem (Gibco). Tet-off HeLa cells (Clontech) that "stably" express GFP-Myo10 were generated as per the manufacturer's instructions. These cells were withdrawn from doxycycline for 1 day to induce expression of GFP-Myo10 and then plated onto glass coverslips and imaged as described above. Only a subset cells expressed detectable GFP-Myo10 following doxycycline withdrawal.

Imaging. Objective type TIRF imaging was performed with a Nikon TE-2000U inverted microscope equipped with a Nikon TIRF-II illuminator (18 mm field of view), a 60x 1.45 NA lens, and a 100 W Hg lamp. TIRF illumination was provided by a 300 mW argon laser and a AOTF was used for rapid wavelength selection and shuttering. For single-molecule experiments, the laser power at 488 nm was adjusted to approximately 40 mW, measured upon exit from the fiber optic cable leading to the TIRF illuminator. During TIRF imaging, all neutral density filters were removed from the beam path in the TIRF-II illuminator. A Chroma #41001 filter cube was used for GFP imaging and images were captured on an ORCA-ER cooled CCD camera (Hamamatsu). Standard camera settings were: low light mode, zero gain, and no binning, resulting in a pixel size of 107 nm. 200 ms exposures were collected at 2-3 frames/s for 30-90 s, with the 488 nm laser line active only during exposures. To avoid pre-bleaching cells prior to a time-lapse series, for most cells we adjusted the laser angle to establish TIRF, shuttered the laser, moved to an adjacent field that had not been

exposed to TIRF, checked focus with DIC, and then activated the laser and acquired the time-lapse. Experiments were performed at 25° C unless indicated otherwise. Metamorph 7.5 software was used to control the microscope, acquire images, adjust contrast, and scale images and Adobe Photoshop and Illustrator were used to generate figures. A particle's velocity were calculated from the slope of its kymograph track.

Kymotracker and data analysis. Imaging data was analyzed using custom software written in Python. This software generates a kymograph based on user-defined lines. The user then traces the particle tracks on the kymograph. This position information is used to seed a fixed-radius Gaussian fit which determines the intensity, background, and subpixel location of the particle in each image. To achieve a more accurate background measurement, the Gaussian fit algorithm ignores nearby pixels which deviate from the Gaussian model by a predefined amount. Kymotracker outputs this data as a file that can be opened in Microsoft Excel for graphing and further analysis. For each track, Kymotracker also captures an image of the spot at each time point. The Kymotracker software is available upon request. Error bars indicate standard deviations. Statistical significance was calculated using a 2-tailed t-test for unequal sample size and unequal variance.

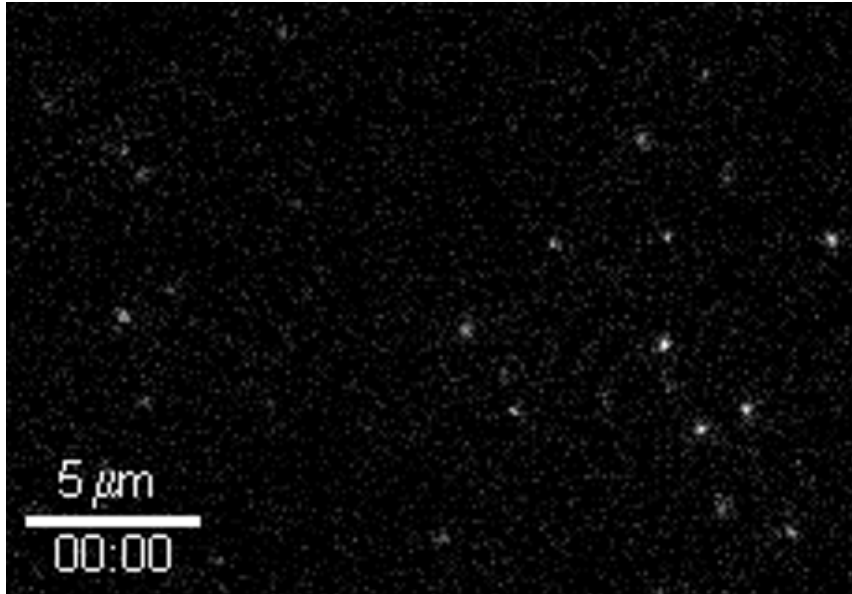
Results

To image the movements of GFP-Myo10 in the filopodia of living cells at the single-molecule level, we used TIRF in combination with a 300 mW laser. We first tested the sensitivity of our TIRF system by imaging pure GFP adsorbed onto coverslips at low concentrations (Movie A2-1). This resulted in the detection of faint spots that were diffraction-limited, underwent stepwise bleaching, and exhibited "blinking", as expected for single-molecule imaging of GFP (Pierce *et al.*, 1997). When living HeLa cells were transiently transfected with full length GFP-Myo10 and imaged by TIRF under the same conditions, we observed bright labeling at the ventral surface of the cell and at the tips of substrate-attached filopodia (Movie A2-2). Most importantly, close inspection of individual filopodia revealed a novel form of movement in which extremely faint particles of GFP-Myo10 moved rapidly towards the tip (Movie A2-3).

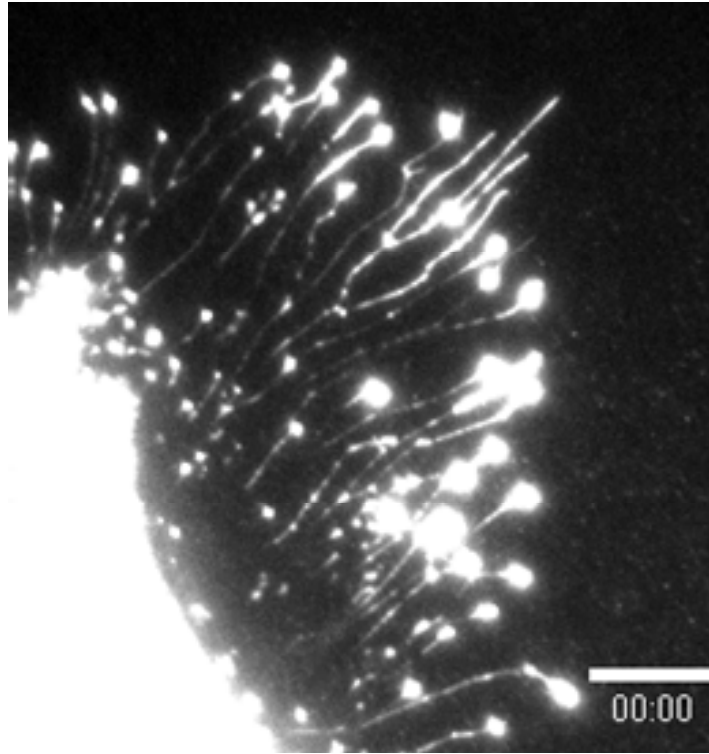
Kymographs along individual filopodia reveal numerous faint tracks that slope gently down to the right (Fig. 1a, b). These tracks correspond to rapid and directed movements of faint particles of Myo10 from the base of a filopodium to its tip. Approximately a dozen such tracks are visible in the 40 s time-lapse illustrated in Fig. 1b, with most of the particles moving the entire $\sim 5 \mu\text{m}$ length of the filopodium. These fast forward tracks appeared to terminate at the tip and were not detected in "control" areas beyond the filopodial tip. Clear examples of fast forward movements were also detected in retraction fibers (Fig. 1c). Although most particles moved in a smooth and apparently processive fashion until they reached the filopodial tip, particles occasionally paused or transiently reversed, generating Z-shaped tracks (Fig. 1d; Supplementary Information, Fig. S1). Rapid forward movements of

Movie A2-1. TIRF microscopy of single GFP molecules adsorbed on a coverslip.

Several faint, diffraction-limited spots are present at the beginning of the time-lapse and exhibit stepwise bleaching. Several spots also "blink" on and off. This time-lapse was acquired using the standard TIRF imaging conditions of 200 ms exposures, 2-3 frames/s, and 107 nm pixels. The calculated penetration depth of the TIRF field (distance to decay to 1/e of intensity at coverslip surface) for 488 nm light at 63° incidence using a 1.45 NA lens is 158 nm. Pure GFP (Clontech) was diluted with TBS, adsorbed to #1.5 glass coverslips, and washed several times with TBS before imaging. Time stamps indicate minutes:seconds.



Movie A2-2. TIRF microscopy of GFP-Myo10 in HeLa cell filopodia. This time-lapse was acquired under the same imaging conditions as Movie 1 and shows GFP-Myo10 at the tips of the numerous substrate-attached filopodia/retraction fibers. Most importantly, faint particles of GFP-Myo10 can be detected moving within these filopodia. GFP-Myo10 can also be detected in the thicker part of the cell at the bases of the filopodia, but much of this region of the cell is saturated under the imaging and scaling conditions used here. When TIRF and wide-field illumination were compared under identical exposure conditions, the tips of substrate-attached filopodia were approximately an order of magnitude brighter with TIRF and also exhibited greatly decreased background.



Movie A2-3. TIRF microscopy reveals fast forward movements of faint particles of GFP-Myo10 in a filopodium. This time-lapse movie illustrates the rapid and directed movements of several faint particles of GFP-Myo10 towards the tip of a filopodium. This is the same filopodium illustrated in Figure 1A-B and was acquired under the standard TIRF imaging conditions described above.

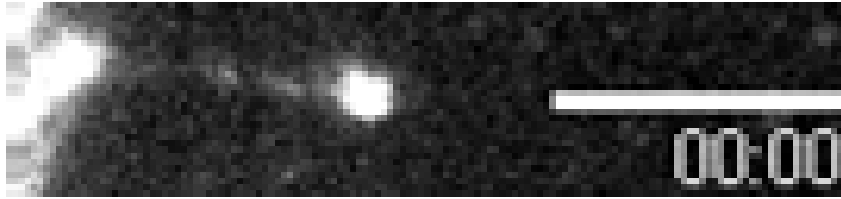
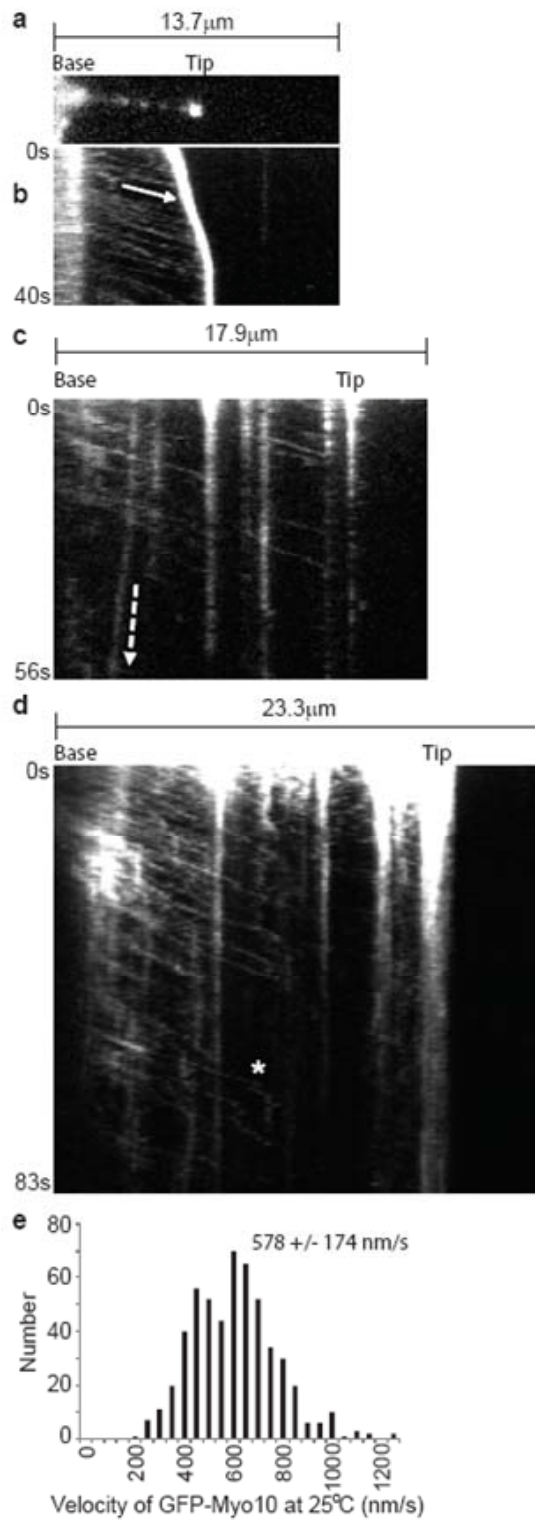


Figure A2-1. TIRF microscopy reveals fast forward movements of faint particles of GFP-Myo10 in living cells. (a) TIRF image of a single filopodium from a HeLa cell expressing GFP-Myo10 showing a bright punctum of GFP-Myo10 at the tip of the filopodium, several faint particles of GFP-Myo10 along the shaft, and diffuse fluorescence at the base of the filopodium (See Movie 3). (b) Kymograph generated from time-lapse imaging of the same filopodium revealing numerous faint tracks (arrow) corresponding to rapid movements of faint particles towards the tip. The bright track that slopes more steeply down to the right corresponds to the tip of the filopodium, which was initially extending forward at ~ 100 nm/s and then stopped. The faint vertical track beyond the tip corresponds to a faint particle of fluorescent debris. (c) Kymograph from a branched retraction fiber in a HeLa cell stably expressing GFP-Myo10. This kymograph shows faint tracks from fast forward movements as well as vertical tracks from stationary particles. One track slopes steeply down to the left and corresponds to GFP-Myo10 that was moving slowly rearward (dashed arrow). (d) Kymograph from a HeLa cell expressing GFP-Myo10 showing numerous faint tracks that terminate midway along a filopodium. One particle moved rapidly forward, transiently reversed, stopped for a few seconds, and then disappeared suddenly (track marked by an asterisk). (e) Velocity histogram for fast forward movements of faint GFP-Myo10 particles.



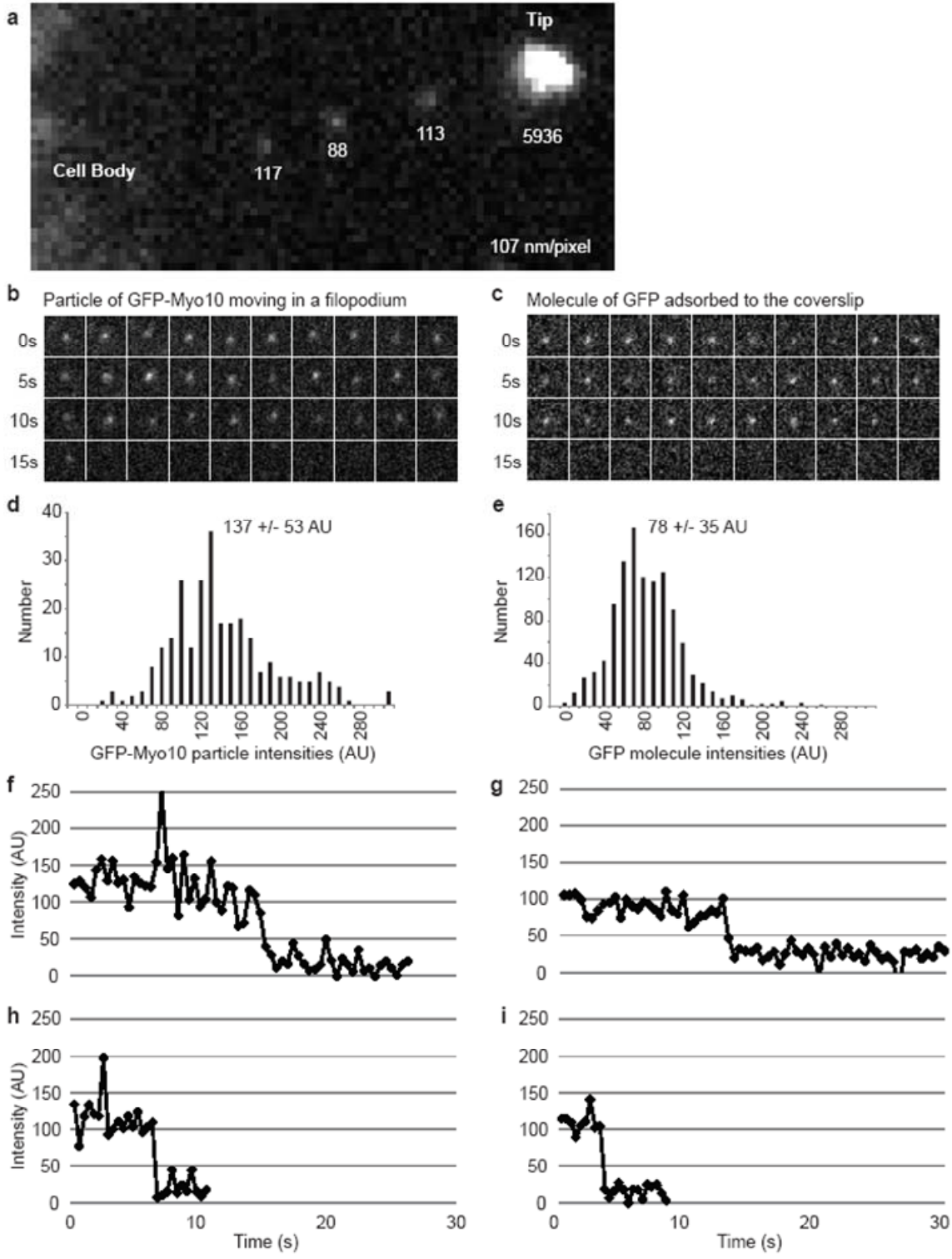
faint Myo10 particles were detected under a variety of TIRF imaging conditions, including the use of different camera settings, different magnifications, and a different TIRF illuminator (Supplementary Information, Fig. S1). The faint particles of Myo10 moved forward at an average velocity of 578 ± 174 nm/s at 25° C (Fig. 1e) and 840 ± 210 nm/s at 37° C. The fast forward movements of the faint particles detected here using TIRF occur at velocities 5-10 fold greater than the relatively infrequent forward movements of bright puncta of GFP-Myo10 detected previously using wide-field microscopy (Berg and Cheney, 2002). Importantly, the velocities of the faint particles of Myo10 detected here in living cells are similar to the 340-780 nm/s reported for individual Myo10 forced-dimers moving on artificial actin bundles *in vitro* (Nagy *et al.*, 2008).

In addition to the fast forward movements, we also detected slow rearward movements of faint particles and bright puncta of GFP-Myo10 (Fig. 1c; Supplementary Information Fig. S1). The average rate of these rearward movements was 23 ± 8 nm/s (137 measurements from 20 filopodia) and is consistent with the hypothesis that GFP-Myo10 moves rearward by binding to actin filaments undergoing retrograde flow. The bright puncta of GFP-Myo10 at the tips of filopodia were generally stationary and thus generated bright vertical tracks that grew gradually dimmer due to photobleaching. Kymographs often showed vertical tracks at different points along a filopodium, indicating that some Myo10 within the filopodial shaft is stationary, perhaps due to association with integrin-based adhesions (Zhang *et al.*, 2004).

We next investigated whether the faint particles of GFP-Myo10 detected by TIRF exhibited properties expected of single molecules (Pierce *et al.*, 1997; Mashanov *et al.*, 2004). High-magnification views show that the faint particles moving within filopodia indeed form diffraction-limited spots with diameters of $\sim 0.3 \mu\text{m}$, whereas the bright puncta at filopodial tips are generally much larger (Fig. 2). Manual measurements indicate that the faint particles have integrated intensities of ~ 100 arbitrary units (AU), which is approximately $1/10^{\text{th}}$ to $1/100^{\text{th}}$ the intensity of a typical tip punctum. To facilitate analysis of the faint particles, we wrote a program called Kymotracker, which uses the position and time coordinates from a line on a kymograph to automatically track the corresponding particle and measure its intensity. As can be seen in the images from Kymotracker of a faint particle of GFP-Myo10 as it moves along a filopodium, the faint particles are diffraction-limited and exhibit relatively constant intensities as they move (Fig. 2b). In some cases, a particle that had been tracked through several frames disappeared suddenly, as would be expected from photobleaching of a single GFP. Using Kymotracker, the average intensity of the faint particles of GFP-Myo10 in filopodia was found to be 137 ± 53 AU. This is comparable to the intensity of single GFP molecules (78 ± 35 AU) adsorbed to coverslips and imaged under the same illumination and exposure conditions (Fig. 2d-e), although it should be noted that the pure GFP was imaged in TBS rather than cytoplasm. Plots of intensity versus time revealed apparent stepwise bleaching events for pure GFP on coverslips and for the faint particles moving within filopodia (Fig. 2f-i). Together these experiments demonstrate that the TIRF system used here can detect single molecules of pure GFP and that the faint particles of GFP-Myo10 detected in living cells correspond to single molecules or small oligomers.

Figure A2-2. Faint particles of GFP-Myo10 exhibit characteristics of single molecules.

(a) High magnification TIRF image of a filopodium showing a bright punctum of GFP-Myo10 at the tip and the diffraction limited nature of 3 faint particles within the filopodial shaft. The numbers indicate the background-corrected, integrated intensity for each spot. (b) Images from Kymotracker showing a single faint particle of GFP-Myo10 as it moved rapidly toward the tip of a filopodium and an apparent bleaching event at ~15 s. (c) Images from Kymotracker showing a single molecule of GFP adsorbed to a coverslip and an apparent bleaching event. (d) Intensity histogram of faint particles of GFP-Myo10 moving rapidly forward in filopodia (268 measurements from 8 filopodia). (e) Intensity histogram of single molecules of GFP adsorbed to coverslip surface (1124 measurements). (f, h) Intensity-versus-time plots from Kymotracker for single particles of GFP-Myo10 that underwent apparent bleaching events as they moved rapidly forward in filopodia. Note that each particle disappeared in a single step rather than gradually fading away. (g, i) Intensity-versus-time plots from Kymotracker for single molecules of GFP adsorbed on a coverslip, illustrating stepwise bleaching.

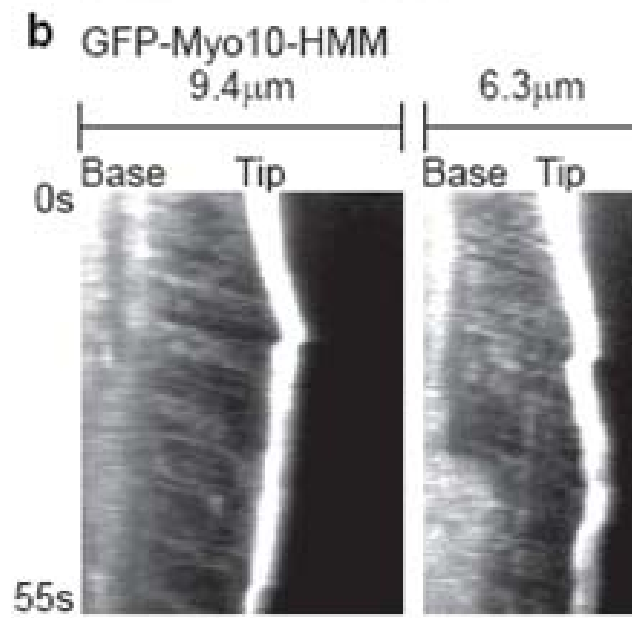
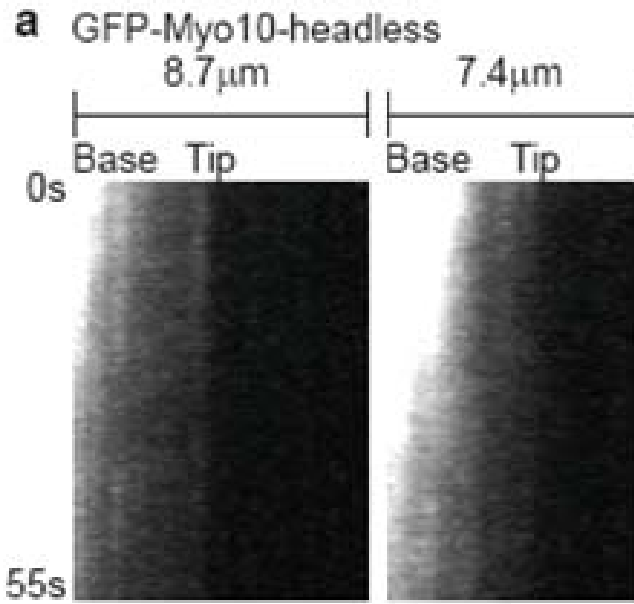


To investigate the mechanisms responsible for the rapid movement of Myo10, we utilized a panel of Myo10 deletion constructs. Rapid particle movements were not detected in HeLa cells transfected with GFP-Myo10-headless, a naturally occurring form of Myo10 that lacks most of the motor domain and thus lacks motor activity (Sousa and Cheney, 2005)(Fig. 3a). We also failed to detect clear particle movements with GFP-Myo10 E456K, a motor domain point mutant engineered to have weak actin binding activity (Supplementary Information Fig. S2). GFP-Myo10-HMM, which consists of the Myo10 motor, neck, and predicted coiled coil, did localize to filopodial tips and underwent rapid movements similar to those of full-length Myo10 (Fig. 3b), suggesting that a dimerized Myo10 head-neck domain is sufficient for fast forward movements. Since systematic analysis of deletion constructs indicated that a forced-dimer construct consisting of the Myo10 head, neck, and first 34 amino acids of the "coiled coil" fused to a GCN4 dimerization domain was the minimal construct able to clearly localize to filopodial tips, we imaged the forced dimer by TIRF and found that it was also capable of fast forward movements in filopodia (Supplementary Information Fig. S2). Together these experiments indicate that rapid movements of faint particles in filopodia require Myo10 motor activity and that a forced dimer is sufficient for fast forward movement.

When HeLa cells expressing GFP-Myo10 were treated with 5 μ M nocodazole, faint particles of GFP-Myo10 still moved forward, indicating that the particle movements do not require microtubules (Fig. 4a). To test whether the fast forward movements are dependent on actin, cells were treated with 1 μ M latrunculin B to depolymerize actin filaments. As expected, this triggered the collapse of filopodia that were not attached to the substrate

Figure A2-3. Fast forward movements require the Myo10 motor domain. (a)

Kymographs from TIRF imaging of GFP-Myo10-headless in filopodia. This construct lacks most of the Myo10 motor domain and does not localize to filopodial tips or exhibit obvious fast forward movements. **(b)** Kymographs from TIRF imaging of GFP-Myo10-HMM. GFP-Myo10-HMM is sufficient for tip localization and faint particles of it undergo fast forward movements.



(not shown) and also caused a spreading or loss of the bright puncta of GFP-Myo10 normally present at the tips of substrate-attached filopodia (Fig. 4b). Most importantly, fast forward movements of GFP-Myo10 were not detected after treatment with latrunculin B, indicating that the fast forward movements are dependent on F-actin.

To test whether other myosins were capable of similar movements within filopodia, we imaged HeLa cells transfected with GFP-Myo1a (brush border myosin I), a monomeric myosin that is non-processive and localizes to microvilli (Tyska and Mooseker, 2002). TIRF showed that GFP-Myo1a yielded a diffuse localization along the filopodia with no obvious enrichment at the filopodial tip (Fig. 5a). Importantly, GFP-Myo1a did not undergo detectable fast forward movements in filopodia, indicating that not all myosins are capable of rapid directed movements in filopodia. We also tested GFP-Myo5a, an intensively studied dimeric myosin that is processive and functions in organelle transport (Trybus, 2008) and filopodial dynamics (Wang *et al.*, 1996). Interestingly, GFP-Myo5a was enriched at the tips of filopodia and faint particles of GFP-Myo5a generated clear tracks corresponding to rapid forward movement (Fig. 5b,c). However, the GFP-Myo5a particles moved at only ~251 nm/s, significantly ($P=0.035$) slower than the ~578 nm/s observed for GFP-Myo10. The velocity of the GFP-Myo5a particles is very similar to the 270-330 nm/s reported for individual molecules of a dimeric Myo5a construct moving on actin bundles *in vitro* (Nagy *et al.*, 2008). It is therefore likely that the rapid and directed movements of GFP-Myo5a detected here correspond to the visualization of individual Myo5a molecules moving along the actin filaments of living cells. As with GFP-Myo10, faint particles of GFP-Myo5a sometimes moved slowly rearward at the retrograde flow rate of ~20 nm/s (Fig 5b). This

observation provides direct evidence that Myo5a can indeed undergo retrograde flow, as recently hypothesized (Liu *et al.*, 2006).

Figure A2-4. Fast forward movements are inhibited by latrunculin B. (a) Kymographs showing that fast forward movements of GFP-Myo10 continue in the presence of nocodazole. Cells treated with 5 μ M nocodazole for 5-10 minutes to depolymerize microtubules and then imaged by TIRF. (b) Kymographs showing that fast forward movements of GFP-Myo10 are blocked by latrunculin B. Cells were treated with 1 μ M latrunculin B for 5-10 minutes to depolymerize actin filaments and then imaged by TIRF.

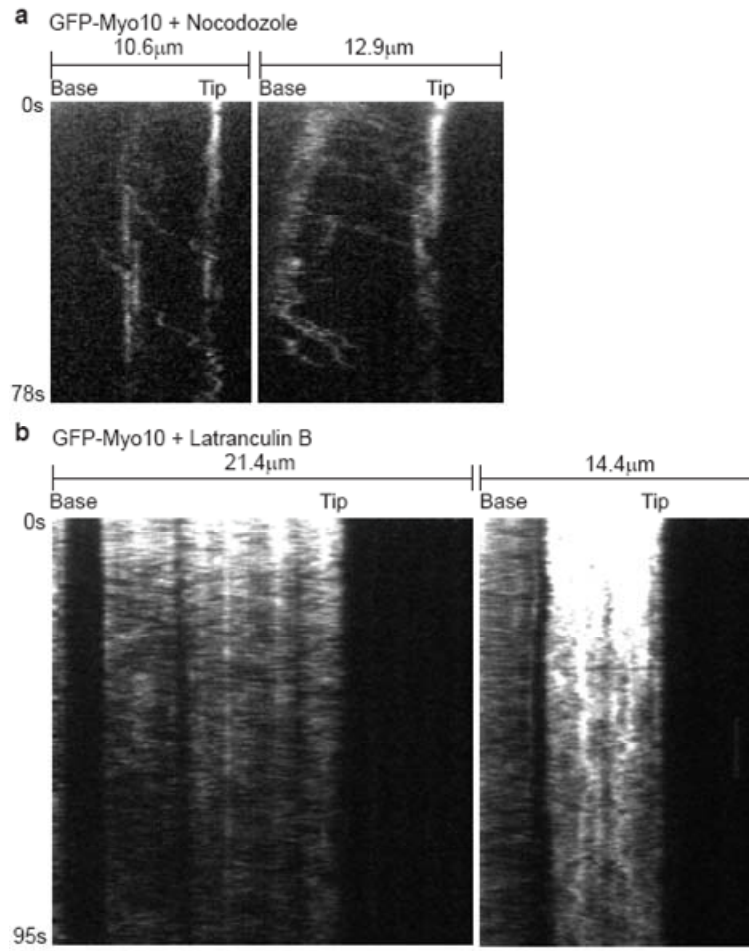
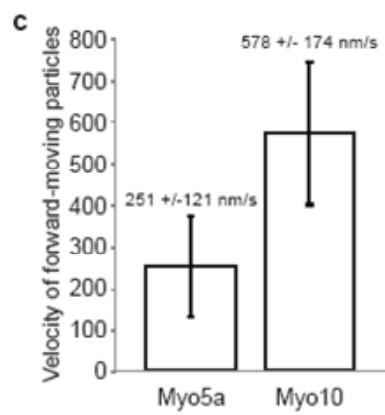
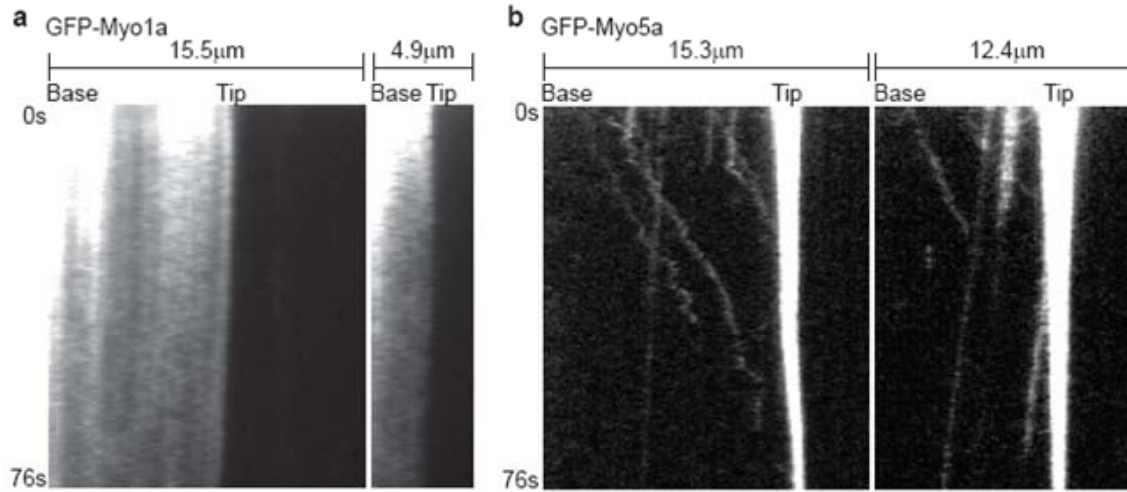


Figure A2-5. Faint particles of GFP-Myo5a can also move forward and rearward in living cells. (a) Kymographs from TIRF imaging of GFP-Myo1a in filopodia. GFP-Myo1a did not localize to the tips of filopodia and no tracks corresponding to rapid forward movement were detected. (b) Kymographs from TIRF imaging of GFP-Myo5a in filopodia. Note that several faint particles of GFP-Myo5a moved rapidly towards the tip while others moved slowly rearward. (c) Histogram comparing average forward velocities of faint particles of GFP-Myo5a (59 measurements from 22 filopodia) and GFP-Myo10 (531 measurements from 65 filopodia).



Discussion

The TIRF experiments reported here clearly reveal a novel form of motility wherein extremely faint particles of GFP-Myo10 move rapidly towards the tips of filopodia over distances of several microns. The fast movements require Myo10 motor activity and actin filaments, but not the Myo10 tail or microtubules. Together, these results strongly support the hypothesis that Myo10 molecules use their barbed-end motor activity to move forward along filopodial actin filaments. The faint particles that we detect with TIRF exhibit a size, intensity range, and bleaching behavior consistent with the imaging of single GFP molecules. It is not yet clear, however, whether these particles correspond to monomers, dimers, or small oligomers of Myo10. Several factors contribute to this uncertainty, including the relatively high and variable background fluorescence present in living cells, the non-ideal behavior of GFP as a fluorophore, variable levels of protein expression, and most importantly, differences in the Z-axis position of filopodia and the molecules within them. It should also be noted that although we can clearly detect the movements of some particles, we cannot guarantee unambiguous detection of every GFP-Myo10 molecule in a filopodium. The development of more sensitive imaging systems, improved fluorophores, and multicolor TIRF is likely to allow for detailed biophysical characterization of the movements of single motor proteins in living cells, and visualization of cotransport with candidate cargo molecules at the single-molecule level.

The discovery of this novel form of motility raises numerous questions, including the identity of factors that regulate the movements of Myo10 and whether similar movements occur in microvilli and stereocilia. It will also be interesting to determine if Myo3a or

Myo15a, myosins that localize to the tips of stereocilia and are necessary for hearing, undergo similar forms of movement (Belyantseva *et al.*, 2005; Liu *et al.*, 2006; Schneider *et al.*, 2006). Finally, it will be important to determine if the rapid movements of Myo10 molecules function primarily as a mechanism to localize this motor protein to the tips of filopodia or as a system for transporting cargo molecules in filopodia in a fashion analogous to intraflagellar transport in cilia.

Acknowledgements

DTJ was supported by a Porter Fellowship from the APS and a UNC Sequoyah Dissertation Fellowship. TY was supported by the Leukemia and Lymphoma Society and OAQ was supported by a UNC SPIRE postdoctoral fellowship from NIH/GM00678. This research was supported by NIH/NIDCD grant RO1 DC03299 to REC and by NIH/NHLBI grant P01 HL080166.

Figure A2-S1. Dynamics of GFP-Myo10 in living HeLa cells imaged with TIRF. (a)

Kymograph of a filopodium imaged using a 60x lens, 1.5x tube lens, 2x2 binning, and camera set to maximum gain. Numerous faint tracks slope gradually down to the right, corresponding to fast forward movements of faint particles of GFP-Myo10. Although most particles move at a relatively constant velocity from base to tip, a few particles appeared to slow down as they approached the tip and others appear to transiently reverse direction, creating Z-shaped tracks. This cell was imaged at 37° C and the pixel size is 142 nm. Note that the particles move so rapidly that most reach the tip prior to bleaching, even at full laser power. **(b)** Kymograph of a filopodium imaged under standard conditions (37° C, 60x, 1x tube lens, no binning, zero gain, and a pixel size of 107 nm) except for use of a Nikon single-molecule TIRF illuminator (11 mm field of view). This kymograph illustrates several different states that Myo10 can exist in, including stationary (vertical lines), moving rapidly forward (tracks that slope gradually down to the right), and moving slowly rearward (tracks that slope steeply down to the left). **(c)** Kymograph of a filopodium imaged under standard conditions where much of the GFP-Myo10 was moving slowly rearward.

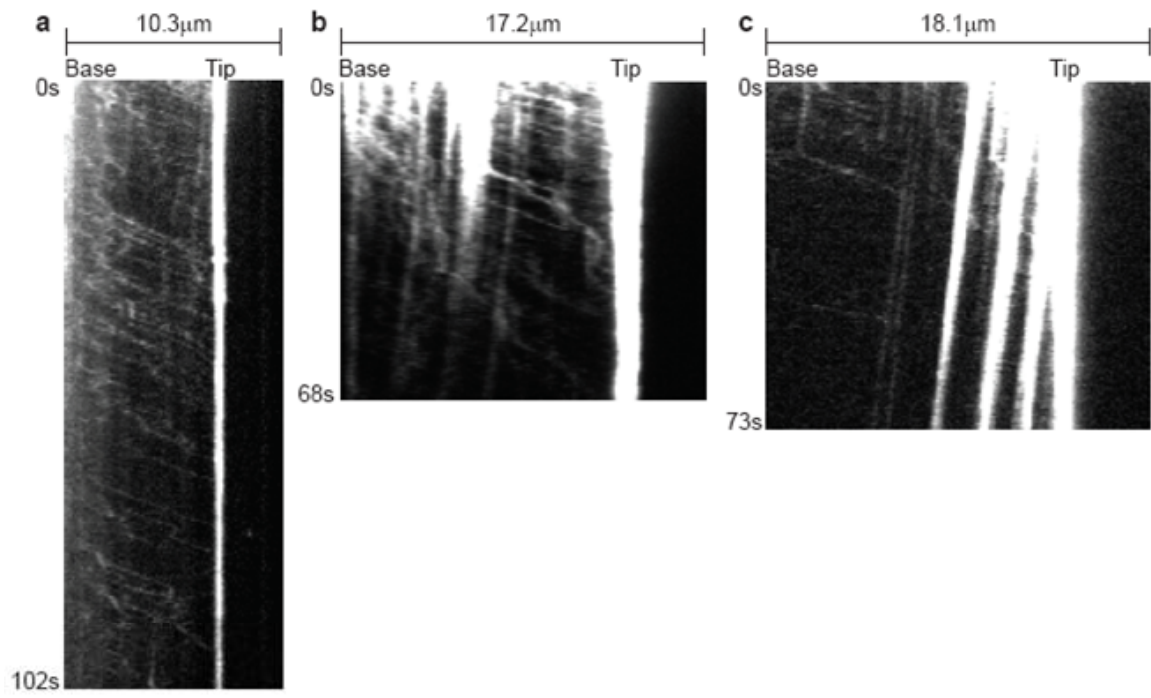
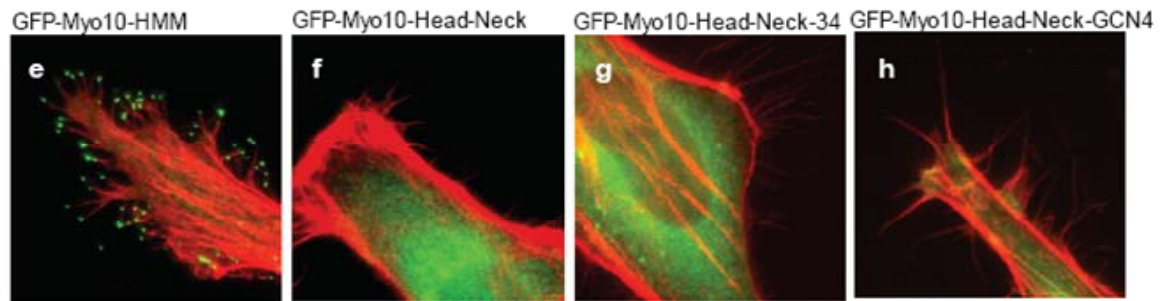
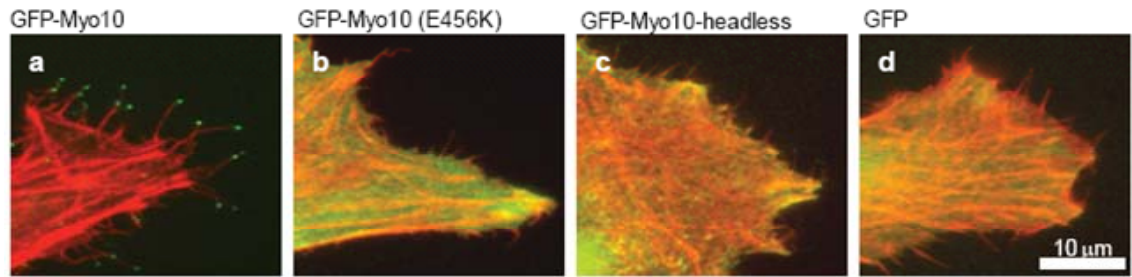
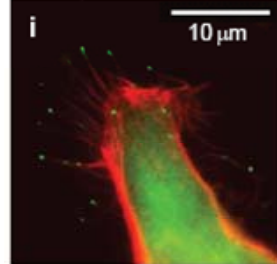


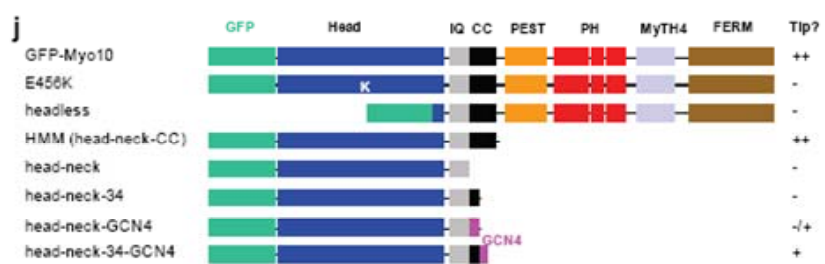
Figure A2-S2. Tip localization of different Myo10 constructs and TIRF imaging of a forced dimer and a motor domain point mutant. (a-i) HeLa cells transfected overnight with the indicated GFP-tagged constructs (green) were replated ~12 hours on glass coverslips, fixed, and then stained with phalloidin (red). (a-d) The full-length, positive control GFP-Myo10 shows clear localization to the filopodial tip, whereas GFP-Myo10 E546K (a motor domain point mutant), as well as the negative controls (GFP-Myo10-headless and GFP alone) show little or no localization to the tip, demonstrating that Myo10 motor activity is necessary for strong tip localization. (E-I) Similar experiment showing that the GFP-Myo10-HMM positive control is clearly sufficient for localizing to filopodial tips, whereas the GFP-Myo10-head-neck, GFP-Myo10-head-neck-34, and the GFP-Myo10-head-neck-GCN4 forced dimer show little or no tip localization. The slightly longer GFP-Myo10-head-neck-34-GCN4 forced dimer is able to localize to the filopodial tip, although it also exhibits some diffuse labeling of the cell body. (j) Bar diagram summarizing the domain structure of different Myo10 constructs and their ability to localize to the filopodial tip. (k) Kymograph of a filopodium from a cell transfected with the motor domain point mutant (GFP-Myo10 E456K) and imaged by TIRF. The motor domain point mutant showed little localization to the filopodial tip and did not generate clear tracks corresponding to rapid forward movements. (l) Kymograph of a filopodium from a cell transfected with the GFP-Myo10-head-neck-34-GCN4 forced dimer and imaged by TIRF. This construct generated occasional tracks corresponding to fast forward movements, indicating that a forced dimer is capable of rapid forward movements within filopodia.



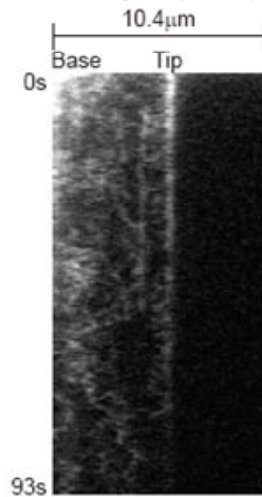
GFP-Myo10-Head Neck-34-GCN4



Summary of tip localization results from widefield fluorescence



k GFP-Myo10 (E456K)



l GFP-Myo10-Head Neck-34-GCN4



References

- Albrecht-Buehler, G., and Goldman, R.D. (1976). Microspike-mediated particle transport towards the cell body during early spreading of 3T3 cells. *Exp Cell Res* 97, 329-339.
- Berg, J.S., and Cheney, R.E. (2002). Myosin-X is an unconventional myosin that undergoes intrafilopodial motility. *Nat Cell Biol* 4, 246-250.
- Berg, J.S., Derfler, B.H., Pennisi, C.M., Corey, D.P., and Cheney, R.E. (2000). Myosin-X, a novel myosin with pleckstrin homology domains, associates with regions of dynamic actin. *J Cell Sci* 113, 3439-3451.
- Friedman, A.L., Geeves, M.A., Manstein, D.J., and Spudich, J.A. (1998). Kinetic characterization of myosin head fragments with long-lived myosin.ATP states. *Biochemistry* 37, 9679-9687.
- Knight, P.J., Thirumurugan, K., Yu, Y., Wang, F., Kalverda, A.P., Stafford, W.F., 3rd, Sellers, J.R., and Peckham, M. (2005). The predicted coiled-coil domain of myosin 10 forms a novel elongated domain that lengthens the head. *J Biol Chem* 280, 34702-34708.
- Liu, J., Taylor, D.W., Krementsova, E.B., Trybus, K.M., and Taylor, K.A. (2006). Three-dimensional structure of the myosin V inhibited state by cryoelectron tomography. *Nature* 442, 208-211.
- Mattila, P.K., and Lappalainen, P. (2008). Filopodia: molecular architecture and cellular functions. *Nat Rev Mol Cell Biol* 9, 446-454.
- Medeiros, N.A., Burnette, D.T., and Forscher, P. (2006). Myosin II functions in actin-bundle turnover in neuronal growth cones. *Nat Cell Biol* 8, 215-226.
- Nagy, S., Ricca, B.L., Norstrom, M.F., Courson, D.S., Brawley, C.M., Smithback, P.A., and Rock, R.S. (2008). A myosin motor that selects bundled actin for motility. *Proc Natl Acad Sci U S A* 105, 9616-9620.
- Pierce, D.W., Hom-Booher, N., and Vale, R.D. (1997). Imaging individual green fluorescent proteins [letter]. *Nature* 388, 338.
- Rogers, M.S., and Strehler, E.E. (2001). The tumor-sensitive calmodulin-like protein is a specific light chain of human unconventional myosin x. *J Biol Chem* 276, 12182-12189.
- Sousa, A.D., and Cheney, R.E. (2005). Myosin-X: a molecular motor at the cell's fingertips. *Trends Cell Biol* 15, 533-539.
- Tokuo, H., Mabuchi, K., and Ikebe, M. (2007). The motor activity of myosin-X promotes actin fiber convergence at the cell periphery to initiate filopodia formation. *J Cell Biol* 179, 229-238.

- Trybus, K.M. (2008). Myosin V from head to tail. *Cell Mol Life Sci* 65, 1378-1389.
- Tyska, M.J., and Mooseker, M.S. (2002). MYO1A (Brush Border Myosin I) Dynamics in the Brush Border of LLC-PK1-CL4 Cells. *Biophys J* 82, 1869-1883.
- Wang, F.S., Wolenski, J.S., Cheney, R.E., Mooseker, M.S., and Jay, D.G. (1996). Function of myosin-V in filopodial extension of neuronal growth cones. *Science* 273, 660-663.
- Weber, K.L., Sokac, A.M., Berg, J.S., Cheney, R.E., and Bement, W.M. (2004). A microtubule-binding myosin required for nuclear anchoring and spindle assembly. *Nature* 431, 325-329.
- Wu, X., Wang, F., Rao, K., Sellers, J.R., and Hammer, J.A., 3rd. (2002). Rab27a is an essential component of melanosome receptor for myosin Va. *Mol Biol Cell* 13, 1735-1749.
- Zhu, X.J., Wang, C.Z., Dai, P.G., Xie, Y., Song, N.N., Liu, Y., Du, Q.S., Mei, L., Ding, Y.Q., and Xiong, W.C. (2007). Myosin X regulates netrin receptors and functions in axonal path-finding. *Nat Cell Biol* 9, 184-192.